University of Nottingham
UK | CHINA | MALAYSIA

Enzyme-responsive hydrogels: Development, characterisation and on-demand modulation of protease activity

Rebeca Lucia Obenza-Otero

Thesis submitted to the University of Nottingham for the degree of Doctor of Philosophy

September 2019

Acknowledgements

Firstly, I would like to acknowledge my supervisors at the School of Pharmacy Dr. Giuseppe Mantovani, Dr. Weng Chan and Dr. Mischa Zelzer for their guidance and support throughout the last three years. In particular Dr Mischa Zelzer for his constant support and encouraging me to learn many new techniques and skills during my PhD. I would also like to like thank industry collaborators Dr. Marianne Ashford and Dr. Paul Gellert for contributing their time to give some extra guidance and support, and very encouraging and kind conversations. I would also like to thank Prof. Simon Johnson and Dr. Debbie Clements from the School of Medicine for having helped me with the design and interpretation of biologically relevant cell assays as well as given me exhaustive training and assistance cell culture throughout the months. I would also like to thank EPSRC for funding this work on the grant EP/L01646X/1 through the CDT in Advanced Therapeutics and Nanomedicines program.

I would like to thank all past and present members in the Functional Biointerfaces group for their helpful scientific discussions and making working in the lab so much grateful. Of course special mention to Emanuele, for his assistance with the synthesis, MMP gels and all these long discussions. But especially for being such a good support in in the lab since we started our PhDs together, you have shown to be great person to work with and learn from. I would also like to acknowledge members of the C22 lab in CBS for their training and help with peptide synthesis and purification. I feel very lucky to have had the chance to meet such wonderful and diverse people during my time at this University, you had all made it an enjoyable place to work.

I would also like to thank the people in my offices, A03 and C15, and of course the CDT family, especially my cohort, for the every-day moral support and reminding me that not all the good skills are learned in the lab. Special thanks to Claudia for always watching over us and helping us, and the technical and admin staff of BSB, CBS and RMQ for their help and making our lives a little easier.

Finally, I want to specially thank my family, friends and partner for supporting me through the PhD and life in general. Grazas á miña familia por estaren sempre ahí, en especial aos meus pais e meu irmán. Grazas por apoiarme en todas as as decisións que tomei, por difíciles que fosen, e por ensinarme a ser quen son, e traballar duro polos meus obxectivos. Grazas ós meus amigos por estar sempre ahí, a tiro de café, de caña ou de videochamada, pois son eses bos momentos os que dan máis enerxía. Gordon, I cannot express how grateful I am, your continuous understanding and support has been immense, and your scientific curiosity is really inspiring.

Table of contents

List of Figures

List of Tables

Abbreviations

4-PEGMal	4-arm-poly(ethylene glycol) maleimide
4-PEGNB	4-arm-poly(ethyleneglycol) norbornene
4-PEG-OH	4-arm-hydroxyl-poly(ethyleneglycol)
AAT	Alpha-1-antitrypsin
AES	Airway Epithelial Cell Growth Supplement
ATR	Attenuated Transmission Reflection
BPE	Bovine Pituitary Extract
BSA	Bovine Serum Albumin
CHCA	alpha-cyano-4-hydroxycinnamic acid
DCM	Dichloromethane
DCTB	(trans-2-[3-(4-tert-Butylphenyl)-2-methyl-2-propenylidene] malononitrile)
DIPEA	N,N-diisopropylehtylamine
DMEM-F12	Dulbecco's Modified Eagle Medium: F-12 nutrient mixture
DMF	N,N-dimethylformamide
DMSO	Dimtehylsulfoxide
Dpa	N-3-(2, 4-Dinitrophenyl)-L-2,3-diaminopropionyl
DTT	D-L-Dithiothreitol
ELISA	Enzyme-linked Immunosorbent assay
ESI-MS	Electrospray Ionisation Mass Spectrometry
Fab	Fragment Antigen Binding
FBS	Foetal Bovine Serum
FD70	70 kDa fluorescein isothiocyanate-dextran
FTIR	Fourier Transform Infrared Spectroscopy
G'	Storage modulus
G''	Loss modulus

HATU	(2-(7-aza-1H-benzotriazole-1-yl)-1,1,3,3-tetramethyluronium hexa-fluorophosphate
HKGS	Human Keratinocyte Growth Supplement
HNE	Human Neutrophil elastase
LAP	Lithium phenyl-2,4,6-trimethylbenzoylphosphinate
LVE	Linear viscoelastic regime
MALDI-ToF-MS	Matrix-Assisted Laser Desorption and Ionisation Time-of-Flight Mass Spectrometry
Mca	(7-Methoxycoumarin-4-yl)acetyl
Mca-PLGL-Dpa-AR-NH2	Mca-Pro-Leu-Gly-Leu-Dpa(Dnp)-Ala-Arg-NH2
NMR	Nuclear Magnetic resonance
Nsuc-AAPV-pNA	N-methoxysuccinyl-Ala-Ala-Ala-Pro-Val-p-nitroanilide
Nsuc-Ala_3-pNA	N-methoxysuccinyl-Ala-Ala-Ala-p-nitroanilide
PBS	phosphate-buffered saline
PEG	poly(ethyleneglycol)
PPE	Porcine Pancreatic Elastase
rhEGF	Recombinant human Epithelial Growth Factor
rhILGF	Recombinant human Insulin-Like Growth Factor
RP-HPLC	Reverse Phase High Pressure Liquid Chromatography-
RP-HPLC-MS	Reverse Phase High Pressure Liquid Chromatography-Mass Spectrometry
SAGM	Small Airway-epithelial Growth Medium supplement
T3	Triiodothyronine
TFA	Trifluoroacetic acid
TIPS	Triisopropylsilane
TRD70	70 kDa Texas red dextran

Mathematical abbreviations

Qm	Mass swelling ratio
Qv	Volume swelling ratio

ρ_p	Density of the polymer
ρ_s	Density of the solvent
$\overline{M}_n$	Molecular weight average of the polymer
Mc	Molecular weight average between crosslinks
X_1	Solvent-polymer interaction parameter
$\overline{(r_0^2)}^{1/2}$	Root mean square of polymer chain end-to-end distance
ξ	Mesh size
M_r	Molecular weight of polymer repeating units
L	C-C bond length average

Amino acids abbreviations

A	Alanine
Ac-	Acetyl-terminated on the N-terminus
C	Cysteine
G	Glycine
I	Isoleucine
K	Lysine
NH_2	Amide-terminated on the C terminus
P	Proline
Q	Glutamine
R	Arginine
S	Serine
V	Valine
W	Tryptophan

Abstract

Bioresponsive materials that are able to release their cargoes in response to disease-specific cues are of great interest for developing targeted therapeutics due to their potential to limit drug release to its site of action, thus minimising side effects. The use of proteases as triggers for biomaterial response is particularly attractive as upregulated activity of proteases, such as elastase, is related to several pathological states such as tissue destruction associated with chronic wounds and respiratory diseases. As elastase also possesses important functions that are crucial for maintaining a healthy status, full enzyme suppression is not desirable. Instead modulation of elastase activity to restore the natural protease/inhibitor balance that favours restoration of tissue integrity would be advantageous.

Feedback-controlled modulation of elastase in response to the level of enzyme activity could be achieved by incorporating inhibitors and elastase-sensitive components in the material. This thesis aims to develop peptide-crosslinked PEG hydrogels able to release the elastase inhibitor alpha-1-antitrypsin (AAT) in response to the level of elastase in its environment, mimicking the body's natural strategy for balancing protease levels to restore tissue integrity. To achieve this, hydrogels were formed by crosslinking of thiol-terminated elastase-sensitive peptides with multi-arm thiol-reactive polymers. Initially the hydrogel crosslinking kinetics, mesh size, mechanical properties and ability to physically entrap molecules were optimised using a model short dithiol. Then, an elastase-responsive peptide sequence with suitable solubility was incorporated into hydrogels via thiol-crosslinking chemistries. Elastase-responsive hydrogels were shown to release a model dextran upon incubation with elastase, while elastase non-responsive gels (fabricated with a scrambled peptide) were unaffected by the enzyme. This confirmed that the responsive release was dictated by the peptide sequence. Further confirmation of the hydrogel's selective responsiveness was achieved by incubation with a non-targeted enzyme, Matrix Metalloproteinase-2, which did not increase macromolecule release.

The ability of AAT encapsulated in elastase-responsive hydrogels to inhibit elastase was demonstrated, as characterised by monitoring the release of a model probe and measuring elastase activity in the *milieu*. Scrambled-peptide crosslinked gels were used as passive release control, and modulated elastase activity to a lower extent than the responsive hydrogels. Finally, the effects of hydrogels in cells and their ability to promote a beneficial effect on cells through elastase activity modulation was studied *in vitro. In vitro* tests confirmed hydrogels did not affect epithelial cell viability and AAT-loaded gels were able to modulate elastase activity in the presence of cells and improved elastase-hindered epithelial repair.

Chapter 1

Introduction

1.1 Introduction to hydrogels

1.1.1 Classification and properties of hydrogels

Hydrogels are defined as three dimensional networks with the ability to retain large amounts of water and mechanical properties characteristic of a solid, although they are mostly formed by liquid[1–3]. Hydrogels present several advantageous properties as drug delivery vehicles such as their porosity, hydrophilic nature, versatility and high water content, that has led to numerous reviews in the field[4–7].

Hydrogels can be classified into chemical hydrogels or physical hydrogels, depending on the mechanism of hydrogel formation. In physical hydrogels the hydrogel network is formed through non-covalent reversible interactions. One example of physical hydrogels are supramolecular hydrogels, which consist of the three-dimensional association via non-covalent interactions of molecules known as gelators. Gelators are small molecular weight compounds such as amphiphilic nucleosides, short peptides, or sugars, able to self-assemble into self-supportive structures that form the gel network, normally upon the action of a trigger[8]. The resulting structures are usually formed of entangled fibrilar networks that entrap large amounts of water[8,9]. Due to their ability to encapsulate active ingredients within the self-assembled structures, supramolecular gels using a vast array of amphiphiles have been used for drug encapsulation and delivery[6,10–12]. Physical hydrogels have also been formed via physical crosslinking of polymeric chains, via a variety of physicochemical interactions (e.g. ionic interactions, hydrophobic or hydrogen bonding)[4]. For instance, hydrogels formed by hydrophobic interactions and ionic interactions between polymers have been particularly advantageous for the encapsulation of small hydrophobic and charged

drugs, respectively[13]. Although physical hydrogels are very versatile, and have the advantage of *in situ* gelation, there is a limited level of control on the hydrogel strength, network pore size and resistance to dilution.

Chemically crosslinked hydrogels provide a better control over crosslink density and pore size, have stronger mechanical properties and allow easy incorporation of functional groups within the hydrogel network. These gels are usually formed by covalently crosslinked hydrophilic polymers with a high affinity for water[5]. Once the chemical crosslinks are formed, the hydrogel network will be prevented from being dissolved into water, but their porous structure will allow water to penetrate between the hydrophilic polymer chains, subsequently causing swelling[14]. Polymeric hydrogels can be formed either by natural or synthetic polymers. Several hydrogels made of natural polymers such as chitosan, hyaluronic acid, chondroitin sulphate or alginate have been used for drug delivery, due to their inherent bio-degradation and biocompatibility [15–20]. Hydrogel preparation with synthetic polymers has the advantage of improved control over hydrogel pore size and mechanical properties by careful selection among a versatile library of polymer types and sizes, and greater flexibility for chemical functionalisations[21–24]. Several derivatives of synthetic polymers with varying physical properties such as charge can be used. For instance, neutral polymers such as poly(vinyl alcohol) (PVA), poly(hydroxyethyl methacrylate) and poly(ethylene glycol) (PEG) or charged polymers such as poly(acrylic acid) (PAA), poly(methacrylic acid) (PMMA) or polyacrylamide (PAAm)[5]. Among these, hydrogels based on PEG (poly-ethylene oxide repeating units) are one of the most widely used biomaterials for biomedical applications. This is due to PEG being biocompatible and non-toxic, approved by the FDA and the option of hydrogels being covalently crosslinked using a variety of methods which can easily incorporate a broad range of functionalities to improve mechanical properties, biocompatibility and controlled release profiles[25–27]. Some of the first uses of PEG were conducted by Merril *et al*., who studied its ability to reduce platelet and protein adsorption and thrombus formation at the implants surface[28]. Since then, PEG-based hydrogels have been designed for many drug delivery applications such as ocular

delivery, sustained release formulations, wound dressings, hydrogel nano- and micro-particulates or *in situ* crosslinking injectable gels[29–33] .

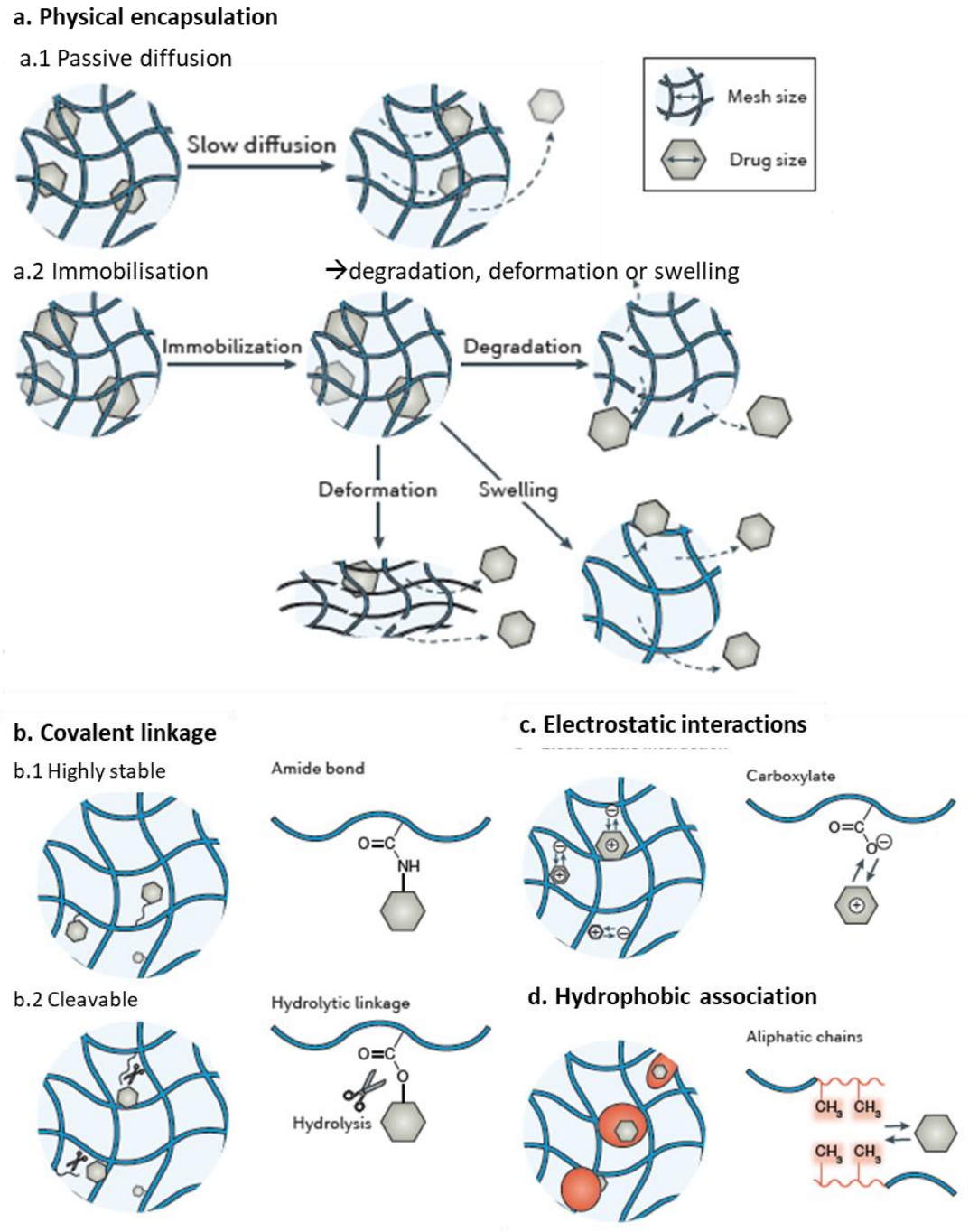

Figure 1.1. Mechanism of drug encapsulation and release into polymeric hydrogels. **a.**) Physical encapsulation of the drug within the hydrogel network. The release mechanism takes place by either passive diffusion, or hydrogel degradation, deformation or swelling, depending on the relative drug/mesh size ratio. **b.**) Covalent linking of the drug to the polymer network, **c.**) encapsulation by electrostatic interactions and **d.**) hydrophobic associations. Figure adapted from[1].

The incorporation of therapeutic molecules into hydrogels can be achieved by different means ranging from physical entrapment, covalent linking, and hydrophobic and electrostatic interactions (Figure 1.1).

1.1.1.1 Physical encapsulation

The most common strategy for drug encapsulation is by physical encapsulation of the molecule within the hydrogel network, since it does not require the use of any chemical modification of the bioactive cargo or the hydrogel. This is especially advantageous for biologics such as proteins, peptides or cells, since their bioactivity can be compromised by chemical linkage or by the use of additional chemicals.

The release kinetics of macromolecules physically entrapped into hydrogels will be determined by the relative size of the molecule with respect to the hydrogel mesh size[22,34]. Hydrogel mesh size is defined as the distance between two adjacent crosslinking points in a polymeric hydrogel (Figure 1.1.a.1). The mesh size is an important parameter for physically encapsulated drugs, since it strongly influences the passive diffusion of the entrapped molecules. Several parameters can be used to tune hydrogels mesh size in order to improve physical entrapment, such as polymer size, concentration and crosslinking degree[22,35,36]. If the mesh size of a hydrogel is much larger than the size of the entrapped molecule (given by its hydrodynamic diameter), then the drug can freely diffuse through the hydrogel network leading to a burst release mechanism[1,14,22]. When the mesh size and drug size are in the same range, then drug diffusion through and out of the hydrogel will be hindered and leading to a release will be slower over time[22] (Figure 1.1.a.1).

If the mesh size is much smaller than the drug size, then the steric hindrance will effectively immobilise the molecule inside the gel. The drug will then remain physically entrapped within the hydrogel until the network of the hydrogel is altered (Figure 1.1.a.2). This allows for the use of stimuli-responsive strategies to trigger the release by causing hydrogel degradation, swelling or

deformation[1,37]. For instance the incorporation of labile groups (e.g. ester) or enzyme substrates within the polymer allows for hydrolytically or enzymatically controlled hydrogel degradation and drug release, respectively[36,38,39]. An alternative approach to trigger the release is to incorporate functionalities that, upon contact with the stimuli, cause hydrogel swelling and subsequent increase in mesh size that leads to the release of the drug[40] (Figure 1.1.a.2).

1.1.1.2 Covalent linking

Another approach for controlling drug release from hydrogels is to covalently bind the drug to the polymer chains. This covalent conjugation is often employed if the therapeutic to be entrap is too small to be physically retained inside the hydrogel, as otherwise the therapeutic would be released in a short time. Normally, the drug will be modified for covalent attachment to the polymer by either a highly stable or cleavable linker (Figure 1.1.b). When linkers with high stability over time are used, such as amide or thioether bonds, the drug will then be released as the bulk hydrogel degrades[41,42] (Figure 1.1.b.1).

Stimuli-responsive release of the drug can be achieved by careful design of a cleavable linker. The covalently attached drug will be released from the hydrogel via degradation of the linker (Figure 1.1.b.2). For instance the incorporation of esters, disulphide or enzymatically degradable linkers allows for pH, oxidative and enzymatic controlled delivery[43–45].

1.1.1.3 Non-covalent drug-polymer interactions

Finally, non-covalent interactions can be exploited to form strong affinity between drugs and the polymer chains. They exhibit some of the beneficial properties of the previous two categories. They do not require any chemical alteration of the encapsulated drug, therefore there is no risk of altering its activity as the drug is physically entrapped. Additionally, they can significantly improve drug retention of charged or small hydrophobic drugs, compared with covalent linking strategies.

Electrostatic interactions by non-specific charge-charge associations between the hydrogel and charged drugs or macromolecules are particularly advantageous for the controlled delivery of charged therapeutics. This can be achieved by the use of charged polymers or by introduction of charged functionalities within the hydrogel. For example, hydrogels containing polymers that are negatively charged at physiological pH, such as alginate or chondroitin sulphate have been shown to efficiently encapsulate positively charged proteins such as growth factors [20,46]. Alternatively, when the polymer does not carry any charges, it can be functionalised with charged end-groups. For instance, Kim *et al.* have incorporated pendant charges with either negative (Sulfonate) or positive (trimethylammonium chloride) net charge in PEG hydrogels to retain and control the release of positively or negatively charged proteins[47]. Negatively charged proteins albumin and insulin, were better retained in the positive functionalised gels while they underwent faster release from negatively charged gels (repulsive forces). These studies showed that the use of charged polymers or functionalities can contribute to reducing the passive diffusion and controlling the release of charged therapeutics such as proteins.

Introduction of small hydrophobic functionalities within the polymer chain can improve the entrapment and reduce the passive release of hydrophobic drugs, which otherwise would be problematic to retain due to the hydrophilicity of hydrogels. For instance the introduction of hydrophobic polymers, cyclodextrins or cholesterol molecules in the polymer has been used to improve the encapsulation of hydrophobic drugs[27,48]. Despite the effectiveness of hydrophobic associations for encapsulation of hydrophobic drugs, the incorporation of hydrophobic areas may change hydrogel physical properties. Therefore an appropriate balance of drug encapsulation and maintenance of adequate physical properties must be assessed.

In summary, there are different approaches for the encapsulation of therapeutics into hydrogels. The most suitable will depend on the specific molecule to entrap and the application. This is because there are many factors such as molecule size, charge, and stability, and hydrogel mesh size and composition that can affect both, drug encapsulation and its activity. Among the

previous reports, hydrogels encapsulating drugs by physical entrapment[36,38,39], covalent linking[43–45], and non-covalent interactions[20,46,47] have been shown to achieve controlled release. Thus, controlled release strategies can be achieved independently of the drug encapsulation method, and the choice would depend on each particular case.

1.2 Proteases in health and disease

Enzymes are the main biological catalysts and they play critical roles in all biological processes in living organisms. Enzyme-catalysed reactions are highly specific towards their substrate and a myriad of biochemical reactions are controlled by enzymes (e.g. gene expression, cell adhesion, matrix remodelling, oxidative balance, signal transduction). Thus, adequate regulation of enzymatic activity is essential to maintain homeostasis within tissues and organisms, and many pathological states are characterised by altered level of enzymes.

Proteases are enzymes that degrade peptides and proteins, and are extensively implicated in tissue remodelling. Proteases are involved in a broad array of functions, such as cell migration and detachment, extracellular matrix (ECM) remodelling, regulation of growth factors, acute inflammation and activation of gene regulation pathways[49–53]. Proteases are usually tightly regulated by their physiological inhibitors. Overexpression of protease activity has been associated with several diseases, such as cancer, osteoarthritis, chronic wounds, cardiovascular diseases and inflammatory pulmonary diseases[54–57]. Proteases are usually classified according to their catalytic mechanism as cysteine proteases, serine proteases and matrix metalloproteinases (MMPs).

1.2.1 Unbalanced proteases in chronic inflammatory diseases

Serine proteases and MMPs are the main protease types involved in tissue remodelling, since they are secreted to the extracellular space by various cell types[51,58]. MMPs and serine proteases are endopeptidases (peptide breakage at non-terminal amino acids) with a Zn cation catalytic group and a serine at the active site, respectively. Under physiological conditions both types of

enzymes are tightly regulated by their physiological inhibitors, the Tissue Inhibitors of Proteases (TIMPs, MMPs inhibitors) and Serine Protease Inhibitors (SERPINS). Both enzyme types are overexpressed in certain chronic diseases such as chronic wounds or inflammatory pulmonary diseases

1.2.1.1 Unbalanced proteases in wound healing

Acute and chronic wound healing are usually used as an example of protease activity dysregulation. Wounds are a disruption of normal anatomic structure and function, caused by a pathologic process beginning internally or externally to the involved organ(s)[59]. After a tissue is wounded, a multistep process known as wound healing is triggered in order to restore the disrupted tissue integrity (Figure 1.2.a). Briefly, it begins with the formation of a fibrin clot to prevent excessive bleeding (haemostasis) which leads to an inflammatory response from attracted leukocytes, macrophages and neutrophils that release reactive oxygen species (ROS) and proteases to break down damaged tissue and foreign bodies (inflammation). Then, growth factors are released to promote attraction and migration of fibroblasts and keratinocyte cells to support granulation tissue formation (proliferation). This granulation tissue is then further remodelled to a definitive extra cellular matrix (ECM) architecture that approaches that of normal tissue (re-epithelialization and wound contraction)[58,60–62]. The proteolytic activity of MMPs and serine proteases is essential for cell migration and detachment, and remodelling and contraction of the ECM during the different phases of wound healing[49,52,58]. In normally healing wounds, protease activity fluctuates during the different phases of healing. This proteolytic activity regulation is achieved by a tight balance between proteases and their endogenous inhibitors that allows equilibrium of matrix deposition and degradation favourable to tissue regeneration.

Chronic wounds fail to progress through the normal phases of healing, remaining usually at the inflammatory phase [63,64]. It is estimated that chronic wounds or non-healing wounds affect

1-1.5% of the population of the industrialised world. The related treatment costs makes up 4% of healthcare budgets in Europe, with a £4.5-5.1 billion annual expenditure in the UK [65–67].

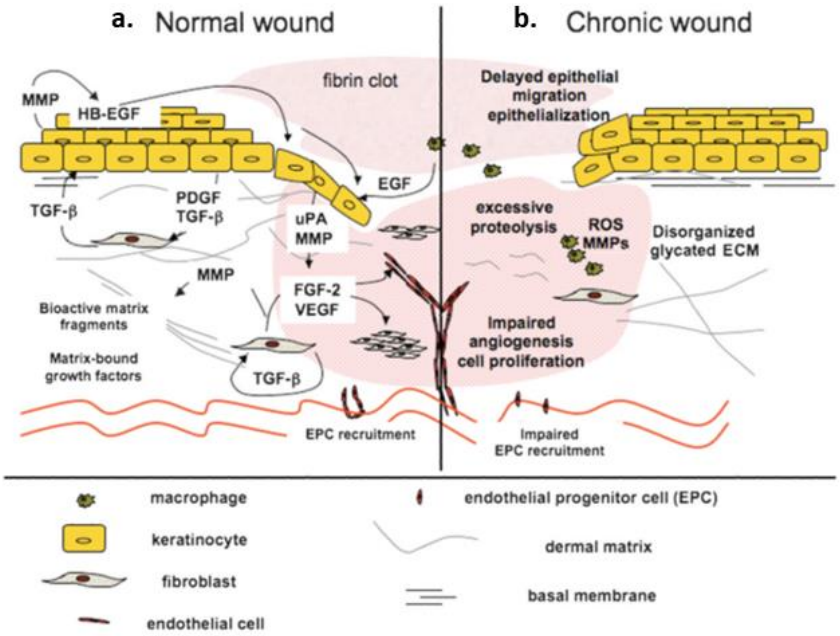

Figure 1.2. Comparison of **a.**) normal healing wound and **b.**) chronic wound bed environment. **a.**) normal healing wounds present organised ECM, growth factors, more matrix synthesis than degradation and modulated proteases activity. **b.**) Chronic wound is characterised by persistent inflammation, proteolysis and degradation of growth factors, and ECM, from Demidova-Rice *et al*[58]

Chronic wounds often present a complex environment and high patient to patient variability. In general, the chronic wound stage is characterised by elevated pro-inflammatory cytokines, oxidative stress and increased activity of proteases, as illustrated in Figure 1.2.b[60,68–71]. It is well known that the protease/inhibitor balance is significantly affected in chronic wounds[54,72–74]. The expression of protease inhibitors is very low, which results in excessive protease activity, causing ECM and connective tissue degradation as well as cytokine and growth factor inactivation[68,75]. All these factors have been associated with impaired healing[60,71,76–78]. The overexpressed proteases are mainly MMPs and serine proteases. MMPs include collagenases and gelatinases that are involved in collagen remodelling and chemokine degradation[49,50,70,72,76], with described activities that can be up to 30 times higher than acute wounds [72].

The main serine protease associated with wound chronification is Human Neutrophil Elastase (HNE), which has been associated with growth factor degradation and MMP activation, contributing to impaired healing[54,68,75,76,79].

1.2.2 Roles of Human Neutrophil Elastase

Human Neutrophil Elastase (HNE, E.C 3.4.21.37) is a serine protease produced mainly by neutrophils and immunocompetent cells under normal conditions[80]. HNE cleaves peptide sequences after small neutral amino acids, such as valine and alanine with a higher specificity for valine (BRENDA:EC 3.4.21.37[81]). Among its physiological functions are pathogen degradation, host pathogen destruction, bactericidal activity, degradation of ECM components and plasma proteins, cleavage of growth factor receptors, and activation of other proteases[82]. Thus, under physiological conditions, elastase has an important role in cell signal regulation, immune response, tissue remodelling and inflammation.

Elastase can be highly tissue destructive when present extracellularly in high concentrations[82]. In addition to chronic wounds, some other chronic inflammation diseases such as the pulmonary diseases Chronic Obstructive Pulmonary Disease (COPD) and Acute Lung Injury (ALI) present excessive levels of extracellular elastase that has been correlated with poor prognosis[80,83]. These pathological conditions display a much higher elastase activity than in healthy tissues[79,83]. COPD is a heterogeneous and slow progressing disease characterised by persistent airflow limitation and chronic inflammation. The exact molecular mechanisms underlying COPD are not fully understood, but it is believed excessive ECM turnover may promote the structural changes that accelerate COPD progression[83]. Elastase is one of the main proteases believed to contribute to COPD progression, due to high degradation of elastin and other components of the ECM in the lung epithelium[84]. This hypothesis is based on an elastase/elastase inhibitor imbalance theory. In physiological conditions the main physiological inhibitors of elastase are alpha-1antitrypsin (AAT), Secretory Leukocyte Proteinase Inhibitor (SLPI) and elafin[82]. In a similar way to

previously explained for chronic wounds, these elastase inhibitors (in particular AAT), tightly regulate HNE activity in the lung. Under chronic inflammation conditions, such as smoke-induced inflammation, the high infiltration of neutrophils leads to a rise in HNE activity. HNE physiological inhibitors are not able to adequately control these levels of elastase which causes the excessive proteolysis and tissue damage[85].

This hypothesis is supported by the alpha-1-antitrypsin deficiency (AATD) disease. AATD is an hereditary disorder characterised by very low levels of circulating AAT. The low levels of active AAT that reach the lung are not enough to inhibit HNE, and as a consequence patients experience the emphysematous changes observed in COPD[86]. The current treatment for AATD patients is augmentation therapy, by intravenous administration of AAT[86].

Additionally, preclinical models show an association between high elastase activity and inflammation and epithelial damage. For instance wound models using Secretory Leukocyte Proteinase Inhibitor (SLPI) deficient mice lead to high elastolytic activity and wound chronification[87]. Intratracheal instillation of elastase is used as preclinical model of pulmonary emphysema[88,89]. These *in vivo* models give an insight on the damaging effects of elastase to healthy epithelium in chronic diseases.

These *in vivo* data, together with COPD and chronic wounds clinical pathology, and the evidence of augmentation therapy for AATD treatment, suggest that the elastase/inhibitors balance is an important factor in maintaining healthy epithelium, whether it is in wound healing or inflammatory lung diseases.

1.2.3 Strategies and challenges for modulation of excessive proteolytic activity

Many chronic wound and pulmonary inflammatory diseases treatments have aimed to reduce elastase activity.

To date the only approved elastase inhibitor for pulmonary diseases is AAT, indicated only for augmentation therapy in AATD patients[86]. Although several synthetic HNE inhibitors have been studied for pulmonary diseases, only Sivelestat® has reached the clinic for COPD and Acute Lung Injury and it is only approved in Japan and South Korea [90,91]. This shows that the systemic administration of elastase inhibitors has so far achieved limited success in modulating HNE activity[92]. This could be due to HNE modulation rather than full inhibition being required, due to the beneficial functions of elastase at low concentrations.

A review of recent literature revealed two predominant approaches to reduce proteolytic activity in the wound environment (Table 1.1):

i) Incorporation of broad spectrum elastase inhibitors in wound dressings. Inhibition or reduction of protease activity has been achieved with polyvinyl pyrrolidone iodine,[93] direct administration of synthetic elastase inhibitors[94,95], oligosaccharides[96] and derivatives of tetracyclines [49] (Table 1.1.i).

ii) Protease activity modulation by "mopping up" strategies (Table 1.1.ii). These are wound dressings that act by binding the enzymes decreasing their activity in the wound bed [97,98]. A dressing composed of collagen and oxidised regenerated cellulose (ORC) has been commercialized to "modulate" excessive protease activity in chronic wounds (Promogram®) The ORC and collagen matrix "modulate" protease activity by sequestering several proteases, drastically decreasing their presence in wound exudate *in vitro*[75,99]. Synthetic sequestering protease dressings have also been developed as chemically modified gauzes[100] and polymer-based super absorber dressings and particles that can additionally help to manage wound exudates[63,101]. Despite the variety of mechanisms described above, Promogram® is the only protease modulating wound dressings that has reached clinical applications within this category of dressings[75]. This product reduces

protease activity by an unspecific and uncontrolled mechanism, affecting many other enzymes and which could lead to unpredictable levels of elastase.

In summary, more targeted and regulated methods of elastase inhibition would be beneficial for chronic wounds and inflammatory lung diseases. Previous reports have either shown a lack of efficacy or are based in unspecific mechanisms, and therefore need to be improved. A system that allows for elastase modulation rather than full inhibition would be advantageous, since it will re-balance the elastase/inhibitor ratio found in healthy tissues. Therefore more specific and targeted therapies may be required.

Table 1.1. Strategies to decrease protease activity in chronic wounds. (i) Incorporation of inhibitors and (ii) decrease in activity by sequestering of enzymes/coenzymes in the dressing matrix.

Entry	Inhibition	Target Enzyme(s)	Product composition	Mechanism of action	Ref
1	(i)	Gelatinases, plasmin, elastase	Polyvinyl pyrrolidone (PVP) – iodine	Inhibition of proteases	93
2	(i)	Elastase	MeOSuc-AAPV-CMK	Inhibition of elastase	95
3	(i)	Elastase	Elastase peptide inhibitors, elastinal	Inhibition of elastase	94
4	(i)	Elastase	MGWCTASVPPQCYG, GWCTASVPPQCYG(GA)7 and elastinal	Inhibition of elastase	102
5	(i)	Proteases	Nano-olligosacharide (NOSF) (UrgoStarts®)	Inhibition of proteases	96
6	(ii)	Elastase	Dialdehyde modified cotton gauze (DAG)	Binding/sequestering elastase	100
7	(ii)	MMP-2,-9, elastase, plasmin	Collagen/Oxidised regenerated cellulose (ORC) (Promogram®)	Binding/sequestering proteases	75,99,103

1.3 Controlled drug delivery

Over recent years there has been increasing interest on designing strategies to modify and control the release of drugs. This can be achieved in different ways, depending on the application and the dosage requirements of a specific drug and disease (Figure 1.3). Most advanced drug delivery strategies are based on engineering of the materials and they can be classified as stimuli-responsive or non-responsive drug delivery. Non-responsive drug delivery

systems control drug release either by restricting drug diffusion through the material, or by offering a slow erosion of the material over time. In the particular case of hydrogels, diffusion and either erosion through hydrolysis have been employed for controlling the release of several proteins[36,104].

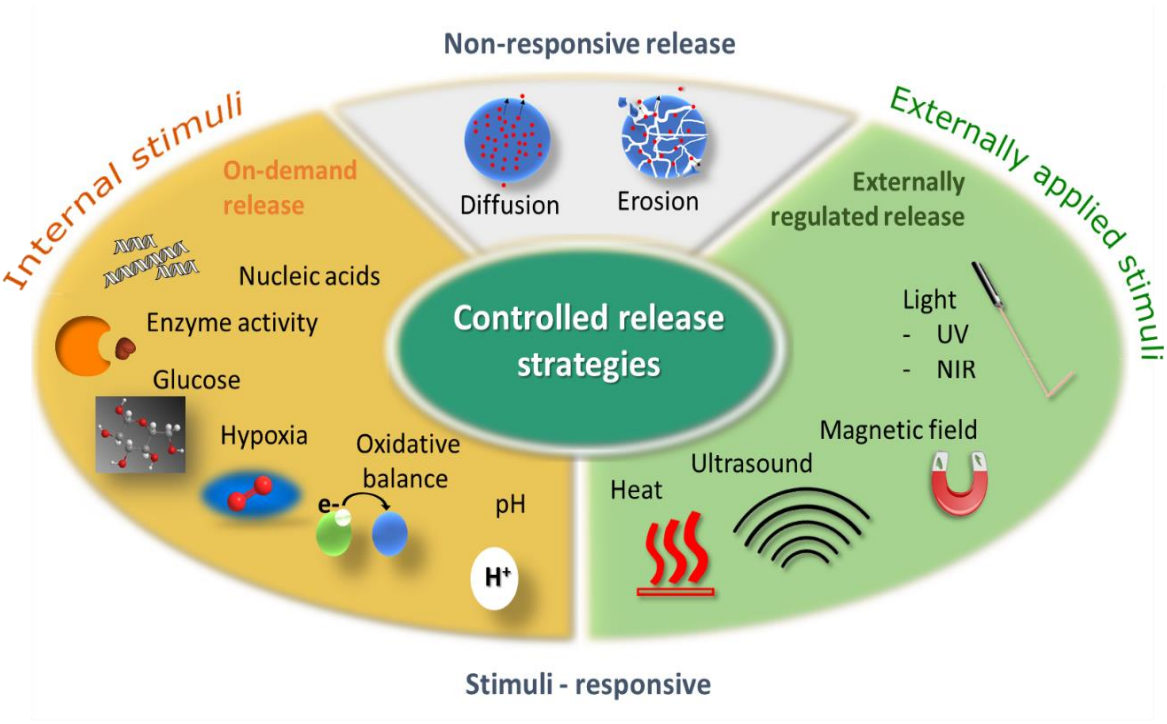

Figure 1.3. Common controlled release strategies, including stimuli-responsive and non-responsive mechanisms.

1.3.1 Stimuli-responsive drug delivery

Stimuli-responsive materials contain functional motifs that are sensitive to particular stimuli incorporated into the delivery system. Upon contact with the target stimuli, the functional motif will cause a change in the delivery system that triggers release. The target stimuli can be either an externally applied stimulus (e.g. light, magnetic fields, ultrasound or heat) or an internal stimuli (e.g. nucleic acids, enzymes, glucose, hypoxia, oxidative stress and pH)[105]. Materials responsive to externally applied stimuli have been widely used for drug delivery, since it allows user-defined spatial and temporal control of the release. For example, temperature controlled

delivery can be achieved by fabricating hydrogels using thermally reversible crosslinking points[106]. Hydrogels able to release their cargo in response to externally applied light, and ultrasounds have also been developed[26,27,107].

The application of an external stimuli may not be always feasible (e.g. accessibility to the drug location), and it may affect the biological environment of the delivery system (e.g. tissue damage). The development of materials able to release their cargo in response to internal stimuli offers an alternative approach to limit drug release specifically to the disease site. Therefore by targeting internal stimuli characteristic of the target disease, the delivery can be optimised and limited to the site of action. pH-responsive hydrogels for drug delivery are probably among the most investigated stimuli-responsive delivery system, due to their application to treat diseases or body organs characterised by altered pH, such as cancer and gastrointestinal tract, respectively[13,108,109]. Several glucose-responsive delivery systems have also been largely investigated. This is because hydrogels that release insulin in response to glucose levels have the potential of achieving an autonomous delivery of insulin[11,110]. Other internal stimuli related to pathological states have also been explored for the development of bioresponsive drug delivery hydrogels such as oxidative stress, hypoxia and genetic material[44,45,111].

1.3.2 Enzyme-responsive materials

A particularly interesting group of 'smart' stimuli-responsive biomaterials are enzyme-responsive materials. Enzymes play critical roles in all biological and metabolic processes in living organisms and many pathological states are characterised by an altered level of different enzymes[60,112]. Moreover, enzymes are very selective towards their substrates which would allow for specific and biologically-inspired release mechanisms[113]. For this reason, materials whose properties can be regulated by enzymes have been of increased popularity for several biomedical applications, such as injectable degradable scaffolds and cellular supports[114], drug delivery[39,115,116] and diagnosis[117,118].

This young class of bio-responsive materials are known as enzyme-responsive materials (ERMs) and they were first defined by Uljin in 2006[119]. Since then the research on that type of functional systems has substantially grown leading to multiple review papers and book chapters on the field[7,120–122]. ERMs are currently defined as 'materials that change their functionality as a result of the action of an enzyme on the material'[121]. There are four requirements that need to be fulfilled to achieve functional ERMs[121]. First, the system must be able to operate in conditions of enzymatic activity. Then, they need to incorporate an enzyme sensitive functionality (i.e. enzyme substrate, Figure 1.4.a) and be able to translate this activity of the enzyme to the sensitive part of the material (Figure 1.4.b). Finally, this translation needs to change some of the materials properties that generate a response in the material (Figure 1.4.c). A fifth consideration is required when considering the use of ERMs for efficient enzyme-responsive drug delivery. The material response to enzyme action has to trigger the release of the encapsulated drug.

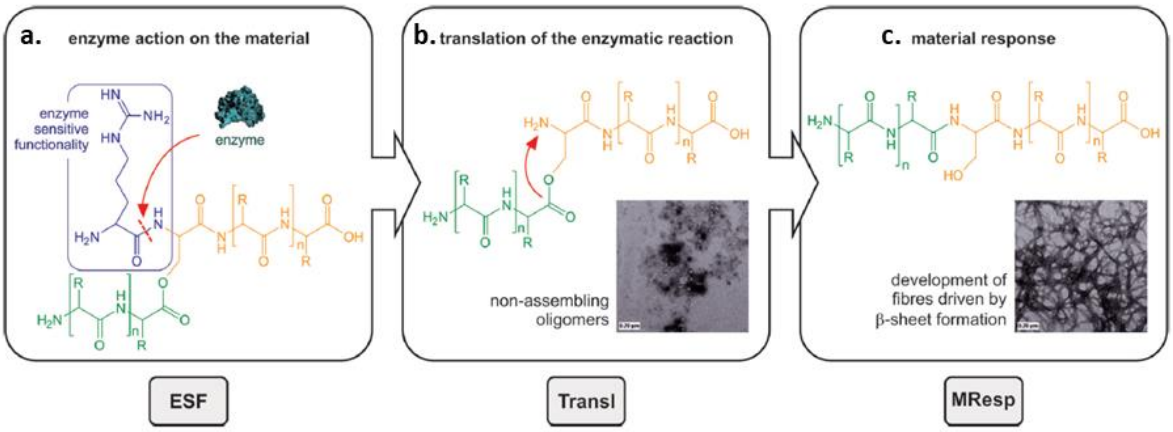

Figure 1.4. Illustration of the requirements of ERMs. Enzyme sensitive functionality (ESF), translation of enzymatic action (Transl) and material response (MResp), using as an example a self assembling switch peptide. Adapted from [121].

1.3.2.1 Mechanisms of enzyme-responsiveness and drug release

As the research in ERMs grows, these functional materials are seen as a great opportunity for improving drug delivery [7].

Considering a broader definition of ERMs and including materials where the release is triggered indirectly by the enzyme, there are several release mechanisms that can be exploited to achieve appropriate enzyme-controlled delivery (Figure 1.5). The most common approach is to include enzyme-sensitive moieties within the hydrogel that would lead to drug release controlled by the material cleavage upon enzyme action (Figure 1.5.a). These moieties can either link the drug to the polymer or be part of the hydrogel network[39,123–126]. Other approaches for release through enzyme-controlled cleavage are more common from nanoparticle systems, and they include cleavage of an outside shell layer, and removal of a cage in a porous system[127,128]. The enzyme-controlled drug delivery can also be indirect, for instance, by exposure of targeting ligands for cell internalisation upon enzyme action on the material[129] (Figure 1.5.b). Finally, the release may be indirectly caused by specific product generated by the enzyme [11,113] (Figure 1.5.c).

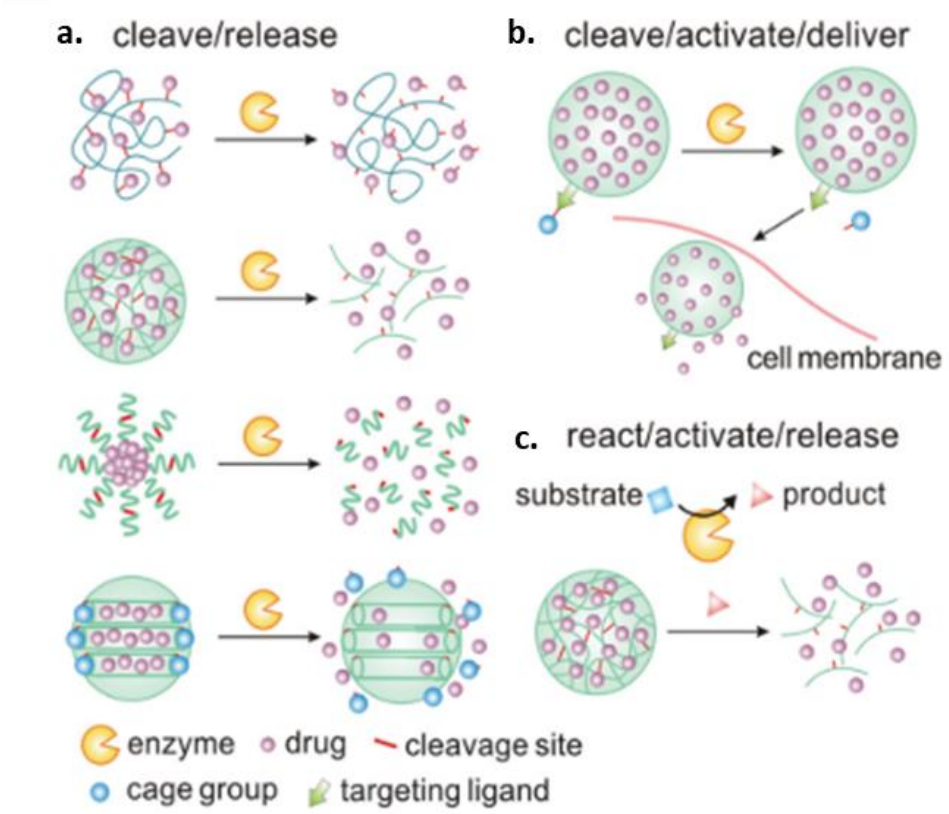

Figure 1.5. Mechanisms of enzymatically-controlled trigger of drug delivery. Release via **a.**) direct cleavage of enzyme-sensitive linkers, matrix, and shell cages (from top to bottom), **b**.) enzyme activation to expose targeting ligands, and **c.**) indirect activation via enzyme-generated products. Adapted from [122].

Several classes of enzymes have been considered as triggers for enzyme-controlled drug delivery taking advantage of their imbalance in certain pathological states[113]. Examples of widely targeted enzymes for enzymatic controlled release are proteases[39,43], phospholipases[130] and oxidoreductases[131]. Among these, proteases have been a widely exploited target for enzyme-controlled drug delivery strategies and many delivery systems responsive to proteases such as elastase[39,132], trypsin[133], chymotrypsin[134], thrombin[43,135], plasmin[136], cathepsins[137] and Matrix Metalloproteinases[41,115,138] have been developed recently. The concentration range of enzyme that lead to responsive drug delivery is highly variable between different studies depending on the target enzyme, desired extent of release, and units of concentration (e.g. molar concentration, weight concentration or activity units). For instance drug delivery from elastase-responsive hydrogels was achieved within 24 h of incubation with elastase at concentrations between 100 nM and 1 µM, while very low release took place in absence of the enzyme[39,132]. Delivery systems for the controlled release of therapeutic proteins, such as Bone Morphogenic Protein 2 (BMP-2)[138], Tissue Inhibitor of Proteases- 3 (TIMP-3)[115], Vascular Endothelial Growth Factor (VEGF)[41,139] and Immunoglobulin G in response to MMP concentration have also been developed[41]. The concentration of enzyme used varied between publications from 1 to 200 U/mL of collagenase (a mixture of MMPs). However all publications demonstrated a higher extent of release in presence of MMP with respect to extent of release in the absence of enzyme[41,138,139]. An increase in the release rate of the encapsulated protein at higher concentrations of MMPs[115,138], demonstrating a clear protease-controlled mechanism of release has also been developed. Similar to MMPs and elastase examples, drug delivery systems responsive to thrombin have also been developed. Again, the total release increased with the concentration of thrombin in the medium (2 – 45 nM) and depended on the selected enzyme sensitive functionality incorporated into the materials[43,140]. Although it is difficult to compare between studies due to the use of different normalisation and quantification of enzyme levels, the previous reports demonstrated that the release from ERMs takes place at a higher extent in presence of higher concentrations of target enzyme[41,43,115,132,138,139].

A clear correlation between the enzyme concentration range in pathological states and the protease concentrations required for achieving responsive delivery from ERMs remains unclear, and it is another challenge in this field. It has been broadly stablished in preclinical and clinical studies that diseases such as chronic wounds, pulmonary diseases and cancer have higher activity of certain proteases such as MMPs and elastase with respect to healthy individuals. However, the lack of unified methods for the enzyme quantification makes comparison between isolated studies

and the acquisition of an absolute numbers of enzyme concentration difficult. For instance, elastase and MMPs levels have been described to be overexpressed in chronic inflammatory diseases, such as chronic wounds and pulmonary diseases, but different techniques have been used for quantification. Some studies are based on the quantification of proteases levels by Enzyme-Linked Immunosorbent Assay (ELISA), and Mass Spectrometry based quantifications[68,141,142]. Although these techniques are highly specific for the targeted protease and allow for accurate quantifications, they are not always able to differentiate between active protease (related to disease progression and state), and inactivated protease (not necessarily related to disease state). Other studies are based on measuring proteolytic activity of the active protease. This is achieved either by quantification of enzymatic hydrolysis rate of a model substrate (units of enzyme activity) or by quantification of the protease degradation products in patient samples[71,79,83]. Although this technique has the advantage of measuring the active enzyme, which is the marker of disease activity, the lack of standardisation between studies (e.g. the definition of units of activity, substrate choice, sample/substrate ratio and normalisation) difficults comparison between different studies. Although the existence of a variety of techniques and lack of standardisation for protease quantification makes difficult to predict the protease levels the ERMs for drug delivery will need to be responsive to, it can be concluded that the activity of these proteases is overexpressed by a several folds in chronic/disease state respect to healthy/acute states[54,68,72,79]. Nevertheless, recent experiments have shown that enzyme-responsive drug delivery can be effectively achieved *in vivo* with improved therapeutic outcomes. For instance, MMP-responsive delivery of TIMP-3 achieved improved cardiac function of a porcine model of myocardial infarction and limited TIMP-3 action to the infarction region for a two week time frame[115]. In two separate studies Foster *et al.* and Phelps *et al.*, have shown MMP-responsive delivery of VEGF improved *in vivo* vascularisation and showed extended delivery respect untargeted therapy (IV administration of VEGF)[41,139]. These studies confirm that the levels of

enzyme-responsiveness of recently developed ERMs is adequate to achieve enzyme controlled release *in vivo*, which is an important first step for clinical translation of this delivery.

Enzyme-responsive drug delivery systems include many types of different materials, such as hydrogels, microparticles, nanoparticles and micelles[39–41,127,129,143,144]. A lot of research on ERMs for drug delivery have focused on developing enzyme-responsive hydrogels. This is due to hydrogels porosity, hydrophilic nature, versatility and high water content offering mild conditions for both, drug encapsulation and enzyme interactions, so these will be explained in more detail in section 1.4.

1.4 Enzyme-responsive hydrogels for drug delivery

ERMs can be found in both categories of hydrogels, most commonly developed enzyme-responsive hydrogels are supramolecular (physical hydrogels) and polymeric (chemical hydrogels). Proteases are the most targeted enzymes, due to their implications in many pathologies. However hydrogels targeting other pathologically relevant enzymes for controlled release, such as glycosidases[145,146], hyaluronidase[19] or phospholipases[147] have also been developed.

- *Supramolecular hydrogels*: Since the formation of supramolecular hydrogels is driven by non-covalent self-assembly, the incorporation enzyme-responsiveness into these gels can be quite complex, requiring a high level of rational design. For this, a self-assembly molecule needs to be covalently crosslinked to the enzyme-sensitive moiety. The resulting conjugate has to fulfil several requirements in order to guarantee hydrogel formation and subsequent enzymatically-controlled degradation: i) maintain suitable assembly properties to form gel fibres, while ii) guaranteeing that the enzyme-sensitive moiety is exposed to the outside of the assembled structure, and iii) the conformational change caused upon enzyme activity causes enough structural changes which lead to hydrogel dis-assembly[148]. This approach has been used to obtain supramolecular protease-responsive hydrogels, by combining a protease-

cleavable peptide with self-assembling sequences within the same peptide molecules[148–150]. Similarly, the covalent linkage between a small amphiphilic molecule and disaccharides has been described for the design of glycosidase-responsive supramolecular gels[146].

- *Polymeric hydrogels:* Enzyme-responsive moieties are usually introduced in these hydrogels by chemically crosslinking polymers with enzyme-sensitive molecules. These crosslinkers are usually formed of two functional parts: one responsible for the enzyme-responsiveness, which will determine the specificity and kinetics of enzyme degradation, and the crosslinking points, responsible for the linking to the polymer[140,151,152].

1.4.1 Preparation of protease-responsive hydrogels

In most cases, for incorporation of protease-responsiveness into polymeric hydrogels, an enzyme-sensitive peptide sequence is modified at both termini with functionalities that are reactive towards the polymer (crosslinking points). Peptide sequences for protease-responsive materials are usually synthesised via solid phase peptide synthesis (SPPS). SPPS is based on the step-wise coupling of individual amino acids to a solid support, constructing the desired peptide sequence with a high degree of control. This versatile method can be used to synthesise up to medium chain polypeptides (usually around 30 amino acids). Normally sequences of 6-10 amino acid length are enough to achieve appropriate enzyme responsiveness, and therefore SPPS is the peptide synthesis technique of choice[117,123,153].

The most commonly used chemical crosslinking methods to introduce protease-sensitive peptides in polymeric hydrogels are based on highly efficient and facile reactions which take place in aqueous environment. Common crosslinking chemistries to fabricate protease-responsive materials are summarised in Figure 1.6.

- *Azide-alkyne cycloaddition* (AAC, Figure 1.6.a): This crosslinking requires modification of both the peptide and the polymer to introduce azide or alkyne functionalities to form a

triazole link. AAC is the most prominent 'click chemistry', it has a high reaction rate and can be performed under very mild reaction conditions. Copper(I)-catalysed AAC between both bis-azido peptides and multivalent alkyne polymers[154,155], or alkyne-terminated peptides and multi azido-polymers has been described[156]. Copper free variants of AAC have also been developed, due to the toxicity of copper. DeForest *et al.* fabricated enzyme-responsive hydrogels via Strain-Promoted AAC between multi-azido polymers and bis-cyclooctyne peptides which allowed encapsulation of living cells [157].

- *Hydrazone crosslinking* (Figure 1.6.b). Aldehyde functionalised polymers can be crosslinked with complementary hydrazide fucntionalised peptides into a hydrazone bond to form hydrogels under physiological conditions which do not affect encapsulated protein bioactivity[115,158].
- *Radical polymerisation* (Figure 1.6.c). Peptides sequences can be end-functionalised with polymerisable groups such as acrylates or methacrylates. These can then be incorporated into multi-acrylate polymers via radical polymerisation to form the hydrogel network[159]
- *Thiol-based crosslinking chemistries* (Figure 1.6.d and e). Two crosslinking mechanisms are grouped within this category, Thiol Michael addition (Figure 1.6.d) and thiol-ene photopolymerisation (Figure 1.6.e), both involving the addition of a thiol over an alkene to form a thioether bond. Thiol-based crosslinking chemistries have been widely used for developing hydrogels for enzyme-responsive delivery for biomedical applications[160–166]. This is due to the fact that they can be carried out in mild aqueous conditions, they do not require complex peptide modifications, and they can lead to fast formation of hydrogels [160–162,167]. The main advantage is that the thiol functionalities can be obtained by addition of cysteine residues at both ends of the peptide linker during peptide synthesis, avoiding any chemical functionalisation. Both reactions mechanisms will be explained in detail.

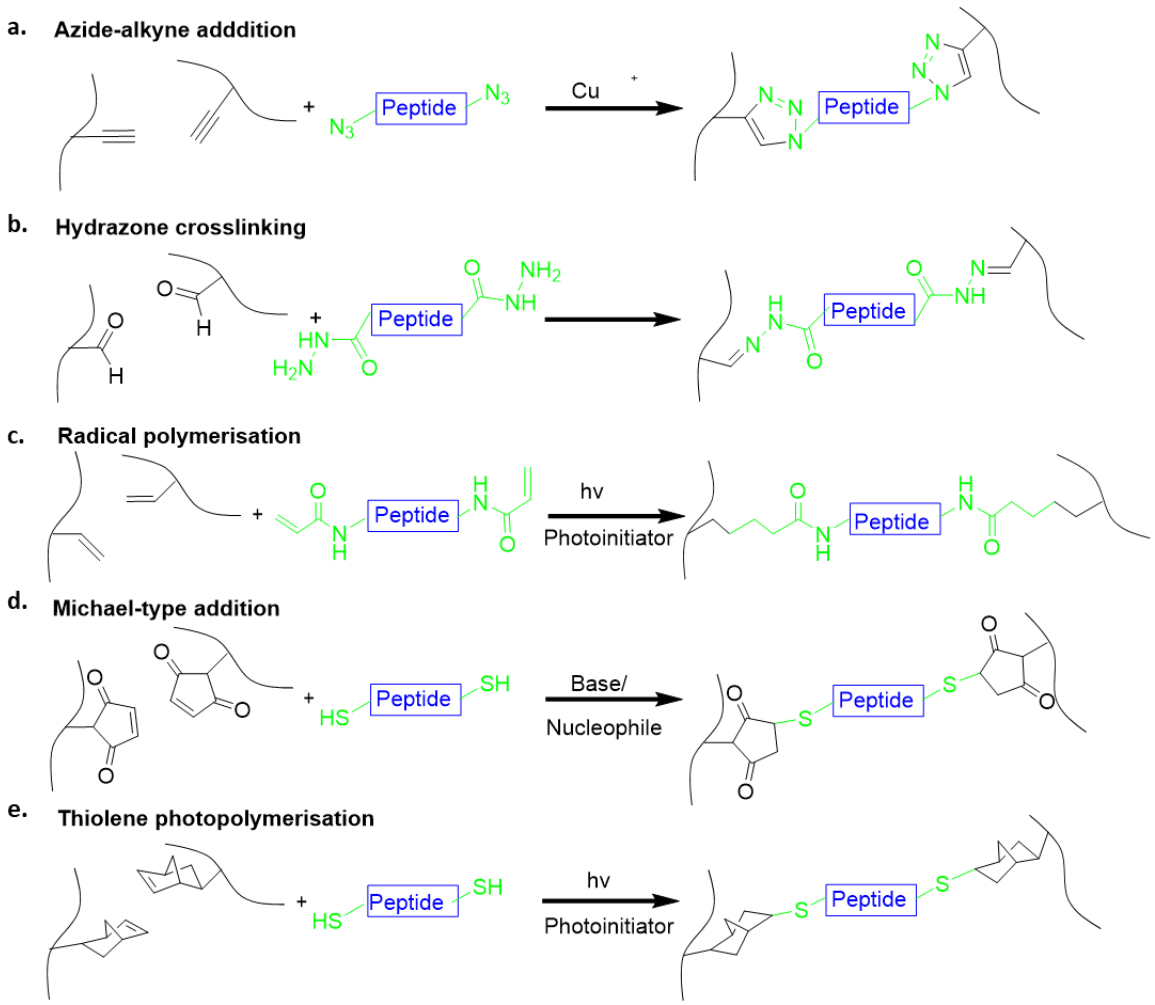

Figure 1.6. Simplified schematic of methods to introduce protease-sensitive peptide crosslinkers into polymeric hydrogel networks**.**

1.4.1.1 Michael-type addition and thiol-ene photopolymerisation for the preparation of protease-responsive hydrogels

Michael-type addition and thiol-ene photopolymerisation are widely used to incorporate peptides cleaved by the target enzyme into the hydrogel network, by crosslinking multisubstituted vinyl polymers with dithiol peptides[43,164]. Their mild reaction conditions have made them particularly useful for encapsulation of biologics, such as proteins[22,35,39,43,138,139], peptides[152] and cells[114,168].

- *Thiol-ene photopolymerisation*. Thiol-ene photopolymerisation proceeds under aqueous conditions and is based on the use of photo-generated radicals to initiate the addition of a thiol to an electron-rich alkene[169,170]. Commonly used photoinitiators are Irgacure 2959 (2-hydroxy-1-[4-(hydroxyethoxy)phenyl]-2-methyl-1-propanone) and Lithium phenyl-2,4,6-trimethylbenzoylphosphinate, and commonly used alkenes include electron rich norbornene, or vinylethers[161,171]. The reaction requires the photo-generated radical initiator to attack the thiol yielding a thiyl radical (Figure 1.7.a). The thiyl radical then attacks the alkene forming the thioether addition product and generating a new thiyl radical[170,172]. Since the reaction only proceeds once and where UV light is applied, this allows for control over the spatial and temporal hydrogel formation [39173]. This has led to a wide use of thiol-ene photopolymerisation to prepare protease-responsive hydrogels for sensing and drug delivery[38,39,160].
- *Michael-type addition.* Michael-type addition consists of the 1,4 addition of a thiol over an electron deficient vinyl group such as maleimides, vinyl-sulfones, acrylates and methacrylates to form a thioether bond (Figure 1.7.b,**c**) [174]. Since this reaction can be efficiently performed in aqeuous buffers and at physiological pH, hydrogels formed by crosslinking of multifunctional vinyl polymers with cysteine-terminated peptides through MTA are considered suitable for biomaterial design and have been used even for *in situ* cell encapsulation and injectable hydrogel scaffolds [114,164] Michael type addition reactions can be classified based on the catalyst used, since they can be initiated either by a catalytic amount of a base or nucleophile, such as triethanolamine and Tris(2-carboxyethyl)phosphine hydrochloride, respectively[175].
    - The *Base catalysed Michael-type addition* requires the use of catalytic amounts of a base to initiate the reaction by extracting a proton from the thiol to generate a thiolate anion [S-] (Figure 1.7.b). This anion is a strong nucleophile which can attack the electron deficient beta carbon of the ene. This yields a strong carbon centered

anion which can then subtract a proton form the conjugated acid of the catalysts, generating the thioether product and regenerating the base catalyst[176].

- The *Nucleophile-catalysed Michael-type addition* usually involves the use of phosphines such a tris(2-carboxyethyl phosphine chloride (TCEP) and it has been described to yield faster reaction rates at trace amounts[174,175]. In this reaction, the phosphine reacts with the electron deficient ene to generate a strong base which then deprotonates the thiol leading to formation of the thiolate anion (Figure 1.7.c). The thiolate anion will then attack another vinyl group forming the thioether product[174,176].

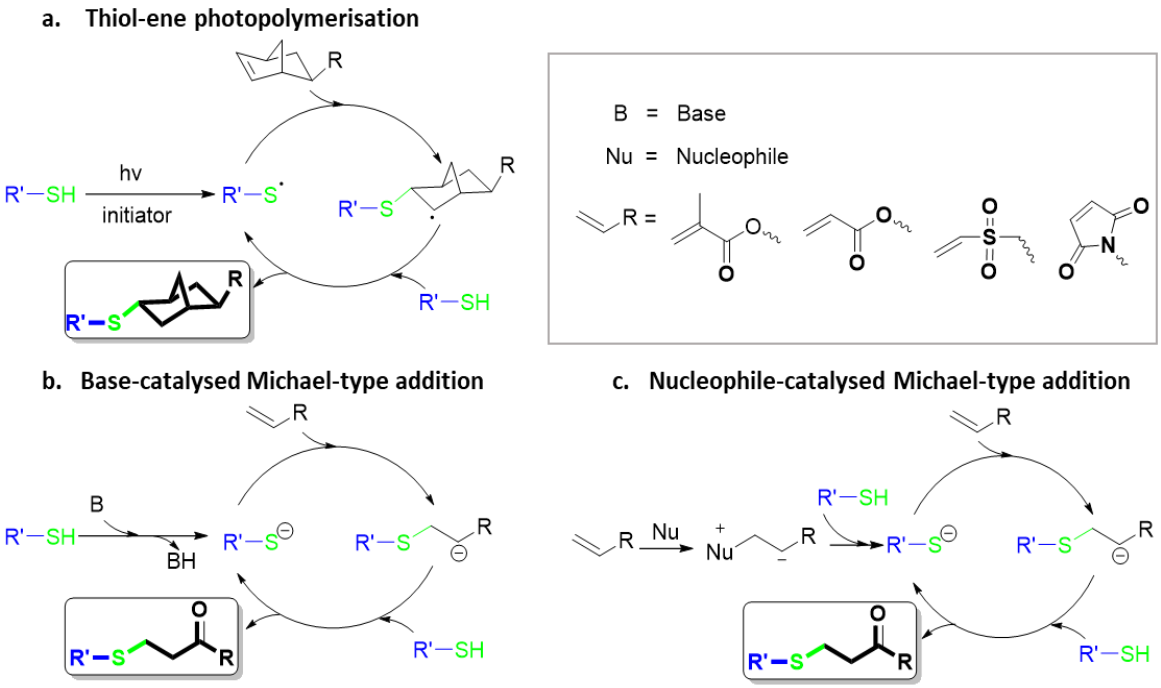

Figure 1.7. Mechanism of thiol-based crosslinking chemistries. **a.**) Thiol-ene photopolymerisation between norbornene and thiols. **b.**) Base-catalysed and **c.**) nucleophile catalysed Michael-type addition with electron deficient alkenes.

The first hydrogels prepared via Michael-type addition were formed between cysteine containing peptides and acrylates[143,177]. Then vinyl sulfone functionalised polymers were introduced since they showed improved reaction kinetics and mechanical properties[166,176,178] . Maleimide is the most reactive of the Michael type acceptors, showing superior reaction kinetics and reactivity than vinyl sulfones and acrylates. Recently, hydrogels prepared via Michael addition

with maleimide-functionalised polymer were shown to require a lower concentration of catalyst for obtaining hydrogels with improved mechanical properties and cytocompatibility[164]. Due to their higher reaction efficiency, maleimide crosslinked hydrogels can even be obtained without using any base or nucleophilic catalysts[41,173,179], which could otherwise affect cell viability and the stability of encapsulated proteins[168,180,181]

Since both reactions can be efficiently performed in aqueous buffers and physiological pH, hydrogels formed by crosslinking of multifunctional polymers with cysteine containing peptides have been largely prepared by both, thiol Michael type addition[41,114,115,123,138], and thiolene photopolymerisation[22,152,161,16815]. The lack of use of initiators is a key advantage of maleimide Michael type-addition over thiol-ene photopolymerisation reactions. Initiators often used for photopolymerisation generate radical species that can have toxic effects on cells and damage proteins, reducing their bioactivity during hydrogel formation step[180,181]. The inhibitor encapsulated in this project and used for achieving elastase inhibition is a protein, therefore the use of such initiators could affect the inhibitor bioactivity, which is a key aspect of the project. Additionally, the use of maleimide-PEG as reaction for the PEGylation of proteins is well established and characterised[25], with a solid precedent *in vivo* and clinical trials studies[25,182,183]. For these two reasons Michael-type addition with maleimide functionalised polymers was the crosslinking reaction of choice to start with in this work for the preparation of functionalised hydrogels.

1.4.2 Drug delivery applications of protease-responsive hydrogels

Protease overexpression has been associated with pathological diseases such as cancer, chronic wounds, cardiovascular diseases and inflammatory pulmonary diseases[60,112,184]. They are therefore major targets as internal stimuli for selective and controlled release. In an early report from West *et al*., they developed a protease-responsive hydrogel that could be selectively degraded by either collagenase or plasmin[185]. Since then there have been many reports of

enzyme-responsive hydrogels targeting proteases for controlled release, such as plasmin[186], matrix metalloproteinases[125,149,187,188], trypsin[133,136], chymotrypsin[40], thermolysin[40], thrombin[189] and elastase[39].

The use of protease-responsive hydrogels can restrict drug release spatially and temporally to the desired site of action by appropriate selection of the target protease and material design [115,116]. Once at the targeted site, drug release is triggered via enzyme-controlled peptide degradation, decreasing the amount of off-target effects and achieving therapeutic efficacy as shown by Purcell *et al* in their *in vivo* model [115].

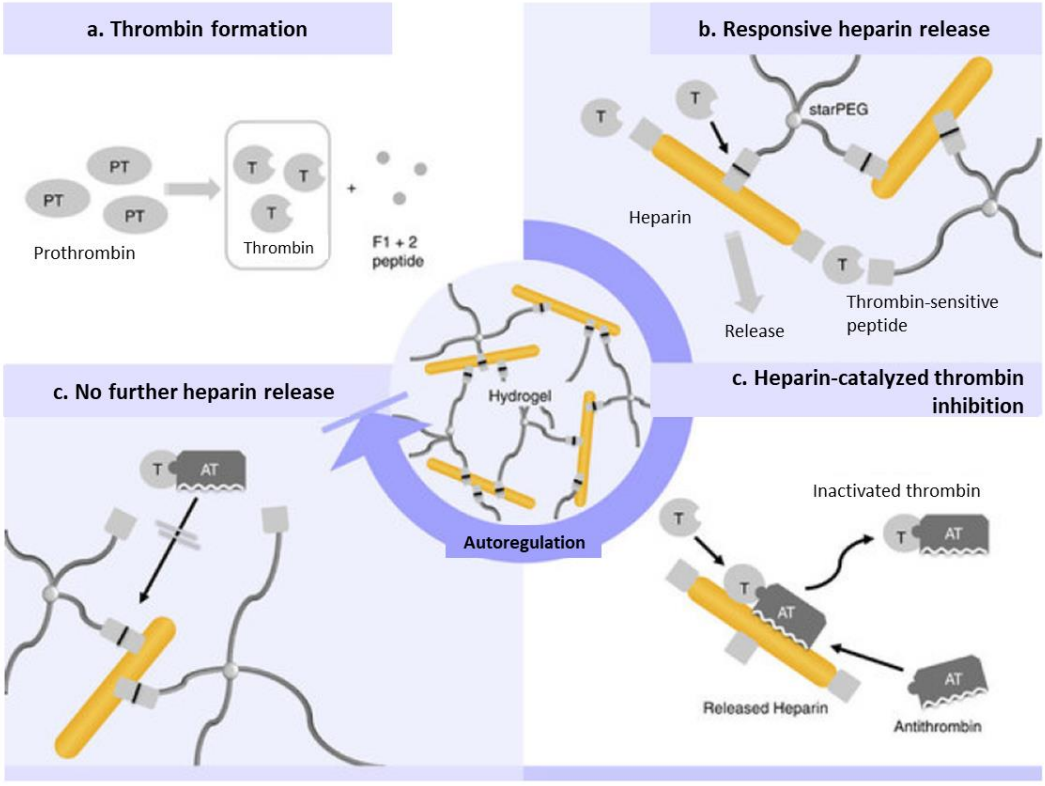

Figure 1.8. Mechanism of protease activity autoregulation, using as example heparin release from thrombin-sensitive hydrogels, adapted from[43]. **a.**) Protease activation (thrombin), **b.**) selective cleavage of the crosslinking peptide (by thrombin) triggering the protease inhibitor release (heparin), **c.**) Released inhibitor (heparin) catalyses the inactivation of the protease (thrombin) and **d.**) the inhibition of the protease terminates gel degradation terminates and further inhibitor release (heparin).

Protease-responsive hydrogels not only offer the possibility of obtaining protease-controlled release but also of achieving self-regulated enzyme activity modulation. By incorporation of inhibitors of the target protease within the protease-responsive hydrogels, the inhibitor can be

release on-demand depending on the activity levels of the target protease. This approach has been recently explored by Maitz *et al.* and Purcell *et al.* for the local on-demand inhibition of thrombin and MMPs, respectively. Maitz *et al.* developed a system for autonomous regulation of coagulation. In the presence of thrombin (Figure 1.8.a) the hydrogel will be degraded and the inhibitor (heparin) released (Figure 1.8.b). This will lead to the protease inhibition (thrombin via the heparin-antithrombin complex) (Figure 1.8.c), subsequently stopping hydrogel degradation and any further inhibitor release (Figure 1.8.d). A similar feedback-controlled release mechanism could be developed for the inhibition of other physiologically relevant proteases, such as elastase.

1.5 Aims and objectives

1.5.1 Challenges in the field

The overexpression of elastase in chronic inflammatory diseases with respect to healthy tissue has been widely described[79,80,83]. Although clinically important, introduction of elastase inhibitors to tackle elastase overexpression has been of limited clinical effectiveness to date[92]. Thus far, responsive delivery strategies to tackle enzyme overexpression are scarce. Only some isolated studies have developed controlled delivery systems for the modulation of enzyme activity based on enzyme-responsive delivery of inhibitors. Although release kinetics and *in vivo* efficacy and compatibility of the materials was demonstrated, their ability for sustained release of inhibitor, detailed inhibition kinetics and effects of inhibitor/protease ratio in a biological environment has not been systematically studied[43,115]. Furthermore, to date, a bio-responsive delivery strategy has not been developed to address elastase overexpression. A responsive hydrogel able to release an elastase inhibitor in response to the levels of elastase will be advantageous, since it will provide an on-demand inhibition of the enzyme. Since the inhibitor release is dependent on elastase concentration, the system could contribute to restoration of the elastase/inhibitor balance of healthy tissue and spatially and temporarily limit the release of the

inhibitor to the site where elastase is highly expressed, increasing potency and reducing side effects. Some challenges still need to be addressed for the development of these complex enzyme-responsive materials:

i. Establishing a relationship between hydrogel composition, physicochemical properties and physical entrapment of macromolecules.
ii. Development of an array of elastase-responsive peptide crosslinkers with high water solubility tailored to Human Neutrophil Elastase.
iii. Study of specificity and selectivity of the enzyme-controlled release, for instance, investigations of the release in presence of a non-targeted enzyme.
iv. Establishment of required amount of inhibitor and ability to regulate different levels of enzyme activity.
v. Elucidation of the effect of hydrogels on cells, their ability to modulate enzyme activity in presence of cells and establishment of whether enzyme modulation leads to any improvement in cell function with a suitable model.

1.5.2 Aim and objectives of the project

This work aims to develop a hydrogel-based delivery system able to modulate elastase activity by releasing an elastase inhibitor on-demand, responsive to different activity levels of enzyme in the environment (Figure 1.9). With this purpose elastase-sensitive peptides will be used to crosslink multi arm PEG polymers and encapsulate alpha-1-antitrypsin. Before we can proceed to the testing of the materials responsiveness and modulatory capabilities, physicochemical properties and physical encapsulation properties of the hydrogels obtained with two different thiol-reactive polymers (4-arm-PEG-norbornene and 4-arm-PEG-maleimide) will require investigation.

This work can be split into five different objectives, as summarised below:

i) Characterisation of hydrogel gelation kinetics, mechanical properties, mesh size and passive entrapment of model macromolecules with a model crosslinker dithiol (Chapter 3).

ii) Development of a water soluble elastase-cleavable peptide crosslinker, incorporation into hydrogels and initial assessment of elastase-responsiveness (Chapter 4).

iii) Fabrication of peptide-crosslinked hydrogels for improved macromolecule entrapment, assessment of their specificity and cross-reactivity of release in presence of other proteases (Chapter 5).

iv) Encapsulation of alpha-1-antitrypsin and characterisation of hydrogel degradation and modulation of different levels of elastase activity in solution (Chapter 6).

v) Determination of the biocompatibility of hydrogels and testing of their ability to modulate elastase activity in presence of cells and improve elastase-hindered cell repair

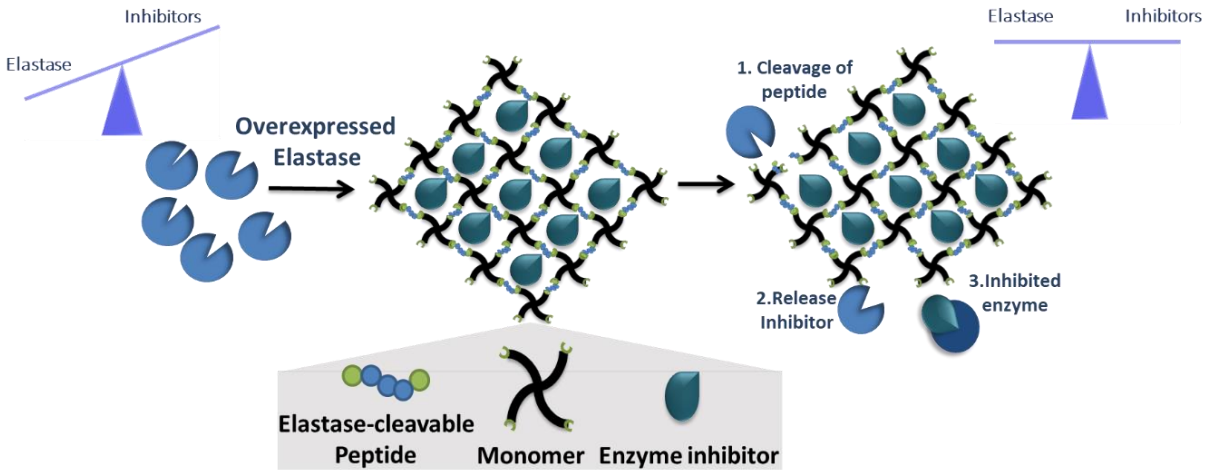

Figure 1.9. Preparation of elastase-responsive hydrogels and proposed on-demand modulation of enzyme activity.

Chapter 2.

Materials and Methods

2.1 Materials

Unless otherwise stated, all general chemicals were purchased from Sigma-Aldrich Ltd (Dorset, UK), amino acids from Bachem AG (Bubendorf, Switzerland) and solvents from Fischer Scientific UK Ltd (Loughborough, UK). All water used was obtained from an ELGA purification system. Peptide synthesis grade N,N-dimethylformamide (DMF) was purchased from Rathburn Chemicals Ltd (Walkerburn, UK); 5 kDa and 10 kDa 4-arm PEG-maleimide (4-PEGMal) from Advanced Biochemicals LCC (Lawrenceville, GA , USA); 5 kDa and 10 kDa 4-arm-hydroxyl-PEG (4-PEG-OH) from Creative PEGWorks (Chapel Hill, NC, USA), D-L-dithiothreitol (DTT) from Alfa-Aesar (Heysham, UK); fluorescamine from Across Organics (Geel, Belgum); and Amicon Ultra centrifugal filters (3.5 kDa molecular weight cut-off (MWCO)), NHS-fluorescein and Texas-Red Dextran 70 kDa (TRD70) from Fisher Scientific UK Ltd (Loughborough, UK). Human Neutrophil Elastase and Rink amide Novagel^{TM} resin for peptide synthesis were purchased from Merck (Darmstadt, Germany). The dialysis membrane (0.5 - 1 kDa MWCO) was purchased from Spectrum Chemical Mfg. Corp (New Brunswick, NJ, USA) and SolventPlus Kinesis Omnifit (Diba) solvent reaction column for peptide synthesis (10 mm dimeter × 100 mm length) from Kinesis Ltd (Cheshire, UK). Matrix Metalloproteinase 2 and Mca-Pro-Leu-Gly-Leu-Dpa(Dnp)-Ala-Arg-NH_2 was acquired from R&D systems (Minneapolis, MN, USA).

2.2 Analytical techniques

Fourier Transform Infrared Spectroscopy

Fourier Transform Infrared Spectroscopy (FTIR) spectra were acquired on an Agilent technologies Cary 630 FTIR instrument equipped with an attenuated transmission reflection (ATR)

module. Spectra were recorded in the 4000 – 650 cm^{-1} range with 128 scans collected for each sample.

Nuclear Magnetic Resonance

Nuclear Magnetic Resonance (NMR) spectra were acquired in a Bruker 400 MHz NMR spectrometer at 298 K. Unless otherwise stated spectra were acquired in 5 mm diameter NMR tubes (Wilmad®, Sigma Aldrich) using the solvents indicated in each case. All chemical shifts are reported in ppm relative to the solvent peak (D_2O 4.79, $CDCl_3$ 7.26, $(CD_3)_2SO$ 2.50 ppm). Spectra analysis was conducted with Mestrenova 9.0.1 © 2014 MestreLab research S.L. Abbreviations for multiplet description: s = singlet, d = doublet, t = triplet and m = multiplet.

Mass Spectrometry

Soluble and low molecular weight samples (<2000 Da) were analysed by Electrospray Ionisation Mass Spectrometry (ESI-MS). Low solubility peptides and synthesised polymers were analysed by Matrix-Assisted Laser Desorption and Ionisation Time-of-Flight mass spectrometry (MALDI-ToF-MS).

Electrospray Ionisation Mass Spectrometry (ESI-MS): ESI-MS measurements were conducted in a Bruker ApexIV FT-ICR spectrometer in Electrospray Ionisation (ESI) positive or negative ionisation mode, as specified.

Matrix-Assisted Laser Desorption Ionisation Time-of-Flight Mass Spectrometry (MALDI-ToF-MS). MALDI-ToF-MS measurements were conducted in a Bruker Daltonics Ulatraflex II MALDI-ToF-MS in the positive ion mode. Polymers were analysed using a DCTB (trans-2-[3-(4-tert-Butylphenyl)-2-methyl-2-propenylidene]malononitrile) as a matrix and sodium trifluoroacetate as a cationising agent. 10 µL (10 mg/mL) of polymer sample were mixed with 10 µL of sodium trifluoroacetate (10 mg/mL, acetonitrile) and 20 µLµL of matrix solution (saturated, acetonitrile). 2 x 1 µL of the mixture were spotted onto a MALDI plate and left to fully dry before analysis. Low solubility peptides were also characterised by MALDI-ToF-MS

using the alpha-cyano-4-hydroxycinnamic acid (CHCA) matrix. 20 µL (0.5 mg/mL, 19:1 water:TFA) of peptide solution were mixed with 20 µL sodium trifluoroacetate (10 mg/mL, acetonitrile) and 20 µL of CHCA matrix (saturated, acetonitrile). 6 × 5 µL of the mixture were spotted onto a MALDI plate and left to fully dry before analysis. Spectra were acquired with the PepMix RP (positive) method.

Reverse Phase High Pressure Liquid Chromatography-Mass Spectrometry

Reverse Phase High Pressure Liquid Chromatography-Mass Spectrometry (RP-HPLC-MS) spectra were acquired in a Shimadzu UFLCXR system coupled to an Applied Biosystems API2000 with a C18 Phenomenex Gemini-NX 50 × 2mm 3µm-110A column. Sample gradient started with 1 min equilibration at 5% Solvent B (0.1% Formic acid in acetonitrile) and 95% Solvent A (0.1% formic acid in water) for 0.5 min, 10 to 98% B for 2min, 98% B for 3min and 98 to 5% B in 0.5, and 5% B for one min. Flow rate was 0.5 mL/min with UV detection at 220 nm.

2.3 Peptide synthesis, purification and characterisation

2.3.1 Peptide synthesis

Peptides were synthesised using Fmoc (Fluorenylmethyloxycarbonyl) solid phase chemistry on a rink amide Novagel resin (Merck) in a reaction column (Kinesis Ltd). The peptide sequence was assembled by sequential coupling of the corresponding Nα-Fmoc-protected amino acids to 0.1 or 0.2 mmol of the resin previously swollen overnight. Side functionalities in cysteine, arginine and serine were Trt (trityl), Pbf (2,2,4,6,7-Pentamethyldihydrobenzofuran-5-sulfonyl) and tBu (tert-butyl**)** protected respectively. Nα-Fmoc-protected amino acid (4 eq) activated with carboxyl-activating reagent (2-(7-aza-1H-benzotriazole-1-yl)-1,1,3,3-tetramethyluronium hexa-fluorophosphate (HATU, 3.9 eq) and N,N-diisopropylehtylamine (DIPEA, 8 eq) were dissolved in peptide grade dimethylformamide (DMF) and left to react for 4 h at room temperature (20 °C) in the reaction column. After each amino acid coupling, the resin was washed under continuous flow

(3 mL/min) first with DMF, then with 20% v/v piperidine in DMF and finally with DMF using a NOVA SYN® GEM manual peptide synthesiser. Each DMF and piperidine washing step was conducted over several minutes until Fmoc group and excess amino acids were fully removed from the column, as determined by post-column absorbance monitoring at 355 nm.

N-acetylation of the sequences was achieved by reacting the N-terminal cysteine of the sequence with 10 eq of acetic anhydride (Ac_2O) and 1.5 eq of DIPEA for 30 min. The resin was rinsed with DMF, dichloromethane (DCM) and hexane before cleavage (10 mL each). The peptide sequence was then simultaneously cleaved from the solid support and deprotected using trifluoroacetic acid (TFA)/triisopropylsilane (TIPS)/water (95/2.5/2.5 % v/v) for 4h. The resin was separated by gravity filtration and the filtrate was dried under vacuum and triturated with cold diethyl ether (5 × 1 mL).

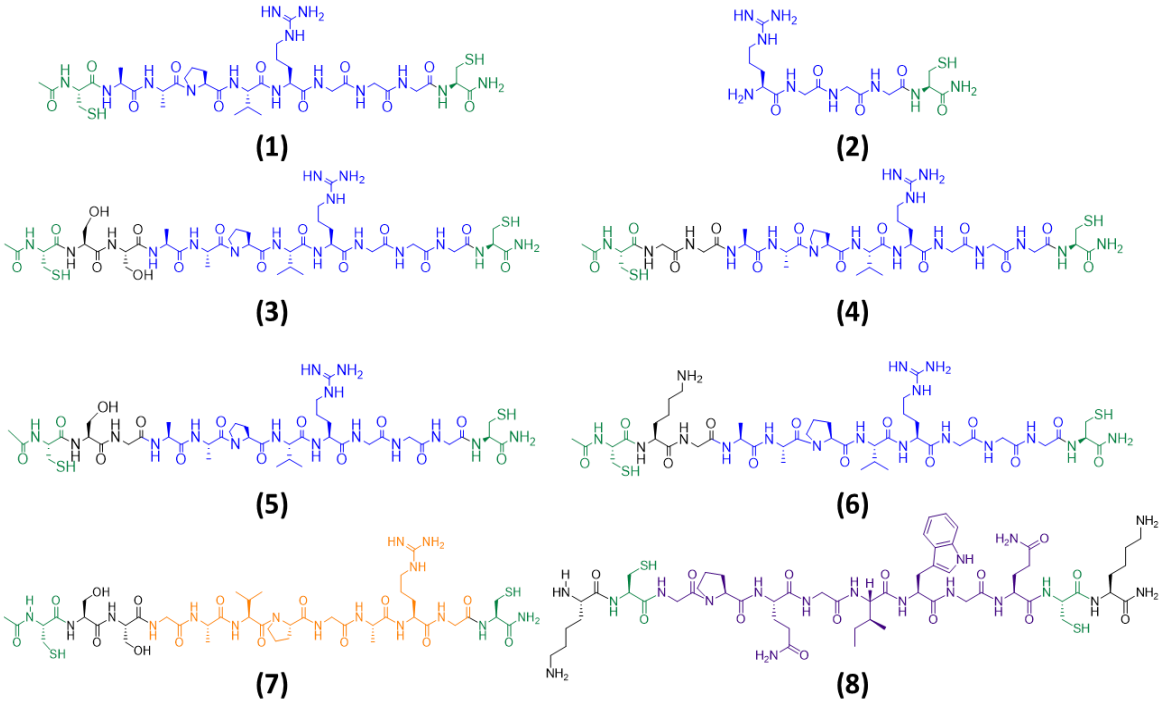

Figure 2.1. Structures of peptides. (**1**) Initial elastase-cleavable sequence Ac-CAAPVRGGGC-NH_2, (**2**) Peptide for elastase cleavage control H-RGGGC-NH_2. (**3-6**) Elastase-cleavable analogue for improved solubility: (**3**) Ac-CSSAAPVRGGGC-NH_2, (**4**) Ac-CGGAAPVRGGGC-NH_2, (**5**) Ac-CSGAAPVRGGGC-NH_2, (**6**) Ac-CKGAAPVRGGGC-NH_2.(**7**) Non-responsive elastase sequence Ac-CSSGAVPGARGC-NH_2 obtained from scrambling the responsive sequence (**3**). (**8**) Matrix Metalloproteinase (MMP) responsive sequence KCGPQGIWGQCK-NH_2. Cysteine moieties to allow crosslinking are represented in green, hydrophilic amino acids additionally added to increase solubility in black, elastase-sensitive amino acid sequence is in blue, elastase scrambled amino acids in orange and MMP sensitive sequence in purple.

2.3.2 Peptide purification and RP- HPLC characterisation

Peptides were purified by semi-preparative Reverse Phase High Pressure Liquid Chromatography (RP-HPLC) in a Waters HPLC with UV detection at a flow of 9 min/mL.

Purified peptides were characterised by RP-HPLC, and ESI-MS. RP-HPLC analysis was conducted in a waters HPLC equipped with a Waters 2487 detector at 214 nm and using an Onyx monolithic C18 HPLC column (C18 Phenomenex 100 x 4.6mm, 2µm, 130Å) at a flow rate of 3 mL/min. 25 or 50 µL of 1mM of crude or pure peptide were injected per analysis. Solvent A consisted of 0.06% TFA in water, and solvent B was 0.06% TFA in 90:10 HPLC grade acetonitirile:water.

Method 1: 1 to 20% B over 8 min, 3.0 mL/min

Method 2: 5 to 23.5% B over 8 min, 3.0 mL/min

Method 3: 5 to 35% B over 8 min, 3.0 mL/min

Method 4: 5 to 40% B over 14min, 3.0 mL/min

2.3.3 Relative solubility of peptides 3 – 6.

An approximation of the relative solubility of peptides **3 – 6** was obtained by comparing the Area Under the Curve (AUC) of the HPLC peak of the peptide at a fixed concentration with an Fmoc-Glycine internal standard. Crude peptides were prepared at 20 mM in water and centrifuged at 15000 *g* for 5 min at room temperature to remove the insoluble fraction. 10 µL of the supernatant was diluted with 190 µL of water and 20 µL of the Fmoc-Glycine internal standard (1mM). 200 µL of each sample were analysed by RP-HPLC (method 4) and the percentage of the AUC from the peptide to the internal standard calculated in order to compare the relative solubility of peptides **3 - 6**. Calculations are based on the assumption that i) the higher solubility of the peptide the higher the AUC of the peak in the spectra, ii) the UV absorbance of peptides 3-

6 is comparable due to the absence of aromatic amino acids and the number of aliphatic residues is the same in all peptides and iii) that the products are of similar purity

2.3.4 Quantification of free thiols

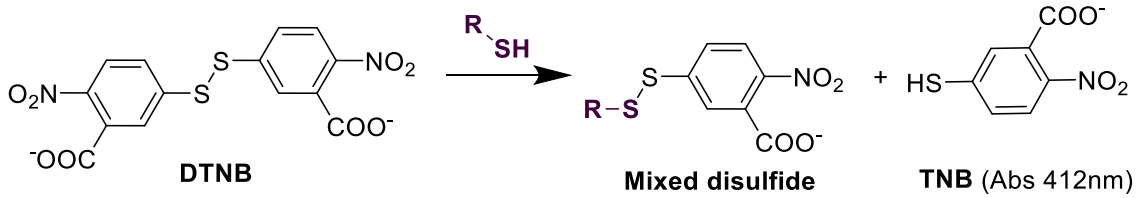

Figure 2.2. Determination of thiol contents in peptides with Ellman's assay. Reaction of Ellman's reagent 5,5'-dithio-bis(2-nitrobenzoic acid) (DTNB) with free sulfhydryl yielding a mixed disulphide and the colorimetric compound 5-thio-2-nitrobenzoic acid (TNB).

Free sulfhydryl groups in all peptide batches were quantified by 5,5-dithiobis(2-nitrobenzoic acid) (DTNB) colorimetric assay[190]. The quantification methods is based on the reaction of free thiols present in the peptide sequences with DTNB reagent forming a mixed disulphide and generating compound 5-thio-2-nitrobenzoic acid (TNB) in an equimolar ratio, which can be quantified spectroscopically (Figure 2.2). Briefly, peptides were dissolved in deionised water (2 and 4 mM). 5 mL of DTNB solution (2 mM, 4 mg) were prepared in sodium acetate buffer (20.5 mg, 50 mM). TRIS buffer consisted of tris(hydroxymethyl)aminomethane 1 M at pH 8.0 (pH adjusted with 1 M HCl). For analysis, 10 µL of the peptide containing sample were added to 840 µL of water, 100 µL of TRIS buffer. Then 50 µL DTNB solution were then added to each sample and incubated for 5 min. Absorbance at 412 nm was read in a Varian UV-Vis spectrophotometer. The percentage of free thiols in each peptide batch was then used to adjust the experimental thiol to -ene ratio for the preparation of peptide-crosslinked hydrogels.

After chemical characterisation, verification of hydrogel formation and adequate enzyme responsive properties, the elastase-responsive sequence Ac-CSSAAPVRGGGC-NH_2 was purchased from SynPeptide Co Ltd instead of in-house synthesised.

All purchased peptides were analysed routinely as described above via ESI-MS, RP-HPLC and quantification of free thiols.

Characterisation of synthesised peptide Ac-CAAPVRGGGC-NH_2 (**1**): **ESI-MS**: $[M+H]^+$ predicted 931.424, observed 931.424; $[M+Na]^+$ predicted 953.402, observed 953.406. Oxidised peptide: $[M_{oxid}+H]^+$ predicted 929.41, observed 929.41; $[M_{oxid}+Na]^+$ predicted 951.39, observed 951.39. **RP-HPLC**: retention time (r.t.) 3.4 min (containing predominantly $[M_{oxid}+H]^+$, $[M_{oxid}+Na]^+$)and 3.7 min (containing predominantly $[M_{oxid}+H]^+$, $[M_{oxid}+Na]^+$) (Method 2).

Characterisation of synthesised peptide H-RGGGC-NH_2 (**2**): **ESI-MS**: $[M+H]^+$ predicted 448.21, obtained 448.21. **RP-HPLC**: r.t. 0.7 min (Method 1).

Characterisation of synthesised peptide Ac-CSSAAPVRGGGC-NH_2 (**3**) **ESI-MS**: $[M+H]^+$ predicted 1105.49, obtained 1105.49, $[M+H+Na]^{+2}$ predicted 564.24, obtained 564.24, [M+TFA] predicted 1241.46, obtained 1241.47. **RP-HPLC**: r.t. 3.9 min (Method 2).

Characterisation of synthesised peptide Ac-CGGAAPVRGGGC-NH_2 (**4**) **ESI-MS**: $[M+H+Na]^{2+}$ predicted 564.24, obtained 564.24. **RP-HPLC**: r.t. 3.5 min (Method 2).

Characterisation of synthesised peptide Ac-CSGAAPVRGGGC-NH_2 (**5**) **ESI-MS**: $[M+H+Na]^{2+}$ predicted 549.23, obtained 549.23. **RP-HPLC**: r.t. 3.6 min (Method 2).

Characterisation of synthesised peptide Ac-CGGAAPVRGGGC-NH_2 (6) **ESI-MS**: $[M+2H]^{2+}$ predicted 558.78, obtained 558.78. **RP-HPLC**: r.t. 3.2 min and 3.5 (Method 2)

Characterisation of purchased peptide Ac-CSSGAVPGARGC-NH_2 (**7**): **ESI-MS**: $[M+H]^+$ predicted 1105.49, obtained 1105.49, $[M+2H]^{2+}$ predicted 553.25, obtained 553.25, $[M+H+Na]^{2+}$ predicted 564.24, obtained 564.24. **RP-HPLC**: r.t. 4.3 min (Method 2).

Characterisation of purchased peptide KCGPQGIWGQCK-NH_2 (**8**): **ESI-MS**: $[M+H]^+$ predicted 1304. 73, obtained 1303.64, $[M+2H]^{2+}$ predicted 652.33, obtained 652.33. **RP-HPLC**: r.t. 4.3 min (Method 3).

2.4 Synthesis of 4-arm poly-(ethylene glycol)-norbornene (4-PEGNB)

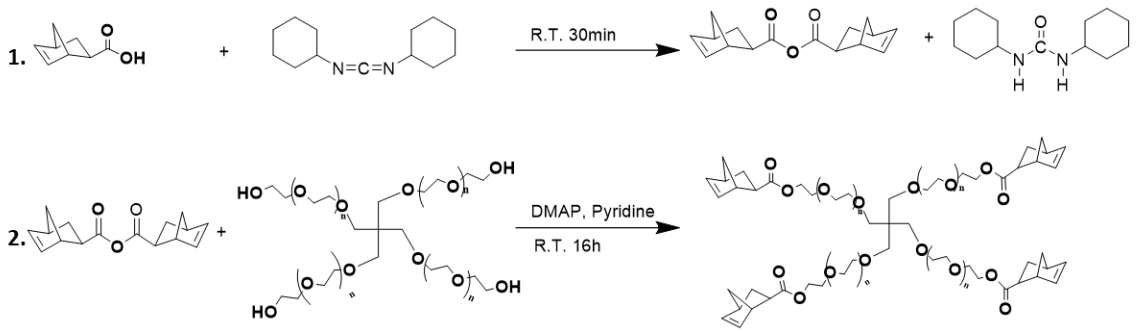

Figure 2.3. Schematic of 4-arm Poly-(ethylene glycol)-norbornene (4-PEGNB) synthesis. **1**.) Synthesis of Norbornene-anhydride. **2**.) Synthesis of 4-PEGNB.

4-arm Poly-(ethylene glycol)-norbornene (4-PEGNB) was synthesised from 4-arm-hydroxyl-PEG (4-PEG-OH, Creative PEGWorks, Mn~5000) similarly to previously described methods [39,161]. All glassware was dried overnight. Equivalents are calculated relative to hydroxyl group concentration. 4-dimethylaminopyridine (DMAP) (0.5 Eq) and pyridine (5 Eq) were added to a 4-arm-hydroxyl-PEG (PEG-OH) (1 Eq) previously dissolved in DCM. In a separate round bottom flask, norbornene-2-carboxcylic acid (5 eq) was reacted with N,N'-Dicyclohexylcarbodiimide (DCC) (2 eq) in anhydrous DCM for 30 min at room temperature to form the norbornene anhydride. The anhydride was then filtered to remove the dicyclohexylurea byproduct and added dropwise to the PEG solution under nitrogen. The reaction was left at room temperature for 16h. Then the product was concentrated under vacuum and precipitated in cold diethyl ether (3x). The crude 4-PEGNB was purified by dialysis against 4 L distilled water (MWCO 1kDa, Spectrum Chemical Mfg. Corp.) for 72 h (water changed 3 times/day). Purified 4-PEGNB was finally lyophilised and hydroxyl conversion characterised by NMR and MALDI-ToF-MS.

^{1}H NMR (400 MHz, D_2O, δ, ppm): δ 6.33 – 6.14 and 6.01 – 5.95 (m, 2H, C=C), 4.39 – 4.18 (m, 2H, CH2OCO), 3.93 – 3.44 (m, 124H, CH2CH2O), 3.29 – 2.95 and 2.44 – 2.28 (m, 3H), 2.02 – 1.81 (m, 1H), 1.54 – 1.25 (m, 3H).

FT-IR: 2880 cm^{-1} (υ_{CH}), 1951 cm^{-1}, 1728 cm^{-1} ($\upsilon_{C=O}$), 1650 cm^{-1}, 1464 cm^{-1}, 1431 cm^{-1}, 1279 cm^{-1}, 1240 cm^{-1}, 1099 cm^{-1}, 960 cm^{-1}, 841 cm^{-1}.

MALDI-ToF-MS: $[M+Na]^+$ predicted 5491.7, $[M+Na]^+$observed 5489.9, repeating unit 44 (-CH_2CH_2O). (From PEG starting material $[M+Na]^+$ predicted 5002.4, $[M+Na]^+$ observed 5003.4).

2.5 Hydrogel preparation by Michael-type addition and thiol-ene photopolymerisation

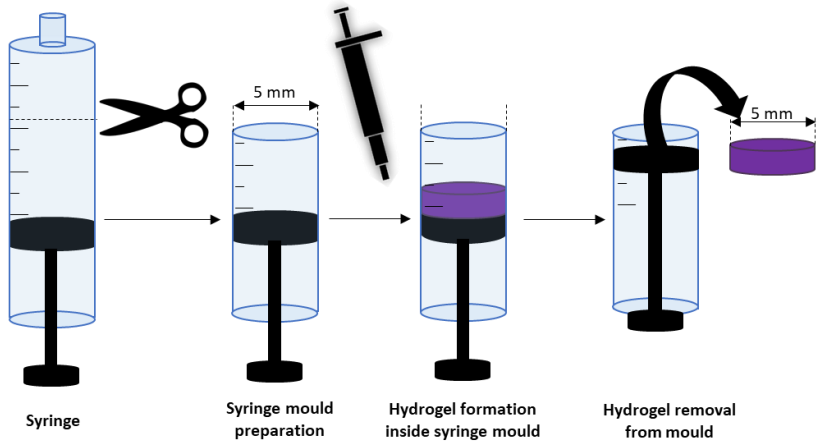

Figure 2.3. Schematic of general procedure for the preparation of hydrogel disks using cut-open syringes as moulds.

25 or 50 µL hydrogels were prepared in 1 mL syringes with cut open tops as moulds, in order to avoid any possible effects of hydrogel geometry on drug release and enzyme degradation kinetics (explanatory schematic in Figure 2.3). All buffers were purged with nitrogen before reaction in order to minimise thiol oxidation. A summary of the different types of hydrogels prepared is shown in table 2.1.

Table 2.1. Hydrogel classification according to their polymer and crosslinker composition and associated functionality.

Hydrogel type	Polymer	Crosslinker	Functionality
Thiol - maleimide hydrogels	4-PEGMal (5 kDa or 10 kDa)	Any	-
Thiol-norbornene hydrogels	4-PEGNB (5 kDa or 10 kDa)	Any	-
Non-responsive hydrogels	Any	DTT*	Not degraded by enzymes
Elastase responsive	Any	Ac-CSSAAPVRGGGC-NH_2	Degraded by elastase
Elastase unresponsive (Scrambled)	Any	Ac-CSSGAVPGARGC-NH_2	Not degraded by elastase
MMP-responsive	Any	KCGPQGIWGQCK-NH_2	Degraded by MMP-2

*DTT= dithiothreitol, all hydrogels prepared at a 1:1 SH:C=C ratio.

2.5.1 Preparation of PEG-based hydrogels via Michael addition

PEG-based hydrogels were synthesised by Michael-type addition between the maleimide functionalities of 4-PEGMal 5 kDa and 10 kDa and a dithiol crosslinker with modifications from the literature[164,173]. Employed crosslinkers were either D-L-dithiothreitol (DTT), or the elastase-responsive peptide (Ac-CSSAAPVRGGGC-NH_2). Buffers consisted in 0.1 M citrate buffer at a range of pH (3, 4, 5 and 6). 25 or 50 µL hydrogels containing different w/v percentages of PEG (5, 10, 20 and 30% w/v) were formed in a single step by addition of the dithiol crosslinker to the 4-PEGMal at an equimolar ratio of thiol to maleimide functional groups and left to react overnight before any further analysis.

2.5.2 Preparation of PEG-based hydrogels via thiol-ene photopolymerisation

4-PEGNB 5 kDa was used to prepare peptide crosslinked hydrogels via thiol-ene photopolymerisation. 4-PEGNB was combined at an equimolar [thiol]:[norbornene] ratio with the elastase responsive, elastase-scrambled and MMP-2 responsive sequences Ac-CSSAAPVRGGGC-NH_2, Ac-CSSGAVPGARGC-NH_2, and KCGPQGIWGQCK-NH_2, respectively (see table 2.1). Reaction was conducted in presence of the photoinitiator lithium phenyl-2,4,6-trimethylbenzoylphosphinate (LAP, 1.7 mM). The resulting solution was exposed to 365 nm UV light for 5 min (absence of protein inhibitor) or 2 min (for encapsulation of alpha-1-antitrypsin inhibitor). 25 or 50 µL were then used for further characterisation.

2.6 Physical characterisation of hydrogels

2.6.1 Characterisation of crosslinking by ^{1}H NMR

Hydrogels for ^{1}H NMR characterisation were prepared according to the general protocol for either Michael addition or thiol-ene photopolymerisation (Section 2.5) inside 3 mm diameter

NMR tubes (Norell®Select Series™, Norell Inc.). Hydrogels were fabricated at a 5 % w/v polymer and 1:1 [thiol]:[ene] ratio in a total volume of 220 µL D_2O.

Thiol-maleimide hydrogels were prepared in 0.1 M citrate pH 4 in D_2O. 4-PEGMal polymer (11 mg) was dissolved in 50% of the reaction volume (110 µL) and added with a syringe to the 3mm NMR tube. Then, the dithiol crosslinker was added (1 eq SH, 110 µL) and thoroughly mixed up and down with the syringe-needle avoiding air bubble formation in the hydrogel network. NMR spectra were acquired 30 min or 14h after the addition of the crosslinker.

Thiol-norbornene hydrogels were prepared in deuterated water (D_2O). A 4-PEGNB solution (11 mg, 110 µL) was mixed with the peptide (1 eq SH, 88 µL) and the LAP photoinitiator (17 mM, 22 µL) in a 1.5 mL HPLC vial. The mixture was then transferred with a syringe to a 3 mm NMR tube, and exposed to 365 nm UV light for 5 minutes before NMR analysis.

2.6.2 Determination of hydrogel mesh size

Hydrogel mesh size was determined based on the swelling ratio measurements as described by Flory-Rehner and Canal and Peppas equations[34]. 50 µL hydrogels were prepared as previously described in section 2.5 and swollen in 1 mL phosphate-buffered saline (PBS) at 37 °C. At each time point hydrogels were collected and the mass of the equilibrium - swollen networks (M_s) was recorded. After four days hydrogels were freeze-dried in a Biopharma Freeze drier to obtain the dried mass of the gels (M_D).

The mesh size (ξ) is defined as the distance between two adjacent crosslinking points in the hydrogel. It was calculated as described by the Canal-Peppas equations[34] (Eq 2.1 to Eq 2.6).

As a first step towards the mesh size characterisation, the molecular weight average between crosslinkers (Mc) was calculated (Eq 2.1) as described by Flory-Rehner and broadly used for PEG hydrogels[36,38,191].

$$\frac{1}{\bar{M}c} = \frac{2}{\bar{M}_n} - \frac{\frac{\bar{v}}{V_1}[ln(1-v_2)+v_2+X_1v_2^2]}{v_2^{1/3}-\frac{v_2}{2}} \quad (2.1)$$

Where $\bar{M}_n$ is the Mw average of the polymers, V_1 the molar volume of the solvent (18 cm^3/mol), v_2 is the polymer volume fraction in equilibrium swollen hydrogel (equal to the reciprocal volume swelling ratio, (Q_v)), $\bar{v}$ the specific volume of polymer (ρ_{sp}/ρ_p). The solvent-polymer interaction parameter (X_1) is 0.426 for PEG-water systems and it was considered constant for this work[192]. In order to calculate Mc, the mass (Q_m) and volume (Q_v) swelling ratio were determined with equations 2.2 and 2.3, respectively. Where ρ_p and ρ_s are the density of the polymer (1.12 g/cm^3 for PEG) and of the solvent, respectively.

$$Qm = \frac{M_S}{M_D} \quad (2.2)$$

$$Q_v = 1 + \frac{\rho_p}{\rho_s}(Qm - 1) \quad (2.3)$$

The Mesh size (ξ) was then calculated by Eq 2.4, where the number of bonds in the crosslink (n) and root mean square of the end-to-end distance of polymer chain $\overline{(r_0^2)}^{1/2}$ can be obtained from Eq 2. 5 and 2.6.

$$\xi = v_2^{-1/3}.(r_0^2)^{1/2} \quad (2.4)$$

$$n = 2\frac{\bar{Mc}}{Mr} \quad (2.5)$$

$$\overline{(r_0^2)}^{1/2} = l\, C_n^{1/2} n^{1/2} \quad (2.6)$$

Here, M_r is the molecular weight of the repeating units of the polymer (44 for PEG). l is the C-C bond length average (0.146 nm)[34], and C_n is the ratio characteristic of the polymer chain (4.0 for PEG)[192].

2.6.3 Rheological characterisation of hydrogels

Viscoelastic properties of hydrogels were analysed in oscillatory mode in an Anton Paar Physica MCR 301 Rheometer using an 8 mm parallel plate setup with temperature controlled to 20 ◦C.

Determination of mechanical properties of preformed gels. For rheological characterisation of preformed gels, hydrogels were prepared between two glass slides covered with teflon laminate and separated by 1 mm spacers. After crosslinking, gels were swollen overnight in PBS at 37 °C. Hydrogels were then punched with an 8 mm biopsy punch for ensuring 8 mm diameter. The gap between the parallel plates was fixed to 0.7 mm to ensure sample contact and avoid slipping. Linear viscoelastic (LVE) regime of hydrogel was assessed by conducting frequency and amplitude sweeps. Frequency sweeps were conducted between 0.1 Hz to 15 Hz at constant 0.5 % amplitude and amplitude sweeps from 0.01 to 10 % at constant frequency of 0.5 Hz. Routine determination of storage and loss modulus (G' and G'', respectively) was conducted at fixed 0.5 Hz frequency and 0.5% amplitude as those values fell in the LVE regime for the samples.

***In situ* gelation**. Gelation kinetics were characterised by monitoring the increase on storage modulus (G') and loss modulus (G'') with time at a fixed 0.5 mm gap, 0.5 Hz and 0.5% strain. Hydrogel components were added between the two parallel plates and their viscoelastic properties recorded every 15 seconds. The gelation time or gel time was defined as the crossover point of G'> G'', and the final G' of gelation was used to compare hydrogels mechanical properties.

2.7 Encapsulation and passive release of model dextrans from non-responsive hydrogels

Encapsulation and passive diffusion from DTT-4-PEGMal hydrogels was assessed with a 70 kDa Texas red dextran (TRD70) as model macromolecule. 25 µL hydrogels were formed as previously explained in section 2.5 with TRD70 being incorporated during polymerisation at final concentration of 10 µg/µL. Not physically entrapped dextran was removed by washing with PBS (2 x 1 mL for 5 min) and used to calculate the encapsulation efficiency (expressed as percentage of the theoretical maximum, Eq 2.7). Release experiments were conducted by incubation of

hydrogels in 5 mL PBS at 37°C for 15 days. 500 µL aliquots were collected for analysis at each time point and replaced with fresh medium. The amount of TRD70 released was quantified in a Tecan plate reader at $\lambda_{Ex/Em}$ = 580 nm/625 nm, Gain 81. Release was expressed as the percentage of the total TRD70 dextran encapsulated.

$$Encapsulation\ Efficiency\ (E.E) = \frac{amount\ encapsulated\ macromolecule\ (\mu g)}{Total\ amount\ macromolecule\ (\mu g)} \times 100 \qquad (2.7)$$

Where encapsulated macromolecule is the amount of dextran inside the gels at time 0h and the total dextran is the entrapped dextran and the one released during the medium washes before starting the release.

2.8 Fluorescamine assay for characterisation of the enzymatic degradation of hydrogels and peptide in solution

Enzymatic degradation of peptides in solution. 200 µL of 3 U/mL of elastase (Porcine pancreatic elastase or PPE) were added to 200 µL of 2mM peptide Ac-CAAPVRGGGC-NH2 (**1**) in PBS and incubated at 37 °C. After 3h incubation fresh enzyme was added to the medium. Two controls corresponding to the peptide in buffer and the enzyme in buffer were kept under the same conditions. At determined time points the reaction medium was sampled and centrifuged through 3.5 kDa MWCO filters at 14000rpm for 5 min (Hermle Z 160 M benchtop centrifuge) at room temperature to remove the enzyme prior to analysis. Samples were diluted 1/80 in distilled water and 150 µL of sample were then reacted with 50µl of a 3 mg/mL solution of fluorescamine in acetone. After 10 min incubation fluorescence was read in a Tecan SPARK plate reader from above at $\lambda_{Ex/Em}$ 400 nm/460 nm for quantification of free amino groups (n=3). Additionally, samples and controls were analysed by RP-HPLC-MS and compared to peptide (**1**) and enzyme controls and the peptide fragment synthesised (**2**).

Enzymatic degradation of hydrogels. 25 µL 10% w/v peptide-crosslinked hydrogels (n = 3) were incubated in 0.5mL phosphate buffer pH 8 with porcine pancreatic elastase as the model elastase (12.5, 25 and 50 mU/mL elastase for total enzyme activities of 6.25, 12.5, and 25 mU respectively). Controls of each enzyme concentration without gels and gels incubated in buffer (0 U/mL enzyme) were also conducted. At each time point the supernatant was removed and replaced with fresh medium. The increase in cleaved primary amines from peptide-crosslinked hydrogels was quantified by fluorescamine assay[123,193,194]. Briefly, samples were diluted 1/20 in distilled water and 150 µL of sample were then reacted with 50 µL of a 3 mg/mL solution of fluorescamine in acetone for quantification of total primary amines content. After 10 min incubation fluorescence was read in a Tecan SPARK plate reader at $\lambda_{Ex/Em}$ 400 nm/460 nm for quantification of free amino groups. Results were normalised to mg of polymer and presented as the increase with time of primary amines due to cleavage (nmol NH_2/mg polymer). The maximum degradation rate was obtained from the slope of the steepest region of the degradation curve and expressed as nmol NH_2/mg polymer/h.

2.9 Elastase-controlled release from peptide-crosslinked hydrogels

Encapsulation efficiency and passive and enzyme-controlled release from peptide crosslinked hydrogels were assessed with a 70 kDa Texas red dextran (TRD70) or fluorescein isothiocyanate-dextran 70 kDa (FD70) as model macromolecules.

25 µL hydrogels were formed as previously explained in section 2.5 with the dextran being incorporated during polymerisation at final concentration of 10 µg/µL. Gels were incubated with 1 mL release medium for 12 h (2x) to release not physically entrapped dextran and calculate the encapsulation efficiency (Eq 2. 7). Release experiments were conducted by incubating hydrogels in 500 µL of release medium at 37 °C with pancreatic elastase (6.25 mU), Human Neutrophil Elastase (10 - 40 nM) or just buffer. At each time point, all medium was removed for analysis and

replaced with fresh one. Release medium consisted on either 0.1 M phosphate buffer pH 8, zymogram (50 mM Tris_HCl, 10 mM $CaCl_2$, 150 mM NaCl, 1 µM $ZnCl_2$, 0.05% w/v Brij35, pH 7.5) or Dulbecco's Modified Eagle Medium: F-12 nutrient mixture (DMEM-F12) supplemented with 0.1% w/v Bovine Serum Albumin (BSA) and Airway Epithelial Supplement (AES).

Hydrogels were degraded at the end of the release experiments by incubation with 1 mL porcine pancreatic elastase (PPE) (10 µg/mL) for more than 4 h. This provided the amount of dextran remaining inside the gels at the endpoint of release (not released). The amount of dextran released was expressed as the percentage of the total amount encapsulated as determined experimentally.

2.10 Cross-release in presence of Matrix Metalloproteinase-2 (MMP-2)

20% w/v peptide-crosslinked hydrogels were incubated for 12 h in 2 × 1 mL of zymogram medium to release unentrapped dextran. Hydrogels were then incubated in 0.5 mL zymogram medium consisting on Matrix Metalloproteinase-2 (MMP-2, 16 nM in zymogram), HNE (10nM in zymogram) or just zymogram buffer. At each time point the supernatant was removed and the dextran released quantified. All remaining dextran at the endpoint of the experiment was released from the not-degraded hydrogels by incubation with 1 mL 20 µg/mL collagenase overnight. Encapsulation and release of fluorescein isothiocyanate-dextran 70 kDa was conducted following the same protocol and quantified with fluorescent readings at $\lambda_{Ex/Em}$ = 470 nm/515 nm, Gain 45.

2.11 Fluorescent labelling of alpha-1-antitrypsin

2 mg of human α-1-antitrypsin (AAT) were dissolved in 0.1 M Na_2CO_3 buffer at pH 8.5. A stock solution of 20 mg/mL stock of NHS-fluorescein in DMSO (2 µmol) was added dropwise under

stirring. Reaction was left overnight at room temperature. Fluorescently labelled AAT protein (AATF) was purified through PD-10 columns and its purity was analysed by HPLC.

2.12 Encapsulation and passive release of alpha-1-antitrypsin

Fluorescently labelled AAT was added during 25 µL hydrogel preparation, as described in section 2.5 of this chapter. Unentrapped protein was left to diffuse out of the gels for 24 h before starting release experiments. For the release experiments, the release medium (PBS) was replaced every 24 h and the AAT release quantified via fluorescent measurements in a Tecan plate reader ($\lambda_{Ex/Em}$ 492nm / 537nm).

2.13 Enzyme activity assays

2.13.1 Porcine Pancreatic Elastase activity assay

N-methoxysuccinyl-Ala-Ala-Ala-p-nitroanilide (Nsuc-Ala_3-pNA) was used to determine the activity of pancreatic elastase. Nsuc-Ala_3-pNA is cleaved to yellow compound pNA upon the action of pancreatic elastase. 50 µL of elastase were incubated at 37 °C with 1.45 mL of 0.29 mM substrate in either Tris-HCl buffer 100 mM or phosphate buffer 0.1M pH 8. The rate of hydrolysis was monitored every 15 seconds at 410 nm for 6 min to obtain the ΔA_{410nm} in the linear range. One enzyme unit (U) was defined as the amount of enzyme needed to cleave 1 µmol of Nsuc-Aal_3-pNA per minute under the previous conditions. Enzyme activity was calculated as shown in Eq 2. 8.

$$U/_{ml} = \frac{(\Delta A_{410nm/min} sample - \Delta A_{410nm/min}\ blank) \times V \times Df}{Ce \times Ve} \quad (2.8)$$

In equation 8, $\Delta A_{410nm/min} sample$ is the increase in absorbance of the sample, $\Delta A_{410nm/min}\ blank$ is the increase in absorbance of a substrate solution, *V* is the volume of

reaction, *Df* is the dilution factor of the enzyme solution, *Ce* is the coefficient of extinction of pNA, and *Ve* the volume of enzyme added into the reaction medium.

2.13.2 Human Neutrophil Elastase activity assay

The cleavage of the substrate N-methoxysuccinyl-Ala-Ala-Pro-Val-p-nitroanilide (Nsuc-AAPV-pNA, Sigma Aldrich) by HNE to release the colorimetric compound p-nitroaniline (p-NA) was used to determine the activity of native Human Neutrophil Elastase (HNE)[76,195]. 10 µL of HNE (200 nM – 400 nM) were added to 80 µL of buffer (Phosphate 0.1 M pH 8) in a transparent 96 well plate. 10 µL of 2 mM Nsuc-AAPV-pNA were then added to the medium and the increase in absorbance at 37 °C was immediately monitored every 30 seconds in a Tecan plate reader. Controls of substrate in buffer were also included. The amount of p-nitronaniline (p-NA) cleaved during 30 min was calculated by comparing to a p-NA standard curve and expressed as µmol/min. One enzyme unit (U) was defined following the manufacturer instructions as the amount of enzyme that will hydrolyse 1 µmol of Nsuc-AAPV-pNA per minute at pH 8.

For the analysis of HNE activity in release samples and cell culture supernatants, 90 µL or 140 µL of the sample containing HNE were incubated with 10 µL of 2 mM Nsuc-AAPV-pNA and pNA formation was monitored as described above.

2.13.3 Alpha-1-antitrypsin activity quantification

The inhibitory activity and stability of alpha-1-antitrypsin was assessed based on its ability to inhibit HNE activity. It was therefore quantified by assessing its ability to hinder HNE-mediated conversion of Nsuc-AAPV-pNA to the yellow compound pNA as described in the previous section. In order to achieve this, 10 µL of AAT were incubated with 10 µL 200 nM HNE in 70 µL buffer for 10 min prior to addition of the substrate and measurement of the HNE activity as stated above. AAT activity was expressed as percentage inhibition of the native HNE in absence of the AAT inhibitor.

2.14 Activation and characterisation of Matrix Metalloproteinase 2 activity

Activation and characterisation of Human recombinant Matrix Metalloproteinase 2 (MMP-2) was conducted by Mr. Emanuele Russo. MMP-2 proenzyme (RnD systems, 10 µg) was activated by incubation with p-aminophenylmercuric acetate (APMA). Pro-MMP-2 was diluted to 100 µg/mL in zymogram buffer and incubated at 37 °C for 1 hour in presence of 1 mM APMA in DMSO. Activated enzyme was then aliquoted at different concentrations (10 µg/mL or 100 µg/mL).

Enzyme activity was assessed by using the quenched MMP fluorogenic substrate Mca-Pro-Leu-Gly-Leu-Dpa(Dnp)-Ala-Arg-NH2 (Mca-PLGL-Dpa-AR-NH2, RnD systems) [Mca=(7-methoxycoumarin-4-yl)-acetyl; Dpa=N-3-(2,4- dinitrophenyl)-L-α-β-diaminopropionyl]. Mca fluorescence is quenched by the Dpa group until cleavage by MMPs at the Gly-Leu bond. 50 µL of 0.2 ng/µL activated enzyme solution were added to 10 µL of 100 µM Mca-PLGL-Dpa-AR-NH2 and 40 µL of zymogram buffer in a 96 black well-plate. The rate of substrate hydrolysis was continuously monitored at 37 °C for 1 hour using a TECAN plate reader ($\lambda_{Ex/Em}$ = 320 / 405 nm). The enzyme activity was then calculated using Eq 2.9.

$$Specific\ MMP\ activity = \left(\frac{pmoles}{\min \mu g}\right) = \frac{Vmax\left(\frac{RFU}{min}\right) * CF\left(\frac{pmoles}{RFU}\right)}{\mu g\ enzyme} \quad (2.9)$$

Where RFU/min was the slope of the linear part of the curve, CF is the conversion factor obtained by the ratio pmols/RFU using the calibration curve of control peptide Mca-Pro-Leu-OH (y = 63.9x + 64.48, CF= 0.015 pmol/RFU).

2.15 Cell culture

2.15.1 Cell culture reagents

Lung epithelial cells A549 were purchased from ATCC (American Type Culture Collection, Manassas, VA, USA), Gibco Dulbecco's Modified Eagle Medium: F-12 nutrient mixture (DMEM-F12 medium), Gibco™ Human Keratinocyte Growth Supplement, Prestoblue™ and GIbco™ Foetal Bovine Serum (FBS) from Fisher Scientific UK Ltd (Loughborough, UK). Small Airway Growth Medium Supplement was obtained from Lonza (Basel, Switzerland), from Airway Epithelial Cell Growth Supplement from Promocell (Heidelberg, Germany), Peprogrowth Supplement from PeproTech EC (London, UK) and penicillin-streptomycin (10000 U/mL penicillin, 10 mg/mL streptomycin, Sigma).

2.15.2 General Human Lung Alveolar Epithelial (A549) cell culture

Lung epithelial cells A549 were maintained in T-75 cell culture flasks (Corning®). Cells were cultured with Dulbecco's Modified Eagle Medium: F-12 nutrient mixture (DMEM-F12 medium) supplemented with 10 % v/v Foetal Bovine Serum (FBS) and 1 % v/v penicillin-streptomycin at a final concentration of 100 U/mL penicillin and 100 µg/mL streptomycin (complete medium). Cells were incubated in a humidified atmosphere at 37 °C with 5 % CO_2 and passaged when they reached around 80 – 90 % confluence by trypsinisation with Trypsin-EDTA solution (1x). After cell detachment trypsin was deactivated by addition of complete medium (1:2 of trypsin: medium). Cells were then centrifuged for 5 min at 200 *g* (MSE Mistral 3000i), resuspended and transferred to a new flask at an adequate dilution. Medium was replaced every 2-3 days after splitting.

Cells were frozen for long term storage in 10 % v/v of DMSO in FBS. Cryovials were cooled at -1 °C/min to -80 °C in the freezer and transferred into liquid nitrogen storage after 48h. Cryopreserved vials were recovered by thawing in a water bath at 37°C and then transferred to DMEM-F12 + 10 % FBS. The obtained cell suspension was centrifuged at 200*g* (MSE Mistral 3000i)

for 5 min. Cell pellet was then resuspended in fresh DMEM-F12 and seeded in a T-75 flask, and cultured with the general procedure stated above.

2.15.3 Media composition for assays containing Human Neutrophil Elastase

Human Neutrophil Elastase (HNE) showed not to be active in standard culture conditions with 10 % FBS DMEM-F12 medium. Assays with neutrophil elastase were therefore conducted in serum reduced (4 %, 2 %, 1 %, 0.5 % v/v FBS in DMEM-F12) or serum free media alternatives.

Initial assessment of neutrophil elastase toxicity and recovery by administration of AAT was conducted in Small Airway Growth Medium Supplemented DMEM-F12 (SAGM). 500mL of medium were supplemented with the following volumes of the SAGM Bullet Kit ,as suggested by the supplier: 2mL Bovine Pituitary Extract, 500 µL insulin, 500 µL hydrocortisone, 500 µL transferrin, 500 µL recombinant human Epithelial Growth Factor (rhEGF), 500 µL ng/mL triiodothyronine, 500 µL epinephrine and 1 mL of Bovine Serum Albumin (BSA). The supplements of Retinoic Acid and Gentamycin-Amphotericin provided by the supplier were not included.

Due to interruption in the supply of the SAGM supplement by the manufacturer, alternative serum-free media with similar compositions were tested. This included DMEM-F12 supplemented with:

- Human Keratinocyte Growth Supplement (HKGS). HKGS was diluted 1/100 in DMEM:F12 basal medium for a final concentration 0.002 mL/mL BPE, 1 µg/mL recombinant human insulin-like growth factor (irhILGF), 0.18 µg/mL hydrocortisone, 5 µg/mL bovine transferrin, 0.2 ng/mL hEGF).
- Peprogrowth Supplement, containing 1/200 v/v lipid mixture solution and 1/100 serum replacement solution, diluted according to supplier instructions.
- Airway Epithelial Cell Growth Supplement (AES). AES was diluted according to supplier instructions to a final concentration of 0.004 mL/mL BPE, 5 µg/mL insulin, 0.5 µg/mL

hydrocortisone, 10 µg/mL transferrin, 10 ng/mL recombinant human Epithelial Growth Factor (rhEGF), 6.7 ng/mL triiodothyronine and 0.5 µm/mL epinephrine).

All media were tested with and without BSA supplements and compared in their ability to support cell viability and migration. For this cells plated in DMEM-F12 + 10 % FBS were gradually transferred in the test medium, by adding 50 % DMEM-F12 + FBS and 50 % test medium 48 h before the assay and 100 % test medium 24 h before the assay. Afterwards cell migration and viability were assessed as described below.

2.15.4 Determination of cell viability: Prestoblue® assay

Quantification of metabolic activity with Prestoblue™ assay was conducted to assess cell viability after treatment with hydrogels, AAT and HNE, and compare cell viability under different conditions. Prestoblue™ is a resazurin containing reagent that evaluates the reducing ability of cells. Healthy cells will reduce Prestoblue™ to the highly red fluorescent compound resorufin. In contrast, unhealthy cells will not be able to conduct the reduction of resazurin, therefore not yielding the fluorescent product.

Toxicity of Human Neutrophil Elastase and α-1-antitrypsin

Cells were seeded at 8×10^3 cells/well in a 96 wells plate and incubated with either HNE, AAT, or HNE-AAT combinations in a humidified atmosphere at 37°C with 5 % CO_2. The treatment was removed at every time point, replaced with 90 µL of fresh medium and 10 µL of Prestoblue™, and incubated for 1 h at 37 °C. Then, 90 µL of the medium were plated in a black 96 well plate and fluorescence was read at $\lambda_{Ex}/_{Em}$ 560/590 nm in a FlexStation 3 (Molecular Devices). Metabolic activity was normalised to untreated cells at the same time points as described in Eq 2.10.

$$\%\ Cell\ viability = \frac{AFU\ treated\ cells\ t_x}{AFU\ untreated\ cells\ t_x} \times 100 \quad (2.10)$$

Where $AFU\ treated\ cells\ t_x$ and $AFU\ untreated\ cells\ t_x$ are the fluorescent signal at each time point expressed as arbitrary fluorescent units (AFU).

Toxicity of thiol- thiol-norbornene hydrogels

Hydrogels preparation was conducted as specified in section 2.5 and under sterile conditions. Cells were seeded at 5×10^4 cells/well in a 24 well plate and incubated in a humidified atmosphere at 37 °C with 5 % CO_2 with PEG-maleimide or PEG-Norbornene. Hydrogels were placed in a Transwell® insert (6.5 mm diamater, 8 µm pore, Corning®) to avoid physical damage of the cell monolayer. At every time point, hydrogels were removed and 570 µL of fresh medium and 30 µL of Prestoblue™ were added to the cells and incubated for 1 h at 37 °C. Then, 90 µL of medium were plated in a black 96 well plate and fluorescence was read at $\lambda_{Ex}/_{Em}$ = 560/590 nm in a FlexStation 3 (Molecular Devices). Metabolic activity was normalised to untreated cells at the same time points (Eq 2.10).

2.15.5 Migration Assay

The scratch wound migration assay was used to assess the ability of cells to repair disrupted cell monolayers, as described elsewhere[195,196]. Cells were grown in a 24 well plate until they reached 95% confluence. Then cells were serum starved for 24 h in the test medium used for migration, corresponding to either SAGM or AES supplemented DMEM-F12 for experiments containing Human Neutrophil Elastase. After 24 h, a wound was created by scratching vertically the cell monolayer with a 200 µL pipette tip and wells were washed with 3 × 1 mL of cell medium to remove detached cells.

25 µL hydrogels were placed in a Transwell® insert placed in the 24 well plates, in order to avoid physical damage of the cell monolayer and the scratch. Treatment was then added to the cells in a total volume of 600 µL in the receptor chamber and 100 µL in the Transwell®. Images of the wound were taken every 24 h under an Olympus Inverted Microscope CKX53 with XM10 digital camera and CellSens software at 4x magnification. Wound closure was assessed by measuring the wound area with ImageJ 1.52a Software[197] (National Institute of Health, USA, https://imagej.nih.gov/ij/index.htmL) at each time point and comparing it to the originally created

wound size. Wound closure was expressed as a percentage of the original wound, and calculated with Eq 2.11.

$$\%\, Wound\ closure\ = \frac{Wound\ size\ t_{0h} - Wound\ size\ t_{xh}}{Wound\ size\ t_{0h}} \quad (2.11)$$

Where $Wound\ size\ t_{0h}$ is the area of the created wound at time 0h, and $Wound\ size\ t_{xh}$ corresponds to the area of the wound at each time point analysed.

2.16 Statistical Analysis

GraphPad Prism 7 version 7.04 for Windows (GraphPad Software, La Jolla California USA, www.graphpad.com) was used to perform all statistical analysis.

Data is reported as mean ± standard deviation for dependent samples and as mean ± standard error for independent experiments. The number of repeats are stated as N for independent experiments and n for dependent experiments. When independent experiments were compromised of dependent replicates within the experiment, both N and n were stated.

Chapter 3.

Fabrication and characterisation of PEG-maleimide–based hydrogels

3.1 Introduction

Polymeric hydrogels are of growing interest in biomedical applications, such as drug delivery and tissue engineering[43,114]. Their high porosity, hydrophilic nature and high water content make them an attractive drug delivery platform, as they can encapsulate high amounts of therapeutic macromolecules, cells and nanoparticles within the polymeric network under mild conditions[138,164,198]. In particular, poly(ethylene glycol) (PEG) based hydrogels possess tuneable properties and can be easily modified with a broad range of functionalities to impart improved mechanical properties, high biocompatibility and controlled release profiles[22,39,114,140].

It is the aim of this thesis to develop hydrogels for the efficient protease-responsive delivery of inhibitors of proteases. One of the remaining challenges when formulating hydrogels for responsive drug delivery is to reduce passive diffusion from the hydrogels porous structure and therefore minimise unspecific drug release[1991]. Passive release can be reduced by: i) covalent linking of the drug,[41] ii) gel-macromolecule ionic or hydrophobic interactions[47], iii) formulation of the therapeutic into secondary delivery systems such as nanoparticles[200], and iv) modification of hydrogel physicochemical properties for improved passive encapsulation[22], with the latter one offering the mildest and most suitable conditions for physically entrapped macromolecules.

Thiol crosslinking chemistries (thiol-ene photopolymerisation or thiol Michael addition reaction), are the most commonly used method for the fabrication of protease-responsive materials for biomedical application[160–165]. Thiol Michael addition consists of the 1,4 addition of a thiol to an electron deficient vinyl group such as maleimides, vinyl-sulfones, acrylates and methacrylates leading to a thioether bond formation (Fig3.1a)[174]. This allows for efficient

crosslinking of polymers containing multi-arm vinyl functionalities with multi-cysteine containing peptides, creating the hydrogel network. The use of thiol chemistries eliminates the need for complex chemical modifications of the peptide crosslinkers and can be conducted under mild aqueous conditions, facilitating fast formation of hydrogels[160,161,163,167] The exact mechanism of hydrogel formation via Michael addition and other alternative chemistries for hydrogel fabrication are discussed in more detail in section 1.4.1.

Due to their higher reaction efficiency, maleimide crosslinked hydrogels can be obtained without using any catalysts[41,173,179], which could otherwise affect cell viability and the stability of encapsulated proteins[168,180,181]. Additionally, the use of maleimide-PEG to PEGylate proteins is well stablished and it has led to commercialised products such as Cimzia®(Certolizumab pegol)[25]. Cimzia® is an anti-Tumour Necrosis Factor (anti-TNF) antibody Fab (fragment antigen binding) PEGylated with a multiarm PEG-maleimide currently used in the treatment of several inflammatory diseases such as Crohn's disease and rheumatoid arthritis [25,182,183]. For those two reasons, thiol Michael addition was the crosslinking reaction of choice in this work for the preparation of functionalised hydrogels as summarised in Figure 3.1.a.

3.1.1 Michael-addition hydrogels: properties that affect drug release

There are two key aspects which can influence drug encapsulation in hydrogels prepared via Michael addition: the kinetics of crosslinking and the mesh size of the polymeric hydrogel network.

3.1.1.1 Crosslinking kinetics

Crosslinking kinetics are a key parameter in hydrogel fabrication by Michael addition, since uniformly crosslinked gels are required for reproducible macromolecule encapsulation and release.

Although the superior reactivity of maleimides has made them good candidates for biocompatible hydrogel preparation, their higher reaction efficiency also implies faster

crosslinking kinetics[173]. This can lead to the crosslinking reaction, and therefore hydrogel formation, taking place faster than the speed at which hydrogel precursor components can be mixed together[173,179]. The resulting hydrogels would have non-uniform hydrogel networks with domains containing low and high crosslinking densities within the same hydrogel[173]. As a result, the distribution of macromolecules within the hydrogel matrix would be heterogeneous and drug diffusion would be highly variable[179], therefore altering release. On the other hand, too slow gelation kinetics have been associated with irregular distribution of the gels cargo resulting from sedimentation before crosslinking takes place[179]. Therefore this balance of both aspects has to be considered during optimisation of gelation speed, in order to guarantee kinetics slow enough to achieve homogeneous reproducible drug distribution and release, but not so slow as to allow drug sedimentation before gel formation. Despite the wide use of maleimide hydrogels for tissue engineering and protein release, a systematic assessment of different parameters on crosslinking kinetics has been mostly overlooked in the field, except for two key works by Darling *et al*., and Jansen *et al*.[173,179] Darling and co-workers observed that gelation kinetics of 4-arm-PEG-maleimide (4-PEGMal) were too fast under physiological conditions and lead to micro-domains of varying crosslinking densities. They studied the effect of polymer concentration, pH and pka of the thiol on the crosslinking kinetics and concluded that slowing gelation by changing the pka of the thiol was the most suitable strategy to slow gelation for cell encapsulation and spread[173]. Jansen *et al.* also observed that 4-PEGMal polymers reacted rapidly with thiols at physiological pH without any catalyst. They systematically studied the effect of lowering polymer concentration, buffer pH and concentration and the use of more electronegative thiols on gelation kinetics. All changes lead to slower gelation and usually more uniform hydrogels, presenting less variable diffusion of small molecules through the network[179].

There are several factors that can affect hydrogel gelation kinetics of hydrogel formation through Michael addition which are summarised in Figure 3.1.b and can therefore be used to modulate gelation kinetics:

- *Thiol crosslinker*. Increasing number of cysteine residues and therefore number of thiols available for crosslinking has been described to speed gelation kinetics[178]. Additionally, the pka of the thiol can drastically change the crosslinking kinetics of Michael addition[173,177,179,201]. The use of negatively charged amino acids adjacent to the cysteine can increase the pKa of the thiol and reduce gelation kinetics up to ~100 fold, allowing uniform mixing without compromising hydrogel mechanical properties[173,179].
- *Polymer and vinyl group*. An increase in the concentration of the polymer and therefore the vinyl groups accelerates crosslinking kinetics[143,179]. Additionally, lower molecular weight of PEG or an increase in the number of arms per polymer will effectively lead to more vinyl groups available for crosslinking, being therefore associated with faster gelation[143,178]. Another strategy to modulate gelation kinetics could be by changing the vinyl group functionality. Maleimides are the most reactive –enes for Michael type addition, and vinyl sulfone and acrylate functionalised polymers show slower kinetics (reactivity: acrylate < vinyl sulfone < maleimide, Figure 3.1.b bottom right)[173,178]. Although this strategy efficiently slows gelation, it has been shown that acrylate and vinyl sulfone polymers require the use of higher amount of catalyst to form hydrogels under same conditions than maleimide ones, which has shown to affect cell viability[164]. It has also been shown that vinyl sulfone and acrylate lower reactivity with thiols decreases the efficiency in thiol incorporation, leading to more loosely crosslinked networks with weaker mechanical properties[164].

- *pH of the buffer*. Altering the pH of the reaction buffer has been described as another valid option for modulating Michael addition kinetics. Hydrogel formation via crosslinking between thiols and vinyl groups has been shown to take place in a pH range between 3 to 10[143,173,179]. This is because pH values below 3 may lead to too

low a concentration of thiolates and could affect the stability of other functional groups such as ester bonds, thus hindering crosslinking reactions. Neutral and slightly acidic pH values keep the reaction selective towards thiols, minimising any possible reactions of maleimides with primary amines in the peptides, and gelation is usually conducted at pH below 8 - 8.5[18,41,114,164,166]. Additionally, lowering the buffer pH will modulate the thiol/thiolate equilibrium towards the protonated form (thiol). This reduces the thiolate concentration, which is the active species for Michael addition and therefore slows gelation kinetics (Figure 3.2.b top right)[173,179]. Varying the buffer pH has been shown to not affect final mechanical properties of the hydrogels[173].

- *Temperature*. The temperature of reaction can also affect crosslinking kinetics. Darling *et al*. and Elbert *et al.* have shown that a decrease in the temperature can slow crosslinking reaction kinetics leading to significantly slowing gelation[143,173]. Although varying temperature could be an efficient approach to control gelation kinetics of hydrogels formed via Michael-type addition, it has less impact on maleimide-crosslinked hydrogels[173]. Additionally, the preparation of hydrogels under low temperature presents impracticalities and difficulties to be implemented into routine hydrogel preparation. For these reasons, this parameter has not been varied in this work, and hydrogel formation was conducted at 20 °C throughout this work.

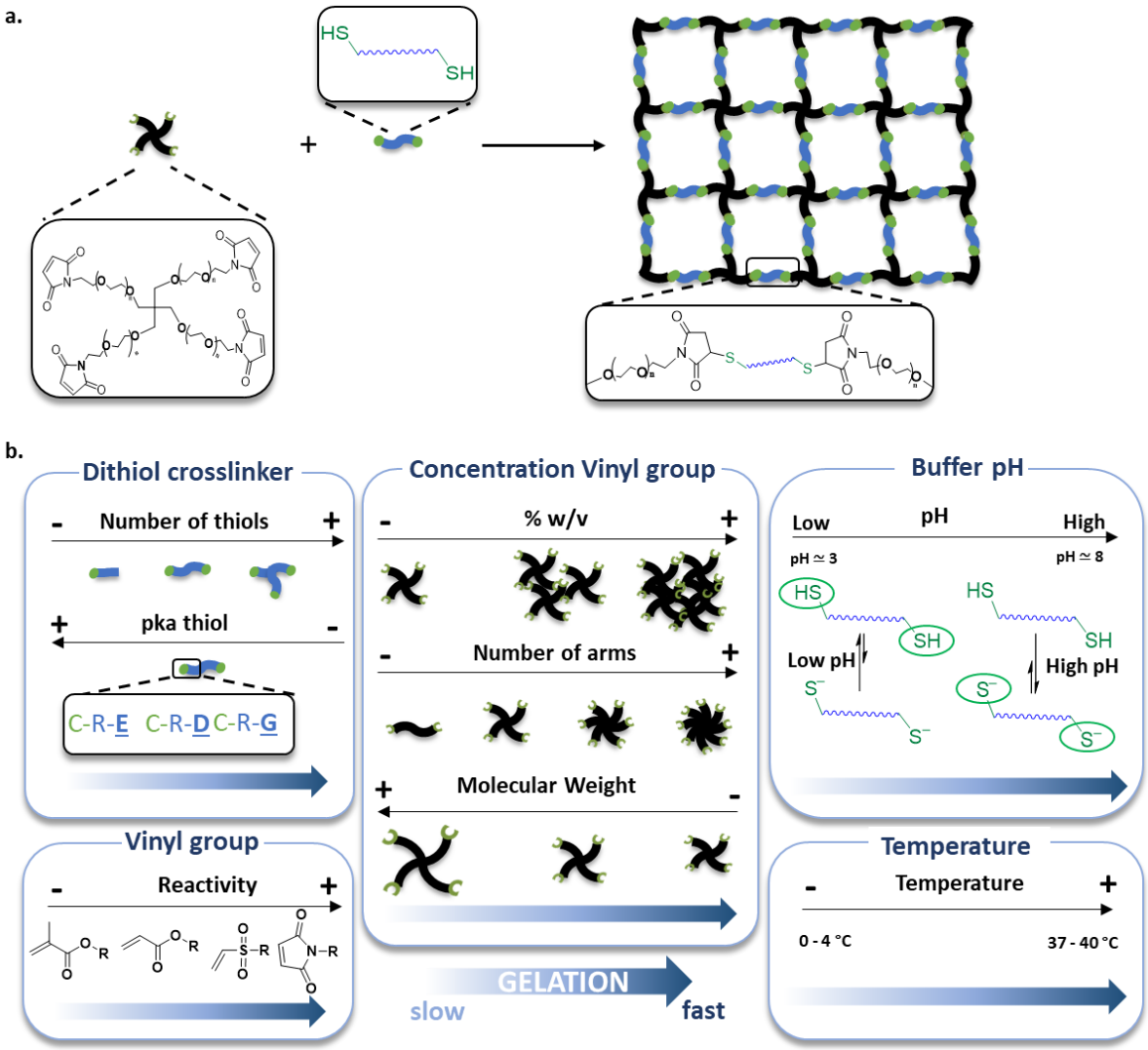

Figure 3.1. Thiol Michael addition reaction for functionalised hydrogel preparation. **a.)** Simplified schematic of crosslinking reaction between dithiol crosslinkers and maleimide polymeric networks(hypthetical 2D structure). **b.)** Parameters affecting gelation kinetics via Michael addition (ordered from slowest to fastest gelation condition left to right within each category).

3.1.1.2 Hydrogel mesh size

Hydrogel mesh size (ξ) corresponds to the distance between two adjacent crosslinking points in the hydrogel network, being a key parameter dictating effective drug encapsulation and passive release[22,34]. Several parameters can affect hydrogel's mesh size, and therefore entrapment and passive release from hydrogels. Some of the parameters have also been described to have an effect on gelation kinetics (section 3.1.1.1) and therefore their effect on the final macromolecule release can be complex to predict for hydrogels fabricated via Michael addition:

- *Molecular weight and concentration of polymer*. An increase in the polymer concentration and reduction in the molecular weight produces hydrogels with reduced mesh size values, due to the higher density of crosslinking points in both cases[22,36]. Zustiak *et al*. and Rehmann *et al*. have described that this also altered the passive diffusion of proteins through the gel,[36] affecting passive release of different size proteins[22].
- *Number of arms of polymer*. An increase in the number of arms of the polymer, and therefore the number of vinyl functionalities available for crosslinking for the same Mw has been described to reduce hydrogel swelling[178] and the mesh size[36]. This is due to the higher spatial distribution of arms around the polymer core leading to lower interpenetration and overlap of arms and reducing local fluctuation, leading to higher crosslinking density[178].

Since one key aspect of this thesis is achieving enzyme-controlled release, guaranteeing the lowest passive release possible, in order to achieve more efficient enzyme-controlled release is essential. Thus, mesh size quantification and characterisation and its influence on passive release is crucial.

3.2 Aim and objectives

This chapter explores the synthesis and characterisation of poly(ethylene glycol) (PEG) hydrogels via Michael addition of 4-arm-PEG-maleimide and dithiol crosslinker dithiothreitol (DTT) for the delivery of macromolecules. DTT is used throughout this chapter as a cost-effective model dithiol, in order to characterise the effect of different variables on hydrogel properties relevant for drug delivery.

It is our aim to systematically study how the buffer pH, Mw and concentration of polymer affect i) hydrogel formation conditions between PEG maleimide and crosslinker dithiols, ii) hydrogel's mechanical properties and mesh size, and iii) the passive release of a fluorescent dextran as a model macromolecule.

The objectives of this chapter are as follows:

- Synthesis of DTT-crosslinked 4-arm-PEG-maleimide gels and confirmation of hydrogel formation.
- Characterisation of the effect of pH, molecular weight and polymer concentration on gelation kinetics and mechanical properties of DTT-4-PEGMal gels.
- Characterisation of the effect of molecular weight and polymer concentration on the mesh size of crosslinked hydrogels.
- Reduction of passive release of model macromolecules from 4-arm-PEG-maleimide gels by tuning the molecular weight and concentration of polymer.

3.3 Results and discussion

3.3.1 Crosslinking of multi-arm-PEG-maleimide with dithiols to form chemically crosslinked hydrogels

Michael-type addition between 4-arm-PEG maleimide (4-PEGMal 5 kDa and 10 kDa) and the crosslinker dithiol dithiothreitol (DTT) was used to obtain chemically crosslinked hydrogels (Figure 3.2.a). Hydrogel formation was assessed by ^{1}H-NMR and rheological characterisation of the swollen hydrogels (as described in sections 2.7.1 and 2.7.3 of the methods chapter, respectively).

^{1}H-NMR has been extensively used to confirm hydrogel formation [9,201]. Chemical crosslinking was confirmed by disappearance of the maleimide characteristic protons at a chemical shift of 6.8 - 6.9 ppm in the NMR spectrum (labelled as protons **a** in Figure 3.2) which indicates complete reaction between maleimides and the dithiol crosslinker within the detection limit of NMR.

Oscillatory rheology is routinely used to describe the flow of viscoelastic materials, such as hydrogels, and characterise their mechanical properties and gelation kinetics.[167,173] Hydrogel

formation and stiffness were determined by measuring the storage modulus (G') and the loss modulus (G'') by oscillatory rheology. The former, G', is indicative of the elastic solid behaviour of the sample. The latter, G'', is indicative of the viscous liquid behaviour of the sample, therefore representing the solid and liquid components of the system, respectively.

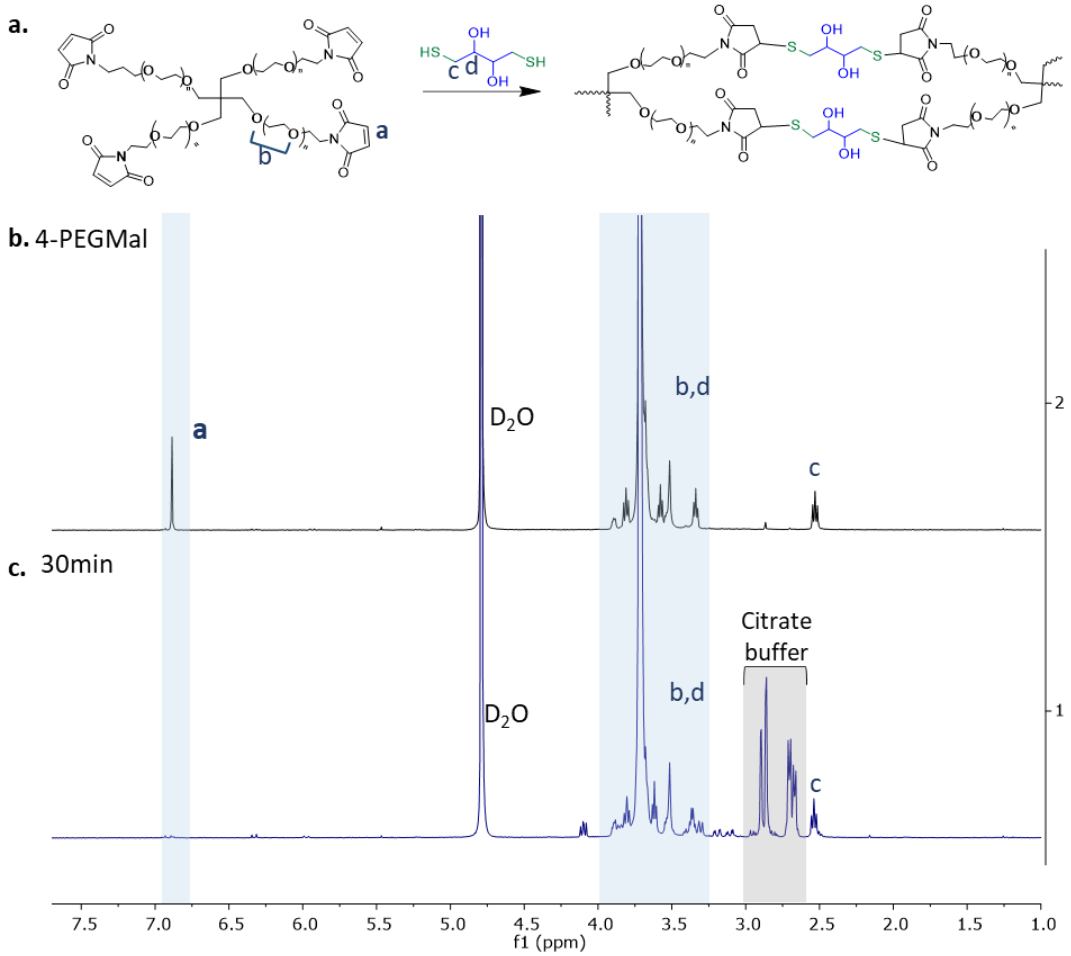

Figure 3.2. Chemical monitoring of hydrogel formation. **a.**) Michael-type addition reaction between 4-arm PEG-maleimide (4-PEGMal) and dithiol dithiothreitol (DTT), a protons highlight maleimide protons. ^{1}H-NMR of 5 kDa 4-PEGMal **b.**) before and **c**.) 30 minutes after reaction with DTT (5 % w/v in 0.1M citrate pH 4 in D_2O) showing disappearance of maleimide protons.

Hydrogels consist of macroscopic networks that limit the flow of the aqueous phase, behaving macroscopically as a viscoelastic solid. Therefore, if a hydrogel is obtained, the resulting product will be characterised by a higher storage modulus (G'>G'' predominant solid behaviour) throughout the linear viscoelastic (LVE) region. The LVE region corresponds to the amplitude (Figure 3.3.a) and frequency (Figure 3.3.b) range in which the mechanical properties of the sample

(G') are. LVE is therefore defined as the range of frequencies and strains where G' reaches a plateau.

Successful synthesis of thiol-maleimide hydrogels via Michael addition was confirmed by oscillatory rheology as storage moduli values were much higher than loss moduli in the LVE, indicating a gel-like structure (Figure 3.3). The obtained hydrogels had strong mechanical properties, with a storage modulus in the kPa range.

A frequency of 0.5 Hz and an amplitude of 0.5 % were selected for further rheological experiments as they both fall well within the LVE (0.16 to 3.17 Hz at 0.5 % strain and 0.0631 to 5 % strain at 0.5Hz). Those strain and frequency values will therefore guarantee hydrogel integrity during rheological experiments. Therefore, observed rheological properties are only due to changes in hydrogels structure.

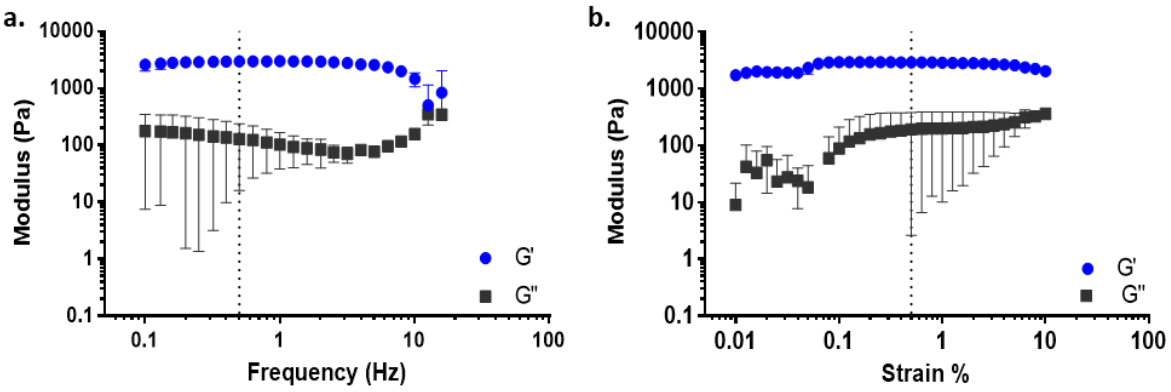

Figure 3.3. Determination of mechanical properties and linear viscoelastic region of DTT-4-PEGMal hydrogels by oscillatory rheology. **a.**) Frequency and **b**.) amplitude sweeps of preformed hydrogels swollen in PBS (10 % 10kDa 4-PEGMal, n=2). Dotted lines represent chosen amplitude and frequency within the LVE selected for further rheology measurements of 4-PEGMal hydrogels (Strain 0.5 %, Frequency 0.5 Hz).

3.3.2 Influence of pH, polymer concentration and molecular weight on mechanical properties and gelation kinetics of hydrogels prepared by Michael-addition

Physicochemical properties of hydrogels such as mechanical strength, gelation kinetics and mesh size are key when formulating hydrogels for drug delivery, as they can alter hydrogel strength, homogeneity and macromolecules encapsulation[22,173]. For this reason, the impact of pH, molecular weight and concentration of polymer on the properties of thiol-maleimide hydrogels

obtained by Michael addition reaction between 4-PEGMal and the model dithiol DTT was studied. In general, either a base or nucleophile are required as catalysts for Michael addition hydrogel formation[174]. Maleimide is the most reactive of the Michael addition acceptors and has shown superior kinetics and requires less catalyst for improved hydrogel properties[164]. We therefore aimed to obtain and characterise 4-PEGMal crosslinked hydrogels without using any catalyst, since the use of extra catalysts may compromise the biocompatibility and cytotoxicity of the materials[164].

The effect of pH on hydrogel formation was investigated as it has been shown that pH affects Michael type addition reactions[143,173,179]. Thiolates (deprotonated thiols) are the active species in Michael addition, hence, lowering the pH can effectively slow polymerisation kinetics,[174] increasing gelation time[38]. The influence of pH on hydrogel gelation kinetics was characterised by monitoring the storage (G') and loss modulus (G'') of 5 % w/v 10 kDa 4-PEGMal and DTT at pH 4, 5 and 6 (Figure 3.3 a,b) and 10 % w/v at pH 3, 4, 5 and 6 (Figure 3.3.c-e). G'' or loss modulus, indicative of viscous behaviour of the sample, does not increase after addition of the dithiol crosslinker (Appendix Figure A.1.a-d). Conversely, the storage modulus, (G'), indicative of the elastic solid behaviour of the sample, starts at lower initial values and increases as the crosslinking reaction between dithiol and 4-PEGMal takes place, until plateauing at a maximum once gelation is complete, reflecting hydrogel network formation (Figure 3.3.a and c)[143]. The gel point was used as numerical value to compare gelation kinetics at different conditions and it was described as the time at which G'>G'' (Crossover point) during gelation[39,202]. The gel point was attained within 5 min for pH 4-6, while pH 3 showed a delayed onset of gelation of ~30 min for 10 % 10 kDa hydrogels (Figure 3.3.c and Table A.1in the Appendix). pH dramatically affected gelation kinetics by reducing the gel point from 27.2 min to 0.4 min from pH 3 to pH 6 (Figure 3.3.c, Table A.1 in the Appendix). pH also affected the final G' after 1h gelation, with significantly stronger hydrogels at pH 6 than 4 (Figure 3.3.d). However, there was no significant difference in the mechanical properties of hydrogels prepared at different pH after being left to cure overnight and then

swollen in PBS (Figure 3.3.e). This data shows that while varying the pH of the medium modulates gelation kinetics, with substantial changes in gel times, it did not affect the final mechanical properties of the hydrogels.

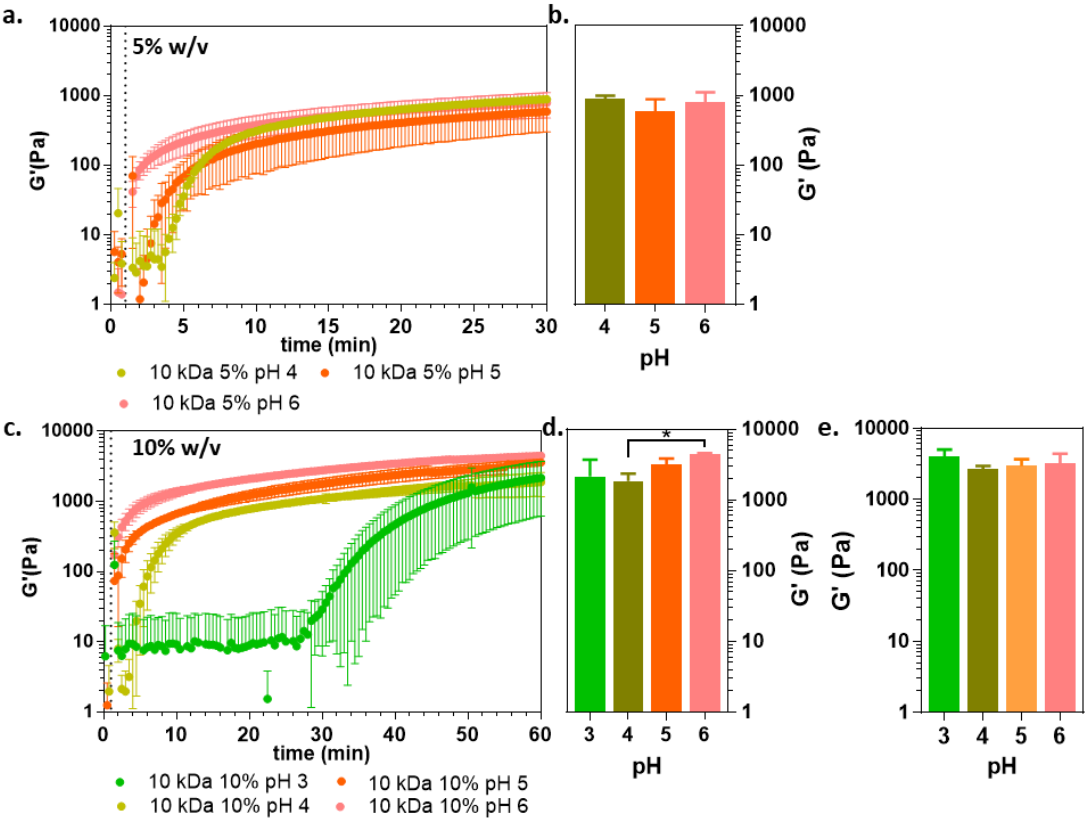

Figure 3.3. Influence of pH, on hydrogel formation kinetics and mechanical properties of 4-arm-PEGMaleimide (4-PEGMal) gels monitored by oscillatory rheology (0.5 %Strain, 0.5Hz). Effect of pH on **a,c.)** gelation kinetics, **b,d**.) storage modulus at the end of gelation, e.) storage modulus equilibrium swollen 4-PEGMal DTT-crosslinked gels. **a.**) and **b.**) represent 5 % w/v 10 kDa 4-PEGMal gels and **c.**), **d**.) and **e**.) represent 10 % w/v 10 kDa 4-EGMal data. Gelation kinetics of 5 % w/v 10 kDa gels at pH 3 are not included sinde gelation was not observed within 1 h (data not shown). * indicates statistically significant difference of G' by one-way ANOVA with Tukey post-comparisons ($p<0.05$, n=3, mean ± standard deviation). Dashed line represents addition of the crosslinker to initiate polymerisation. In gelation kinetics assays, only alternate data points of G' are shown for clarity. Gelation kinetics showing G' and G'' corresponding to graph a.) and c.) can be found in Figure A1.a. and b in the Appendix.

Similar observations were found when the concentration of polymer was lowered to 5 %. The gel point decreased with increasing pH values in a similar trend to the 10 % gels (Figure 3.3.c). As expected, decreasing the concentration of polymer and crosslinker leads to slower kinetics of crosslinking compared to 10 % hydrogels. Longer gel points than the 10 % gels at each pH were observed with 12.5, 2.5 and 0.3 min for pH 4, 5 and 6, respectively (Figure 3.3.b, Appendix Table

A.2,). Longer gel points, mean that samples will remain longer as a viscous liquid (G''>G'). This would allow for more homogeneous mixing during hydrogel preparation for 5 % hydrogels. 5 % 10 kDa hydrogels showed significantly lower G' than 10 % gels, reflecting weaker mechanical properties of the gels, as expected due to lower amount of polymer and crosslinker[179] (Figure 3.3.a-b).

Hydrogel mechanical properties and gelation kinetics can be further tailored by changing the size and concentration of the polymer[167]. Therefore the effect of the concentration of polymer (w/v) on the kinetics and mechanical properties of hydrogels was investigated more systematically. 5 kDa 4-PEGMal hydrogels were prepared at pH 3 and 4, from 5 to 30 % w/v of polymer at a 1:1 [Thiol]:[Maleimide] ratio (Figure 3.4.a-d). Increasing the polymer concentration lead to faster gelation (shorter gel points, Figure 3.4.a and c.) and significantly higher storage moduli at the endpoint of gelation at both pH (Figure 3.4.b and d) as similarly observed by other researchers[143,167]. Higher storage modulus (G') at increased polymer content indicates higher crosslinking densities

and stronger gels[22,164].

Interestingly, the mechanical properties of 20 and 30 % w/v hydrogels were not significantly different, indicating similar crosslinking densities. Similar to as shown previously with the 10 kDa 4-PEGMal gels, pH 4 hydrogels had an overall faster reaction rate (Figure 3.4.c), with shorter gel points and G' values achieving a plateau faster than the same conditions at pH 3 (Figure 3.4.a). This is due to the pH control over thiolate formation, with lower proportion of thiolate anions present at pH 3 than at pH 4, leading to slower hydrogel formation[173]. Lowering the pH is therefore promising as means to slow gelation kinetics to obtain more homogeneous hydrogels.

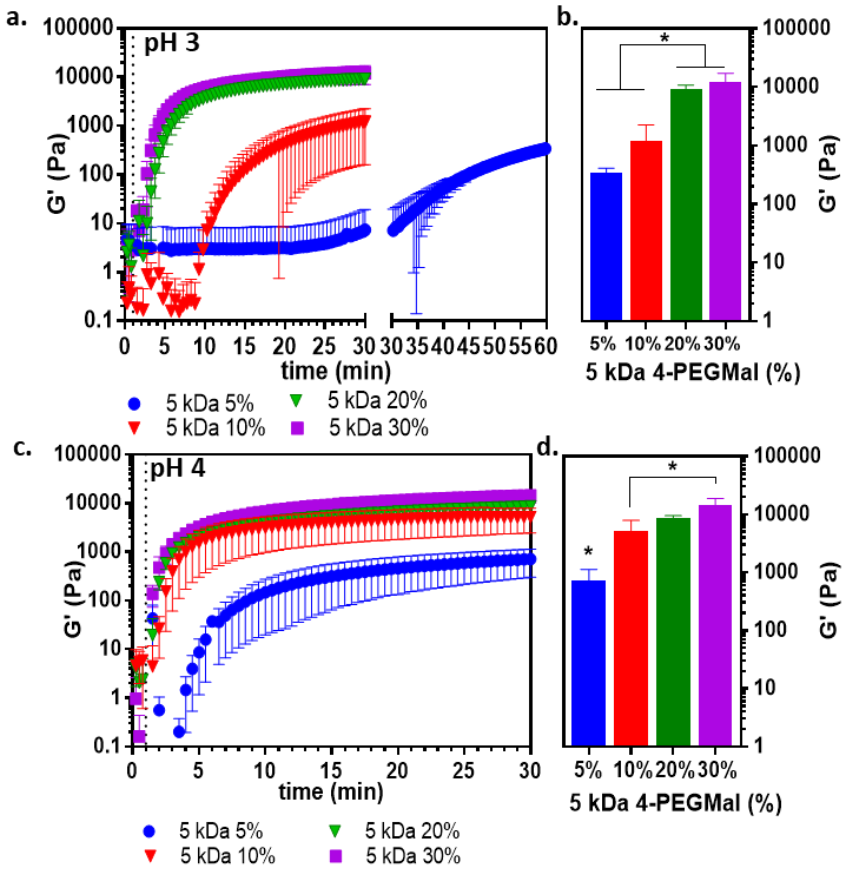

Figure 3.4. Effect of polymer concentration on the gelation kinetics (a.,c.) and final storage modulus (b.,d.) at pH 3 (a.,b.) and pH 4 (c.,d.) of 5 kDa 4-PEGMal DTT-crosslinked hydrogels. * indicates statistically significant difference of G' by one-way ANOVA with Tukey post-comparisons ($p<0.05$, n=3 mean ± standard deviation). Dashed line represents addition of the crosslinker to initiate polymerisation. In gelation kinetics assays, only alternate data points are shown for clarity.

Figure 3.5 summarises the gel points of 4-PEGMal hydrogels obtained at different polymer size and concentration (w/v) at pH 3 and 4. Overall, the gelation time was higher for hydrogels prepared at pH 3 compared to pH 4 at all polymer concentrations and Mw. Gel time was higher for the same polymer concentration for 10 kDa 4-PEGMal in comparison to the 5 kDa. 5 kDa hydrogels contain double molar concentration of maleimide groups, with an increase in the concentration of maleimide groups available for crosslinking leading to faster gelation[178]. 20 % and 30 % w/v for 5 kDa 4-PEGMal at pH 4 had very fast gel times (0.7min), versus 1.4min and 1.8 min for the same conditions at pH 3 (Figure 3.5, Table A.2 in the Appendix).

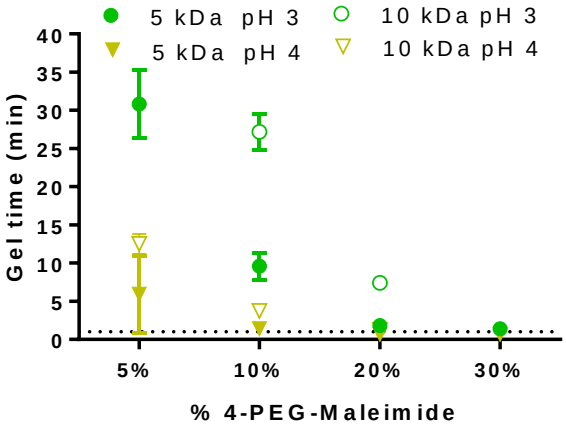

Figure 3.5. Summary of gelation times at different w/v % of polymer for DTT-crosslinked 10 kDa 4-PEGMal and 5 kDa 4-PEGMal at pH 3 and 4 measured by oscillatory rheology (n=3, mean ± standard deviation).

Too fast gelation kinetics can compromise hydrogel uniformity due to polymerisation occurring faster than mixing, leading to heterogeneous hydrogels containing high and low crosslinking density domains within the same gel, making hydrogels performance unpredictable[173]. Jansen *et al*. have shown that diffusion of macromolecules through heterogeneous hydrogels due to too fast gelation is more variable[179], and could lead to more variable release profiles. In this section three strategies were investigated to slow gelation kinetics of 4-PEGMal gels: varying the size and the concentration (% w/v) of the polymer, and reduce the pH of the buffer. We observed that decreased concentration and higher size of the polymer could efficiently slow gelation, increasing gel point. But those conditions also produced weaker hydrogels. Weaker gels formed at bigger polymer size and lower concentration of polymer have been associated with bigger mesh sizes in the network in the literature, leading to worse entrapment and passive release of macromolecules[36]. Therefore due to the potential effect of polymer size and concentration on mesh size and passive release of cargoes, they were not the chosen strategy to modulate hydrogel kinetics with applications for drug delivery and their effect on passive release should be further investigated. We have shown that while the pH of the buffer efficiently slows gelation, it does not affect the final mechanical properties of the hydrogels (Figure 3.3.e), pH 3 was chosen for the preparation of 4-PEGMal hydrogels for further experiments. This will allow longer times for homogenisation of hydrogel components at the

different polymer concentration and Mw without compromising the strength and crosslinking degree of the hydrogel networks[41].

3.3.3 Effect of molecular weight and polymer concentration on the mesh size of DTT-crosslinked hydrogels

The mesh size (ξ) is defined as the distance between two adjacent crosslinking points in the hydrogel network. It is considered a key parameter dictating effective drug encapsulation and passive release[22,34]. Polymer concentration and MW of the polymer in PEG hydrogels can influence their mesh size, altering macromolecule entrapment and passive diffusion through the hydrogel network, thus modifying their passive release. This is due to bigger mesh sizes offering less hindrance to the diffusion of macromolecules, whereas smaller mesh sizes allow higher entrapment of macromolecules within the hydrogel network, reducing their relase[22,35,36]. It is therefore important to evaluate the effect of polymer concentration and size on the mesh size of the obtained hydrogels, since it will condition the encapsulation and passive release of the entrapped macromolecules.

The effect of polymer concentration (5, 10 and 20 % w/v) and size (5 kDa and 10 kDa) on the mesh size of 4-PEGMal hydrogels crosslinked with DTT as a model dithiol was evaluated. Mesh size was calculated based on hydrogel swelling ratio (see TABLE A. 2 in the Appendix for swelling values), as described in section 2.7.2, and widely used for PEG hydrogels[22,36,191].

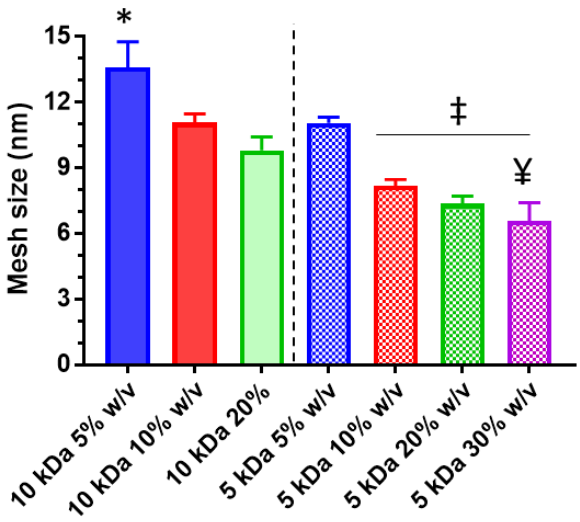

Figure 3.6. Effect of polymer concentration and Mw on the mesh size of DTT-crosslinked hydrogels. Symbols indicate statistically significant differences by one-way ANOVA with Tukey post-comparisons ($p<0.05$, n=4). *indicates different from all; ‡ from 10 kDa 10 %, 10kDa 20 % and 5kDa 5 %; ¥ from 5kDa 10 %.

The molecular weight of the polymer had a significant effect on the mesh size, with 5 kDa hydrogels showing significantly smaller mesh sizes than their 10 kDa equivalents at all polymer concentrations (Figure 3.6). This is due to the smaller molecular weight polymers having shorter PEG chains per molecule and, at the same mass, increased molar concentration of maleimide groups available for polymerisation. Overall, smaller size and increased concentration of polymer lead to a reduction in the mesh size of 4-PEGMal hydrogels (Figure 3.6). This trend indicates higher crosslinking densities are achieved at higher polymer concentrations and smaller Mw, being consistent with the increased mechanical properties (Figure 3.3 and 3.4), and with reported values in the literature[22,167]. The obtained mesh size values are within the same range as other PEG-based hydrogels prepared under similar conditions by Zustiak *et al.*[38]and Rehmann *et al*.[22]. The reduced mesh size values below 10 nm obtained are promising for efficient physical entrapment of macromolecules, as they are in the same range as the hydrodynamic dimeter (D_h) of several therapeutic macromolecules[14,22,36].

3.3.4 Effect of molecular weight and concentration of polymer on passive release of dextran from DTT-crosslinked hydrogels

Since the different crosslinking conditions of 4-PEGMal hydrogels affect the structure of the resulting network, it is important to understand the effects these crosslinking conditions can have on the encapsulation and release of macromolecules. The influence of Mw and concentration of polymer on the ability of 4-PEGMal hydrogels to encapsulate and modulate the release of a 70 kDa fluorescent dextran (Texas Red, TRD70) as the model macromolecule (Dh ~ 12 nm) was assessed. TRD70 was used as the model fluorophore since it has a similar size to the elastase inhibitor that will be encapsulated in this project (alpha-1-antitrypsin) and will be indicative of the release profiles that could be achieved with the protein under same conditions.

Dextran was incorporated during hydrogel formation and its encapsulation (10 μg/μL) and release was measured by periodical analysis of the release medium as described in section 2.7. Only 10 % and 20 % w/v hydrogels are represented as 5 % w/v hydrogels did not reproducibly lead to hydrogel formation. A trend was observed displaying improved encapsulation efficiency at higher concentration of polymer and lower size, with the 20 % 5 kDa gels showing the best entrapment (Figure 3.7.a). All hydrogel formulations showed an initial burst release during the first 6h (Figure 3.7.b) with a much slower release from 48 h onwards. This can be attributed to the swelling of hydrogels in aqueous medium, which occurs during the first 24 h and then it stabilises at an equilibrium swelling value (see Table A.1 and Figure A.2 in the Appendix).

It has been shown that reduced release of macromolecules can be achieved by either reduced molecular weight or increased concentration of the polymer[22,35,36]. This is due to the increase in crosslinking hindering the diffusion of the macromolecules through the hydrogel network, therefore controlling the release rate[35,36]. We therefore expected the maximum amount of dextran released (D_{max}) to be directly related to the crosslinking degree of the hydrogels (highest D_{max} for 10 kDa 10-PEGMal 10 % w/v and lowest for 20 % w/v 5 kDa). D_{max} from 10 %

5kDa 4-PEGMal gels was significantly higher than all the other hydrogel conditions (Figure 3.7). As hypothesised, 5 kDa 4-PEGMal hydrogels showed better retention of dextran with a significantly lower Dmax after 15 days than the 10 % w/v ones although it was not significantly different from 10 % 10 kDa and the 20 % 10kDa (Figure 3.7, Table.A.2 in the appendix).

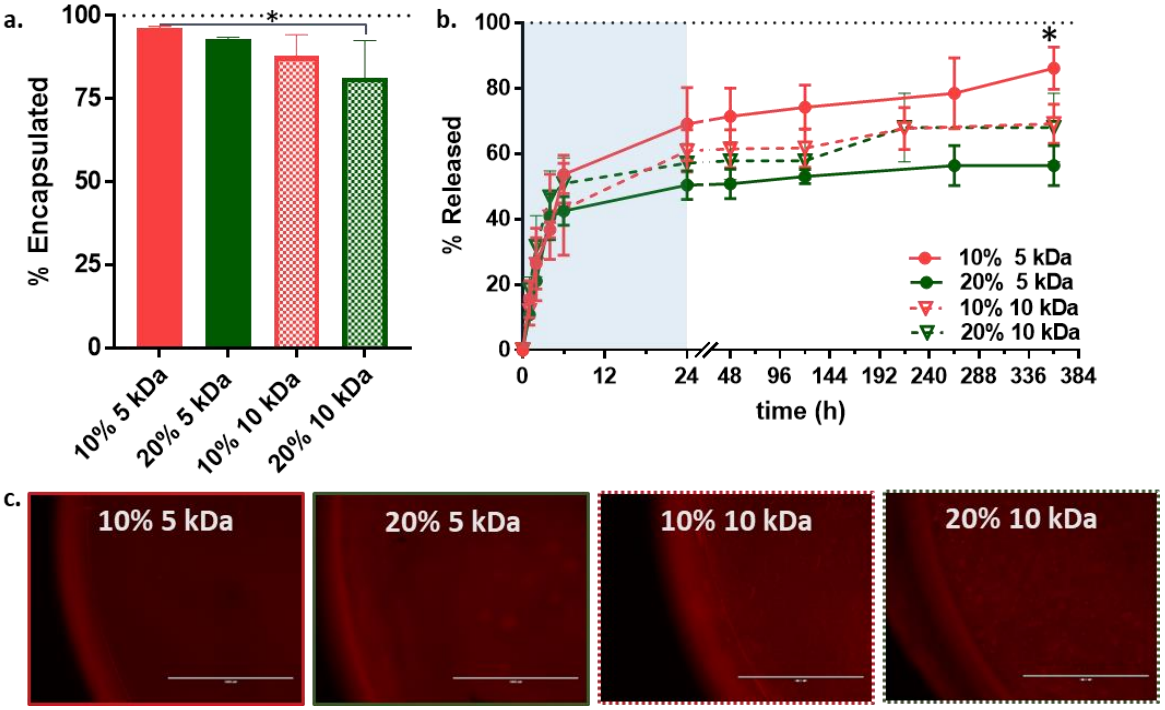

Figure 3.7. Encapsulation and release of 70kDa dextran (TRD70) from DTT-crosslinked hydrogels. Effect of polymer concentration and size on **a.**) Encapsulation and **b.**) passive release of 70 kDa dextran. **c.**) Fluorescence microscopy images of hydrogel-medium interfaces at release endpoint, confirming TRD70 is confined within the gel area (day 15, scale bar 1 mm).* indicates statistically significant difference on encapsulation efficiency and on final amount released by one-way ANOVA with Tukey post-comparisons ($p<0.05$, n=4, mean ± standard deviation).

3.3.5 Correlation between hydrogel mesh size and dextran release from DTT-crosslinked hydrogels

The value of mesh size obtained for a given hydrogel composition has been used as an approximate prediction of their efficiency and release kinetics and encapsulation of macromolecules of known sizes[22]. Although some deviations of predicted release from mesh size data can occur[22], in general a reduction of mesh size correlates with a reduction in the amount of macromolecule released. If the mesh size is much bigger than the hydrodynamic diameter (Dh) of

the encapsulated molecule (Dh<<ξ), the diffusion of the molecule will be essentially unaffected, leading to a burst release profile and near 100 % release from the gel (Figure 3.8.a)[1,14,22]. In contrast, hydrogels with mesh sizes smaller than the size of the encapsulated cargo (Dh>>ξ) usually lead to macromolecule diffusivities close to zero, achieving almost total encapsulation and 0 % release. Intermediate situations (Dh~ξ) lead to hindered diffusivity through the hydrogels, typically resulting in an initial burst release followed by a slow release phase with a variable amount of macromolecule effectively being retained depending on the conditions (Figure 3.8.a)[1,14,22].

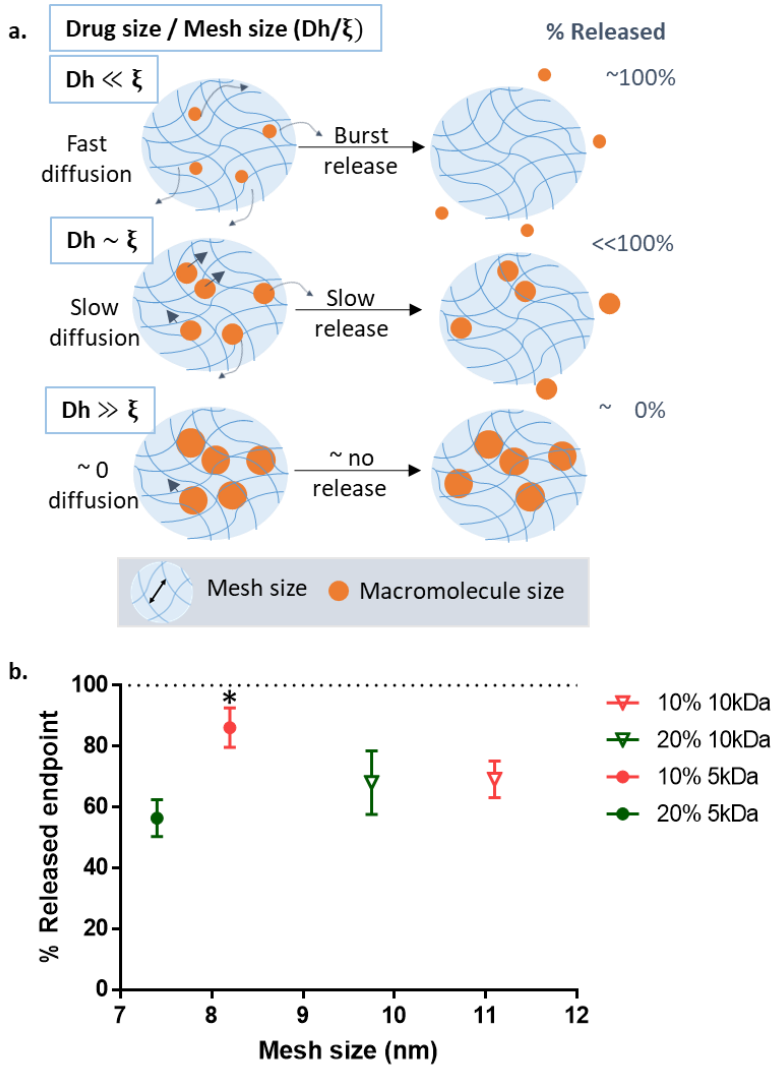

Figure 3.8. Mesh size and passive release from hydrogels. **a.**) General mechanism of macromolecule release from hydrogels depending on the relative relation between the mesh size (ξ) and macromolecule sizes measured as their D_h. **b.**) Correlation between hydrogel mesh size determined by swelling and the total amount (in %) of 70 kDa dextran (Dh ~12 nm) released at the endpoint of release experiment (day 15).* indicates statistically significant difference of final amount released by one-way ANOVA with Tukey post-comparisons ($p<0.05$, n=4, mean ± standard deviation).

TRD70 is approximately 12 nm in diameter and the mesh size of the hydrogels ranged from 6.6 to 11 nm, placing the developed 4-PEGMal hydrogels in the latter category of similar mesh and macromolecule sizes (Dh~ξ). Our release results are in agreement with those observations; as all hydrogels showed a burst release and then slow release (Figure 3.7a), with dextran still remaining in all formed hydrogels at the endpoint of release (Figure 3.7.c). In order to further correlate mesh size and dextran release, Figure 3.8 shows the maximum concentration of dextran released at the endpoint of the release (D_{max}) as a function of the determined mesh size of the hydrogels. With the exception of the 10 % 10 kDa hydrogels, an overall increase in the mesh size led to an increase in D_{max}. This is in agreement with similar PEG-based hydrogel systems and macromolecules studied in the literature[22,35].

3.4 Conclusions

The scope of this chapter was to develop and characterise the formation of PEG hydrogels by Michael addition and to evaluate the effect of buffer pH, and polymer size and concentration on the kinetics of gelation, mesh size and macromolecule entrapment. PEG hydrogels prepared via Michael addition between multi-arm PEG-maleimide and the model dithiol (DTT) as crosslinker showed full maleimide crosslinking and led to strong mechanical properties in the kPa range. Lowering the pH of the reaction solution affected the crosslinking kinetics, but not the mechanical properties of hydrogels. Decreasing the polymer concentration slowed gelation kinetics but also affected hydrogel strength and increased passive release. Therefore lowering the pH of the buffer to 3 was used as strategy to obtain slower kinetics, suitable for homogeneous hydrogel preparation. Under those conditions, the influence of the molecular weight and concentration of 4-PEGMal effect on mechanical strength, mesh size and passive-diffusion from DTT 4-PEGMal hydrogels was characterised. Higher concentration and smaller Mw of the PEG macromere led to stronger hydrogels with smaller mesh size and improved passive release of dextran, used here as

a model macromolecule. A direct relationship between mesh size and passive release from hydrogels was observed, with the 20 % w/v hydrogels showing a superior performance in reducing passive release of TRD70 and being the selected composition for protease-responsive hydrogel preparation.

Chapter 4.

Development of elastase-responsive hydrogels for controlled release

4.1 Introduction

In this chapter we will develop an elastase-responsive peptide dithiol which will then be used as crosslinker between polymer strands to generate elastase-responsive hydrogels. The incorporation into hydrogels will be conducted via Michael addition with the fabrication method optimised in Chapter 3 using a model dithiol.

4.1.1 Elastase-controlled drug delivery

The development of stimuli-responsive delivery strategies is a growing field within drug delivery, particularly the development of materials offering stimuli-responsive delivery upon contact with disease-specific molecular cues[7,105]. For instance, hydrogels able to undergo selective degradation by enzymes overexpressed in pathological states are an attractive strategy restricting drug release temporally and spatially to the desired site of action. This is achieved by appropriate selection of the target enzyme and material design[7,115]. Recent research showed that once the material is at the targeted site, drug release is triggered via enzymatic degradation of the hydrogel, decreasing the amount of off-target effects and achieving therapeutic efficacy *in vivo* model[115].

In order to achieve the enzyme-controlled release mechanism, peptides that are recognised as substrates by the targeted protease need to be incorporated in the hydrogel network, as represented in Figure 4.1.a. Then, in the presence of the targeted protease, the enzyme will recognise the targeting sequence (Figure 4.1.b), leading to cleavage of the peptide and triggering drug release. This will then translate into hydrogel degradation and cause the release of the entrapped cargo (Figure 4.1.c).

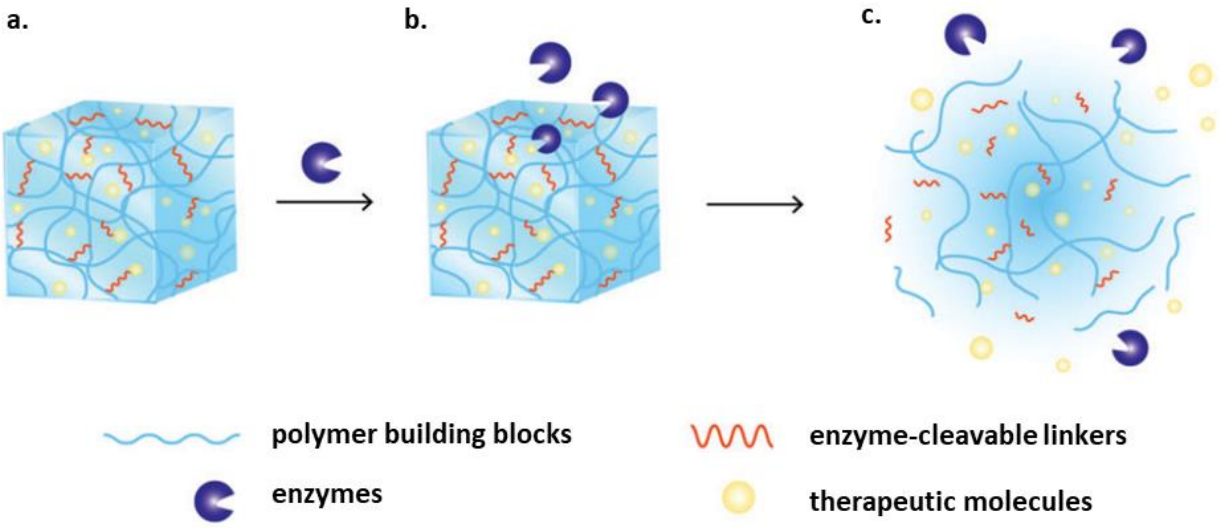

Figure 4.1. Mechanism of controlled release from enzyme-responsive hydrogels. **a.**) Incorporation of enzyme-recognised elements. **b.**) Degradation of the linkers by the targeted enzyme. **c**.) Cleavage of the enzyme-substrate linker translates into degradation of the hydrogel and release of the therapeutic molecules. Image adapted from Chandrawati[7].

4.1.1.1 Introduction of elastase-sensitive functionalities

As described in section 4.1.1, selection of a linker which can be specifically recognised and degraded by the target enzyme is a key requirement to achieve efficient enzyme-controlled release. Since elastase is the targeted protease, it is necessary to select a peptide sequence that can be cleaved by elastase and incorporate it into the polymeric backbone of the hydrogel. The design of synthetic peptides which can be selectively cleaved by elastase has been investigated for sensing[117,203–206], drug delivery[39,132] and tissue engineering[207,208] applications.

Despite its clinical implications, the literature available on short synthetic elastase–sensitive peptides is limited and is summarised in table 4.1. Human Neutrophil Elastase (HNE) cleaves peptide sequences after small neutral amino acids, such as valine and alanine with a higher specificity for valine (BRENDA:EC 3.4.21.37[81]). Accordingly, the peptide sequences found could be grouped into three classes: i) poly-alanine containing sequences where the peptide is cleaved between alanine residues; ii) peptides cleaved after an isoleucine residue; and iii) peptides cleaved after a valine residue.

i) *Poly-alanine sequences* (cleavage between alanine residues, entries 1-5 in Table 4.1). Sequences containing several consecutive alanine residues of lengths varying from 2 to 8 amino acids have been reported to be cleaved by elastase[40,203,207,208]. Although some of these references have employed Porcine Pancreatic Elastase (PPE) in their assays and some did not specify which type of elastase was employed. PPE (E.C. 3.4.21.36) is considered as a different enzyme to HNE with broader specificity. PPE cleaves peptides after small amino acids with a preferential cleavage site after alanine residues (BRENDA:EC3.4.21.36). This was demonstrated by Patrick *et al.* who found that elastase (using PPE) cleaved the peptide AAPV after the alanine residue and not after the valine[203]. Guan *et al*. designed scaffolds incorporating AAK motifs, and showed that elastase-controlled degradation was very slow, taking weeks to achieve 40 % degradation. Interestingly, they reported that their scaffolds were not responsive to collagenase, which indicates some specificity of the sequence[207]. A different approach for obtaining elastase-responsive materials used copolymerisation of amino acids to lead random copolymers of alanine instead of residue by residue assembly[209]. Although this approach has been successful for the design of polymers containing poly-alanine domains, the degree of control of the amino acid sequence is not enough when more complex sequences, involving a specific order of different residues are required.

ii) *Sequences cleaved after an isoleucine residue* (entries 6 -7 in Table 4.1). Korkmaz *et al.* developed several elastase sensitive sequences in order to produce specific fluorogenic HNE substrates not recognised by other proteases. Among the synthesized sequences, the peptide sequence APEEI↓MRR was selectively degraded by HNE, and not degraded by similar enzymes from the serine protease family such as proteinase 3, Cathepsin G and Trypsin[204].

Table 4.1 Summary of elastase-sensitive peptide sequences

Entry	Peptide sequence	Application	Ref
1	$[A]_n[E]_n$	Design elastase-responsive materials	209
2	AAAAA↓AAAAK	Elastase-degradable scaffolds	208
3	$_{DABCYL}$AA↓PVE$_{EDANS}$	Fluorogenic detection and management of elastase (PPE)	203
4	DA↓AR A↓ARGD	Enzyme-responsive hydrogel swelling (PPE) Enzyme-responsive surface modification	40,210
5	A↓AK	Elastase degradable scaffolds (PPE)	207
6	AbzAPEEI↓MRRQ-EDDnp	Design of fluorogenic substrates specific to HNE	204
7	-FI↓RW-	Fluorescence detection of elastase (HNE)	117
8	Suc-AAPV↓-pNA (1) Suc-AAPA↓-pNA (2)	Colorimetric detection of elastase (HNE)	153,206
9	Suc-AAPV↓-AMC (1) Suc-APA↓-AMC (2)	Fluorogenic detection of elastase (PPE and HNE)	205
10	CGAAPV↓RGGGGC CGAAPNva↓GGGGGC	Elastase responsive release (HNE)	39
11	K$_{ROX}$AAPV↓RGGGK$_{QXL}$ AAPV↓RGMG AAPNva↓GGMG	Spatial detection Elastase and responsive release (HNE)	132

Elastase sensitive functionalities are highlighted in blue. Arrows represent protease cleavage site. The type of elastase is indicated when specified by the authors: Porcine Pancreatic Elastase (PPE) and Human Neutrophil Elastase (HNE). Other abbreviations: Dab = 4-{[4-(dimethylami- no)phenyl]azo}benzoic acid, EDANS = 5-[(2-aminoethyl)- amino]naphthalene-1-sulfonic acid, Abz = orthoaminobenzoic acid, EDDnp = Ethylenediamine, p-NA = para-nitroanilide, QXL = QXL® 610 acid, ROX = 5(6)-Carboxyrhodamine, Suc = N-succinyl.

iii) *Sequences cleaved after a valine residue* (entries 8 – 11 in Table 4.1). The AAPV sequence has been the more commonly used motif for elastase-responsive detection[153,205,206] and responsive drug delivery[39,132], and is also widely used and commercially available for the characterisation of elastase activity[195,211]. Edwards *et al* used colorimetric substrates with AAPV and AAPA for quantification of elastase activity for chronic wound applications[153,206]. A later study from the same researchers including fluorogenic detection with the same peptide sequences found increased cleavage of the AAPV sequence with respect to APA by HNE in solution[205]. It was also observed that the APA substrate was more susceptible to cleavage by PPE than HNE[205]. This suggests the alanine residues before cleavage site are more favourable for applications targeting pancreatic elastase while the AAPV sequence, where

cleavage takes place after the valine residues, are more favourable for HNE targeting. This is confirmed by Patrick *et al.* (entry 3) who observed that their FRET substrates containing an AAPV sequence were cleaved after alanine using PPE[203]. The whole elastase sensitive sequence AAPVRGGG has been employed in two publications by Aimetti *et al.* to form elastase-responsive hydrogels with different applications. Although the two crosslinking chemistries were different, in both cases the sequence cleavage by HNE triggered hydrogel degradation[39,132].

Among the previous studies, only a few reports have focused on incorporating the elastase-responsive sequences into elastase-responsive delivery systems that specifically target neutrophil elastase[39,132]. Therefore the fabrication, systematic characterisation of passive entrapment, and enzyme-controlled release from elastase-responsive hydrogels remains unresolved. In order to fabricate hydrogels with suitable elastase-responsive properties the selection and synthesis of a peptide with suitable water-solubility, and specificity towards Human Neutrophil Elastase is important. With this purpose, the elastase-sensitive sequence AAPVRGGG developed by Aimetti *et al.*[39,132], was selected as to be integrated into crosslinkable peptides. The crosslinker would be subsequently incorporated into hydrogels in order to characterise their capabilities for physical entrapment of macromolecules and elastase-controlled release.

4.2 Aim and objectives

The aim of this chapter is to fabricate and characterise elastase-sensitive hydrogels suitable for the encapsulation of macromolecules.

In order to achieve this aim, the objectives of the chapter are:

- The design of a soluble elastase-responsive peptide suitable for crosslinking via thiol chemistries.

- The crosslinking of elastase-sensitive peptides with 4-arm-PEG-Maleimide (4-PEGMal) for the fabrication and physicochemical characterisation of hydrogels via Michael addition.
- The characterisation of the passive and elastase-controlled release abilities of the developed hydrogels.

4.3 Results and discussion

4.3.1 Design and synthesis of an elastase-sensitive sequence for incorporation into hydrogels

4.3.1.1 Synthesis of elastase-sensitive peptide and characterisation of elastase-responsiveness

To achieve elastase-controlled delivery hydrogels it is important to design a suitable elastase-cleavable crosslinker. The initial peptide was designed including an elastase-sensitive sequence AAPVRGGG[39,132] flanked by two terminal cysteine residues in order to allow reaction with 4-arm-PEG-Maleimide polymer (peptide **1**, structure on Figure 4.1.a). All synthesised peptides (peptide **3 – 6,** Figure 2.1) were acetylated on the N-terminus and amide-terminated on the C-terminus. This avoids the presence of charges in the vicinity of the thiols which could lead to altered reaction kinetics by Michael addition[173,177].

The crude peptide (**1**) was analysed by ESI-MS to confirm that the synthesis was successful. Both protonated and sodium adducts corresponding to the reduced (protonated thiols) and oxidised (oxidised thiols) forms of the peptide were observed in the spectrum (Figure B.1 in Appendix B).

The confirmation of cleavage of the crude peptide (**1**) was assessed by incubation with the model elastase PPE (Figure 4.2.a). Concentration of PPE is stated as U/ml throughout this work, and the method of unit calculation can be found in section 2.13.1 in the methods chapter. The

proteolytic cleavage of peptidyl bonds in the peptide was confirmed by monitoring the appearance of *de novo* primary amine groups with the fluorescamine assay[123,193,212]. Controls consisting on peptide in buffer and enzyme in buffer were also conducted in order to account for primary amines present in both samples. The fluorescence increase in the peptide samples when incubated with elastase but not in the enzyme or peptide alone, suggests an increase in free amino groups due to the proteolytic cleavage of the peptide (Figure 4.2.b). The high magnitude of increase of fluorescence in the reaction medium could be due to cleavage taking place at more than one point in the sequence. Alternatively, since the crude peptide that was used for the assay was not fully soluble, it was used as a suspension. Therefore as some substrate is degraded by the enzyme, more substrate is solubilised and available for degradation.

Cleavage samples were additionally analysed by Reverse Phase High Pressure Liquid Chromatography Mass Spectrometry (RP-HPLC-MS) in order to confirm cleavage site. For comparative purposes, the C-terminus sequence of the expected cleavage site H-RGGGC-NH_2 (peptide 2) was synthesised and characterised by RP-HPLC-MS as well. Full details of HPLC and ESI-MS confirming synthesis of peptide 2 can be found in Appendix B, Figure B.2. RP-HPLC-MS analysis of elastase substrate (2) revealed appearance of the mass corresponding to the oxidised cleaved peptide fragment H-RGGGC-NH_2 (2, $[M_{oxid}+H]^+$ 447.2) was present only after incubation with elastase, ($[M_{oxid}+H]^+$ 447.2 at r.t. 0.33min. Figure 4.2.d) and absent if the substrate was incubated only in buffer (Figure 4.2.c).

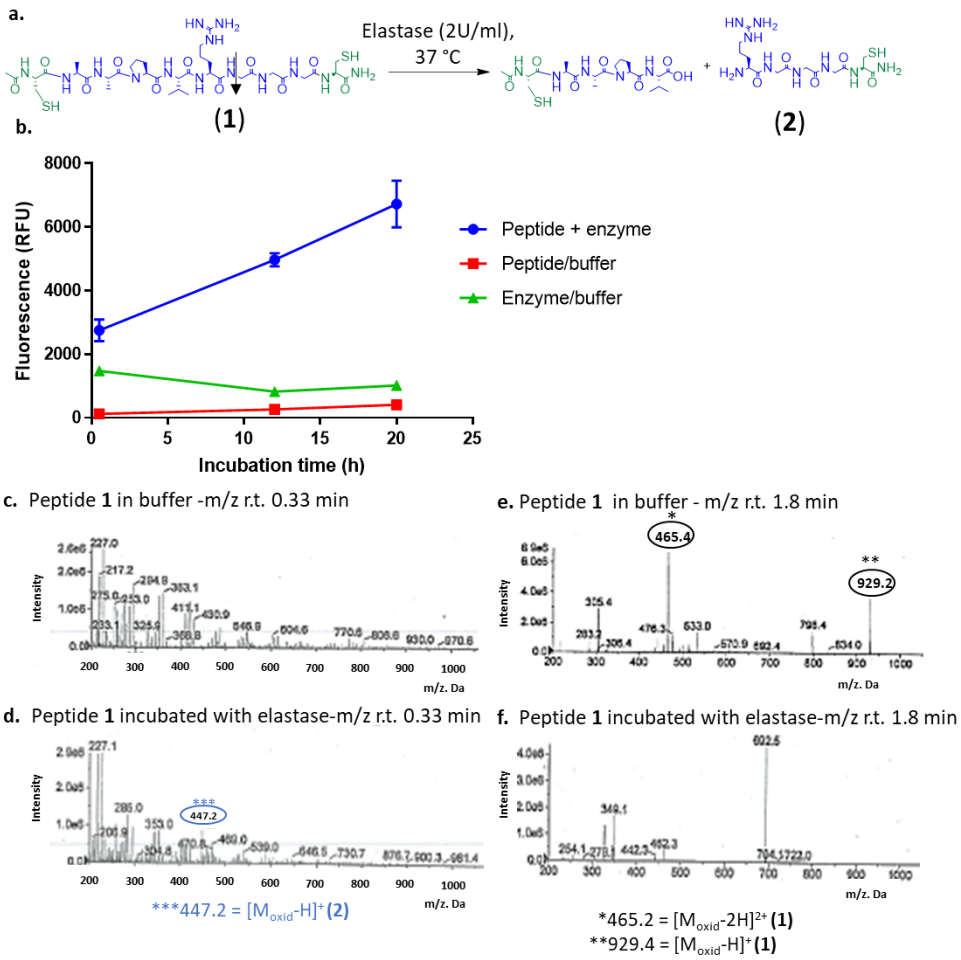

Figure 4.2. Verification of peptide (**1**) cleavage by elastase. **a.**) Schematic of elastase cleavage to predicted cleaved fragments Ac-CAAPV and H-RGGGC-NH_2 (peptide 2), **b.**) Monitoring of cleavage over time with fluorescamine assay (n=3). **c.-f.**) RP-HPLC-MS analysis of enzymatic cleavage assays. **c.**) and **d.**) mass spectra at r.t. 0.33 min from peptide Ac-CAAPVRGGGC-NH_2 (1) incubated **c.**) in buffer and **d.**) with elastase. $[M_{oxid}+H]^+$ of 447.2 corresponding to the thiol oxidised product of cleavage H-RGGGC-NH_2 (2) is only present in the peptide sample incubated with the enzyme d.). e.) And f.) mass spectra at r.t. 1.8 min of the peptide control incubated e.) in buffer and f.) with elastase. $[M_{oxid}+H]^+$ $[M_{oxid}+H]^{2+}$ of 9292.4 and 465.2 from the uncleaved peptide substrate Ac-CAAPVRGGGC-NH_2 (1) are only present in the peptide in buffer control (e.) and absent after incubation with elastase(f.).

Protonated forms that are characteristic of the uncleaved peptide (Ac-CAAPVRGGGCNH$_2$, 1) were present in the samples left in buffer and disappeared after incubation with elastase ($[M_{oxid}+H]^+$ 929.4, $[M_{oxid}+2H]^{+2}$ 465.4, r.t. 1.8 min, Figure 4.2.e and f). This disappearance of the peak characteristic of the uncleaved peptide and appearance of the peak corresponding to the H-RGGGC-NH_2 fragment, confirm the cleavage of the peptide. No peaks associated with the N-terminus fragment of the peptide (Ac-CAAPV) were observed in the samples. This could be

explained since the model elastase (PPE) is a broad spectrum enzyme that cleaves after small aliphatic amino acids such as alanine (BRENDA:EC3.4.21.36, BRENDA database). This can lead to the cleavage of the sequence fragment at other points (e.g. CA↓APV or CAA↓PV)as previously observed[203], being in agreement with the high increase in primary amines observed with fluorescamine assay (Figure 4.2.b). The results of quantification of primary amines together with the mass spectrometry analysis confirm the cleavage of the designed sequence by the model elastase. It also suggest that the cleavage may take place at more than one point. More importantly, the cleavage of the sequence will allow elastase-triggered release from peptide-crosslinked hydrogels, regardless of cleavage taking place at more than one sites in the peptide sequence.

In order to be used for hydrogel formation, the elastase responsive peptide (**2**) was purified. Since the m/z of the peptide was observed in two fractions of the HPLC chromatogram (Appendix B, Figure B.1), both fractions with r.t. 3.36 min (designated as fraction 1) and 3.68 min (designated as fraction 2) were purified by RP-HPLC. Due to solubility issues it was impossible to dissolve the purified products for further characterisation. The two purified fractions were insoluble at 0.1 mg/mL in several solvents with different polarities (water, DMF, methanol, isopropanol, hexafluoroisoproanol [HFIP] and DMSO). Both purification fractions were dissolved in 10 % TFA/ water (1mg/mL) to allow characterisation by MALDI-ToF-MS. It was shown that both reduced and oxidised forms of the peptide ($[M_{oxid}+H]^+$ 929.4, $[M+H]^+$ 931.4, and ($[M_{oxid}+Na]^+$ 951.4, $[M+Na]^+$ 953.4) were found in both HPLC fractions (Figure 4.3) Distribution of the oxidised and reduced form of the peptide varied between both fractions, with the oxidised form being the predominant in the first fraction and the reduced in the second. This confirm the purification of peptide (**2**) and that the presence of two HPLC fractions was not due to impurities, but due to differences in peptide oxidation. Although the peptide could be solubilised in a mixture of TFA-water, this is not suitable for any further application, due to high toxicity of TFA.

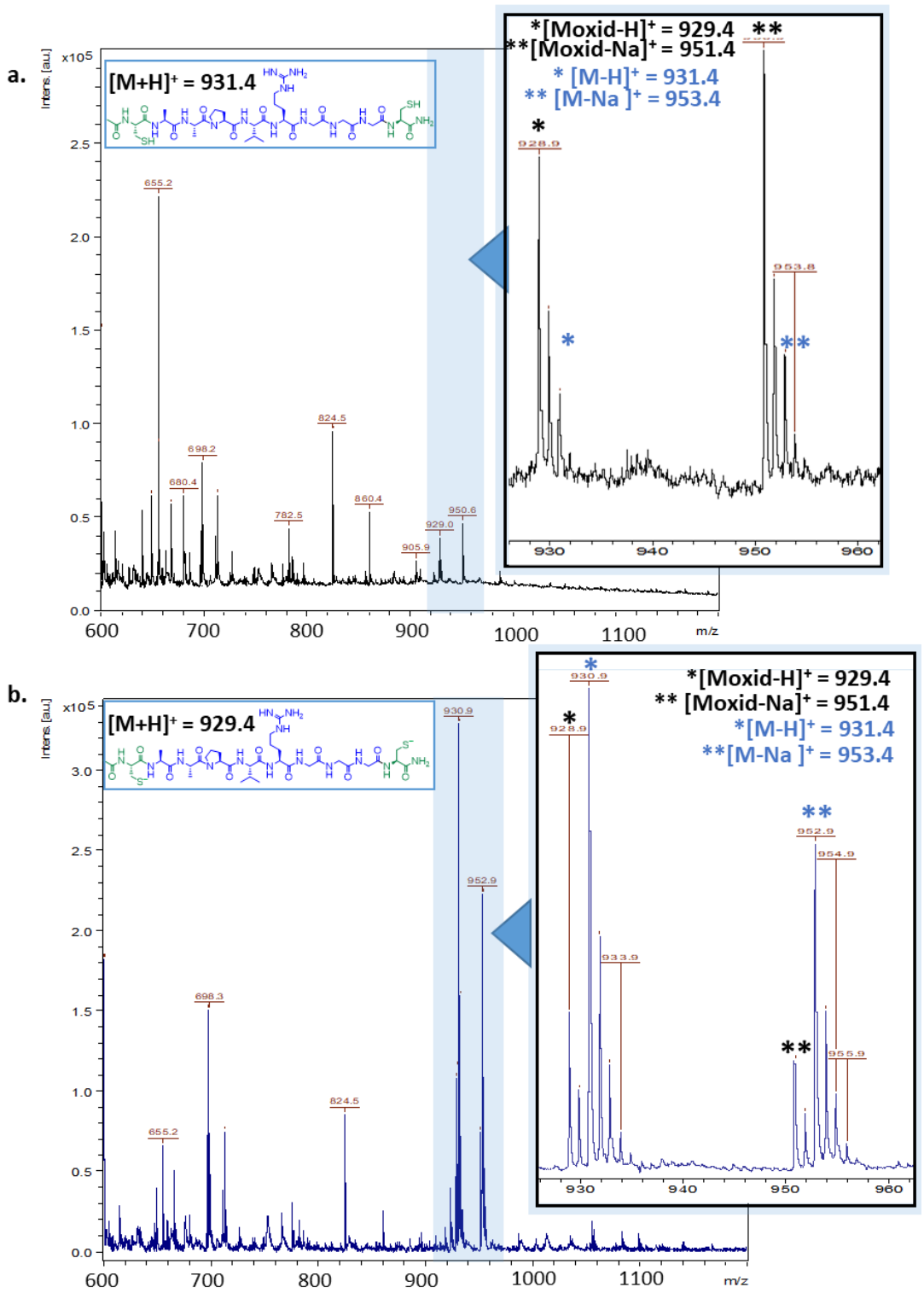

Figure 4.3. MALDI-ToF-MS of the two RP-HPLC purified fractions from peptide Ac-CAAPVRGGGC- NH_2 (**1**). **a**.) RP-HPLC fraction 1 (r.t 3.4min in RP-HPLC), **b**.) RP-HPLC fraction 2. (r.t. 3.7min in RP-HPLC). Detail of peptide region and assignment of adducts from reduced and oxidised forms of peptide for both fractions included. $[M+H]^+$ and $[M+Na]^+$ adducts for the oxidised peptide are noted in black ($[M_{oxid}+H]^+$ predicted 929.4, $[M_{oxid}+Na]^+$ predicted 951.4; $[M_{oxid}+H]^+$ observed 928.9, $[M_{oxid}+Na]+$ observed 950.9). $[M+H]^+$ and $[M+Na]^+$ adducts for the reduced peptide ($[M-H]^+$ predicted 931.4, $[M+Na]^+$ predicted 953.4; $[Moxid+H]^+$ observed 928.9, $[M_{oxid}+Na]^+$ observed 950.9) are noted in blue. m/z= 698 was also found in the matrix blank (data not shown).

4.3.1.2 Synthesis of elastase-responsive peptides with enhanced solubility (3 – 6)

Since the low water solubility of peptide **1** meant it could not be used for hydrogel formation, a series of peptide analogues were designed to improve the hydrophilicity of the molecule (Figure 4.4.a). For this purpose two hydrophilic and charged amino acids were incorporated between the elastase sensitive section and the cysteine residues at the end of the sequence (peptides 3 - 6).We hypothesised that this approach could improve solubility while maintaining both elastase sensitivity and thiols for crosslinking. The synthesis of the sequences was confirmed by ESI-MS (Appendix B, Figure B.3).

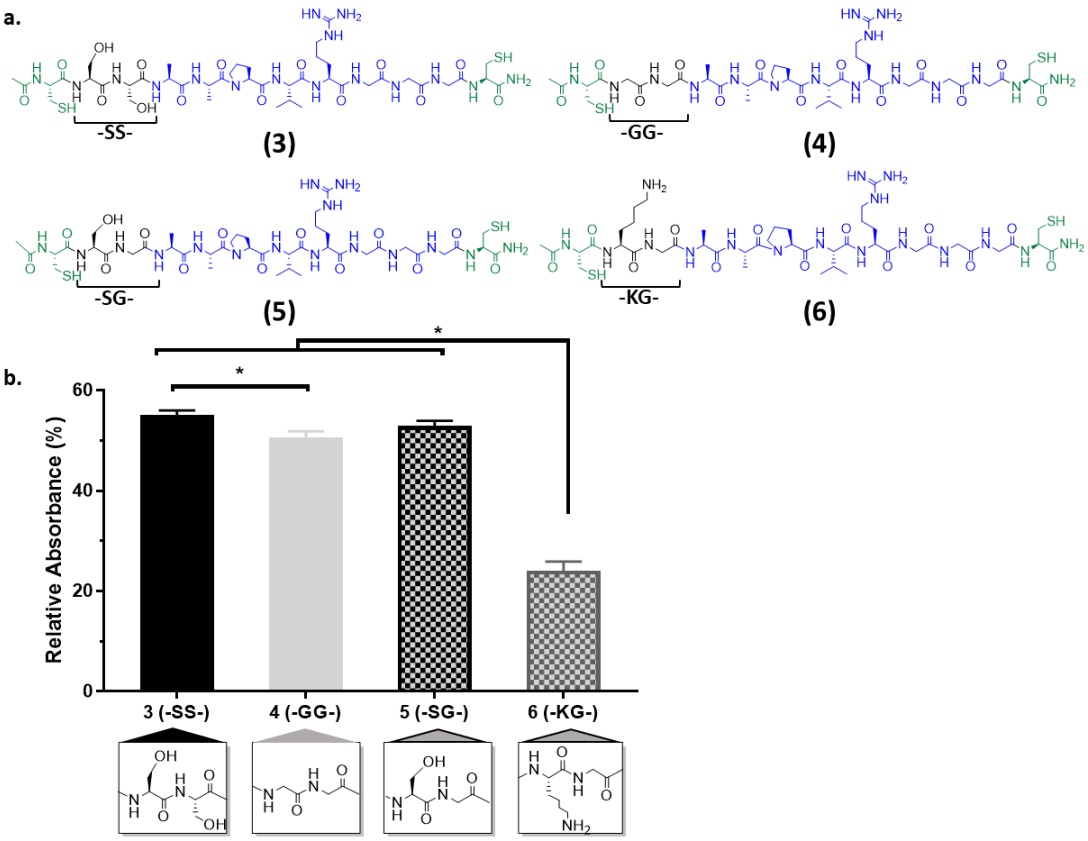

Figure 4.4. Elastase-cleavable peptide analogues for improved water solubility. **a**.) Peptide structures: (3) Ac-CSSAAPVRGGGC-NH_2, (**4**) Ac-CGGAAPVRGGGC-NH_2, (**5**) Ac-CSGAAPVRGGGC-NH_2, (6) Ac-CKGAAPVRGGGC-NH_2. Cysteine moieties are represented in green, elastase-sensitive sequence is in blue and hydrophilic amino acids additionally added to increase solubility in black and highlighted.**b**.) Estimation of relative solubility of peptides 3 – 6. Relative absorbance (concentration AUC of peptide respect to Fmoc-Gly internal standard) of each elastase-responsive peptide analogue. (**3**) Ac-CSSAAPVRGGGC-NH2, (**4**) Ac-CGGAAPVRGGGC-NH2, (**5**) Ac-CSGAAPVRGGGC-NH2, (**6**) Ac-CKGAAPVRGGGC-NH2. The structures of varied amino acids in each sequence are highlighted in bold and represented under the X axis. * indicates statistical difference using a 2-way-ANOVA test with Tukey post comparison (n=3, mean ± standard deviation).

In order to compare the solubility of peptides **3 – 6,** an approximation of their relative solubility was obtained by RP-HPLC. Crude peptides were dissolved in water at 20 mM and the soluble fraction analysed by RP-HPLC together with an internal standard (see section 2.3 for experimental procedure details). The concentration of the Area Under the Curve (AUC) of the HPLC peak of the peptide with respect to a Fmoc-Glycine internal standard was calculated (Figure 4.4.b). Calculations are based on the assumption that i) the higher the solubility of the peptide, the higher the AUC of the peak in the spectra will be, ii) the UV absorbance of peptides **3- 6** is comparable due to the absence of aromatic amino acids and the equal number of aliphatic residues in all peptides and iii) that the products are of similar purity. The peptide with highest percentage of absorbance (and approximated relative solubility) was the -SS- analogue, displaying significantly higher absorbance than the -GG- and -KG- analogues (2-way ANOVA with Tukey post comparison). Although the difference in absorbance was not statistically significant from the -SG-, the -SS- analogue (**3**) was selected as the sequence for hydrogel preparation. RP-HPLC and mass spectrometry characterisation of purified peptide 3 are shown in Figure 4.5.

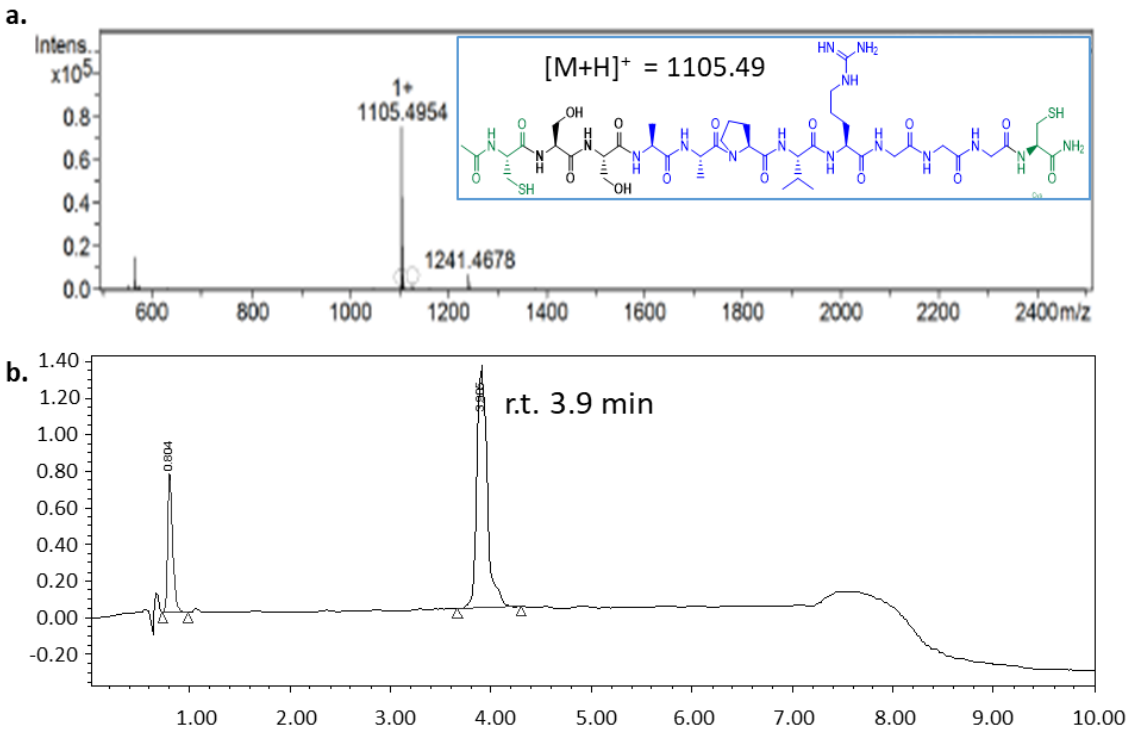

Figure 4.5. Characterisation of purified Ac-CSSAAPVRGGGC-NH2 peptide (3). **a.**) ESI-MS spectra: predicted $[M+H]^+$ 1105.49, observed 1105.49; $[M+NaTFA]^+$ predicted 1241.46, observed 1241.47. **b.**) RP-HPLC chromatogram of peptide (**3**), r.t. 3.9 min.

4.3.2 Preparation of elastase-responsive hydrogels

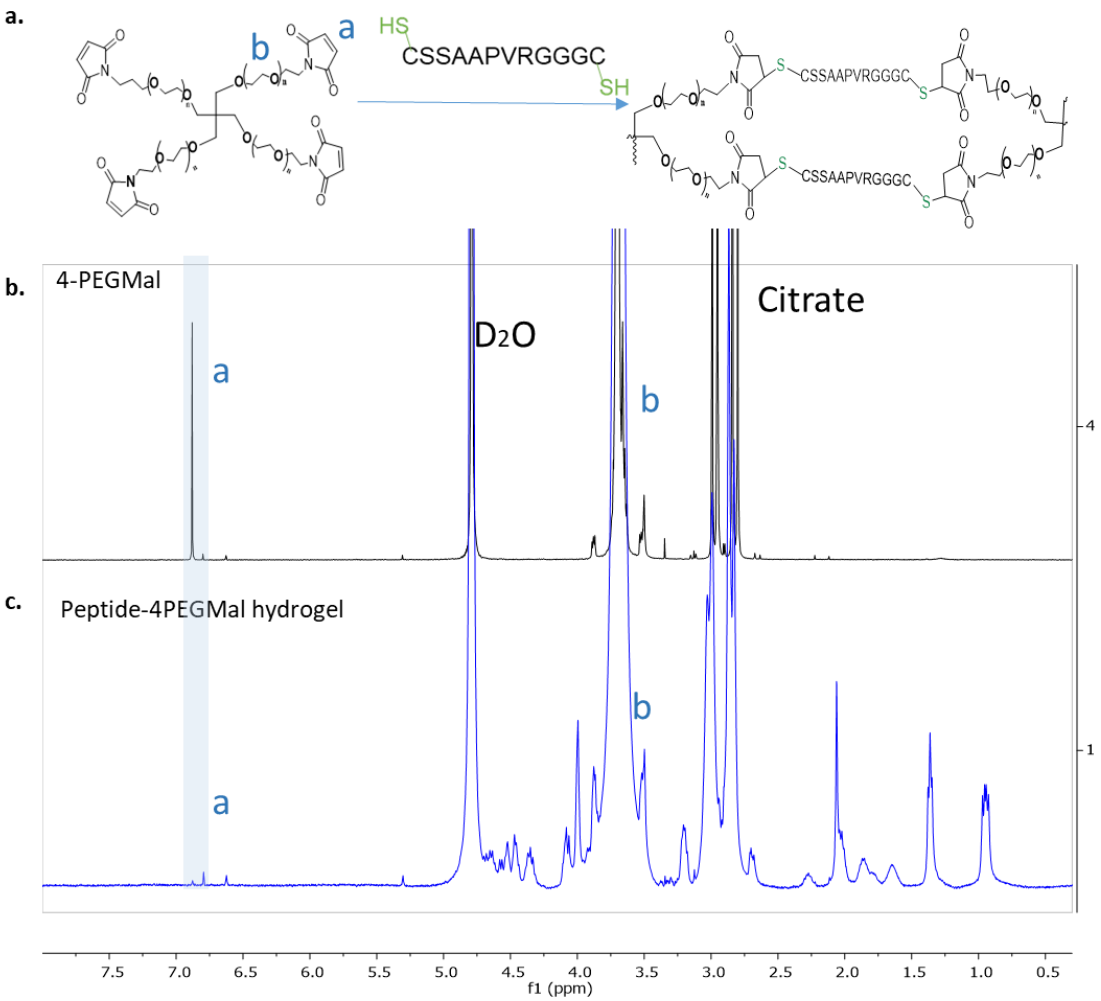

Figure 4.6. Chemical characterisation of hydrogel formation. **a.**) Michael-type addition reaction between 4-arm PEG-maleimide and elastase-responsive dithiol Ac-CAAPVRGGGC-NH_2, a protons highlight maleimide protons. ^{1}H NMR of 5 kDa 4-PEGMal in D_2O **b.**) before and **c.**) after reaction with peptide (5 % w/v).

Michael addition between vinyl groups and thiols has been widely used in material chemistry to form peptide-polymer hybrids with applications in drug delivery and functional materials [114,115,143,164]. This is due to peptides introducing a wide range of bio-functionalities to polymers and polymers increasing stability and delivery of peptide or protein based therapeutics. In particular, maleimide-terminated PEG polymers have been used to crosslink cysteine-terminated peptides in order to obtain hydrogels for protease- responsive drug delivery[41,43,139,164].

This section focuses on developing and characterising elastase-responsive hydrogels. In order to achieve elastase–controlled delivery, hydrogels were formed via Michael addition between 4-arm-PEG-maleimide (4PEGMal) and the elastase-responsive sequence developed in section 4.3 (peptide **3**) (Figure 4.6.a).

The extent of hydrogel crosslinking was determined by ^{1}H NMR (5 % w/v hydrogels, at 1:1 SH:C=C ratio, in 0.1 M citrate buffer in D_2O). The disappearance of the maleimide proton signal between 6.8 -6.9 ppm confirmed near full reaction between maleimides and the peptide dithiol, with over 97 % maleimide conversion as detected by NMR (Figure 4.6.c).

The use of different crosslinkers can affect properties of hydrogels obtained by Michael addition, such as crosslinking kinetics or mechanical strength, therefore potentially having an effect on mesh size and drug release[38,177,213]. For this reason, the mechanical properties of peptide-crosslinked hydrogels were compared to those of the previously studied hydrogels crosslinked with the model dithiol DTT (Figure 4.7.a-c). First, the linear viscoelastic regime (LVE) and mechanical strength as determined by the storage modulus (G') of equilibrium swollen peptide-crosslinked hydrogels were compared to those of DTT-crosslinked gels (Figure 4.7.a). Peptide-crosslinked (peptide- 4-PEGmal) hydrogels showed viscoelastic properties with a LVE and G' values comparable to the equivalent DTT-crosslinked hydrogels (DTT-4-PEGMal), for both 5 kDa and 10 kDa 4-PEGMal hydrogels. Peptide- 4-PEGmal hydrogels have slightly faster gelation kinetics than DTT one s(Figure.4.7.b). 10 kDa and 5 kDa Peptide-4-PEGMal gels achieved the gel point (crossover point where G'>G'') at 2.63 and 3.3 min respectively, while the gel points for the same conditions were 3.8 and 9.6 min for DTT-4-PEGMal (Figure 4.7.b, exact gel time numbers can be found in Table A.1 of the Appendix). These slight differences in polymerisation kinetics could be due to the effect of differences in pK_a of the thiols[177,214] or size between both crosslinkers[38] on Michael addition polymerisation. Although the gelation times were slightly different for the peptide- 4-PEGMal gels, these gelation times are in same order of magnitude, so the optimisations in pH and

polymer concentration conducted in Chapter 3 to obtain homogenous DTT – 4-PEGMAl hydrogels can be assumed to be applicable to peptide-4-PEGMal hydrogels.

No significant difference between mechanical properties of hydrogels crosslinked with either DTT or peptide crosslinker were found (Figure.4.7.c). In a similar work, Rehmann *et al.* did not find differences in mechanical properties, swelling and mesh in similar PEG-based hydrogels prepared with different crosslinkers (PEG-dithiol and peptides)[22]. This highlights that hydrogels with comparable kinetics and mechanical properties were obtained with both DTT and peptide crosslinkers.

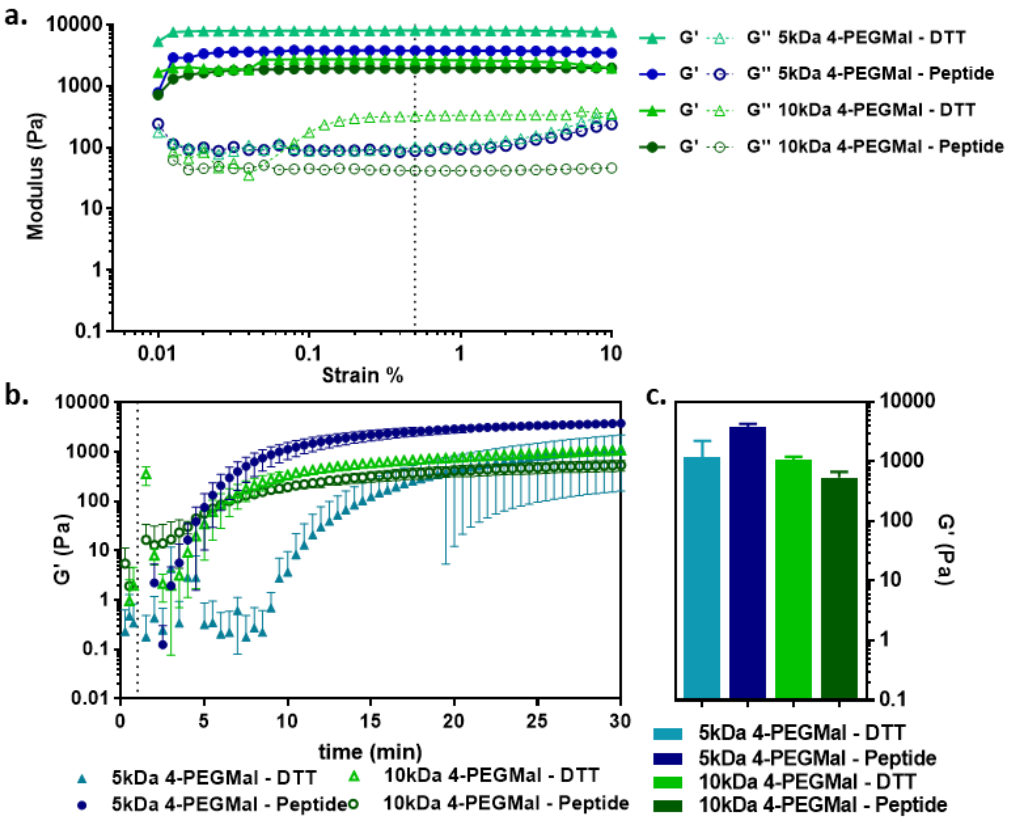

Figure 4.7. Comparison of DTT and peptide (3) crosslinked hydrogel mechanical properties. **a**.) Amplitude sweep to confirm LVE for peptide hydrogels. Effect of crosslinker type in storage modulus of 10 % 4-arm-PEGMal 5kDa and 10kDa on PBS equilibrated swollen hydrogels. Effect of crosslinker type in 10 % 4-arm-PEGMal 5kDa and 10kDa. **b.**) gelation kinetics and **c**.) final storage modulus during gelation. *No difference of G' by one-way ANOVA with Tukey post-comparisons ($p<0.05$, n=3 DTT, n=2 peptide).

4.3.3 Elastase controlled degradation and drug release from 4-PEGMal hydrogels

Having confirmed the incorporation of the elastase-sensitive peptide into 4-PEGMal hydrogels via Michael addition, hydrogel degradation in presence of elastase was evaluated. Hydrogels were prepared as previously described in section 4.3.2 and then incubated at 37 °C with increasing concentrations of elastase for 24 h. Medium samples were taken periodically and a fluorescamine fluorescent assay was used for quantification of hydrogel cleavage by the targeted enzyme. As elastase-controlled cleavage of the hydrogels takes place, the concentration of *de novo* primary amines released upon enzymatic hydrolysis of peptide crosslinkers within the matrix increases and can be quantified with the fluorescamine assay[123,193,194]. The maximum degradation rate (nmol NH_2/mg polymer/h) was calculated from the steepest region of the degradation curve for each enzyme activity condition and used to compare degradation kinetics (Figure 4.8.a). Degradation of the peptide-crosslinked hydrogels depended on the enzyme activity with faster degradation kinetics achieved at higher elastase activities (25 mU). Hydrogels incubated without elastase showed negligible degradation. These results highlight the potential of the developed peptide-crosslinked hydrogels to be used as elastase-controlled drug delivery systems.

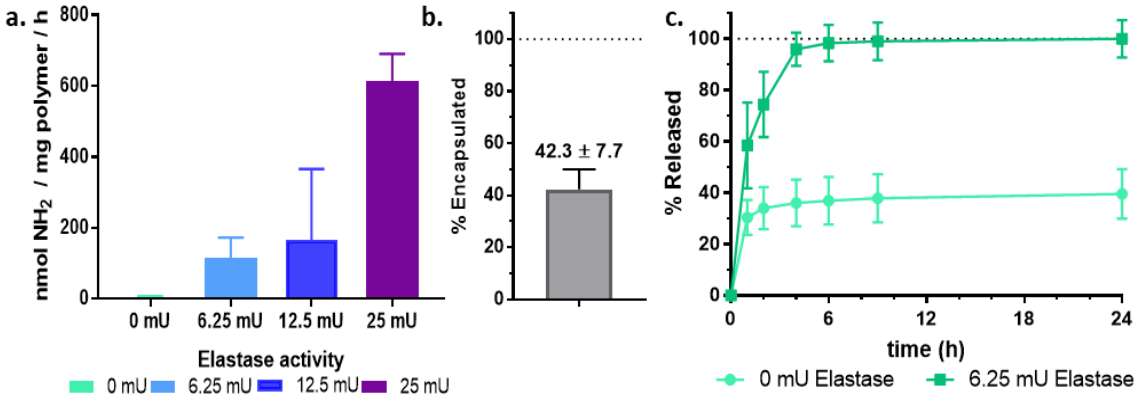

Figure 4.8. Elastase-controlled degradation and release from peptide crosslinked 4-PEGMal hydrogels. **a**.) Hydrogel degradation kinetics under different activity levels of elastase assessed by quantification of *de novo* primary amines (n=3, mean ± standard deviation). **b. – c**.) Encapsulation and elastase-controlled release of 70 kDa Texas red dextran (TRD70): b.) Entrapment efficiency of TRD70 (n=6, mean ± standard deviation), **c.**) Release of TRD70 in absence (0 mU) and presence (6.25mU) of pancreatic elastase (n=3, mean ± standard deviation).

Knowing that elastase-triggered degradation of the peptide crosslinked hydrogels was possible, their utility as elastase-controlled delivery systems was investigated. 70 kDa Texas Red labelled dextran (TRD70) was used as the model macromolecule.

In order to have elastase-controlled release, it is crucial to avoid mixed release mechanisms by keeping passive diffusion of the macromolecules from hydrogels to a minimum. Since similar mechanical properties were observe between DTT and peptide-crosslinked hydrogels, we selected the composition of hydrogels which showed optimal mesh size and passive release of dextran from DTT-crosslinked gels optimised in Chapter 3. Hence, 10 % 5 kDa peptide - 4-PEGMal at pH 3 was used for the following assays, as this showed the best encapsulation and lowest passive release of dextran. Although this composition had a significantly bigger mesh size than the 20 % w/v 5 kDa 4-PEGMal gels, their release performance was not significantly different and they require substantially less peptide for their preparation.

Release assays were conducted according to section 2.9. Before starting the release experiments, hydrogels were swollen in buffer for 24 h to release any loosely trapped dextran, as it was shown that most of the burst release occurs in the first 24 h with DTT-crosslinked hydrogels. The percentage of TRD70 retained inside the hydrogels at this time was used to calculate the encapsulation efficiency of the hydrogels (% TRD70 encapsulated). The encapsulation efficiency was 42.3 %, meaning that most of the dextran had escaped out of the hydrogel before starting the release experiment (Figure 4.8.b) Hydrogels were then incubated at 37 °C in the presence (6.25 mU) or absence (0 mU) of elastase. Dextran released at each time point from peptide 4-PEGMal hydrogels was quantified and the amount released was expressed as percentage of the total dextran released (Figure 4.8.c). Hydrogels incubated with elastase achieved a 100 % release within 6 h as opposite to circa 50 % of dextran released in 24 h from hydrogels incubated without enzyme (Figure 4.8.c). These trends are in agreement with the elastase-responsive release found by Aimetti *et al*. from their photopolymerised hydrogels.[39] In their work, Bovine Serum Albumin (BSA) was physically encapsulated inside elastase-responsive hydrogels with the same elastase

sensitive sequence AAPVRGGGC. In the presence of enzyme, they observed hydrogel degradation and BSA release taking place within 6 h while BSA release did not take place in absence of elastase.

4.3.4 Suitability of peptide – 4-PEG-maleimide hydrogels for elastase-controlled drug delivery applications

Although the release data, together with the fluorescent monitoring of the degradation, confirm the elastase-triggered degradation and release from the fabricated peptide-crosslinked hydrogels, the encapsulation efficiency and the passive release of TRD70 are not optimal.

Since this work will explore the encapsulation of a protein enzyme inhibitor (Chapter 6), it is extremely important to guarantee a higher encapsulation efficiency and a lower passive release. Achieving a higher encapsulation efficiency guarantees that the maximum amount possible of inhibitor added during fabrication remains inside the hydrogels until the start of the assay. A lower passive release guarantees that the biological effect of the inhibitor on the enzyme is dictated only by controlled release due to the presence of specific enzyme. Both encapsulation efficiency and passive release should therefore be further improved.

The hydrogel composition used for the elastase controlled release in this chapter was the one that showed the lowest passive release from 4-PEG-Mal hydrogels as optimised in Chapter 3. It was hypothesised that another hydrogel characterised by a smaller mesh size will lead to a) improved encapsulation efficiency and b) lower passive release than the achieved with peptide 4-PEGMal hydrogels. Unpublished data within our group has shown that the mesh size of 4-arm-PEG-norbornene hydrogels crosslinked with DTT via thiol-ene photopolymerisation can be up to 3 nm smaller than that of the equivalent compositions described in this work (Table B.1, Appendix). Thus, their ability to physically entrap macromolecules is much higher than the 4-PEGMal hydrogels.

4.4 Conclusions

Initial steps towards the development of elastase-responsive hydrogels have been conducted. An elastase-sensitive crosslinker was designed and demonstrated to be cleavable by elastase. The purified peptide (2) demonstrated limited solubility and tendency to aggregation, limiting its use in aqueous medium.

Four peptide analogues were synthesised by adding two extra hydrophilic amino acids to the sequences showing improved solubility **(3-6**). The peptide Ac-CSSAAPVRGGGC-NH_2 was selected for crosslinking with 4-PEGMAl in order to obtain elastase-responsive hydrogels. The crosslinking with 4-PEGMal polymer resulted in full maleimide conversion by NMR and had strong mechanical properties (kPa range) similar to the DTT crosslinked hydrogels obtained in Chapter 3. The hydrogels were elastase responsive, showing to be specifically degraded in presence of elastase and the elastase-controlled delivery was demonstrated with a 70 kDa fluorescent dextran as the model probe. Hydrogels incubated with elastase achieved full release of entrapment dextran within 6h while a lower release was observed on hydrogels incubated without elastase.

Despite the selection of a hydrogel formulation with the lowest passive release, the entrapment efficiency and the passive release of the model macromolecule were still improvable. This data indicates that ideally both parameters should be further improved when enzyme inhibitors are encapsulated in later chapters in this thesis (Chapter 6 and Chapter 7). This will allow improved treatment effectiveness and allow for a delivery mechanism controlled exclusively by elastase.

It can be concluded that hydrogels prepared with the synthesised elastase-responsive peptide successfully demonstrated an elastase-controlled release mechanism. Since low encapsulation and high passive release profiles were found, further investigation in the next chapter will address this issue. The use of an alternative crosslinking mechanism will be explored, thiol-ene

photopolymerisation, to obtain hydrogels which keep the elastase-responsive functionality and improved release.

Chapter 5.

Fabrication of elastase-responsive hydrogels via thiol-ene photopolymerisation

5.1 Introduction

In the previous chapter an elastase-sensitive peptide was synthesised and used to prepare elastase-responsive hydrogels via Michael addition, characterised by a high passive release. Chapter 5 builds on this knowledge by fabricating elastase-responsive gels via thiol-ene photopolymerisation for improved macromolecule entrapment, assessing their specificity and cross-reactivity of release in presence of other proteases.

5.1.1 Hydrogel fabrication by thiol-ene photopolymerisation

Thiol-ene photopolymerisation, together with Michael addition (explored in Chapter 3 and 4), is one of the most common methods for the fabrication of protease-responsive materials. Protease-responsive hydrogels can be prepared under mild conditions in an aqueous environment via crosslinking of thiol terminated peptides with multifunctional norbornene polymers via thiol-ene photopolymerisation[161]. The crosslinking reaction is a highly efficient and radical mediated reaction between electron rich alkenes and thiols, requiring a photoinitiator and light to catalyse the initiation (Figure 5.1.a). In the presence of the UV light the photoinitiator generates strong radicals that attack the thiol generating a thiyl radical (Figure 5.1.b top) which then reacts specifically with a norbornene-terminated polymer forming a thioether bond (Figure 5.1.b. bottom). Since the reaction only proceeds once UV light is applied, this allows for more control over the spatial and temporal hydrogel formation (e.g. adequate premixing of the hydrogel components before gelation), leading to very homogeneous hydrogels[39173].

Several biologicals, such as proteins[22,35,39], peptides[152] and cells[168], have been encapsulated using multi-arm PEG-norbornene. The aqueous environment and mild crosslinking conditions have been shown to preserve both macromolecules functionality and cell viability after release[22,35,39,152,168]. This is possible due to the use of low toxicity photoinitiators such as lithium phenyl-2,4,6-trimethylbenzoylphosphinate (LAP)[168,171]. McCall *et al.* have shown that 4-PEGNB hydrogels can be prepared with very low concentrations of LAP initiator, which allowed the maintenance of full bioactivity of encapsulated proteins (lysozyme and TGF-β)[168]. LAP was first synthesised by Majima *et al.*[215], and first used for hydrogel photopolymerisation by Fairbanks *et al* [171], showing advantages such as high water solubility, cytocompatibility, and improved polymerisation kinetics compared with previously used photoinitiators such as Irgacure 2959[171]. LAP was first used for thiol-ene photopolymerisation of 4-PEGNB and peptide dithiols to obtain protease-responsive hydrogels by the same group. This showed faster initiation of the crosslinking and at lower concentrations (~50 μM) than commercial initiators[161]. This has led to a wide use of this technique to prepare protease-responsive hydrogels for sensing and drug delivery[38,39,160]. Hydrogels prepared with PEG-norbornene designed for protease-controlled release have shown a good entrapment of proteins and macromolecules with a low passive release[39], and are therefore good candidates to be used in this work.

Although 4-PEGNB hydrogels prepared by thiol-ene photopolymerisation and 4-PEGMal hydrogels prepared by Michael addition have been widely used for biomedical applications, there have been limited reports comparing the properties of both types of gels. *Darling et al*. have shown that hydrogels formed via thiol-ene photopolymerisation were more microscopically uniform than 4-PEGMal ones prepared at neutral pH, affecting cell attachment and spread[173]. When 4-PEGMal hydrogels were prepared with conditions that slowed maleimide gelation kinetics to allow homogeneous mixing, both hydrogel types were uniform and equally supported cell spread. Although 4-PEGNB have slightly stronger mechanical properties, and crosslinking density

the authors did not found significant differences. To date, there are no reports on the effect of the two different crosslinking chemistries on macromolecule entrapment and release.

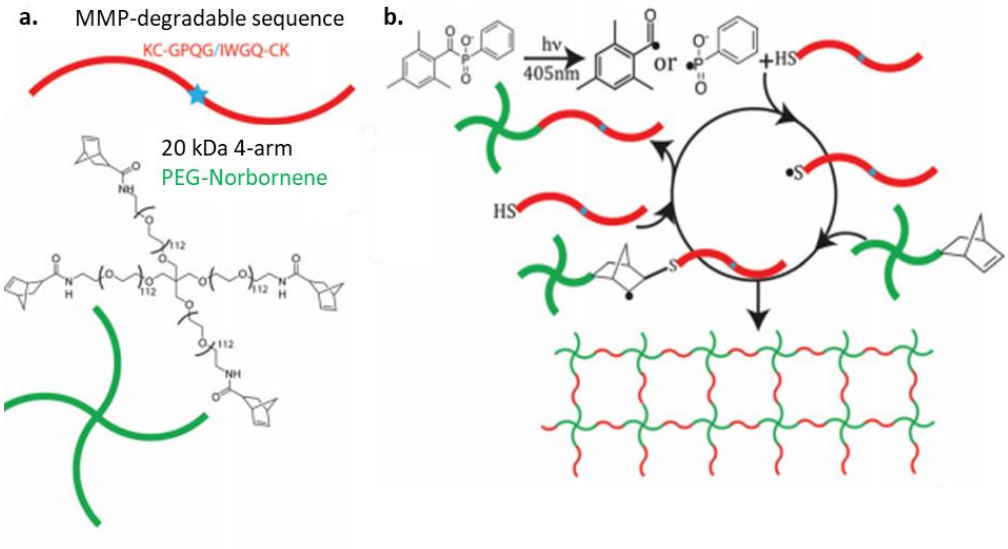

Figure 5.1. Fabrication of protease-degradable peptide crosslinked PEG-norbornene gels formed using thiol-ene click chemistry and LAP as a photoinitiator. **a.**) Chemical structures of network components, including MMP-degradable sequence and multi-arm PEG-norbornene. **b.**) Hydrogel formation via radical-mediated thiol-ene photopolymerisation to form step growth networks. Adapted from [216].

5.2 Aim and objectives

In this chapter we aim to obtain elastase-responsive hydrogels with reduced passive release of macromolecules, and characterise their elastase-controlled responsiveness and selectivity. In order to achieve this aim, the objectives of the chapter are:

- Crosslinking of elastase-sensitive peptides with 4-arm-PEG-norbornene (4-PEGNB) for the fabrication of hydrogels via thiol-ene photopolymerisation.
- Comparison of 4-PEGMal and 4-PEGNB hydrogels abilities to encapsulate and reduce passive release of a model 70 kDa dextran.
- Characterisation of the specificity of release in presence of elastase from elastase-responsive and non-responsive 4-PEGNB hydrogels.
- Study of the susceptibility of the elastase-sensitive hydrogels towards degradation and release in presence of Matrix Metalloproteinase 2 (MMP-2)

5.3 Results and discussion

5.3.1 Fabrication of elastase-responsive hydrogels with improved entrapment and delivery

5.3.1.1 Synthesis and characterisation of 4-arm-PEGNorbornene hydrogel components

LAP photoinitiator was synthesised as initially described by Majima *et al*., and adapted by Fairbanks *et al*. [171,215]. LAP photoinitiator synthesis and characterisation was carried out by Mr. Emanuele Russo. Chemical characterisation of LAP can be found in Figure C.1 in the appendix, where Figure C.1.a shows the reaction scheme, Figure C.1.b shows the mass spectra (ESI-MS) and Figure C.1.c. the ^{1}H NMR spectra.

5 kDa 4-PEGNB was obtained from 4-arm-PEG-hydroxyl (4-PEG-OH) following established procedures[39,161] that are described in section 2.4. The purified polymers were analysed by ^{1}H-NMR, FTIR and MALDI-ToF-MS to confirm successful conversion of alcohols to norbornene esters (Figure 5.2). Conversion of alcohols to norbornene esters was determined by the appearance of the peaks corresponding to the norbornene double bond protons (protons a, 6.33-5.95) and ester bond protons (b) in the NMR spectrum (Figure 5.2.a). Successful functionalisation of hydroxyl groups was also confirmed by the appearance of the characteristic stretching/bending band of the C=O bond in the ester at approximately 1730 cm^{-1} ($\upsilon_{C=O}$ =1728 cm^{-1}), and the C-H band from the vinyl group at around 700 cm^{-1} (**$\upsilon_{C\text{-}HVinyl}$** = 716 cm^{-1}**,** Figure 5.2.b). MALDI-ToF-MS of 4-PEG-OH and 4-PEGNB show a shift in the mass peak distribution confirming conversion of four arms from 4-PEG-OH to norbornene ([M+Na]$^{+}$ = 5489.9, Figure 5.2.c). Multiple peaks are observed for both compounds due to the polydispersity of the commercial 4-PEG-OH with repeating units of 44Da, corresponding to the ethylene repeating units of PEG based polymers (-CH_2CH_2O-). This data together with ^{1}H NM, FT-IR data confirm the functionalisation of 4-PEG-OH to 4-PEGNB.

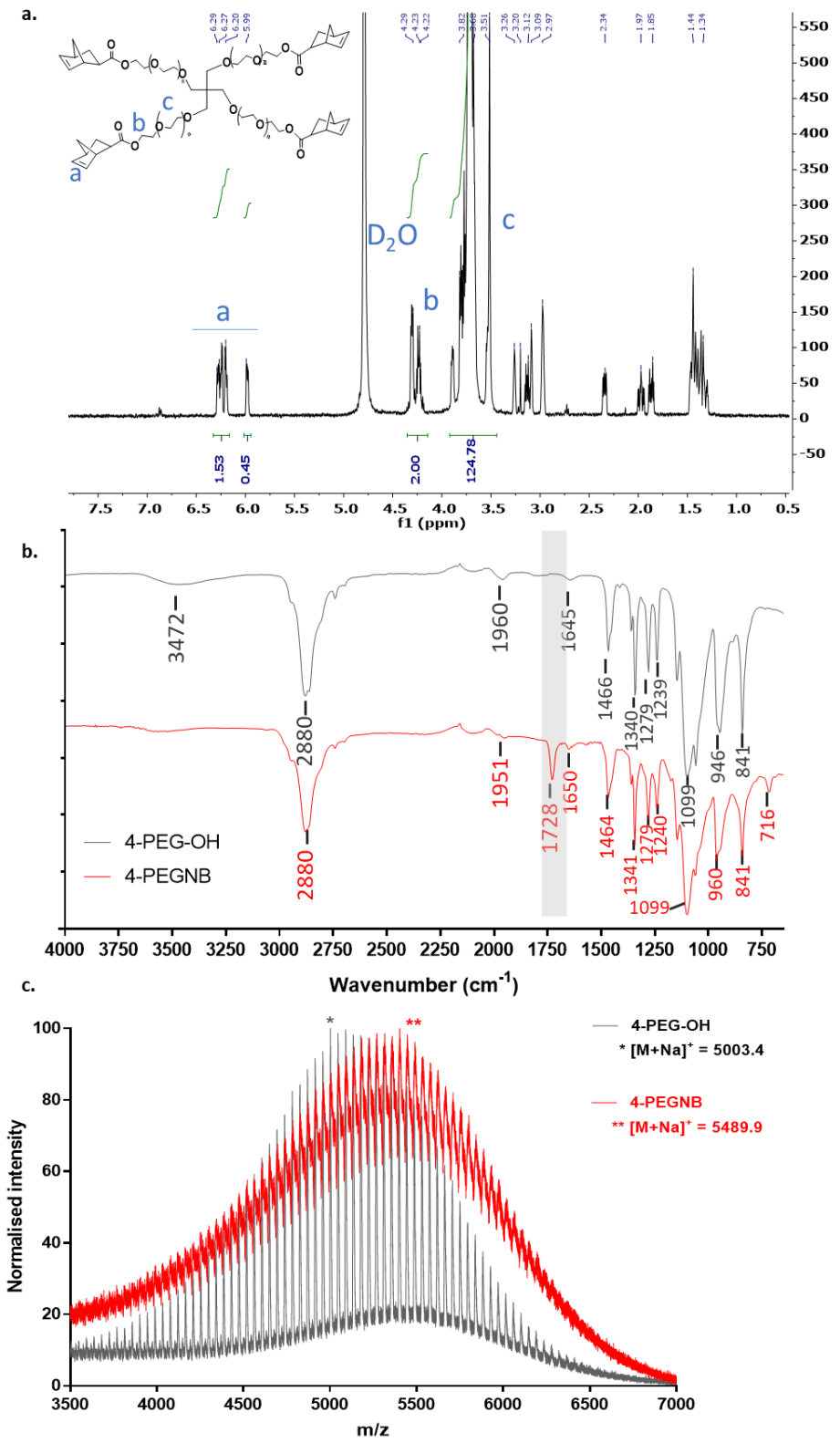

Figure 5.2. Physicochemical characterisation of 4-arm-PEG-Norbornene (4-PEG-NB). **a.**) ^{1}H NMR analysis of 4-PEG-NB showing the integrals of norbornene double bond (6.33-5.95), ester bond (4.39 – 4.18 ppm) and PEG backbone protons (4.93 – 3.33 ppm). **b.**) Comparison of FT-IR spectra of 4-arm-PEG-OH (grey spectrum) and 4-arm-PEGNB (red spectrum). Stretching/bending peak of ester bond ($\upsilon_{C=O}$ = 1728 cm^{-1}) and C-H of the vinyl group ($\upsilon_{C\text{-}HVinyl}$ = 716 cm^{-1}). c.) MALDI-ToF-MS of 4-PEG-OH ([M+Na]$^{+}$ = 5003.4) and 4-PEGNB ([M+Na]$^{+}$ = 5489.9).

5.3.2 Characterisation of hydrogels prepared by thiol-ene photopolymerisation

Elastase-cleavable peptide Ac-CSSAAPVRGGGC-NH_2 was crosslinked with 4-PEGNB to obtain elastase-responsive hydrogels via thiol-ene photopolymerisation as described in Section 2.5.2(Figure 5.3.a). The degree of hydrogel crosslinking was determined by ^{1}H NMR (5 % w/v polymer, 1:1 SH:C=C ratio, 1.7mM LAP, D_2O). The disappearance of the peaks from the norbornene protons at 6.35 – 5.95 ppm confirmed over 97 % conversion within the detection limits of NMR (Figure 5.3.b). This conversion is similar to the one achieved with 4-PEGMal hydrogels prepared via Michael addition in chapter 4 (Figure 4.5.a). Consequently, comparative experiments between both types of gels as delivery systems were conducted next.

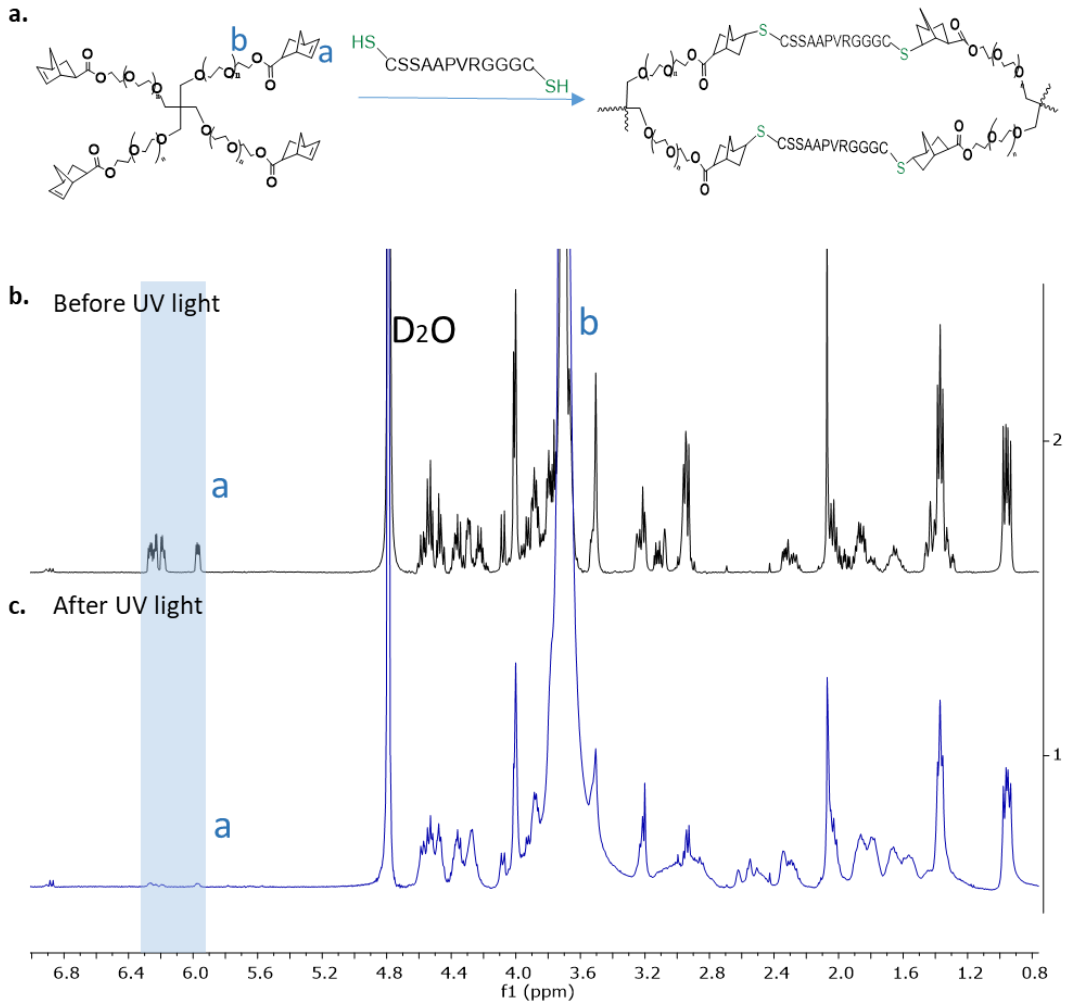

Figure 5.3 Chemical characterisation of peptide – 4-PEGNB hydrogel formation. **a.**) Thiol-ene photopolymerisation between 4-PEGNB and elastase-responsive dithiol Ac-CAAPVRGGGC-NH_2, a protons highlight norbornene protons. ^{1}H NMR of 5 kDa 4-PEGNB and peptide **b**.) before and **c.**) after exposure to UV light.

5.3.3 Comparison of passive release from hydrogels prepared via Michael addition and thiol-ene photopolymerisation

Achieving a high entrapment efficiency and low passive release of macromolecules is important when designing enzyme-controlled delivery systems. In this way, the release of the cargo will be mainly controlled by the effect of the targeted enzyme with minimal contribution of passive diffusion. The peptide – 4-PEGMal hydrogels developed in the previous chapter showed inadequate encapsulation and release of a 70 kDa Texas-Red dextran (TRD70). Unpublished data from the group on the mesh size of DTT – 4-PEGNB hydrogels suggests that 4-PEGNB hydrogels can offer improved encapsulation and passive release than 4-PEGMal ones. For this reason we compared the encapsulation and release of TRD70 as a model macromolecule from 4-PEGMal (Michael addition) and 4-PEGNB (thiol-ene photopolymerisation) hydrogels at a fixed composition (5 kDa PEG, 10 % w/v, 1:1 SH:C=C ratio).

Encapsulation and release of TRD70 (10 μg/ μL) was conducted as described in section 2.9 for responsive hydrogels. The only variant was the washing step to remove loosely entrapped dextran and calculate the encapsulation efficiency. This washing consisted on 2 × 5 min incubation in PBS, as described in section 2.7 and used for non-responsive gels in chapter 3, instead of 24 h as employed in chapter 4. This methodological change was conducted in order to have more data points during the first 24 h of release in medium to better assess the passive release profiles at early times, as it was unknown if the 4-PEGNB hydrogels would perform similarly to 4-PEGMal and have a burst release mostly amid the first 6h.

Encapsulation efficiency of 4-PEGNB hydrogels was significantly higher than 4-PEGMal hydrogels, with the former being over 80 % and the latter ~ 60 % ($p<0.05$, t-test, Figure 5.4.a). The passive release from hydrogels prepared via Michael addition (4-PEGMal) was greater, reaching a plateau of 80 % TRD70 released from 6h (Figure 5.4.b). Hydrogels prepared via norbornene photopolymerisation (4-PEGNB) showed a better passive release profile, with a total dextran

released at the end of the experiment (D_{max}) below 50 %, in contrast with almost 90 % for 4-PEGMal gels (Fig5.4.b and Table 5.1). A t-test was conducted and showed that the maximum dextran released at endpoint was significantly bigger for 4-PEGMal gels. It could be visually appreciated that both the quality of the gels and the remaining dextran were lower for 4-PEGMal hydrogels (Figure 5.4.c). Since both the encapsulation efficiency and the passive release were improved in 4-PEGNB hydrogels this method of hydrogels preparation was employed for further experiments in this work.

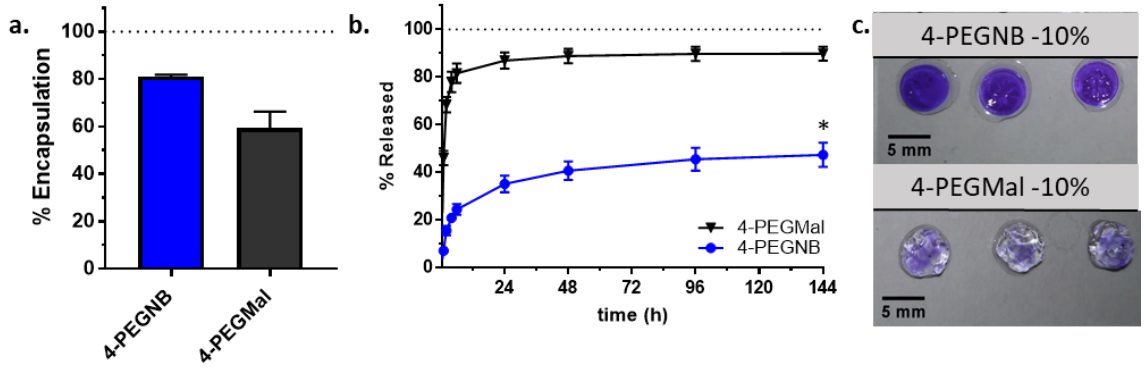

Figure 5.4. Comparison of 4-PEGMal and 4-PEGNB hydrogels as delivery systems using TRD70 as model macromolecule. **a**.) Encapsulation efficiency and **b**.) passive release of TRD70 in from 10 % w/v 5 kDa 4-PEGMal (black triangles) or 4-PEGNB (blue circles) * indicates statistical significance as determined by t-test (*p< 0.05, n=3, mean ± standard deviation). **c**.) Visual appearance of 4-PEGNB and 4-PEGMal hydrogels at the end of release assay (day 6)

In order to further reduce the passive release of macromolecules from 4-PEGNB hydrogels, the effect of varying polymer concentration (w/v) on the model dextran encapsulation and release was investigated. It was expected that the entrapment efficiency would increase and the passive release decrease at higher concentrations of polymer (and crosslinker to maintain 1:1 SH:C=C ratio). We studied the release of TRD70 dextran as model molecule from 5, 10, 15 and 20 % w/v 5 kDa hydrogels with the same release protocol as above.

Table 5.1. Encapsulation efficiency (E.E.) and total percentage of dextran released at 24 h (D24) and 144h (D_{max})

	4-PEGMal 5 kDa	**4-PEGNB 5 kDa**			
	10 % w/v	**5 % w/v**	**10 % w/v**	**15 % w/v**	**20 % w/v**
E.E. Short wash	59.3 ± 7.0	78.8 ± 2.0	81.1 ± 0.7	91.6 ± 1.3	94.1 ± 1.5
D_{24}	86.9 ± 3.4	76.0 ± 1.2	35.3 ± 3.5	26.8 ± 1.6	23.3 ± 8.5
D_{max}	89.8 ± 2.9	85.7 ± 1.1	47.3 ± 5.1	38.4 ± 1.3	36.4 ± 11.7

*E.E. considering as not entrapped the dextran released during the 2 x 5 min washes and 24 h of release experiment.

The amount of encapsulated dextran was higher at the higher crosslinking densities, hydrogels comprising 15 and 20 % w/v polymer encapsulated over 90 % of the dextran (Figure 5.5.a, Table 5.1). The passive release from 5 % hydrogels was much higher than any other conditions, with over 80 % being released and visually less dextran encapsulated at the end of the experiment (Figure 5.5.b an Figure C.2 in the appendix). All other conditions (10 to 20 % w/v) resulted in much lower passive release, which could be explained by higher crosslinking densities offering more hindrance to macromolecule diffusion[35]. Both 15 % and 20 % w/v offer the lowest passive release, with less than 40 % of dextran being released at 24 h and at the endpoint of the assay (D_{24h} and D_{max}, Table 5.1). Although the 20 % hydrogels retained more 70 kDa dextran at the endpoint of the assay than 15 % ones (Lower D_{max}), there was no significant difference between them at any time point of the release (Table C.1 in the appendix contains all significant differences between all samples for the release experiment). This could be due to 15 % and 20 % hydrogels having either a similar mesh size or both having a mesh size smaller than the diameter of the dextran, which would lead to similar release kinetics between both samples[1]. It was therefore concluded that either 15 % or 20 % w/v peptide – 4-PEGNB hydrogels offer the most suitable encapsulation efficiency and passive release, so they were used for enzyme-controlled release experiments.

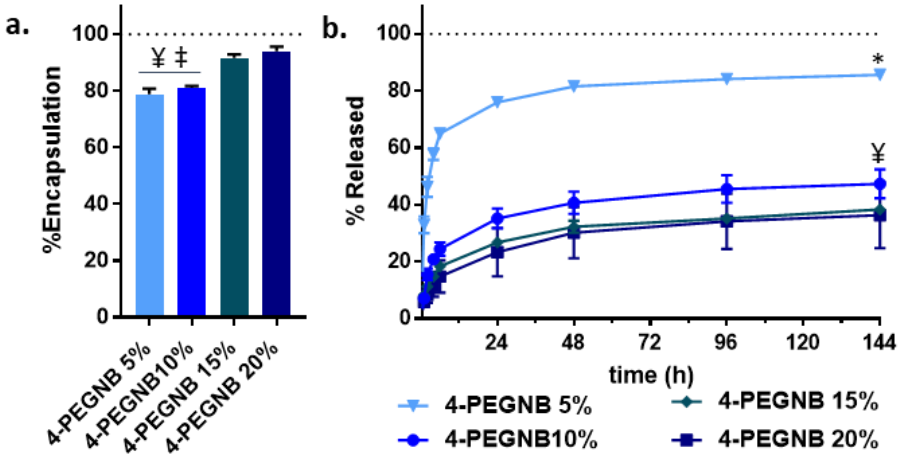

Figure 5. 5. Effect of crosslinking density on encapsulation and release from elastase responsive 4- from 5 %, 10 %, 15 % and 20 % w/v 4-PEGNB hydrogels. **a**.) Encapsulation efficiency. **b**.) Passive release of TRD70 in PBS medium. Symbols indicate statistically significant differences by one-way ANOVA for a. and two-way ANOVA for b with Tukey post-comparison. * indicates different from all, ‡ from 15 % w/v and ¥ from 20 % w/v hydrogels, (n=3, mean ± standard deviation). Only statistical differences at endpoint of release are shown for clarity, all statistical differences can be found in the appendix, Table C.1.

5.3.4 Controlled release from 4-PEGNB hydrogels in response to pancreatic elastase

Porcine Pancreatic Elastase (PPE) was used as model elastase to check elastase-responsiveness of the peptide-crosslinked 4-PEGNB hydrogels. 15 % w/v hydrogels were incubated with increasing concentrations of elastase, as described in section 2.9 (0.5mU and 1.5 mU of PPE in 0.5ml total release volume). Increasing concentrations of elastase lead to faster degradation of the hydrogels and trigger the release of the model macromolecule TRD70 (Figure 5.6). This demonstrates that the hydrogels are not only responsive to elastase, but to the actual concentration of the enzyme. These results suggest the hydrogels may also release higher amounts of encapsulated elastase inhibitors at higher elastase levels, which are usually associated with pathological states.

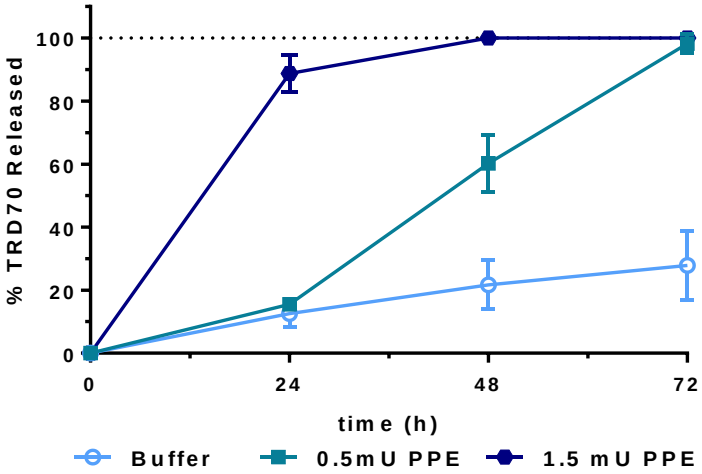

Figure 5.6. Elastase-controlled release of 70 kDa dextran (TRD70) from 4-PEGNB hydrogels with Porcine Pancreatic Elastase (PPE) as model elastase in phosphate buffer pH 8 (n=3, mean ± standard deviation).

5.3.5 Quantification of Human Neutrophil Elastase Activity

Before conducting release experiments, a colorimetric assay was employed to confirm the activity of all the neutrophil elastase batches before conducting release experiments. The activity of HNE was assessed by the ability of the enzyme to cleave the substrate N-methoxysuccinyl-Ala-Ala-Ala-Pro-Val-p-nitroanilide to release the colorimetric compound p-nitroaniline (p-NA) (Figure 5.7.a), as detailed in section 2.14.2. The increase in absorbance at 410 nm was monitored over 3 h for a range of elastase concentrations (1 – 40 nM). The assay was sensitive to different enzyme concentrations tested, showing an increase in absorbance with increasing elastase concentration (Figure 5.7.b). The highest linear correlation between the quantified activity (as determined by absorbance) and the concentration of HNE was obtained when the incubation time was fixed to 30 min (Figure 5.7.c, Figure c.3.b in appendix C for correlations at all incubation times). This will guarantee a better quantification of the HNE concentration in unknown samples, and was therefore the incubation time used to determine the activity of commercial HNE batches as well the activity of elastase in release medium (Chapters 6-7). The obtained values of absorbance were then converted in the international units of enzyme activity using a calibration curve of p-NA in buffer (Figure C.3.b).

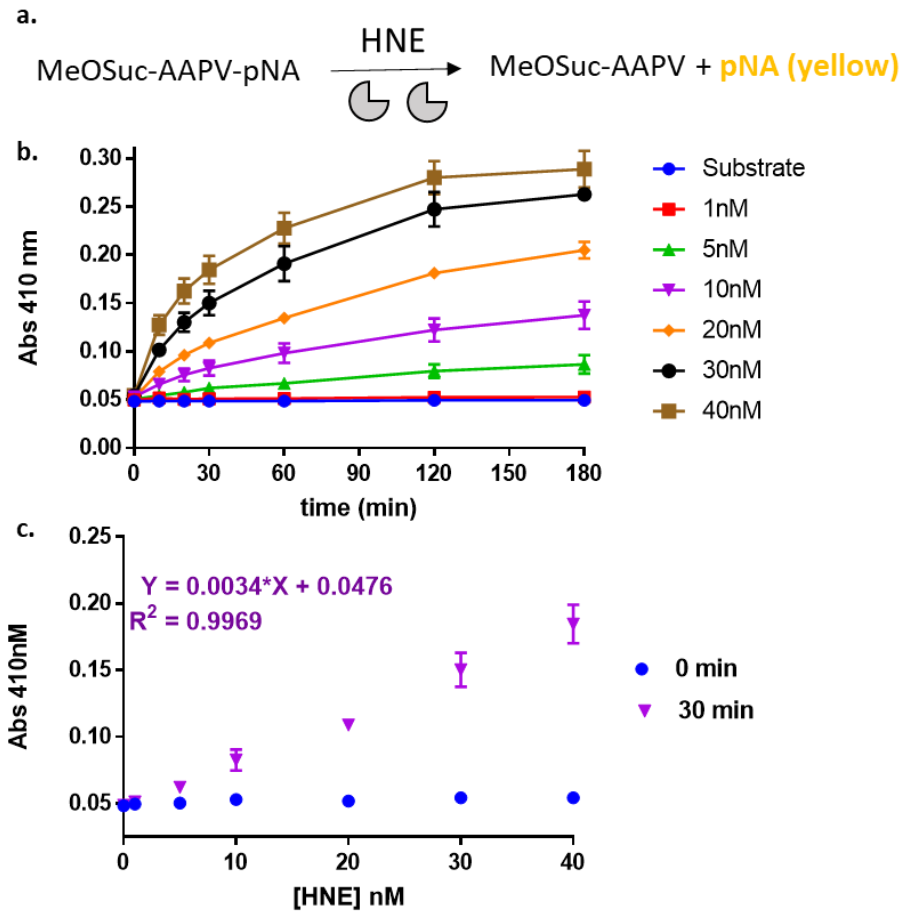

Figure 5.7. Colorimetric assay for quantification of elastase activity. **a.**) Schematic of the assay, showing colorimetric p-NA generation upon cleavage of the substrate. **b.**) Monitoring increase in absorbance with time due to generation of cleaved p-NA at different concentrations of HNE. **c.**) Linearity of absorbance generated by substrate cleavage over 1 – 40 nM HNE at a fixed incubation time of 30 min (0 min used as a control).

5.3.6 Controlled release from 4-PEGNB hydrogels in response to Human Neutrophil Elastase

Once passive release and hydrogels responsiveness to increasing levels of the model elastase PPE were confirmed, release experiments in the presence of Huma Neutrophil Elastase (HNE) were conducted. HNE is the physiologically relevant enzyme overexpressed in various pathologies[54], and it has a slightly different specificity to PPE. Additionally the elastase inhibitor used for further experiments during this project (Chapter 6 and 7), alpha-1-antitrypsin, did not

substantially inhibit PPE. Therefore it is of interest to use HNE since i) it is the physiologically relevant enzyme and ii) enzyme inhibition is necessary in order to complete this project.

Release experiments with HNE were conducted as stated in section 2.9. Release medium consisted on either phosphate buffer supplemented with 0.1 % Bovine Serum Albumin (BSA) or cell medium used in chapter 7 (DMEM-F12 supplemented with 0.1 % BSA), due to observed higher stability of neutrophil elastase in these medium than in non-supplemented phosphate buffer (Figure C.4 in the Appendix). Hydrogels were first incubated with increasing concentrations of HNE in BSA supplemented phosphate buffer (0nM, 20 nM, 40nM). Hydrogels showed a very low passive release in absence of elastase (<~20 %, Figure 5.8.a). Similarly to previously observed with pancreatic elastase, release rates in presence of HNE increased at higher concentrations, achieving a 100 % release within 72h at the highest concentration (40 nM, Figure 5.8.a).

Since in future chapters elastase will be added externally to cells in cell medium, hydrogels sensitivity to HNE and kinetics of release were also tested using the same medium composition (0.1 % BSA supplemented DMEM-F12). Hydrogels incubated with elastase (10nM) underwent full degradation and release of TRD70 in 72h (Figure 5.8.b). A similar extent of hydrogel degradation and elastase-controlled release was achieved, with a much lower concentration of elastase in medium in comparison to the release conducted in buffer (10nM instead of 40nM). This was attributed to the higher stability of neutrophil elastase in BSA supplemented cell medium with respect to BSA supplemented buffer as determined by the HNE activity test (Appendix C, Figure C.4). The difference in enzyme concentrations required to achieve a comparable controlled release profile between both release medium highlights the importance of validating elastase-dictated release profiles in the biological medium, since the same conditions will be used for biological testing of the hydrogels (Chapter 7).

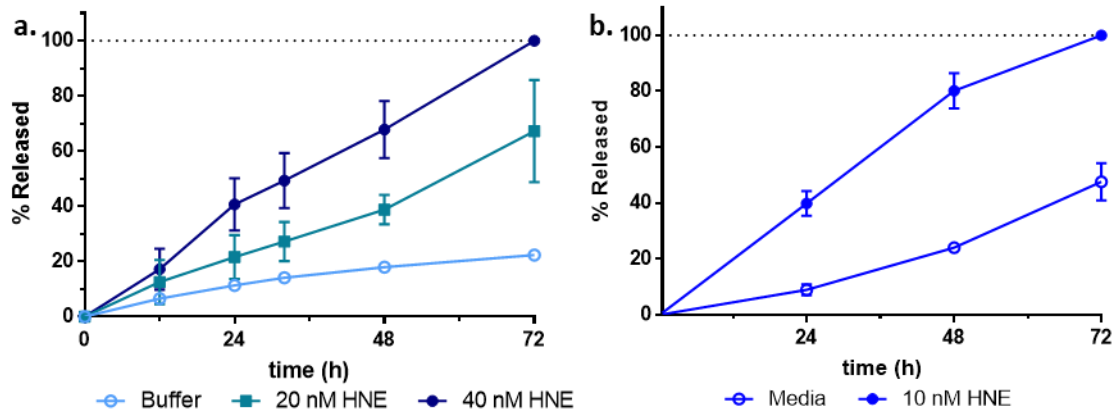

Figure 5.8. Release of 70 kDa dextran (TRD70) from 4-PEGNB hydrogels in presence of Human Neutrophil Elastase (HNE). a.) Release with buffer, 20nM HNE and 40nM HNE in phosphate pH 8 + 0.1 % BSA. b.) Release with medium or 10 nM HNE in DMEM-F12 medium (n=3, mean ± standard deviation).

5.3.7 Evaluation of specificity and selectivity of release

5.3.7.1 Development of non-responsive elastase control hydrogels

Hydrogels fabricated with peptide Ac-CSSAAPVRGGGC-NH_2 have intrinsic elastase-responsive properties. Since the hydrogel will be inherently degraded when incubated with elastase, as a result, the biological effects of entrapped proteins released by passive diffusion in presence of elastase cannot be detached from the effect due to elastase-responsive release. It will therefore be difficult to differentiate in later chapters the effects of encapsulated inhibitors on elastase activity due to an elastase-controlled feedback release and the effects exclusively due to the passive release of the inhibitor under the same condition. Although in Chapter 3 non-responsive hydrogels were developed with dithiothreitol (DTT), this crosslinker is not perfect for establishing these controls. As DTT has different charges and length to the elastase-responsive sequence, it could substantially alter the passive release of proteins.

A better approach for an accurate control of passive release from hydrogels in presence of elastase, is to use a peptide with the same amino acid residues but in a scrambled order. Consequently the crosslinker will have the same length and charge, with the only difference with respect to responsive peptides being the lack of recognition by elastase. Therefore the variability in the release of macromolecules from both types of hydrogels, crosslinked with responsive or scrambled peptides, will be exclusively down to elastase degradation. This has led to a wide use of scrambled peptides as a control of non-degradation by target enzyme in protease-controlled drug delivery[140,152,217] and imaging[218–220]. An exact scrambled version for the elastase-responsive sequence used in this work is not available in the published literature. PEAGVACG is the only sequence found in literature specifically probed not to be significantly degraded by neutrophil elastase[132]. However, the presence of the negatively charged residue at neutral pH glutamic acid (E), instead of the positively charged arginine in our responsive sequence, implies the overall charge of the peptide will be different. Differences in the hydrogel's net charges have been described to significantly modulate the passive release of proteins[47], therefore a scrambled sequence was designed specifically for this project using an online scrambler (https://peptidenexus.com/). Ac-CSSGAVPGARGC-NH_2 was considered as the scrambled sequence (only the amino acid residues giving elastase-responsiveness were scrambled, leaving the cysteine and serine residues in the same position as in the responsive gels). Due to a lack of literature in peptides non-cleaved by elastase, the PROSPER webserver for *in silico* prediction of substrate cleavage by proteases[221] was used to confirm that the scrambled sequence will not be hydrolysed by neutrophil elastase.

To further verify the suitability of the new scrambled sequence as non-responsive to elastase, release experiments were conducted. 70 kDa Texas red dextran was encapsulated in hydrogels prepared with the elastase-responsive (Ac-CSSAAPVRGGGC-NH_2) or non-responsive (scrambled, Ac-CSSGAVPGARGC-NH_2) peptides. Release was conducted in absence (DMEM-F12 medium) or presence of neutrophil elastase (10nM HNE in DMEM-F12 medium). Responsive

hydrogels were degraded by elastase leading to a significantly higher release of TRD70 dextran with respect to medium ($p<0.05$, determined by t-test). In contrast, the release from scrambled peptide functionalised hydrogels in presence of elastase was not significantly different from the release in absence of elastase (Figure 5.9, Figure C.5). This confirms that hydrogels prepared with the designated scrambled peptide are not sensitive to elastase degradation, and proves their suitability to be used as model gels for the passive diffusion of macromolecules in presence of elastase. In both cases the passive release of dextran was considerably low, with less than 50 % of the dextran being released.

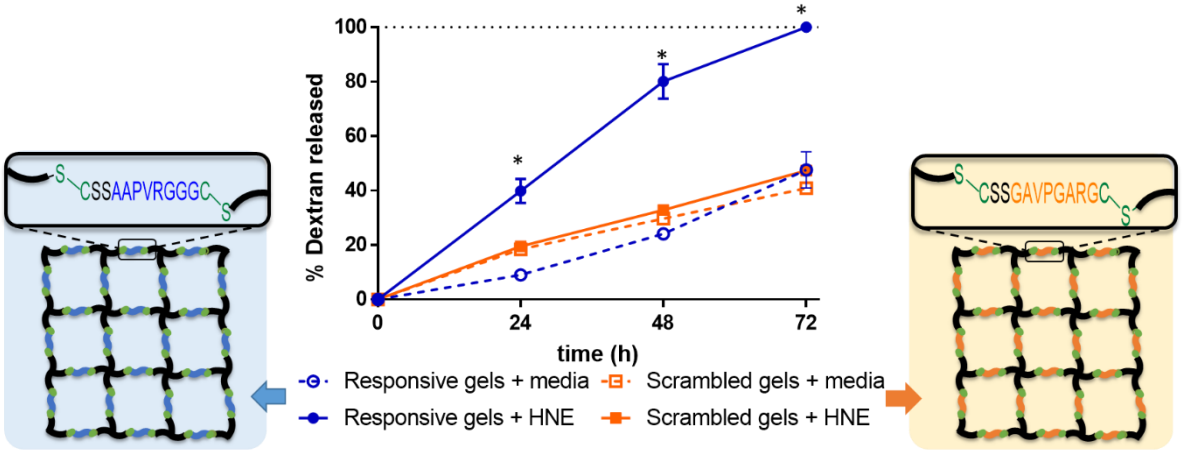

Figure 5.9. Release of 70 kDa dextran from hydrogels formed with either elastase responsive sequence or elastase-scrambled sequence in presence and absence of 10 nM HNE (N=3, mean ± error of the mean). * indicates statistical significance for the same type of gels in presence/absence of HNE as determined by t-test ($p<0.05$).

5.3.7.2 Influence of enzyme cross-reactivity in controlled release profiles

The susceptibility of enzyme-responsive materials to degradation by enzymes other than the targeted one is often not addressed. It would be of interest to understand the susceptibility to cleavage of the responsive hydrogels by other physiologically relevant enzymes. Matrix metalloproteinases (MMPs) are a class of zinc-dependant endopeptidase with a shared similar structure involved in extracellular matrix proteolysis, modulation of cell adhesion and migration and can process a range of growth factors and receptors[56]. Their overexpression has been correlated with several diseases such as cancer, chronic wounds, and pulmonary diseases[56,60,222].

Thus, MMP-2- responsive materials have been extensively reported for biomedical applications in cancer[127,129,149], pulmonary diseases[223], tissue remodelling[41], cardiovascular diseases[115] and chronic wounds[114,126] and MMP-2 degradable sequences are readily available. Therefore some diseases characterised by overexpression of elastase, such as chronic wounds and pulmonary diseases, often present with high levels of metalloproteinase activity as well [54]. It is therefore of interest to establish the selectivity of the release from the developed elastase-responsive hydrogels in the presence of MMPs, since some diseases are characterised by both MMP and elastase overexpression, and diseases characterised by either a high elastase and a high MMP expression could also coexist.

In order to clarify the specificity of the elastase-responsive hydrogels, their release in presence of Matrix Metalloproteinase-2 (MMP-2) as a model MMP was investigated. Release experiments were conducted as explained in section 2.10 using zymogram as release medium, since it is the standard release buffer for MMP-2. MMP-2 was activated and characterised prior to the assays as described in section 2.15 and conducted by Mr.Emanuele Russo. Elastase-responsive hydrogels treated with MMP-2 did not show a release significantly higher than the hydrogels in buffer (Figure 5.10.a). Similar to previous releases with elastase-responsive hydrogels (Figure 5.9), hydrogels incubated with elastase underwent almost 100 % degradation within 72h, being significantly different to the passive release controls in buffer and with MMP-2 (as determined by two-way-ANOVA with Tukey post-comparison, Figure 5.10.a). These results verify the specificity of the hydrogels towards HNE cleavage, since the lack of sensitivity to cleavage by MMP-2 lead to a release profile comparable to the passive release. It also confirms the ability of the hydrogels to maintain an elastase-controlled release mechanism in presence of MMP-2, other overexpressed enzyme in chronic diseases.

We further confirmed that MMP-2 concentration employed for the release study was active and the lack of release was not due to a lack of MMP-2 activity. For this, hydrogels that were specifically sensitive to cleavage by MMP-2 were fabricated and tested, with the kind

assistance of Mr. Emanuel Russo. MMP-2 is a gelatinase, involved in the cleavage of gelatine I, and several types of collagens. Its substrate specificity is quite different from HNE, as it cleaves peptides preferentially between glycine-isoleucine in sequences based on the collagen domain GPQG↓IAGQ (where arrow indicates cleavage site, from BRENDA:EC3.4.24.24 and [224]). The selected peptide for MMP-responsive hydrogel preparation was KCGPQG↓IWGQCK-NH_2 since this sequence has been previously used in the literature for the fabrication of MM-responsive hydrogels[118,163,218].

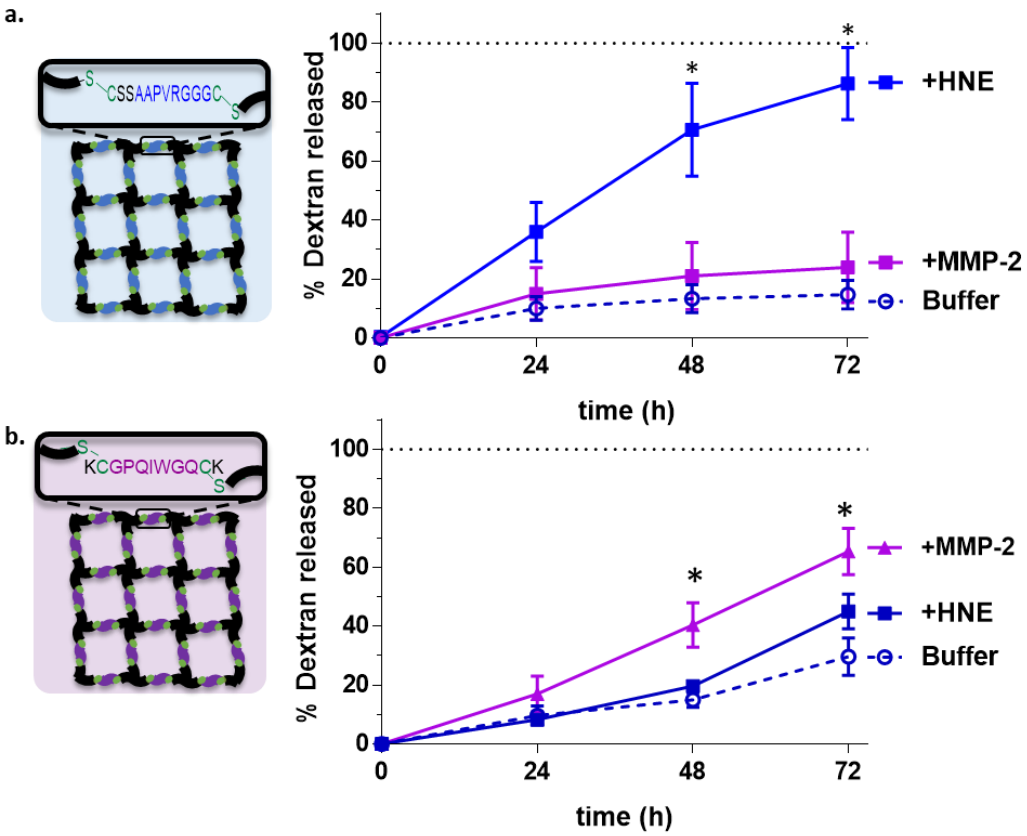

Figure 5.10. Effect of enzymatic cross-reactivity on drug release from elastase-responsive and MM-responsive hydrogels. Release of 70 kDa dextran from **a.**) elastase-responsive or **b.**) MMP-responsive hydrogels in presence of zymogram medium, Human Neutrophil Elastase (HNE, 10nM) and Matrix Metalloproteinase-2 (MMP-2, 16nM). For simplicity, only conditions displaying statistically significant differences from all other samples at each time point are noted as *, as calculated by 2-way-ANOVA test with Tukey post comparison with both MMP-2 and buffer samples (N=3, mean ± error of the mean).

Release from MMP-responsive hydrogels was performed with the same concentrations of MMP-2, HNE and zymogram buffer as previously conducted with the elastase-responsive

hydrogels. Dextran release from MMP-responsive hydrogels incubated with elastase was higher than the passive release controls (Figure 5.10.b, and Table C.2 for all statistical differences). Nonetheless, it was also significantly lower than the release from hydrogels incubated with MMP-2. (Figure 5.10.b), showing a limited degree of selectivity in the release from those hydrogels in presence of HNE. MMP-2 showed significant degradation of the MMP-responsive hydrogels with ~60 % release of dextran over 72h (Figure 5.10.b). The extent of release was significantly higher than for both passive release controls (buffer) and HNE (two-way-ANOVA with Tukey post-comparison). This high release from MMP-responsive hydrogels incubated with MMP-2 confirms that MMP-2 is active enough to trigger MMP-2-controlled released from hydrogels with the adequate sensitive linkers. The same MMP-2 concentration did not previously affect drug release from elastase-responsive gels, reinforcing that elastase-responsive hydrogels selectively lead to elastase-controlled release without interference of MMP-2.

In summary, elastase-responsive hydrogels have shown to be selectively cleaved by elastase, leading to elastase-responsive release, with MMP-2 not affecting the extent of the release from the hydrogels. This suggests that the elastase-responsive hydrogels can potentially be used in diseases where other proteases such as MMP-2 are also highly overexpressed without affecting the elastase-controlled release profiles. MMP-responsive hydrogels were preferentially cleaved by MMP-2, but some increase in the release in presence of elastase was also observed, showing a limited selectivity towards MMP-2 controlled release. This could mean that the release from MMP-responsive hydrogels in pathologies where both enzymes are overexpressed will also be partially triggered by the action of elastase.

5.4 Conclusions

The passive release of a model dextran from elastase-responsive 4-PEGMal hydrogels has been further improved by changing the polymer functionality. Hydrogels prepared via thiol-ene

photopolymerisation between 4-PEGNB showed a reduced passive release of dextran while they kept having suitable elastase-responsive release profiles. Hydrogels underwent almost complete elastase degradation over 72h in conditions similar to the ones employed for future cell-based experiments, indicating the applicability of the hydrogels for future applications.

Specificity of the hydrogels was confirmed by comparing the release of hydrogels prepared with the elastase-sensitive peptide and scrambled peptide (non-responsive). Elastase-controlled release profiles were only observed with the elastase-responsive hydrogels, no release was observed with the scrambled gels. This confirms the specificity of the sequence to elastase degradation and triggered-release, and defines the scrambled sequences as a suitable control for passive release in presence of elastase. This will be important in next chapter, as elastase inhibitors will be encapsulated and a control accounting for their effect in presence of elastase simply due to passive release will be required.

Finally, the lack of MMP-2-controlled degradation of the elastase-responsive hydrogels, at concentrations which have shown to degrade MMP-sensitive gels, confirms the selectivity of the hydrogels to release their cargo in an elastase-controlled manner without being affected by the other protease. On the other hand, MMP-responsive hydrogels were preferentially cleaved by MMP-2 with only a partial increase of the release in presence of elastase. Although the selectivity of the MMP-responsive hydrogels can be further improved, in general, each of the hydrogels lead to a preferential release in presence of the targeted enzyme with respect to the untargeted one. The data presented here signifies a first step to developing dually enzyme-responsive materials for targeting both elastase and MMPs. Those materials would ultimately allow the release of active ingredients from each type of hydrogels selectively in response to the levels of the target enzyme, and be unaffected by the activity of untargeted ones

Chapter 6.

On-demand modulation of elastase activity with inhibitor-loaded hydrogels

6.1 Introduction

The overall aim of this project is to develop hydrogels able to modulate elastase activity by releasing an elastase inhibitor on-demand in response to the levels of protease. The development, passive and elastase-controlled release properties of the hydrogels as well as cross-release in the presence of MMPs has been established in previous chapters (3 to 5). In this chapter, the ability of hydrogels to encapsulate an elastase inhibitor, the ability of elastase to degrade the hydrogel, and the modulation of elastase activity will be studied.

6.1.1 Human Neutrophil Elastase Inhibitors

The high medical need for HNE inhibitors, due to elastase implications in tissue degradation that contributes to the onset and progression of several inflammatory diseases, has led to the development of different types of inhibitors which have been recently reviewed by Von Nussbaum *et al*[92]. The extensive research has made it possible to obtain a variety of elastase inhibitors specifically used for both research and clinical purposes[225]. Elastase inhibitors can be classified as synthetic or physiological, and they are summarised in Table 5.1. Some peptide derivatives have been extensively used for *in vitro* and *in vivo* research such as MeOSuc-AAPA-CMK and MeOSuc-AAPV-CMK. Their mechanism of inhibition is based on the recognition of a tetrapeptide included in the peptide-chloromethylketone molecule, which leads to covalent insertion of the chloromethylketone residue at the catalytic site[226]. Due to their side effects, these inhibitors have been used only in preclinical research[95,204,226,227]. Sivelestat and Alvelestat are two small molecule synthetic inhibitors of elastase with clinical applications. Sivelestat is approved for use in Acute

Lung Injury and Systemic Inflammatory respiratory Syndrome in Japan and South Korea[90]. Sivelestat acts as a suicide substrate, acetylating the active site of HNE[91]. Alvelestat has a similar structure, but with the advantage of being orally active, and it is currently undergoing clinical trial investigation for COPD, Cystic fibrosis and AAT Deficiency[228,229]. The clinical use and ongoing clinical trials of some of these synthetic inhibitors highlights their efficacy and therapeutic potential. But their small size makes it unlikely that a good entrapment efficiency could be achieved in the hydrogels developed in this work.

Table 6.1 : Synthetic and physiological elastase inhibitors

Type	Inhibitor	Size	Uses	Ref
Synthetic	MeOSuc-AAPA-CMK	474.9 Da	Research	204,226
	MeOSuc-AAPV-CMK	503 Da	Research	95
	Elastinal	512.56 Da	Research	94
	Sivelestat	434.46 Da	Clinical: Acute Lung Injury	90
	Alvelestat	545.53 Da	Clinical trials COPD Cystic Fibrosis	230
Physiological (SERPINS)	Alpha-2-macroglobulin	720 kDa	Broad protease inhibitor	82
	SLPI	13 kDa	SERPIN	87
	Elafin	6 kDa	SERPIN clinical trials PAH	231
	Alpha-1-antitrypsin (AAT)	52 kDa	Main SERPIN Clinical: AAT Deficiency COPD	86

MeOSuc = Methoxy succinyl, CMK = Chloromethylketone. SERPIN:= Serine Protease Inhibitors, PAH Pulmonary Arterial Hypertension, SLPI = Secretory Leukoproteinase Inhibitor

Physiological inhibitors of elastase are protein-based inhibitors, therefore possessing a higher size (Table 6.1). The main inhibitors of Human Neutrophil Elastase are alpha-2-macroglobulin, Secretory Leukocyte Protease Inhibitor (SLPI), Elafin and alpha-1-antitrypsin[86,87,92]. Although its high molecular weight (720 kDa) makes alpha-2-macroglobulin a good candidate for hydrogel encapsulation, its wide inhibition spectrum, inhibiting other serine proteases and other classes of endopeptidases such as MMPs makes it too broad for clinical applications[232]. Similarly SLPI and Elafin have a small molecular weight and are not clinically used (Elafin is in clinical trials for Pulmonary Arterial Hypertension, Clinicaltrials.gov identifier NCT03522935[231]), making them

not ideal candidates for this work. The glycoprotein Alpha-1-antitrypsin is a 54 kDa molecule that represents the main physiological elastase inhibitor. Patients having a genetic mutation on the AAT gene possess around 15 % of circulating levels of AAT and develop the disorder known as alpha-1-antitrypsin deficiency (AATD) characterised by severe emphysema and even chronic liver disease[92]. For this alpha-1-antitrypsin is clinically approved and it is currently used as an augmentation therapy in AATD patients[86,233]. Therefore due to suitable size for encapsulation in hydrogels (~50 kDa) and the precedent in its clinical use, alpha-1-antitrypsin was selected as the elastase inhibitor in this project.

The mechanism of AAT inhibition of elastase is complex, characterised by an irreversible suicide substrate mechanism for the AAT[234,235]. The interaction of AAT with elastase can proceed through an inhibitory or a substrate pathway. Figure 6.1 summarises the inhibitory process. Initially the AAT forms a non-covalent complex with elastase (Michaelis Complex, EI in Figure 6.1). Elastase then attacks the inhibitor cleaving a peptidyl bond at the substrate cleavage point of AAT, resulting in a covalent acyl-enzyme intermediate (EI'_{ac}). After this point the reaction can follow either the inhibitory or non-inhibitory pathway. In the non-inhibitory or substrate pathway, elastase cleaves AAT and leads to active elastase (E) and cleaved (inactive) AAT (I*)[234–236]. In the inhibitory pathway, the reaction site loop of AAT is inserted into elastase, causing distortion in the active site of the enzyme and leading to the covalent complex where elastase in deactivated (EI*, Figure 6.1). The extent of substrate or inhibitory pathway will depend on the relative rate of reactive centre loop insertion to the substrate cleavage rate. This will be an important factor to consider when encapsulating AAT into hydrogels since an excess of inhibitor with respect to the concentration of elastase will be required. Supporting this mechanism, others have shown that excess concentrations of AAT (10:1 and 20:1 AAT:HNE ratio) were required to suppress the damaging effects of elastase on cells *in vitro*[195].

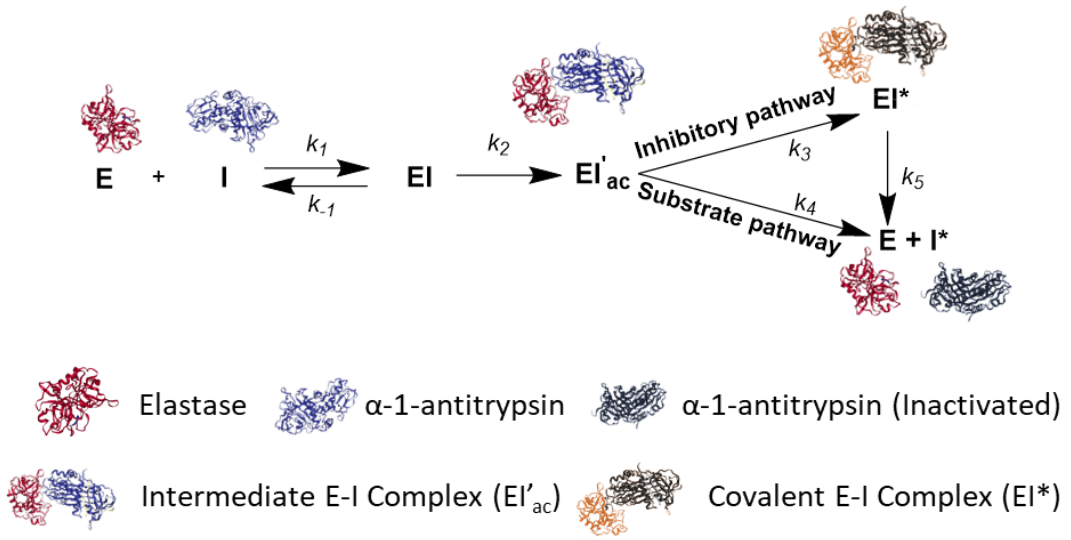

Figure 6.1. Mechanism of alpha-1-antitrypsin (AAT) of elastase, following the general SERPIN pathways. AAT Inhibitor (**I**) forms a non-covalent Michaelis-like Complex with elastase (**EI**). Elastase then hydrolyses the peptidyl bond leading to an acyl-elastase covalent intermediate (**EI'ac**). EI'ac complex can progress through either the inhibitor pathway resulting in inactivated elastase-inhibitor complex (**EI***), or the substrate pathway. The substrate pathway will lead to free (and active) elastase (**E**) and cleaved inactive AAT (**I***). Structures obtained using NGL viewer[237]: Free native pancreatic elastase (PDB entry 1H9L), native AAT (PBD entry 1ATU), cleaved AAT (PDB entry 7API) and complex AAT-PPE (PDB entry 2D26, two colour codes to clearer represent inactive state of elastase and AAT in the EI* complex, where orange is elastase and black AAT).

6.1.2 Dynamic materials for self-controlled modulation of enzyme activity

Enzyme overexpression has been linked to many pathological diseases. For instance, proteases such as Matrix Metalloproteinases (MMPs) and serine proteases are described to be overexpressed in diseases such as cancer, chronic wounds and chronic inflammatory diseases[54,83,142]. The limitation of many protease inhibitor therapies due to high occurrence of side effects and reduced concentration at the disease site has brought attention to the need to develop more efficient delivery systems[115,238]. Additionally many of these enzymes are required in smaller concentrations for the normal functioning of healthy tissue, therefore complete inhibition is not desirable. For this reason, recent researchers have tried to address the challenges of systemic protease inhibitors administration by designing 'smart' materials able to release the enzyme inhibitors on-demand, depending on the level of the targeted enzyme.

As an example, a system aimed for autonomous regulation of coagulation, a coagulation-responsive anticoagulant delivery system was first described by Maitz *et al.*[43]. For this, the anticoagulant heparin was linked to the hydrogel backbone with a thrombin-sensitive peptide. When coagulation occurs, thrombin (coagulation factor) will trigger the release of heparin, inhibiting thrombin and stopping coagulation cascade on one hand and inactivating thrombin on the other, preventing therefore further release. The hydrogels released heparin in response to the concentration of thrombin, reaching pharmacologically relevant levels of heparin release and maintained low coagulation levels[43]. In a recent study the same group did a systematic study, and designed materials with variable degradation speed and expanded the materials to be responsive to other coagulation factors (FX,FXIIa) which are located earlier in the coagulation cascade[140]. More recently, Zhang *et al*., used the same approach in a transcutaneous patch with a feedback-controlled anticoagulant system also responsive to thrombin[189]. The patch was tested in a thrombolytic challenge model, and demonstrated effective protection for acute pulmonary thromboembolism *in vivo*. Some other studies have also used the concept of thrombin-responsive anticoagulant therapies to encapsulate other anticoagulants using alternative delivery systems to hydrogels. Li *et al*. developed thrombin-responsive nanocapsules able to release fibrinolysis activator tissue-type plasminogen activator (t-PA) in response to thrombin levels to be used as surface coatings[135].

The first proof of concept to use enzyme-responsive delivery to release an inhibitor of the targeted enzyme in presence of high levels of enzyme specifically targeting Matrix Metalloproteinases has been developed by Purcell *et al.*[115]. MMP-responsive hydrogels that entrapped a tissue inhibitor of proteases (TIMP-3) by ionic interactions were designed for myocardial infarction treatment, which is characterised by high level of MMPs with respect to healthy tissue[115]. Their *in vivo* work showed that the TIMP-3 loaded hydrogels were able to significantly reduce the MMP activity on the infarction region without increasing the systemic levels of TIMP-3. They also proved that the inhibitor MMP-responsive hydrogels significantly

improved cardiac function 14 days post-injection[115]. In a later study the authors proved that after localized injection of the gels, sustained TIMP-3 effects were even longer with effects seen 28 days post-myocardial infarction. It was also proven that hydrogels administration improved remodelling and ventricular function and reduced key indices associated with heart failure progression[158].

This concept is also being explored for enzymes other than proteases such as β-galactosidase. A lactose-urea Low Molecular Weight Hydrogelator (LMWHG) has been reported to form supramolecular gels which are degraded by β-galactosidase[146]. The degradation kinetics of the material, as measured by the gel to sol transition, depended on the concentrations of β-galactosidase. The authors proved that hydrogels prepared in presence of high concentrations of a β-galactosidase inhibitor were able to modulate β-galactosidase-controlled hydrogel degradation in a concentration-dependent manner. Although it is not clear from the publication if the inhibitor was encapsulated inside the hydrogel or remained between the gel fibres, it exemplifies that the use of specific 'substrate-inhibitor-enzyme' systems for modulation of enzymes has a wider range of applications that just proteases. The authors state as a future application the materials could be explored for controlled drug release applications, since galactosidase is the main enzyme for lactose hydrolysis. As a proof-of-concept they demonstrate degradation of the hydrogel with kiwifruit, which contains high concentration of β-galactosidase[146].

All of the above mentioned studies exploited the overexpression of a pathological enzyme to trigger the release of an enzyme inhibitor, in order to achieve on-demand and site-specific activity modulation. These studies highlight the importance of characterising the inhibitor release kinetics[140], and the effect of different levels of the enzyme [43,115,189] and passive release[43] on inhibition release and biological effects, since they can dramatically affect the efficacy of the system. Therefore these characterisations are required in the hydrogel studies in the present work before conducting *in vitro* studies.

6.2 Aim and objectives

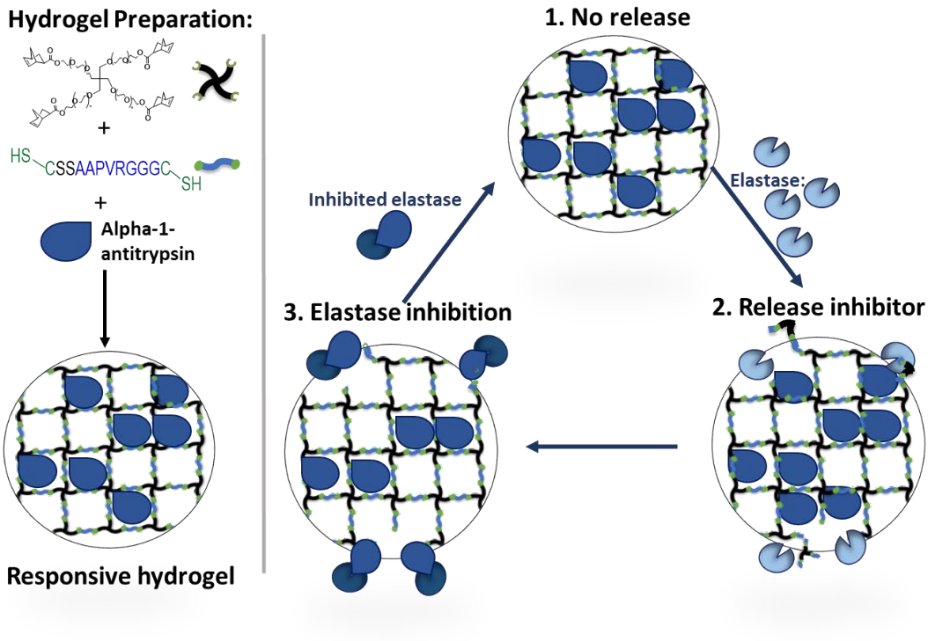

Figure 6.2 Schematic of hydrogel preparation for alpha-1antitrypsin encapsulation (left) and expected mechanism of elastase activity self-regulation for this chapter (right). Mechanism of elastase regulation: **1**) in absence of elastase there is no release of the inhibitor. **2**.) Elastase presence in the medium degrades the responsive hydrogels, triggering the release of the alpha-1antitrypsin inhibitor. **3**) The release of alpha-1-antitrypsin inhibits elastase present in the medium, therefore there is no more release of inhibitor (back to step1.)

In order to be able to modulate protease activity with enzyme-responsive hydrogels in a biologically-relevant disease setting, it is important to assess the kinetics of enzyme-controlled self-inhibition, including assessing the amount of inhibitor required for efficient activity modulation, and its ability to modulate different levels of elastase. The expected mechanism of elastase on-demand activity regulation is explained in Figure 6.2. With this purpose, the aims of this chapter are:

- Characterising the inhibition kinetics and stability of alpha-1antitrypsin in solution.
- Ensuring inhibitor activity under polymerisation conditions and estimate passive release.
- Determining the quantity of encapsulated alpha-1antitrypsin required to inhibit elastase in the release medium.

- Assessing the ability of inhibitor-loaded hydrogels to modulate the activity of different elastase concentrations.

6.3 Results and discussion

6.3.1 Characterisation of alpha-1-antitrypsin inhibition and stability in solution

Before proceeding with the encapsulation of the elastase inhibitor alpha-1-antitrypsin into hydrogels, its inhibitory abilities on Human Neutrophil Elastase were tested. The inhibitory activity of AAT was quantified indirectly by measuring the elastase activity of HNE after incubation with AAT and comparing it to that of untreated HNE. Enzyme and inhibitor were incubated together for 10 min before quantifying the activity of elastase with a colorimetric substrate assay, as described in section 2.13.2 in the methods chapter. AAT had a concentration-dependent inhibition of HNE activity (Figure 6.3). The concentration of inhibitor that reduced elastase activity to 50 % (IC_{50}-) for a 20 nM HNE solution was 14.34nM. This number indicates that the inhibition did not proceed as a 1:1 ratio between enzyme and inhibitor. This could be due to purity of the inhibitor (>70 % as defined by supplier) and due to the described mechanism of AAT inhibition (Figure 6.2). Since AAT interaction forms a complex which can either proceed via an inhibitory pathway (resulting in inactive elastase) or a substrate pathway (resulting in active elastase and inactive AAT). For this reason, it is important to account for an excess of inhibitor when calculating the required amount of inhibitor to be encapsulated.

Then, the stability of alpha-1-antitrypsin in release medium (DMEM-F12) and under hydrogel preparation conditions was assessed. Radical-mediated protein damage has been described at high concentrations of LAP photoinitiator when proteins are incubated with the photoinitiator and exposed to UV light. For this reason solution polymerisations mimicking hydrogel preparation conditions were used to characterise if any loss in inhibitory activity of AAT during radically-mediated thiol-ene reactions was taking place. Compositions were chosen to avoid hydrogel formation and therefore facilitate AAT activity quantification. AAT, AAT and 4-

PEGNB, and AAT and peptide were incubated under UV light exposure in the presence of LAP photoinitiator for three minutes, (mimicking hydrogel preparation conditions). Exposure of AAT to UV light in the presence of LAP photoinitiator drastically reduced its inhibitory activity (Figure 6.4.a). Exposure of the AAT inhibitor to LAP and UV light in presence of the polymer lead to only partial reduction of AAT inhibitory activity. Finally, incorporation of the peptide with the inhibitor had a protective effect on AAT activity, with UV-LAP exposed AAT maintaining the same inhibitory activity over HNE as the control AAT in buffer (Figure 6.4.a). This result is in agreement with previous studies of protein stability[168] and it highlights that no damaging or loss of bioactivity of the AAT inhibitor takes place during photopolymerisation in the presence of other reactive groups (which are present at higher concentrations). Thus, this confirms that the inhibitor is stable under hydrogel preparation conditions and thiol-ene photopolymerisation presents mild encapsulation conditions which maintain the bioactivity of the encapsulated inhibitor.

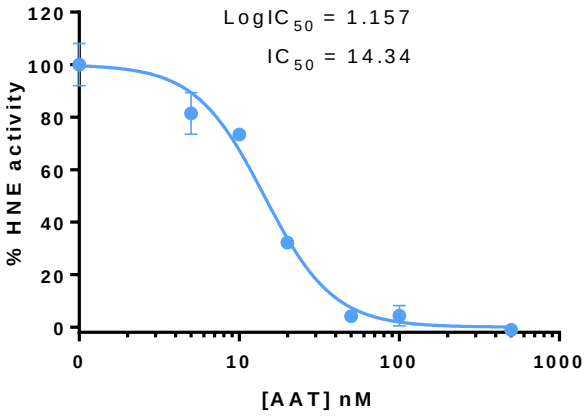

Figure 6.3. Inhibition kinetics and stability of alpha-1-antitrypsin. Concentration-dependent inhibition of 20 nM HNE activity by AAT and determination of IC50 (14.34 nM), n = 4, mean ± standard deviation).

Since the release medium during release studies with the hydrogels is periodically removed every 24 h, stability of AAT in the medium was tested to guarantee its stability for at least 24 h. Alpha-1-antitrypsin was shown to be stable over 72 h in the release media, with inhibitions of HNE comparable to fresh AAT (Figure 6.4.b). These two stability assays together

confirm the suitability of the encapsulation conditions, and the stability of the protein under the selected release medium.

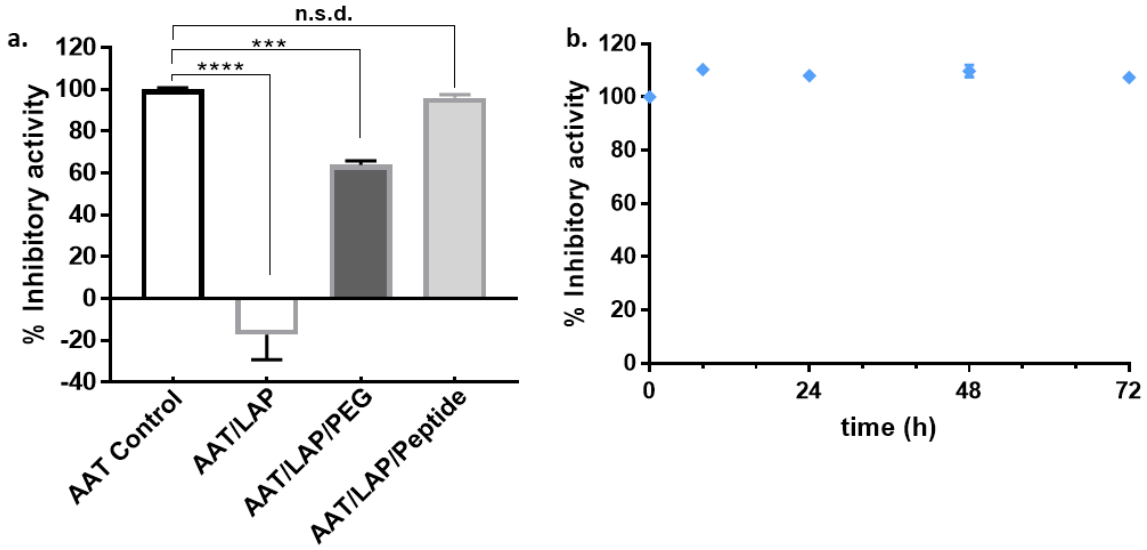

Figure 6.4. Stability of AAT inhibitor. **a.**) Stability of AAT during hydrogel preparation conditions. Percentage of AAT activity with respect to control AAT after exposure to UV light for 2min in presence of LAP photoinitiator only, LAP and polymer (4-PEGNB) or LAP and peptide. (n=3, mean ± standard deviation). Symbols indicate statistical significance by one-way-ANOVA with Tukey post-comparison (p value: ***< 0.001, **** < 0.0001 and n.s.d. not statistically different). **b.**) Stability of AAT incubated in release buffer. (n=4, mean ± standard deviation).

6.3.2 Estimation of the passive release of alpha-1-antitrypsin

Previous studies with Texas red dextran of a similar size to AAT inhibitor (70 kDa) have confirmed that 4-PEGNB hydrogels prepared at 15 % w/v and 20 % w/v allowed for a high entrapment and low passive release of the macromolecule (section 5.3.2). An estimation of the passive release of alpha-1-antitrypsin was conducted in order to confirm a similar encapsulation and release profile than the model dextran. For this, AAT was fluorescently labelled (as indicated in section 2.11 and release was quantified as described in section 2.12). Hydrogels showed a high encapsulation efficiency of the fluorescent AAT, with over 90 % encapsulated. Passive release of the inhibitor was also very low, with only 15 % release over 96 h (Figure 6.5). Although some differences in release could arise between native and fluorescently labelled native inhibitor due

to possible changes in hydrophilicity, charge and size, the good encapsulation and release achieved suggests a similar release may be obtained when encapsulating unlabelled alpha-1-antitrypsin.

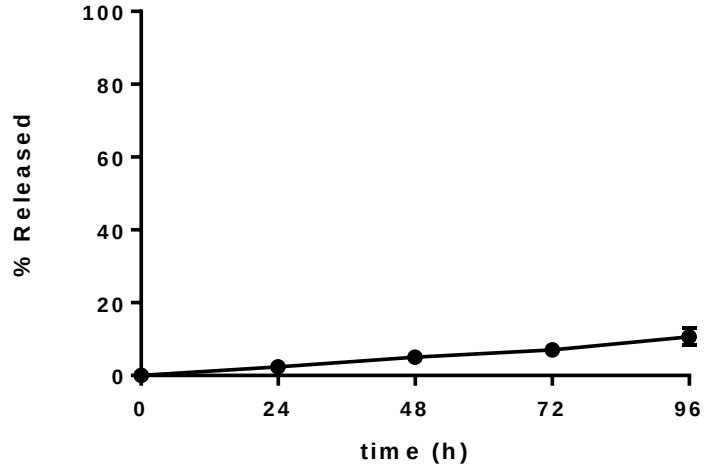

Figure 6.5. Passive release of fluorescently labelled alpha-1-antitrypsin from peptide-4-PENB 5kDa 20 % w/v hydrogels. Encapsulation efficiency was 91.9 ± 2.3 % (n=3, mean ± standard deviation)

6.3.3 Ability of hydrogels to modulate elastase activity

6.3.3.1 Encapsulation of different amounts of inhibitor to achieve modulation of elastase activity

The ability of delivery systems to inhibit enzymes will depend on the relative ratio between the quantities of inhibitor encapsulated and the enzyme in the release medium. If the amount of inhibitor is not enough to regulate the enzyme, enzyme activity will be high and the degradation of the delivery system fast. Only if the quantity of encapsulated inhibitor is high enough will the activity of the enzyme be lowered, causing slower hydrogel degradation and therefore controlled release, similar to a negative feedback loop[43,146].

The ability of alpha-1antitrypsin loaded hydrogels to modulate elastase activity was assessed by monitoring Texas-red dextran (TRD70) release as a probe of hydrogel degradation, and by measuring the HNE activity after each time point. TDRD70 monitoring has previously

shown to be an efficient mechanism to track hydrogel degradation and elastase- controlled-release, since the release of TRD70 increases in proportion to the concentration of elastase (Sections 4.3.6 and 4.3.7). Hydrogels were prepared at a 20 % w/v polymer and TRD70 was co-encapsulated with 5, 10, 20 and 50 µg of AAT and incubated with 10 nM HNE in DMEM-F12 medium, since this medium composition will be the one used for studying *in vitro* effects of hydrogels on cells in Chapter 7. Hydrogels without alpha-1antitrypsin degraded faster than those in medium, with 87 % or TRD70 released over 72h in presence of HNE with respect to the 53 % of passive release controls (no HNE, Figure 6.6.a). Although there were no statistical differences, an inverse relationship between TRD70 and the amount of encapsulated AAT was observed, with 83 % dextran released at the lowest amount of inhibitor encapsulated (5 µg) and 57, 66 and 68 % released at 10, 20 and 50 µg co-encapsulated AAT (Figure 6.6.a). This indicates that a modest effect of the amount of AAT encapsulated on regulating elastase-controlled release was achieved. The lack of stronger trends on elastase-controlled release and statistical differences between hydrogels incubated AAT, could be due to the high passive released observed (53 %). This value was higher than in previous release studies, such as 47 % in DMEM-F12 medium (Figure 5.9) and lower than 25 % when the release was conducted in zymogram medium (Figure 5.10).

Then, the elastase activity at each time point was quantified and expressed as the percentage HNE activity compared to blank hydrogels incubated with HNE (no AAT encapsulated). As shown in Figure 6.6.b, hydrogels containing the lowest amount of AAT (5 µg/gel), did not cause significant reduction of elastase at any time point even though they visually reduced HNE activity at 24 h. Hydrogels containing a higher amount of AAT inhibited HNE activity at earlier time points (24 h for 10 µg and 24 and 48 h for 20 µg gels). This is due to a depletion of the inhibitor at early time points, which does not leave enough inhibitor to efficiently inhibit elastase at the later time points. Only hydrogels encapsulating the highest amount of AAT (50 µg) managed to modulate elastase activity up to 72h (Figure 6.6.b). The lack of a difference between 50 µg gels and blank gels at 24 h was attributed to the high variability of HNE activity for AAT gels at this time point,

since two samples had almost zero activity and the third one showed over 100 % activity with respect to controls (Figure D.1 on the supplement).

It was therefore shown that although no significant differences were found in the release of TRD70, a concentration-dependent effect of the inhibitor on HNE activity modulation was found. Hydrogels containing very low amounts of inhibitor (5 µg) did not modulate the activity of elastase, while increasing amounts of AAT encapsulated led to the gels having an ability to modulate elastase for longer. Only gels containing the highest amount of inhibitor could modulate HNE activity at the last time point.

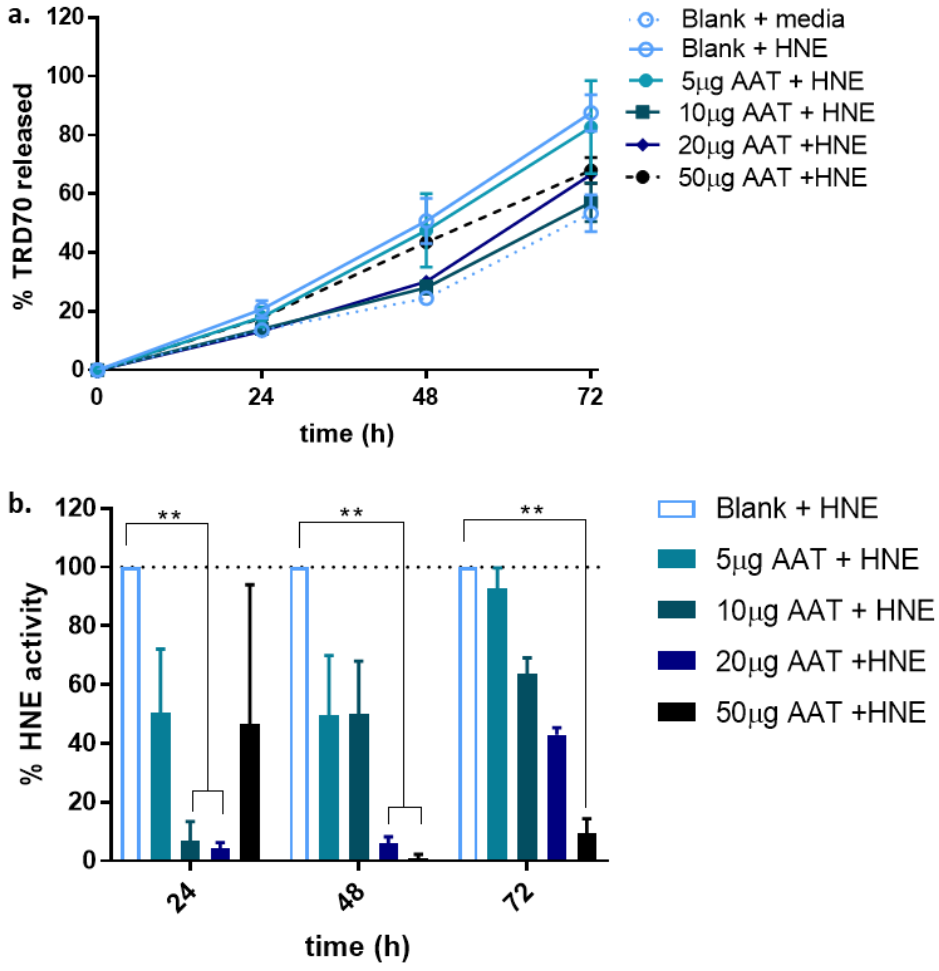

Figure 6.6. Release of dextran from hydrogels containing different quantities of AAT- in presence (+HNE) or absence (+medium)of 10 nM HNE . **a.**) Monitoring release of TRD70 (70 kDa dextran) as model probe of hydrogel degradation. **b.**) Modulation of elastase activity by hydrogels encapsulating different amounts of alpha-1-antitrypsin inhibitor. 0, (blank + HNE) 5 µg (5 µg AAT + HNE), 10 µg (10 µg AAT + HNE), 20 µg (20 µg AAT + HNE) and 50 µg (50 µg AAT + HNE) of inhibitor loaded in each gel and then incubated with 10 nM HNE or medium. N = 3, mean ± standard deviation, symbols represent statically significant differences by two-way ANOVA with Tukey post-comparisons (p value ** < 0.01)

It is impossible to separate the effects on elastase inhibition of AAT released by an elastase-controlled degradation (specific release) from the effects of passively diffused inhibitor (non-specific release) from elastase-responsive hydrogels. This is due to the intrinsic degradability of the responsive hydrogels if they are in contact with elastase. In order to characterise the effects of alpha-1-antitrypsin released by a passive diffusion mechanism on elastase inhibition, ATT was encapsulated in hydrogels prepared with the scrambled peptide (non-responsive hydrogels). Either 20 µg or 50 µg of AAT were incorporated into the hydrogels, since these two conditions rendered a more sustained inhibition of elastase with time with the elastase-responsive hydrogels. It was expected that release of TRD70 would be unaffected by elastase concentration, since it has been already demonstrated in chapter 5 (Figure 5.11) that the gels prepared with scrambled peptides were not degraded by elastase. TRD70 release was not affected by incubation of hydrogels with elastase, neither did AAT encapsulation have any effect on TRD70 release (Figure 6.7). The passive release of TRD70 from scrambled hydrogels was very high, reaching between 65 and 75 % over 72h. Partial degradation of the hydrogels was visually noted and a weaker consistency to the touch (Figure D.2 in the Appendix), which could be for instance due to ester instability in cell culture medium[239]. Both types of hydrogels encapsulating 20 µg or 50 µg were able to modulate elastase activity for the first 48h, but they did not significantly inhibit elastase at 72h (Figure 6.7.b). This effect on elastase activity could be due to the high passive release observed by TRD70 release due to the resulting weaker or partly degraded hydrogels. It has been described that poorly crosslinked hydrogels will lead to an increase of the inhibitor released[43], and would explain the increase of inhibitory effect observed in the first 48h in this work.

Hydrogel composition and mesh size for elastase-controlled release has been selected based on reduced passive diffusion of model dextrans and the fluorescent alpha-1-antitrypsin from the hydrogels. It was hypothesised that a high physical entrapment of the cargo would allow for a release mechanism predominantly controlled by elastase degradation of the hydrogel and

subsequent release of the inhibitor. However, neutrophil elastase is a relatively small protein (approximately 29 kDa in size) and it has been described to infiltrate into hydrogels. Aimetti *et al.*, designed a hydrogel containing some elastase-responsive FRET moieties, and they observed that elastase uniformly penetrated over the full thickness of the hydrogels within 10 minutes (10 % w/v using a 10kDa PEG)[132]. Although the hydrogels used by Aimetti *et al*. had a slightly different crosslinking density, it is possible that a certain extent of elastase infiltration may be taking place in the present hydrogels. This effect would be especially relevant on gels where some degradation had taken place, since the crosslinking density will be much looser. Thus, protease infiltration inside the hydrogel could lead to elastase inhibition through this non-specific mechanism, without the need of the inhibitor to be released to the medium in response to external levels of elastase. This would cause a depletion of the inhibitor at early time points. This could also explain the high extent of inhibition at early time points observed with both elastase-responsive and elastase-scrambled hydrogels.

In summary, although elastase non-responsive hydrogels crosslinked with the scrambled peptide were used initially as a control of the passively released AAT effects on elastase inhibition, they showed a higher passive release of the TRD70 probe than the responsive gels. This suggests some degradation mechanisms other than elastase-controlled one may be taking place in scrambled gels, which led to these hydrogels being able to inhibit elastase activity during the first 48h of release. Therefore, it can only be concluded from this section that although scrambled hydrogels were able to modulate elastase activity at early time points, this was likely due to some non-specific hydrogel degradation. Conversely, elastase-responsive hydrogels encapsulating a high amount of inhibitor were able to modulate HNE activity on the release medium up to 72h. Although elastase-responsive hydrogels with AAT did not significantly alter elastase-controlled hydrogel degradation, they showed an overall improved performance on elastase inhibition with

respect to scrambled ones. This suggests that the elastase-controlled release of the inhibitor is more efficient than only non-specific release mechanisms.

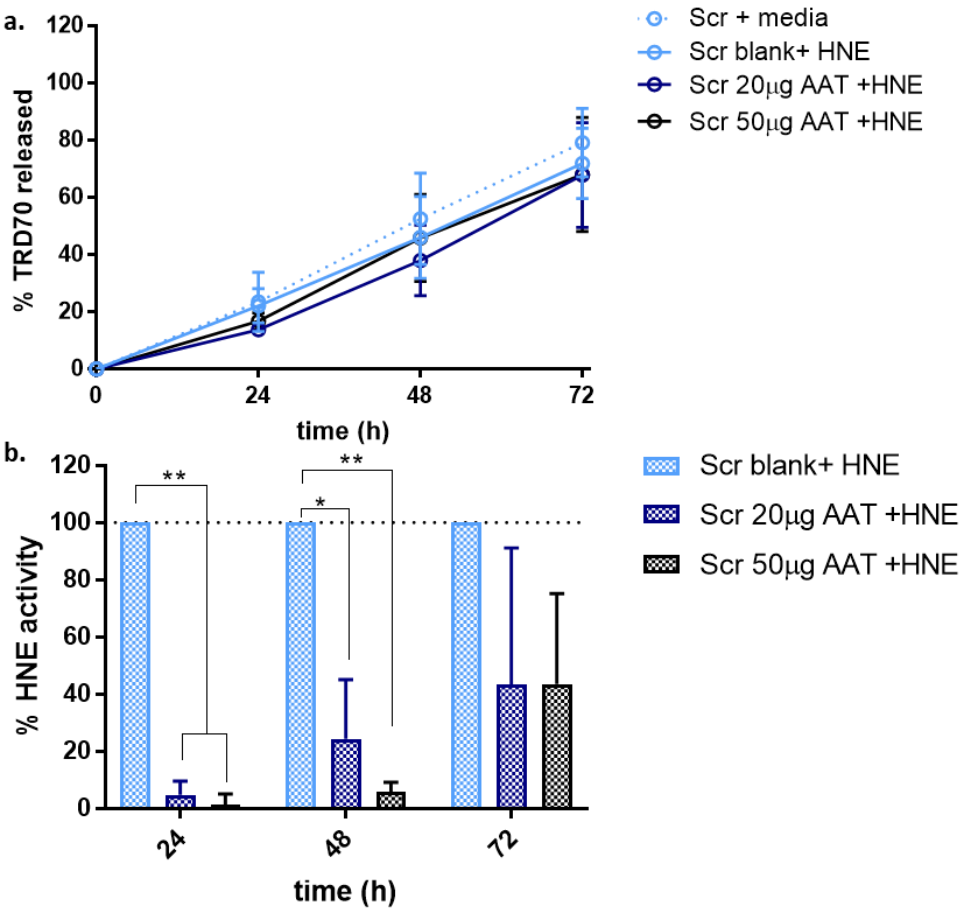

Figure 6.7. Release of TRD70 from hydrogels containing different quantities of AAT and formed with the elastase –scrambled sequence in presence of 10 nM HNE. **a.**) Monitoring release of TRD70 (70 kDa dextran) as model probe of hydrogel degradation. **b.**) Modulation of elastase activity by hydrogels encapsulating different amounts of alpha-1-antitrypsin inhibitor. 0, (blank + HNE), 20 µg (20 µg AAT + HNE) and 50 µg (50 µg AAT + HNE) of inhibitor loaded in each gel and then incubated with 10 nM HNE or medium. N = 3, mean ± standard deviation, symbols represent statically significant differences by two-way ANOVA with Tukey post-comparisons (p value * < 0.05, ** < 0.01)

6.3.3.2 Ability of hydrogels to modulate different elastase activity levels

The concentrations of elastase have been described to be very variable with time and between patients with chronic inflammatory diseases such as COPD and chronic wounds[68,79,240]. Therefore the performance of hydrogels on inhibition of higher concentrations of elastase needs to be investigated. Additionally, increasing concentrations of the target protease have shown to dramatically speed up the material degradation, increasing the release of encapsulated

inhibitor[43,115,241]. It could then be possible that higher concentrations of elastase could degrade the hydrogel faster, leading to inhibitor depletion at early times which would make the hydrogels lose their elastase inhibition properties.

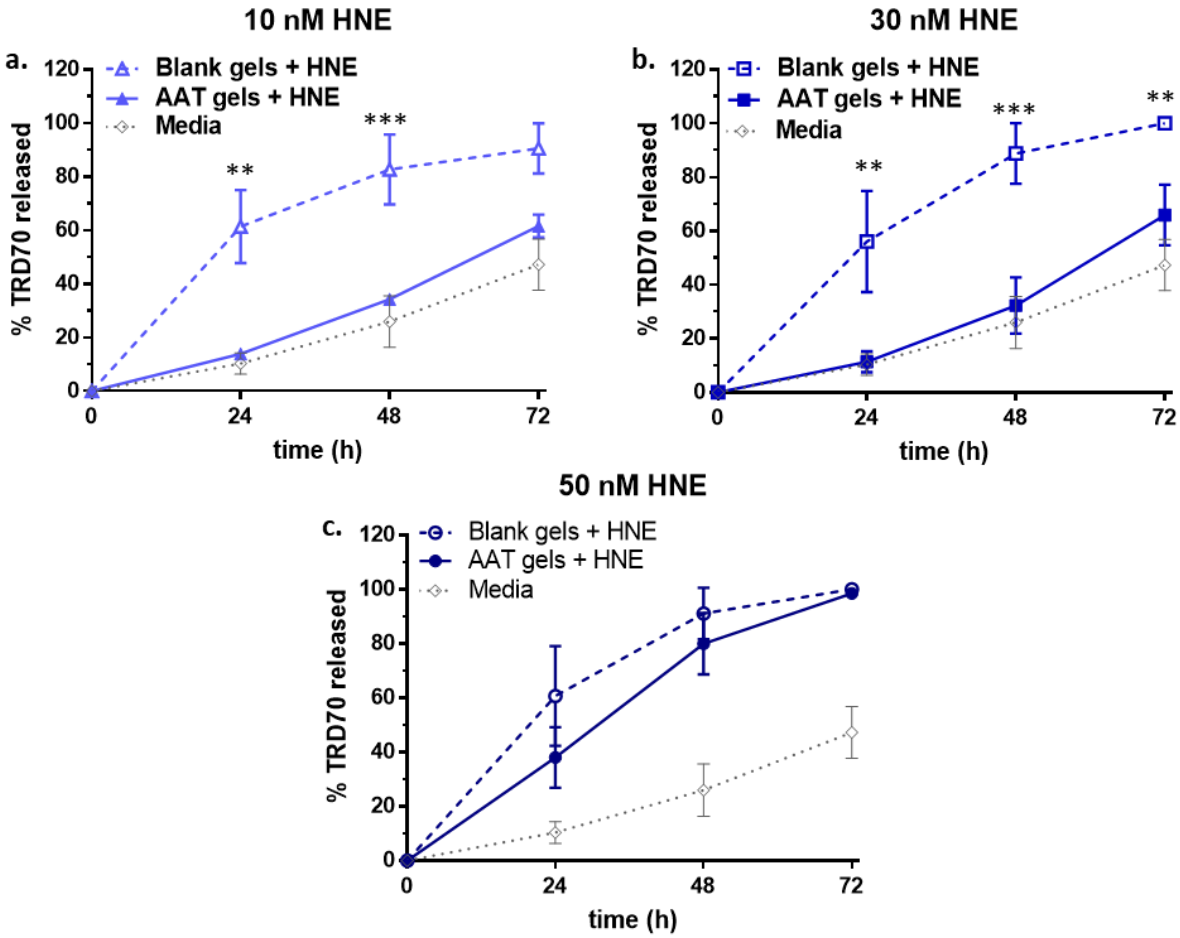

Figure 6.8. Release of 70 kDa TexasRed Dextran from hydrogels loaded without (empty symbols) or with AAT (filled symbols, 50ug) in presence of **a.**) 10nM, **b.**) 30 nM and **c.**) 50 nM HNE. Symbols indicate statistically significant differences by ANOVA with Tukey post-comparisons (p value ** < 0.01, *** < 0.001, mean ± error of the mean, N=3). For simplicity, only differences between hydrogels with (filled symbols) and without inhibitor (empty symbols) are represented. Statistical differences between gels incubated in medium (passive release) and with HNE can be found in Table D.2 in the appendix.

After determining the amount of encapsulated alpha-1-antitrypsin required to inhibit elastase in the surrounding medium, the ability of this formulations to inhibit higher concentrations of elastase was studied. The elastase concentration of 10 nM used in the previous section was initially selected to test the materials since it has shown toxic effect to epithelial cells, which will be described in the next chapter (section 7.3.2). In this section, hydrogels were

incubated with increasing concentrations of elastase (10, 30 and 50nM) in DMEM-F12 medium. 50µg of AAT were encapsulated in each gel, since it had shown better performance on elastase modulation. Hydrogels were prepared at 15 % w/v due to the high variability in release and elastase activity obtained with the 20 % w/v ones in section 6.3.3.1.

Release of TRD70 from blank hydrogels (no containing AAT) showed a faster degradation in the presence of all HNE concentrations of elastase than passive diffusion gels, achieving a total release of 90 % dextran at 10nM and a 100 % release at 30nM and 50nM HNE (Figure 6.8). The encapsulation of AAT had different effects depending on the concentration of elastase. At low concentrations of HNE the hydrogels containing AAT were able to significantly reduce the release of TRD70 with respect to the blank ones (Figure 6.8.a and b, symbols indicate the differences between hydrogels with/without AAT incubated with elastase).

TRD70 release from hydrogels encapsulating the inhibitor was not only lower than blank gels with elastase, but they presented the same profiles as passive release controls (release without elastase, Figure 6.8.a. and b, all statistically significant data in Table D.2. in the Appendix). This indicates that the gels were able to inhibit elastase, causing a reduction in gel degradation and therefore TRD70 released. Other researchers have also described an effective reduction on hydrogel degradation between inhibitor loaded/unloaded hydrogels, demonstrating a sustained inhibition of the protease in the medium[115]. In contrast, hydrogels incubated with the highest elastase concentration (50nM), were not able to modulate HNE in their environment, and as a result the dextran released was not different from blank HNE-treated gels (Figure 6.8, no statistical differences found). Since the stability of AAT on the release medium has been previously confirmed for the time of the release experiments (Figure 6.4), this indicates that the amount of inhibitor was not enough to modulate elastase activity at this highest concentration and therefore did not slow hydrogel degradation and TRD70 release. Maitz *et al*. described a similar protease-controlled mechanism on the inhibitor release profile[43]. They observed a higher release of heparin (inhibitor) from hydrogels incubated with higher concentration of thrombin (protease), but the

hydrogels had a good performance of anticoagulant effect *in vitro*[43]. So it may be possible that although the hydrogels did not modulate release of the 50nM gels, they may have still some significant inhibition of elastase activity.

The elastase activity of the release samples was characterised in order to establish the degree of inhibition achieved with AAT-loaded hydrogels for different HNE concentrations. At 24 h all AAT-hydrogels reduced elastase activity with respect to blank (no AAT) hydrogels although only 30nM and 50nM samples were statistically significant (Figure 6.9.a). This demonstrated that hydrogels were able to largely modulate elastase activity at early time points; however, this inhibition did not translate into a modulation on TRD70 release. Although not significantly different, the inhibitory effect of AAT-loaded gels on elastase activity was still present at 48h, with lower elastase activities achieved with AAT-encapsulating hydrogels at all enzyme concentrations (Figure 6.9.b). Towards the end of the assay (72h) hydrogels did not inhibit higher concentrations of HNE (30nM and 50nM), a visible reduction in HNE activity was only achieved at 10nM HNE, though it was not statistically significant (Figure 6.9.c). This data indicates that the extent of elastase inhibition is enzyme-concentration and time-dependent.

Overall, elastase-responsive hydrogels modulated lower concentrations of elastase more efficiently, achieving only inhibition of high concentrations of elastase at early time points. This was evidenced by the relative changes of the release of a model dextran, and the inhibition of elastase activity.

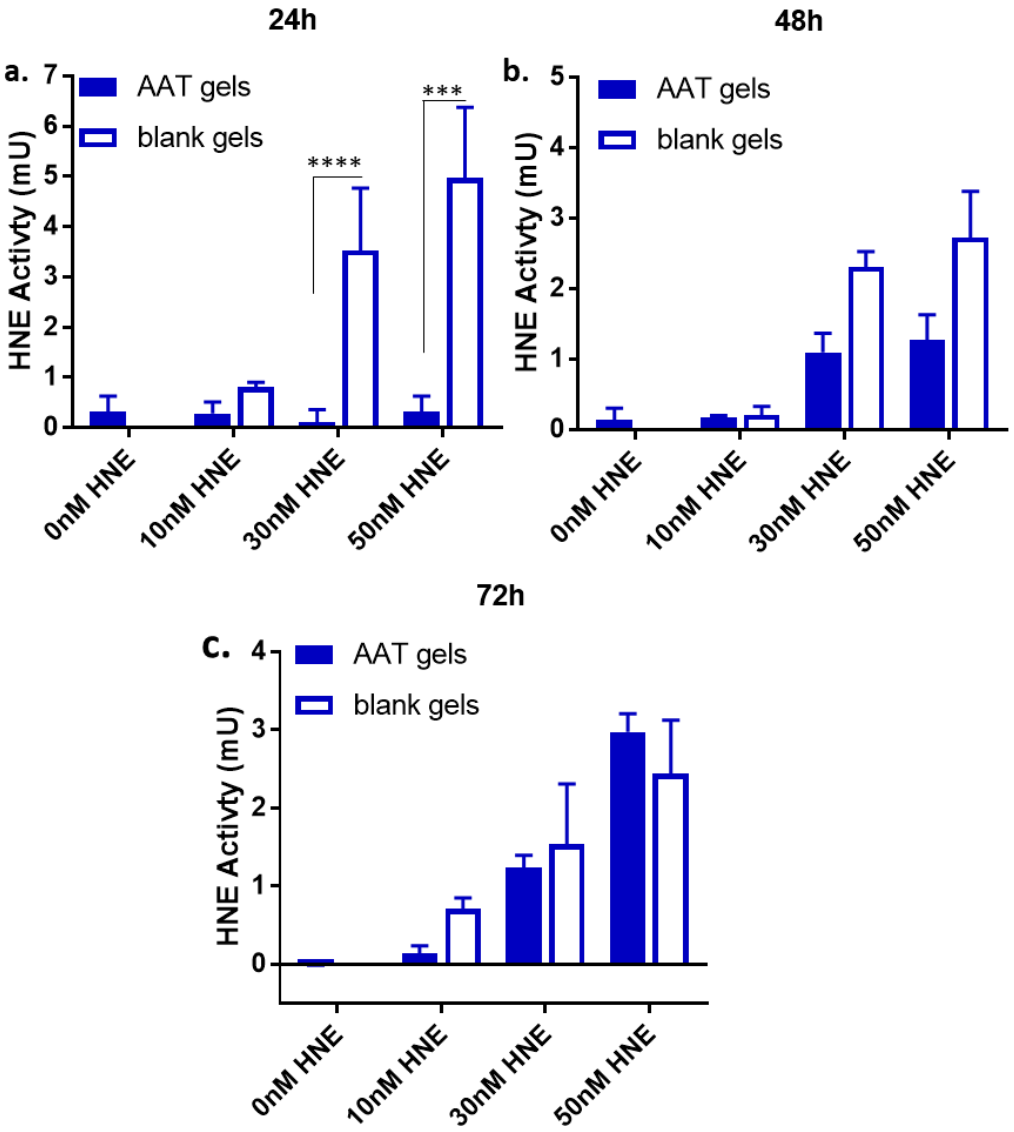

Figure 6.9. Modulation of increasing concentrations of HNE activity (10, 30 and 50 nM) with AAT hydrogels. HNE activity measured on the release medium at each time point with either blank hydrogels (empty bars) or AAT-loaded hydrogels (Filled bars, 50 µg AAT, 15 % w/v gels) at **a.**) 24 h, **b.**) 48 h and **c.**) 72 h. Symbols represent statistically significant differences by ANOVA with Tukey post-comparisons (*** p value < 0.001, **** < 0.0001, mean ± error of the mean, N=3 except 50nM 24 h N=2).

6.4 Conclusions

Alpha-1-antitrypsin inhibitory activity on elastase and its suitable stability during hydrogel preparation and release conditions has been confirmed. The passive release of the inhibitor from hydrogels was estimated with a fluorescein-labelled alpha-1-antitrypsin. The passive release was

very low, below 20 %, being important for achieving subsequent elastase-controlled release in presence of elastase. Although some differences in release could arise due to differences between native and fluorescently labelled native inhibitor the low passive release achieved suggests a similar release may be obtained when encapsulating unlabelled alpha-1-antitrypsin.

Only high amounts (50 µg) of alpha-1-anitrypsin inhibitor encapsulated in elastase-responsive hydrogels achieved sustained elastase inhibition. Although there were no significant changes in the modulation of elastase-controlled release, it was observed that higher concentrations of AAT led to a prolonged inhibition of elastase activity, suggesting that feedback-controlled elastase inhibition could successfully be used to inhibit elastase activity. An overall trend of elastase activity inhibition was observed at early times; however, it is worth noting that at some time points the variability of activity between different hydrogel samples was very high within each hydrogel type.

Scrambled hydrogels encapsulating alpha-1antitrypsin were used as a control of the passively released AAT effects on elastase inhibition as they are non-responsive to elastase. Conversely, some degradation was observed and they showed a higher passive release of the TRD70 probe than the responsive gels, suggesting some other unspecific degradation may be taking place. As a consequence, scrambled hydrogels could also inhibit elastase activity during the first 48h of release. This unspecific release is not fully clear but it is hypothesised that it could be due to non-enzymatic degradation of gels, and the possibility of elastase penetrating weak hydrogels. It has been described that elastase is able to diffuse through hydrogels due to its small size[132]. This elastase penetration of HNE inside the gel could lead to the enzyme being inhibited without the need for the inhibitor to be released, contributing to the high variability in elastase activity and the effect of scrambled hydrogels.

Elastase-responsive hydrogels entrapping with higher amounts of AAT (50 µg) were able to modulate more efficiently lower concentrations of elastase. Inhibition of high concentrations of

elastase was only achieved at early time points, as demonstrated by the relative changes on the release of a model dextran, and the inhibition of elastase activity. This would be particularly important to guarantee effective elastase modulation in a preclinical or clinical context, where the levels of elastase can significantly vary with time and between different individuals.

Overall, although elastase-responsive hydrogels with AAT did not systematically alter elastase-controlled hydrogel degradation, they showed a higher inhibition of activity with respect to scrambled hydrogels. This suggests that non-specific release mechanisms of AAT are less efficient to regulate elastase activity than the elastase-controlled release of the inhibitor, whereby the elastase activity triggers the release of the inhibitor and therefore its own inhibition. Moreover, hydrogels were able to modulate higher concentrations of elastase although for 24 – 48 h. Therefore, elastase-degradable hydrogels able to release AAT in the presence of HNE activity have promising potential to be used to modulate elastase activity *in vitro.*

Chapter 7.

Modulation of elastase activity in an *in vitro* epithelial cell model

7.1 Introduction

In previous chapters, enzyme-responsive hydrogels with enzyme-controlled release and elastase-modulating properties have been developed. The aim of this work is to develop systems that can modulate elastase activity with potential use in biomedical applications. Thus, this chapter will study the cytocompatibility of the prepared hydrogels and their ability to modulate elastase activity *in vitro*.

7.1.1 *In vitro* testing of enzyme-modulating materials

*In vitro c*haracterisation of enzyme-responsive materials or materials aiming to modulate or fully inhibit enzymes often involve general experiments such as cytotoxicity with relevant cell lines, and specific assays for determining enzyme-responsiveness or modulation. The cell-based experiments usually start by the determination of the biocompatibility with cells, to ensure lack of toxic effects of the materials. This can be done by assessing cell membrane integrity[125,195], cell metabolic activity[124,149,164], or a combination of both[38,125,178]. Other researchers have previously shown that peptide-crosslinked PEG hydrogels similar to the system developed here did not have toxic effects on cells[38,124,125,134,164,178]. Therefore it is not expected that the materials developed in this work will have high toxicity *in vitro* although it will be further tested. After these initial *in vitro* toxicity experiments, materials are usually tested *in vivo* for efficacy and/or toxicity. Due to their singularity, some specific tests for enzyme-responsive or modulating materials, such as release and inhibition experiments with the target enzyme or an 'enzyme cocktail', need to be thoroughly characterised, before moving to *in vivo* or *ex vivo* testing[43,115,123,140,145,189].

Since the materials described in this work aim to modulate elastase, an *in vitro* model to test efficient enzyme modulation is required, since accurate characterisation of inhibition profiles would be difficult to establish *in vivo*. As Human Neutrophil Elastase (HNE) enzymatic overexpression has been linked to pathologies such as chronic wounds and pulmonary diseases[79,80,83], some *in vivo* models which give an insight on the damaging effects of elastase on different tissues have been developed. For instance, mice deficient in the elastase inhibitor SLPI (Secretory Leukocyte Protease Inhibitor) have been used to mimic a chronic wound state in mice[87]. Mice lacking this main inhibitor of elastase would experience problems related to elastase overexpression. SLPI knockout mice suffered from delayed wound healing, prolonged inflammation and reduced new matrix deposition causing impaired healing[87]. Intratracheal instillation of elastase is often used as *in vivo* model of pulmonary emphysema. Animals instilled with elastase present lesions characteristic of emphysema characterised by a high inflammatory burden, high activity of metalloproteinases, and marked alveolar extracellular matrix degradation leading to high tissue damage[88,89]. Subcutaneous elastase injection in animal feet pad has also been often been used as *in vivo* model to mimic inflammation and oedema, since elastase administration causes notable microvessel wall destruction, inflammation and swelling [242,243]. These *in vivo* models provide a general understanding of the direct consequences of high elastase activity, mostly associated to high inflammation and epithelial damage.

Some isolated studies have also tried to reproduce *in vitro* the negative effects of elastase on epithelial cells observed *in vivo,* by supplementing cell culture medium with elastase. It has been reported that addition of elastase to different epithelial cells can cause cell detachment[195] and death[227,244–247]. This could be due to a combination of mechanisms, since the enzyme degrades extracellular matrix componets[227] and hinders cell-cell interactions[248]. Garrat *et al* have described that elastase can impede epithelial cell repair in a concentration-dependent manner [195]. Evidence from these studies clearly indicates a negative effect of elastase on epithelial cell viability and migration *in vitro*. However, no comprehensive studies have been undertaken to make use of it

as a biologically relevant *in vitro* model to test elastase modulating agents or materials. Therefore a part of this chapter will focus on the development of a suitable *in vitro* model. Subsequently this model is used to test elastase-modulation abilities of the hydrogels. .

7.2 Aim and objectives

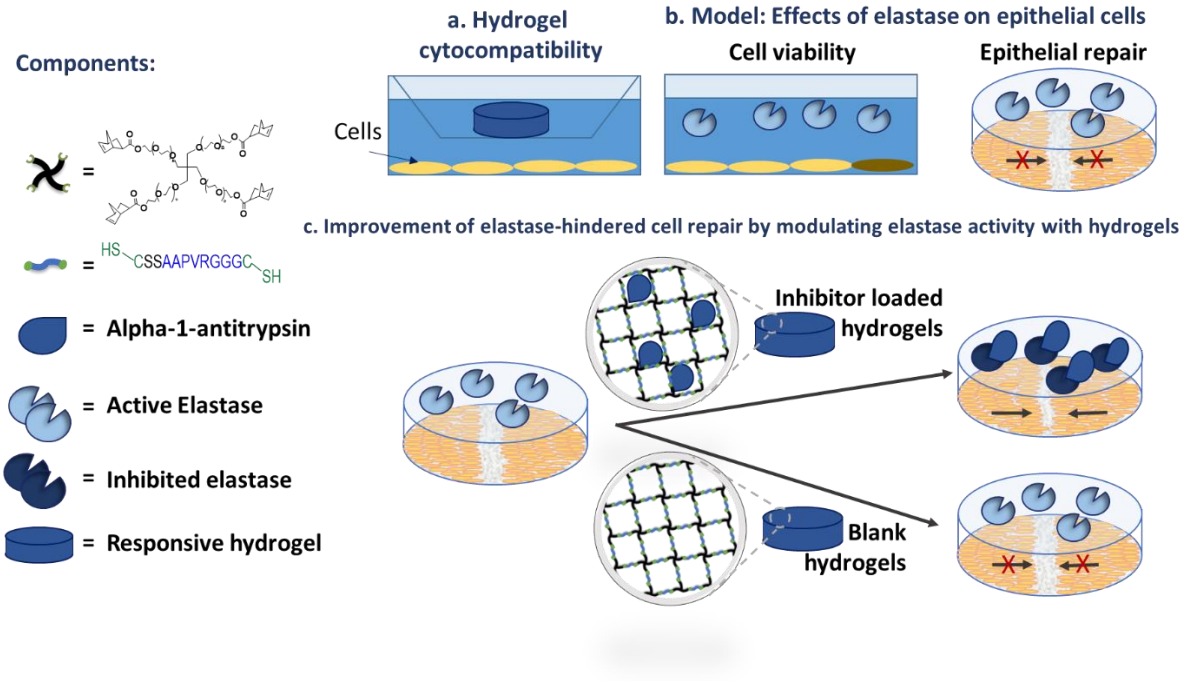

Figure 7.1 Summary of in vitro tests conducted in this chapter. **a.**) Testing of hydrogel components' cytocompatibility. **b.**) Development of a basic cell model environment for the effects of elastase on cell viability and epithelial repair. **c.**) Evaluation of the recovery in epithelial migration through modulation of elastase activity with inhibitor-loaded hydrogels.

This chapter investigates the ability of the gels to modulate elastase activity in presence of cells and improving detrimental effects of elastase on cells. This includes assessing the gels' cytotoxicity and ability to modulate elastase activity and minimise the damaging effects of high elastase activity on epithelial cells.

In order to achieve this aim, the objectives of the chapter are as follows and are summarised in Figure 7.1:

- Incubation of epithelial cells with hydrogel components in order to test cytocompatibility (Figure 7.1.a).

- Systematical study of the effects of elastase on epithelial cell repair and viability, to identify the conditions that can be used as a model of elastase-induced epithelial damage (Figure 7.1.b).
- Characterisation of the ability of hydrogels to promote epithelial repair by modulating elastase activity.(Figure 7.1.c)

7.3 Results and discussion

7.3.1 Effect of hydrogel components on cell viability

Cytocompatibilty of the blank hydrogels and of different concentrations of alpha-1antitrypsin in solution were investigated. Cell viability can be characterised by measuring metabolic activity of the cells, and this method has been broadly used to test biomaterials' cytocompatibility[124,149,164]. These assays are usually based on the reducing power of the live cells and use a substrate that is converted to coloured/fluorescent product upon cell reduction.

The cytotoxicity of elastase-responsive 4-PEGMal and 4-PEGNB hydrogels and the alpha-1-antitrypsin inhibitor in solution was tested on a human lung epithelial cell line, A549. This cell line has been chosen as the model of epithelial cells since it has been widely used as a referent of lung epithelial cells elsewhere[124,125,245,249,250]. Cell viability was assessed throughout this project with the Prestoblue™ fluorescence assay, which evaluates the metabolic activity of the cells[251]. The active ingredient is the non-fluorescent highly cell-permeable compound resazurin. After entering living cells, resazurin is reduced to the highly fluorescent compound resorufin yielding a strong fluorescence signal (Figure 7.2.a). The concentration of resorufin is therefore proportional to the metabolic activity of the cells in the assay medium so it has been used to compare cell viability under different conditions (as explained in section 2.16.3). 4-PEGNB hydrogels were tested for their biocompatibility. Hydrogels were incubated with cells for 72h without showing any toxic effect on the cells (Figure 7.2.b). Metabolic activity of the cells was not significantly reduced as

compared to untreated cell controls as determined by a t-test between each hydrogel type and the respective untreated cell control, confirming the hydrogels did not have a cytotoxic effect on epithelial cells. Other studies have also observed a lack of toxicity of similar PEG-peptide based hydrogels *in vitro* with epithelial cells[124,125] and other types of cells[38,134,164,178].

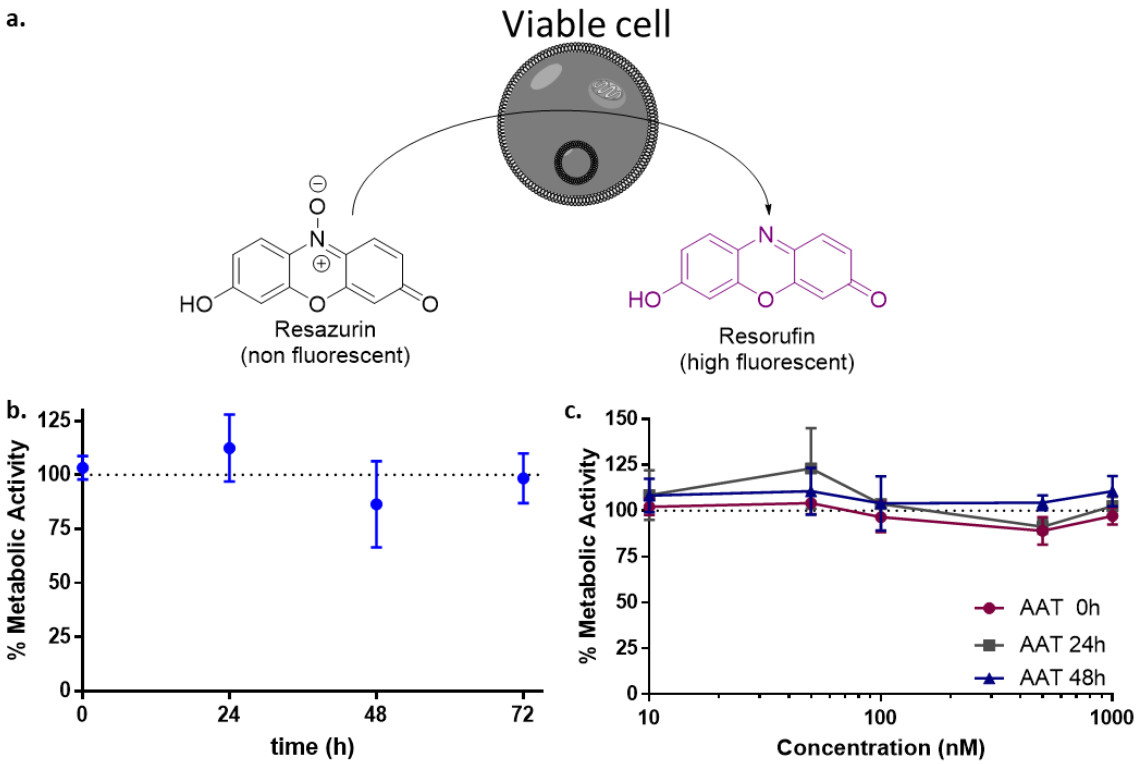

Figure 7.2 *In vitro* cytotoxicity of hydrogel components. **a.**) Reduction of resazurin to fluorescent compound resorufin by viable cells in Prestoblue assay of metabolic activity. Effect of **b.**) blank hydrogels on the viability of A549 epithelial cells measured as % metabolic activity. No significant differences were found by multiple t-test (one per time point) hydrogels with the untreated cell controls at each time point (N = 3 and n=2, mean ± error of the mean). **c.**) Effect of alpha-1-antitrypsin (AAT) inhibitor on the viability of A549 epithelial cells measured as % metabolic activity. No statistically significant differences were found by two-way ANOVA (mean ± error of the mean N = 3, n = 3,). Cell numbers have been normalised to untreated cells for each time point, and dotted line indicates 100 % viability.

The effects of different concentrations of alpha-1antitrypsin (1-1000nM) on cell viability was also investigated. A broad range of concentrations was studied in order to cover the highest concentration expected even in the case that all the encapsulated inhibitor was released at once from the hydrogels. Incubation of epithelial cells with AAT did not affect cell viability at 24 h or

48h, since there was no significant reduction in metabolic activity compared with the untreated cells (Figure 7.2.c).

Overall, these data indicate that blank elastase-responsive hydrogels and the elastase inhibitor human alpha-1antitrypsin are not significantly toxic to the model epithelial cell line A549, as assessed by the metabolic activity experiments.

7.3.2 *In vitro* mimicking of elastase damaging effects to epithelial cells

This section will aim to establish an *in vitro* model that can be used to test the elastase-modulating abilities of hydrogels developed in Chapter 6. Since the hydrogels aim to modulate elastase activity, the *in vitro* model will aim to mimic the harmful effects observed in epithelial cells by overexpressed HNE *in vivo*. It was hypothesised that addition of an adequate concentration of elastase to epithelial cells will cause detrimental effects leading to a reduced metabolic activity and cell migration. For this, a range of media composition and concentration of HNE will be studied in order to find the conditions where HNE concentration reduces cell viability and migration, and the ability of the elastase inhibitor alpha-1-antitrypsin administered in solution to reverse those effects.

7.3.2.1 Selection of adequate cell media

Human lung alveolar epithelial cell line A549 were used throughout this work as the model epithelial cell line, details of the general cell maintenance and culture can be found in section 2.16.1. Standard cell culture conditions for epithelial A549 cells include the supplementation of the basal medium (DMEM-F12) with 10 % v/v of Foetal Bovine Serum (FBS). FBS is widely used in cell culture applications, it has many factors to promote cell growth and cell survival, but its exact composition is undefined. Among these factors there may be a range of protease inhibitors which could inhibit Human Neutrophil Elastase (HNE) activity. Initial experiments showed that HNE did

not have a toxic effect on A549 epithelial cells when incubated in 10 % FBS supplemented medium (Figure E.1). For this reason the suitability of serum-reduced and serum-free media to be used for elastase experiments was investigated. Two factors need to be considered:

- First, the selected medium has to be able to support cell survival and migration. Since cells in medium will be considered as the positive migration control, the selected composition needs to allow for a certain degree of migration which will then be hindered by the addition of elastase.
- Second, HNE needs to have a certain degree of activity in the selected medium. Unless elastase is active in the medium, its effects on epithelial cells will not be observed.

Epithelial cell migration was quantified with the scratch assay. The *in vitro* scratch assay, also known as scratch-wound assay, is widely used to study cell migration *in vitro* and is based on epithelial cells ability to migrate to close gaps created in a confluent cell monolayer[196,252]. Briefly, cells are grown until confluence and then, upon the creation of an artificial gap (or scratch), cells at the edge of the scratch will move toward each other until the wound is closed. Finally, the comparison of images taken at given intervals can be used to assess how effectively the cells migrated to repair the created wound under different conditions[195,250]. This assay is generally accepted as *in vitro* mimic of cell migration, but since differences in cell death and proliferation could also affect the wound closure rate some authors prefer to refer to it more generally as a method to evaluate epithelial cell repair[250]. Experimental details of this assay can be found in section 2.16.4.

Firstly, the ability to support cell repair of five reduced serum media (0.5 %, 1 %, 2 % and 4 % v/v FBS supplemented DMEM-F12) and two serum free media compositions (0 % FBS DMEM-F12 or SAGM [Small Airway Epithelial Cell Growth Medium] supplemented DMEM-F12) was assessed. A range of FBS supplements were tested since the percentage of serum has been described to reduce the ability of A549 to migrate in the scratch assay[250]. SAGM supplement was

selected since it is a serum-free supplement widely used with other epithelial cell lines such as Human Small Airway Epithelial Cells. Cells migrated under all the studied conditions, although the extent of migration increased in general trends with the percentage of serum (Figure 7.3.a). The highest degree of wound closure was observed by cells supplemented with SAGM, and at 1 and 4 % of serum, achieving a 54 %, 49 % and 64 % wound closure respectively. Therefore the ability of these media compositions to support HNE activity was tested.

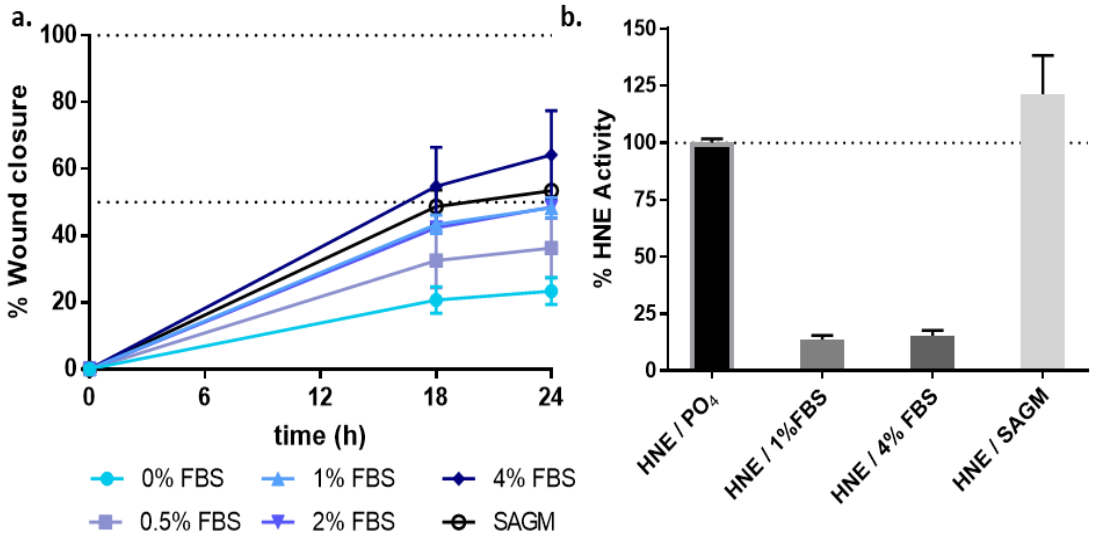

Figure 7.3. Ability of different low serum and serum free media to **a.**) support epithelial cell migration and **b.**) Human Neutrophil Elastase activity. Activity was expressed as percentage of elastase activity in phosphate buffer (n = 3, mean ± standard deviation).

HNE was incubated in 1 % FBS, 4 % FBS and SAGM cell media and phosphate buffer pH 8 as a control. The elastase activity was quantified with the elastase colorimetric assay as described in the chapters (Section 5.4.5) and described in the methods section 2.14.2. The activity of elastase was drastically reduced in cell media containing both 1 % and 4 % FBS, which could be due to the presence of protease inhibitors in FBS. Conversely, SAGM supplemented medium showed a much higher activity of elastase, even higher than the standard phosphate buffer control (Figure 7.3.b). This effect could be due to the absence of serum in SAGM supplemented media, and therefore any protease inhibitors, and to the presence of Bovine Serum Albumin (BSA) which can act as a non-specific protein stabiliser. Since SAGM supplemented medium also allowed both high

epithelial cell migration and elastase activity, it was selected as the medium for HNE-containing *in vitro* experiments.

7.3.2.2 Effect of Human Neutrophil Elastase on cell viability

The effects of HNE on cell viability were evaluated using the Prestoblue assay. SAGM supplemented medium was selected for the experiments as it was shown to promote epithelial cell migration and maintain HNE activity (section 7.4.2.1). Cells were incubated with elastase at a range of concentrations (1 – 140 nM) for 24 h and 48 h. After each time point, the cell viability was calculated and expressed as relative metabolic activity compared to the untreated cells (using equation 2.10). These concentrations were chosen based on the observations of Garrat *et al.* who found that primary airway epithelial cell viability decreased significantly after being incubated with 50 – 100 nM HNE[195].

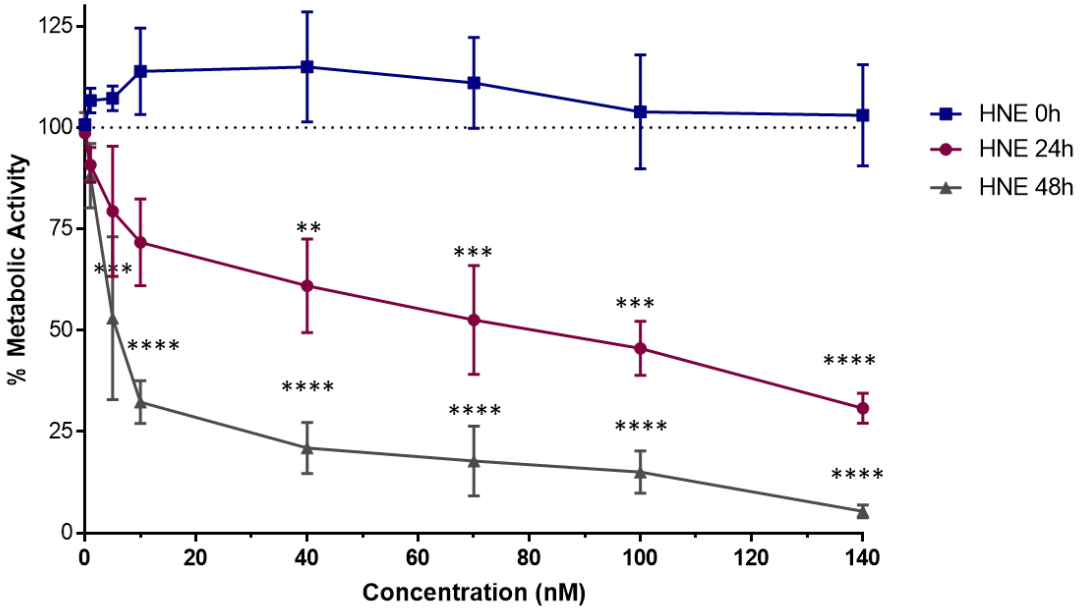

Figure 7.4. Time and concentration-dependent effect of externally supplemented Human Neutrophil Elastase on the viability of epithelial cells (N=3, n=3 on each experiment, mean ± error of the mean). Symbols represent statistical significance by 2-way-ANOVA test with Dunnets post analysis between each concentration respect the control with no HNE at the same time point (p Value ** < 0.01, ***< 0.001, and **** < 0.0001.)

The addition of HNE had a concentration-dependent and time-dependent effect on epithelial cell viability (Figure 7.4.). Concentrations higher than 10 nM lead to a reduction in cell viability within 24 h, and concentrations from 5 nM lead to reduction in viability within 48h. Additionally, it was visually observed that the cell phenotype was altered at high concentrations of elastase, leading to rounded spherical cells and noticeable cell detachment causing reduction in the cell numbers (Figure E.2 in the Appendix). The observed effect of HNE on cell viability may be due to a mixture of mechanisms. These may involve a combination of extracellular matrix degradation[227], alteration of cell-matrix interactions and cell-cell interactions[248] which can cause cell detachment[195] and cell death[227,244–246] leading to the observed reduction in cell viability. Some studies have observed similar effects of elastase or neutrophil conditioned medium on epithelial cells, causing reduced cell viability and cell death[227,244,245,247] . In particular, Song *et al*. have shown reduction in cell viability of the A549 cell line by apoptosis after incubation with elastase[247]. In contrast, one study by Xiaokaiti *et al.* has observed the opposite effect and found an increased cell viability of A549 cells after exposure to HNE[253]. The data of Xiaokaiti *et al.* differs with the results obtained in the previous publications and the present project. It could result from differences in cell media, passage number of cells (unstated), the use of a different cell viability assay, or even due to different mechanism of HNE-cells interactions.

Having shown that elastase has a negative effect on epithelial cell viability, the effect of co-administration of elastase and the elastase inhibitor alpha-1-antitrypsin was investigated. Due to significant reduction in cell viability after 48 h exposure to 5 nM HNE, this concentration was selected for the addition of AAT. An excess of AAT at 2:1 and 10:1 AAT: HNE ratio was employed (10 nM and 50 nM), since it was shown in the previous chapter that AAT requires more than 1:1 ratio to inhibit HNE. HNE addition decreased cell viability at 24 h and 48h. The co-delivery of AAT lead to a recovery of epithelial cell viability, with a significant increase of cell viability at 24 h with the 10 times excess AAT, and at both concentrations at 48 h (Figure 7.5). Although both inhibitor concentrations tested improved cell viability, the extent of cell viability recovery was significantly

higher at the higher inhibitor concentration and cells showed improved morphology (Figure 7.5 and Figure E.3 in the appendix). This highlights the important need of an excess of inhibitor in order to efficiently inhibit HNE-induced reduction of cell viability. These results are in agreement with previous studies assessing the effect of HNE and neutrophil-conditioned medium containing HNE on different epithelial cell types. There, a recovery in cell viability and a reduction in apoptosis was observed by administering an excess of elastase inhibitors such as alpha-1-antitrypsin[227] or sivelestat[247].

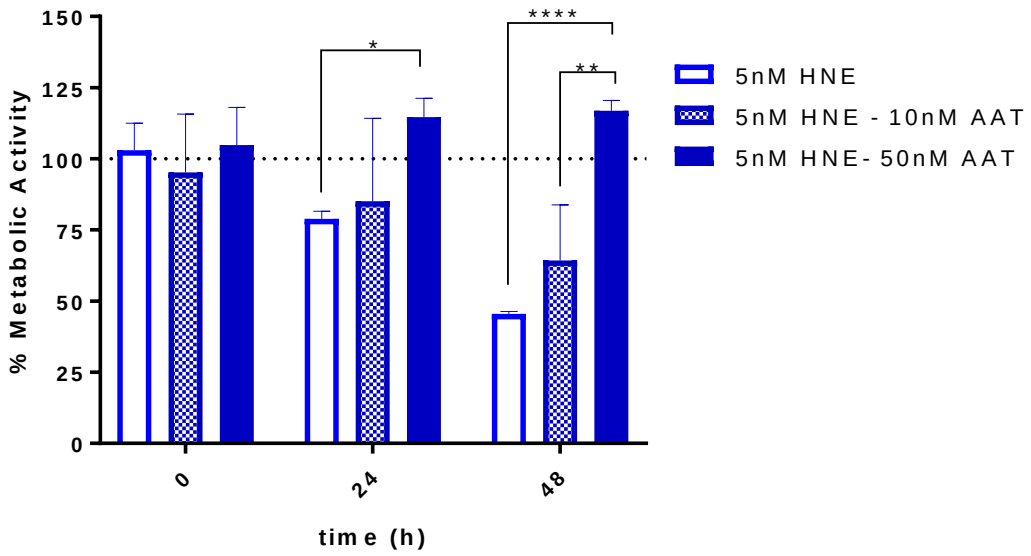

Figure 7.5. Reversibility of 5nM elastase reduction on cell viability by co-administration of AAT (10 nM AAT and 50 nM AAT). Symbols represent statistical significance by 2-way-ANOVA test with Tukey post comparison (p Value: * < 0.05, ** < 0.01 and **** < 0.0001.

In summary, addition of elastase was shown to reduce cell viability in a time and concentration-dependent manner, which is in agreement with previous studies where elastase has been incubated with a variety of epithelial cell lines. More importantly, this elastase-induced reduction in viability could be recovered by co-delivering of an excess of the elastase inhibitor alpha-1antitrypsin.

7.3.2.3 Effects of Human Neutrophil Elastase on epithelial cell repair

Once it had been proven that the presence of HNE can affect viability of epithelial cells, its effect on epithelial repair was investigated. HNE concentrations of 1 nM and 2 nM, which have previously been shown not to affect cell viability after 48h (Figure 7.4), were initially tested. It was hypothesised that although these HNE concentrations did not affect cell viability, they may be high enough to limit epithelial cell migration. Conversely, neither 1 nM nor 2 nM HNE affected cell repair over 48h, with cells migrating at the same rate than the untreated cells (Figure E.5 in Appendix E).

Due to lack of effect of the lowest HNE concentrations on epithelial repair, the two lowest concentrations that caused a decrease in cell viability were tested for their effect on cell migration (5 nM and 10 nM). Exposure of wounded A549 monolayers to HNE (5 nM and 10 nM) for 48h significantly delayed or inhibited the ability of epithelial cells to repair and close the wound, reducing the percentage of wound healing to less than 25 % (Figure 7.6.a and b). In non–NE-exposed controls, rapid migration of cells into the generated scratched area was faster, achieving a ~75 % closure at 48h after wounding. Additionally cells treated with HNE exhibited round spherical morphology and some loss of cell attachment was clearly observed around the wound area (Figure E.5 in the Appendix). The concentration of HNE that affected cell repair is in the nanomolar range, similar to that described by Garrat *et al.* who found that the addition of approximately 50nM elastase hindered cell migration of primary epithelial cells[195]. Another study with intestinal epithelial cells found that neutrophil elastase increased epithelial cell permeability, indicating loss of epithelial barrier function by the cell monolayers[254]. Conversely, Xiaokaiti *et al*., who had also reported an increase in cell viability after incubation with HNE, observed an increase in epithelial cell repair after 24 h incubation with elastase (10 nM) and showed no effect on cell morphology [253]. This was attributed to HNE inducting the migrating ability of A549, used in this work as model lung epithelial tumour cells. The obtained results in this chapter are in accordance

with the first type of works, where elastase was shown to hinder epithelial cell migration and repair.

Since the developed assay will be used to test elastase inhibitor-containing hydrogels, it is important to establish whether the detrimental effects of elastase on epithelial repair are recoverable by addition of the elastase inhibitor alpha-1-antitrypsin. To test the effect of co-administration of alpha-1antitrypsin (AAT) on HNE-inhibited wound repair, scratch assays where cells were incubated with both HNE and AAT were conducted. An excess of AAT at 2:1 and 10:1 AAT: HNE ratio was employed, since it was shown in section 7.3.2.2 that an excess of AAT was required to counteract HNE detrimental effects on viability.

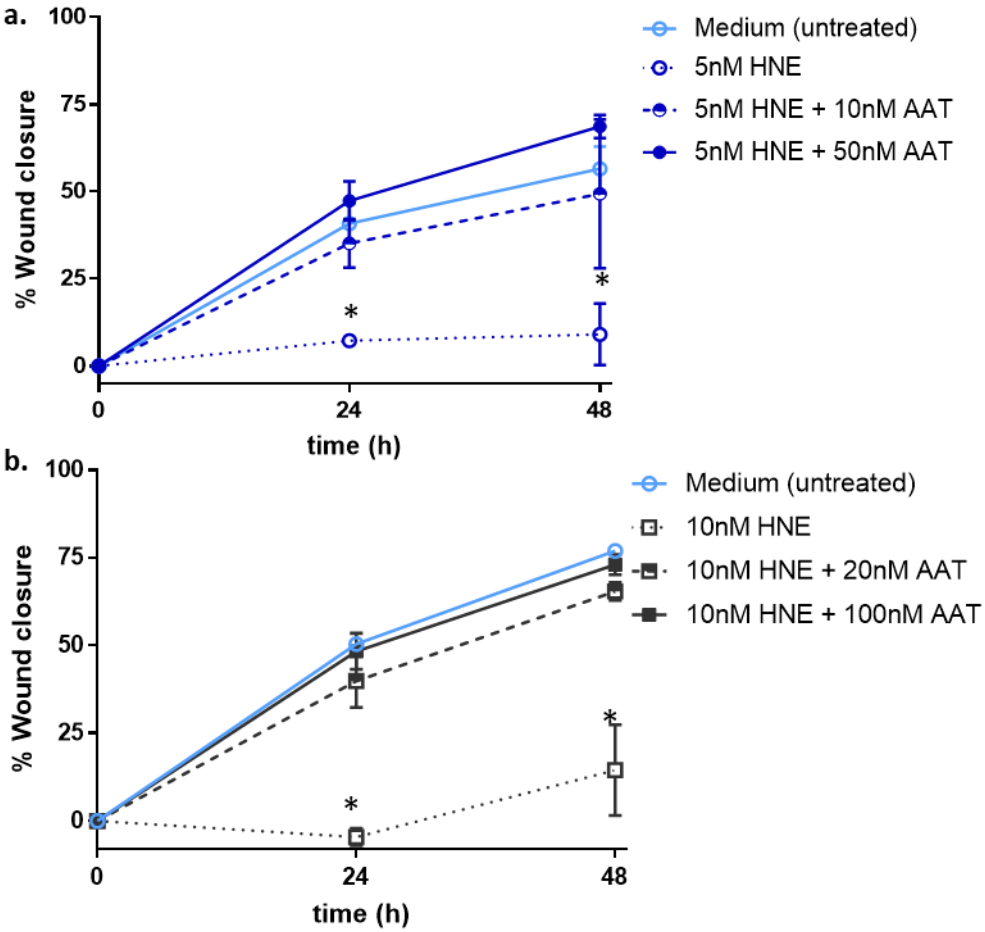

Figure 7.6. Effect of HNE and HNE and co-administered AAT on epithelial cell repair. **a.**) Untreated cells, cells treated with 5 nM HNE and 5 nM HNE and 10, and 50nM AAT. **b**.) Unterated cells and cells treated with 10nM HNE and 10nM HNE and 20nM and 100nM AAT (n=3, mean ± standard deviation). Symbols represent statistical significance by 2-way-ANOVA test with Tukey post comparison (* Value < 0.05, ** < 0.01 and **** < 0.0001.). For clarity, only samples different to all other samples on the same time point are noted, all statistical differences can be found in Tables E.1 and E.2 of the Appendix.

Epithelial repair of 5nM HNE was significantly improved at 24 h and 48 h (Figure 7.6.a). At 48h it was shown that the epithelial cell repair achieved with 10 excess of AAT (50nM AAT) was the same as with untreated cells, but HNE-incubated with only 2x excess AAT (10nM) was significantly lower (all statistical differences can be found in table E.1). Similarly, for epithelial cell migration in presence of 10nM HNE, co-administration of AAT significantly improved cell repair, especially at 48h (Figure 7.6.b). In a similar way to 5 nM HNE samples, a higher AAT:HNE (100 nM) ratio improved cell migration to the same extent as HNE-untreated cells, but the extent of repair in samples containing two times excess of AAT (20nM) was significantly lower than untreated cells (Figure 7.6.b and Table E.2 in the appendix). This could be due to the mechanism of AAT interaction with elastase, which requires an excess of AAT in order to achieve total HNE inhibition. Briefly, upon elastase-AAT interaction, the elastase-AAT complex can follow an inhibitory pathway (resulting in inactive elastase), or a substrate pathway (resulting in active elastase and inactive AAT). The mechanism has been previously described in more detail in section 6.1.1. As a result, higher concentrations of AAT with respect to HNE are required to achieve a full elastase inhibition (described in section 6.3.1). Similarly, Garrat *et al.* found that HNE-inhibited epithelial repair of primary cells from cystic fibrosis patients could be improved by administration of an excess of AAT (10:1 and 20:1 AAT:HNE). Although the epithelial repair capabilities were significantly improved with the administration of AAT with respect to HNE treated cells, epithelial recovery was not complete, and migration was reduced compared to untreated cell controls[195]. This could be attributed to the fact that higher concentrations of elastase (50 and 100 nM) were used and AAT was added 12h after the cells had been incubated with elastase, by which time the protease had started to show some toxic effects on the cells in their experiments. Unlike the present work, full recovery of epithelial repair was achieved by administration of the inhibitor in solution. But based on the observations of Garrat *et al*., it could be possible that only partial recovery of the repair

may be achieved if the inhibitor is released too late or too slowly from the hydrogels in later experiments.

In summary, the reported data shows that HNE at nanomolar concentration reduced the cell viability and epithelial repair of the human A549 epithelial cell line over a time of 48h. It has also been proven that damaging elastase effects on both, cell viability and repair, can be reverted by inhibiting the proteolytic activity of HNE with AAT. Our data shows that the improvement on cell viability and epithelial migration by administration of AAT is dependent on the total HNE concentration and also on the inhibitor:protease ratio. These results confirm the idea that HNE-controlled damage of cell repair could be used as an *in vitro* model to test the efficiency of the AAT-loaded hydrogels in modulating elastase activity in a biologically-relevant model. Although it may be possible that the developed *in vitro* model may not be sensitive enough to show improvements in repair in response to small changes in the release of the inhibitor or too slow release. It has been shown by us and others[195] that once elastase has started to hinder epithelial repair it also causes some cell death and detachment which may prevent complete migration of cells even with the subsequent administration of an elastase inhibitor.

7.3.3 Modulation of elastase activity *in vitro* induced by inhibitor loaded hydrogels

7.3.3.1 Replacement of epithelial cell medium

Due to a discontinuation in the supply of the epithelial growth supplement SAGM by the manufacturer, alternative serum-free medium with similar compositions were investigated. It is important that the new medium can support cell survival and cell repair over 48h at least, and it has to allow elastase activity, so that elastase-induced damaging effects on cells can be observed. Therefore a series of supplements designed for similar epithelial cells were selected based on similarities with the composition of SAGM medium supplement: Human Keratinocyte Growth Supplement (HKGS), Airway Epithelial Cell Growth Supplement (AES) and Peprogrowth supplement. The media composition compared to SAGM medium can be found in Table 7.1,

although Peprogrowth supplement is different in composition to all others, but it was included since it has been defined as suitable for the A549 cell line by the manufacturer. The addition of albumin (BSA) to AES and HKGS supplemented media was also considered, as these supplements are missing this protein component, which is present is SAGM medium (Table 7.1).

The ability of the media to support epithelial cell survival and growth in comparison to the standard 10 % v/v FBS supplemented medium was investigated. Cells were adapted to a 1:1 10 % FBS Medium: test medium for 24 h and then fully incubated in the test medium (AES, HKGS or Peprogrowth Supplemented medium). Similar metabolic activity was observed for cells incubated in media with the different supplements with or without BSA, of around 80 % of the activity of the control cells (incubated with 10 % FBS) as shown in Figure 7.7.a. Although no differences in metabolic activity were found, the cells grown in Peprogrowth supplemented medium showed an altered morphology and did not grow uniformly (Figure E.6 in the appendix).

Table 7.1. Composition of epithelial cell supplements studied.

Composition	SAGM	AES	HKGS	Peprogrowth
For cell line:	hSAEC	Airway epithelial	Keratinocytes	-
BPE	N/S	0.004ml/ml	0.002ml/ml	-
Insulin	N/S	5ug/ml	rhILGF* 1ug/ml	-
Hydrocortisone	N/S	0.5ug/ml	0.18ug/ml	-
Transferrin	N/S	10ug/ml	5ug/ml	-
rhEGF	N/S	10ng/ml	0.2ng/ml	-
G / A	N/A	-	-	-
Retinoic acid	N/A	0.1ng/ml	-	-
BSA	N/S	-	-	-
T3	N/S	6.7ng/ml	-	-
Epinephrine	N/S	0.5ug/ml	-	-
Other:			-	Lipid mixture solution Serum replacement solution

BPE = Bovine Pituitary Extract, G/A = gentamicin /Amphotericin, hSAEC = human Small Airway Epithelial cell, rhEGF, = human recombinant Epithelial Growth Factor, rhILGF = Insulin-Like Growth Factor, T3 = triiodothyronine, N/S = not specified, N/A = not added.

Epithelial repair was then assessed with all the supplements using the scratch wound assay. The ability of AES-BSA supplemented DMEM-F12 medium to promote wound closure was higher than all the other samples, and reached 80 % closure compared to the controls cells migrating in 10 % FBS supplemented medium (Figure 7.7.b). Peprogrowth supplemented cells barely promoted any epithelial repair, achieving only a 40 % wound closure and with most cells adopting a spherical morphology around the wound bed (Figure E.6.b in the appendix). The activity and stability of HNE on AES+BSA supplemented medium was tested and compared to a phosphate buffer standard control. The medium promoted higher HNE activity and led to higher stability of the enzyme in comparison to the buffer control (Figure 7.7.c).

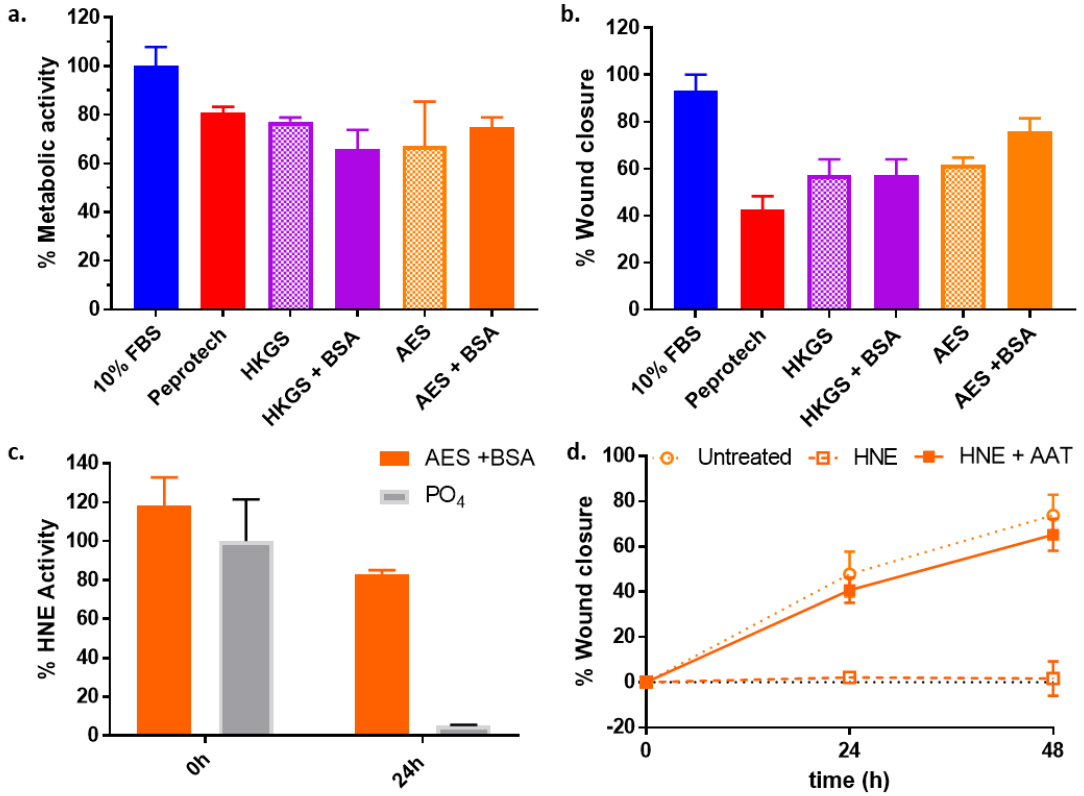

Figure 7.7. Comparison of epithelial supplement support of cell growth and repair of epithelial cells. **a.**) Cell growth after 24 h adaption in 1:1 10 % FBS medium:Assay medium and 24 h in the indicated assay media, compared to 10 % v/v FBS medium. **b.**) Epithelial repair over 72 h in comparison to 10 % v/v/ FBS supplemented medium. **c.**) HNE activity and stability on AES and BSA supplemented DMEM-F12 in comparison to phosphate buffer 0.1 M standard (PO_4). All samples in a-c represent mean ± standard deviation and n=3. **d.**) Effect of HNE (10 nM) and HNE and co-administered AAT (100 nM) and medium (untreated cells) on epithelial cell repair in AES+BSA supplemented DMEM-F12 medium (N=3 and n=3, mean ± error of the mean).

Since AES+BSA supplemented medium offered the best support to cell migration and also enhanced HNE activity it was used for further tests. Epithelial cells were incubated in the presence of 10nM HNE and a combination of 10nM HNE and 100 nM HNE in AES+BSA supplemented medium to confirm the same effect of elastase-induced hindered epithelial repair as shown previously with SAGM could be achieved (Figure 7.6). It was observed that cells in presence of elastase did not migrate (Figure 7.7.d). Cells incubated with elastase and an excess of AAT showed recovered migrating abilities, comparable to the untreated cell controls (Figure 7.7.d). This data follows the same trend as obtained with the SAGM supplement (Figure 7.6.b), confirming the suitability of AES+BSA supplemented DMEM to reproduce the data previously optimised with SAGM medium.

In brief, all media supported cell survival but AES + BSA supplemented medium led to improved cell repair and supported HNE activity and stability. Therefore AES+BSA supplemented medium was selected as substitute for SAGM medium, discontinued in supply, for further *in vitro* testing of the hydrogels.

7.3.3.2 Modulation of elastase activity and epithelial repair with hydrogels

Having established the conditions where HNE-induced poor epithelial repair and shown that normal cell repair could be restored with the co-administration of AAT in solution, hydrogels were tested using this model. It was hypothesised that if the elastase-responsive hydrogels could modulate HNE activity efficiently in presence of the epithelial cells, then HNE-hindered epithelial repair would be improved and a drop in HNE activity could be quantified in the cell supernatant.

Alpha-1-antitrypsin was incorporated on elastase-responsive hydrogels (70 µg per gel). This amount of inhibitor was selected since some of the loaded protein will be lost during swelling of the hydrogels prior to the assay, and an excess of AAT was required in previous *in vitro* experiments for a full recovery of cell repair functions (10:1 AAT:HNE, Figure 7.6.b). Blank

hydrogels (without any inhibitor) were used as a negative control of non-modulation of HNE activity. Hydrogels were placed inside a transwell insert to avoid physical damage to the cell monolayer (as simplified in Figure 7.1.a). This still allows medium exchange between both compartments (one with the cells and one with the gel) through the pores of the insert.

The epithelial repair of HNE-treated cells was significantly improved in presence of AAT-loaded hydrogels but not in presence of blank hydrogels (Figure 7.8.a). However, epithelial repair with AAT-gels was lower than the untreated control cells. Even encapsulation of a higher amount of inhibitor (100 µg per gel) showed improved migration with respect to HNE-treated cells and blank hydrogels, but only a partial recovery of migration capabilities observed in untreated healthy cells. This could be due to the rate of release of inhibitor from the hydrogels depending on the elastase-controlled hydrogel degradation. Elastase will diffuse through the pores on the transwell, degrade the gel and release the AAT, which would then diffuse out and inhibit elastase activity and consequently slow the release of further inhibitor. This complex mechanism of release may cause the release of inhibitor from the hydrogels to be slower than the time by when the cells start experiencing toxic effects of elastase. Then, even if more inhibitor is released it will not be able to reduce cell death. It has previously been shown that even if high excess of AAT (20:1 inihibitor:HNE) is administered after the onset of toxic effects of elastase, only a partial improvement epithelial cell repair is observed[195]. Additionally, due to the release of the inhibitor being dependent on the degradation-inhibition cycles, as explained above, it is possible that only a fraction of the inhibitor will be released. This amount may not be sufficient to inhibit elastase to below the levels at which it shows toxic effects to the cells. Visual inspection of the hydrogels confirmed that most of the hydrogel remained intact after the experiment (Figure E.7 of the appendix), indicating that some inhibitor may not have been released.

Visual inspection of the migrating cell phenotype revealed a marked difference in cell morphology and detachment between cells treated with HNE or HNE and blank gels compared with AAT encapsulating hydrogels (Figure 7.9.). This demonstrates the ability of elastase-responsive hydrogels to promote epithelial repair in HNE-treated cells, although the improvement in migration did not reach the levels of untreated control cells

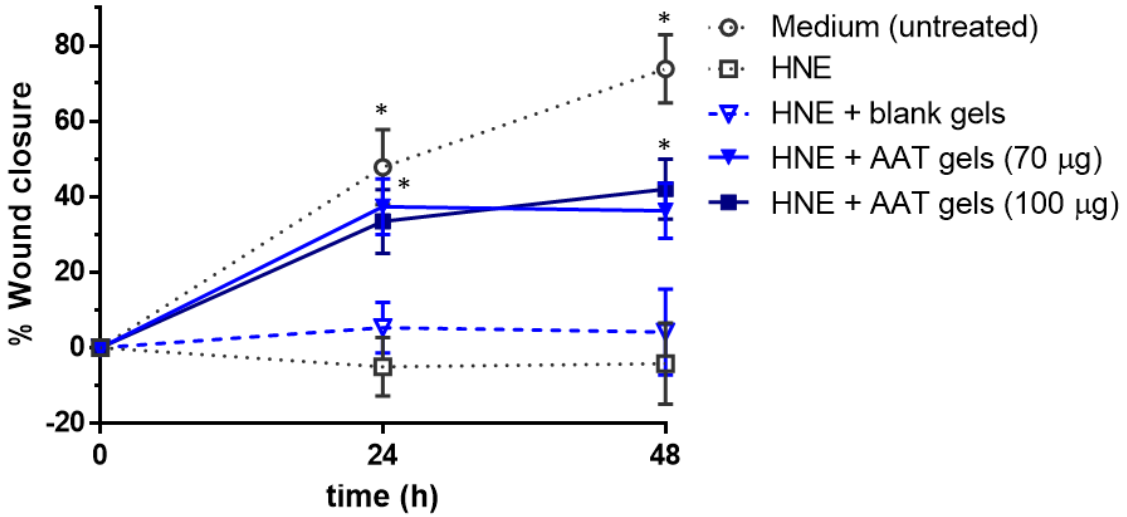

Figure 7.8. Effect of AAT-loaded hydrogels on HNE-impeded epithelial cell repair. Epithelial repair by elastase-responsive hydrogels encapsulating 0 µg (blank), 70 µg and 100 µg of AAT compared to untreated cells (medium) . *represents statistical significance by 2-way-ANOVA test with Tukey post-comparisons, for clarity only samples different from the HNE-incubated cell controls are noted, all statistical differences can be found in Table E3 of the Appendix. Represented mean ± error of the mean; N =3, n=3 for samples not containing hydrogels; N=4, n=2 for responsive hydrogels (70 µg), and N=2,n=2 for responsive hydrogels (100 µg).

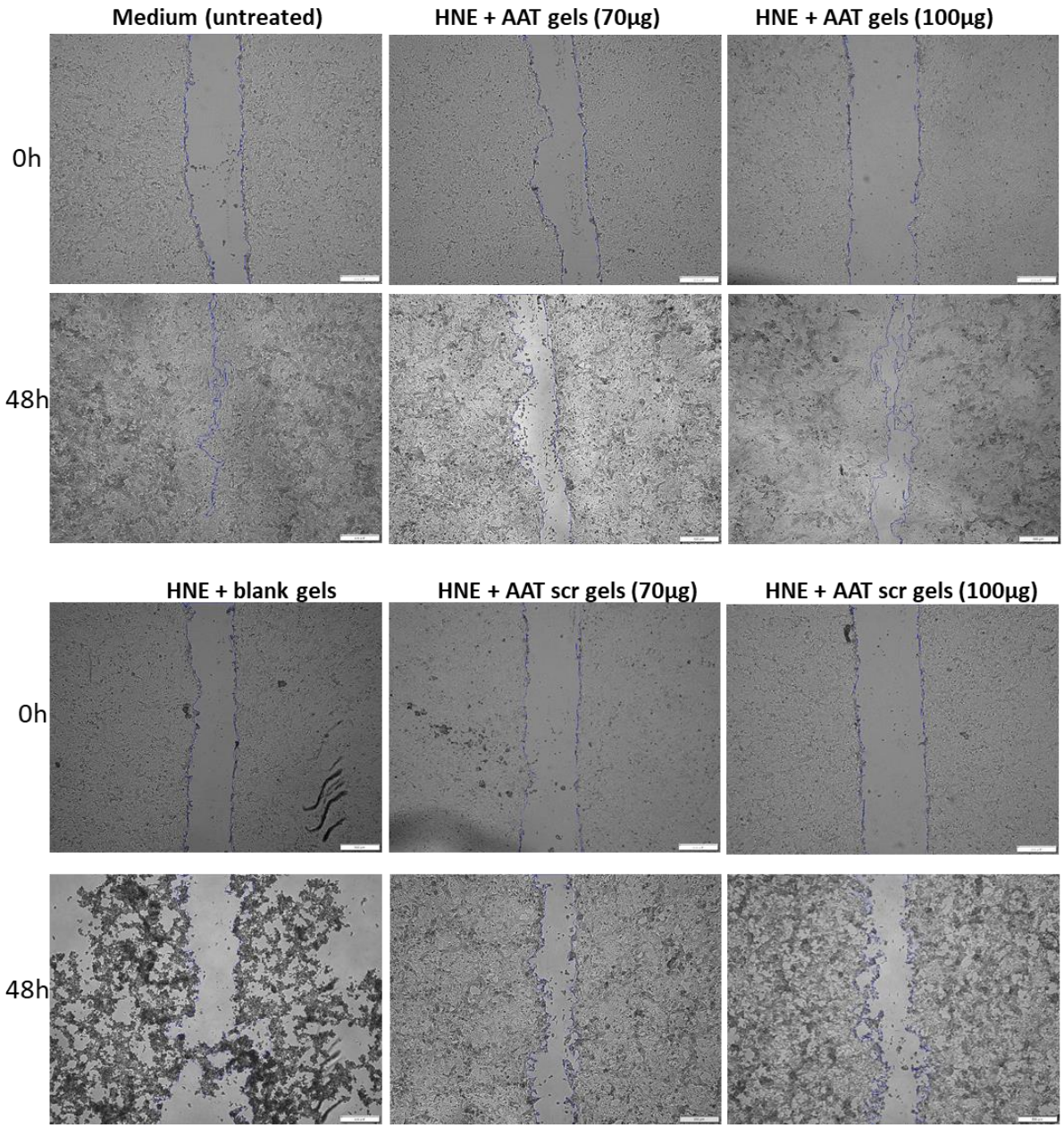

Figure 7.9. Effect of AAT-loaded hydrogels on HNE-impeded epithelial cell repair. Epithelial repair after48 h incubation with only cell medium (untreated) and different hydrogel types, showing morphology and wound closure with elastase-responsive or scrambled (scr) hydrogels. Scale bars are 500 µm

In order to determine the contribution of the inhibitor released by passive diffusion from hydrogels on ameliorating HNE-induced epithelial damage, hydrogels prepared with the elastase non-responsive (scrambled) peptide were tested. Similarly to elastase-responsive hydrogels, a partial improvement in epithelial wound closure with respect to HNE only treated cells was observed on the scratch assay (Figure 7.10) together with an improved visual appearance and

reduced detachment of the cells (Figure 7.9, down). Responsive and scrambled hydrogels promoted a similar extent of epithelial repair, with no statistical differences found between them (Table E.3 in the Appendix summarises all statistical differences). This could either mean that the amount of AAT delivered to the cell medium by passive release is enough to cause a considerable inhibition of elastase. In this case, this could be further investigated by encapsulating lower amounts of inhibitor inside the hydrogels, but this will possibly lower even more the partial improvement in epithelial repair currently observed. Another reason for achieving similar effects on epithelial repair with either elastase-responsive or scrambled gels is due to some degradation of the scrambled gels. Images of the hydrogels at the endpoint of the scratch assay showed that part of the scrambled hydrogels have been degraded (Figure E.7 in the supplement), supporting this possibility of non-selective degradation. Degradation may occur due to 4-PEGNB ester hydrolysis or other cell-secreted proteases may recognise and degrade the scrambled sequences used on the controls hydrogels. For instance, the MMP concentration levels secreted by healthy cells to degrade the extracellular matrix during migration have been shown to degrade hydrogels[163].

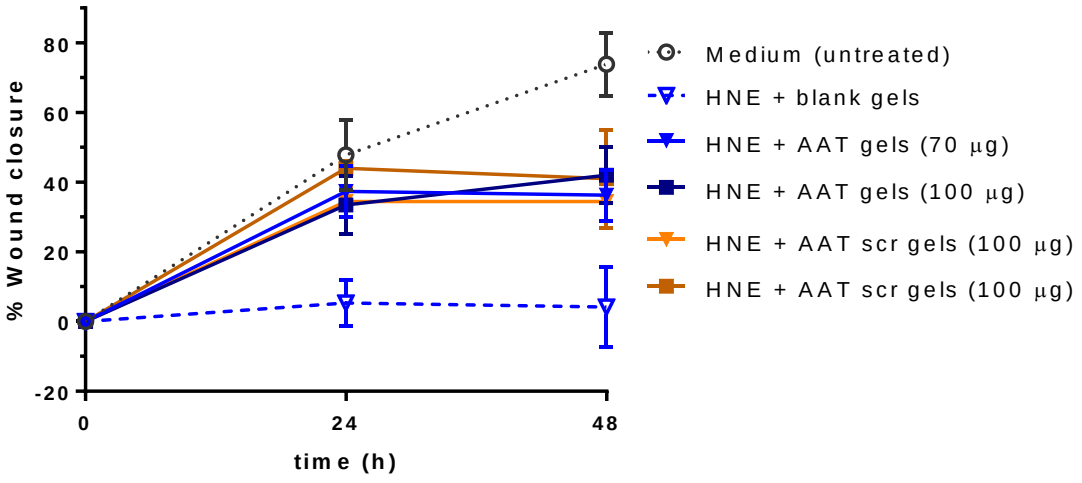

Figure 7.10. Effect of AAT-loaded hydrogels on HNE-impeded epithelial cell repair. Improvement on epithelial repair by scrambled (scr) hydrogels encapsulating 70 and 100µg of AAT respect to untreated (medium) cells and HNE-treated cells. *represents statistical significance by 2-way-ANOVA test with Tukey post-comparisons, for clarity only samples different from the HNE-incubated cell controls are noted, all statistical differences can be found in Table E3 of the Appendix. Represented mean ± error of the mean; N =3, n=3 for samples not containing hydrogels; N=4, n=2 for responsive hydrogels (70 µg), and N=2, n=2 for responsive hydrogels (100 µg) and scrambled hydrogels (70 and 100 µg).

The effects of the released inhibitor are therefore not exclusively due to passive diffusion of the inhibitor. The data from elastase-responsive blank and AAT-containing hydrogels indicates that the elastase-controlled mechanism of inhibitor release effectively down-regulates HNE activity enough to promote a partial improvement of epithelial cell repair in this *in vitro* model.

In order to further understand the degree of HNE inhibition achieved with hydrogels in the presence of the cells, the cell supernatants were collected at each time point and the HNE activity quantified. It was observed that controls with AAT administered in solution where capable of fully suppressing HNE activity at both 24 and 48h (Figure 7.11). This confirms that full recovery on epithelial cell migration with the inhibitor administered in solution is achieved by inhibition of HNE. Blank hydrogels did not reduce HNE activity compared to HNE-treated cells, although a high variability of HNE activity was observed in blank hydrogel samples. At 24 h all AAT-encapsulating hydrogels significantly reduced elastase activity on the cell supernatant compared to HNE-treated cells without reaching full inhibition (Figure 7.11). This data agrees with the cell repair experiments, where scrambled and responsive hydrogels promoted improved epithelial repair, but did not achieve the full repair capabilities of healthy control cells. This also indicates that a higher degree of inhibition of HNE on the medium may be required in order to achieve complete migration of the cells. Conversely, at 48h only elastase-responsive hydrogels significantly inhibited the activity of HNE (Figure 7.11 and table E4), while scrambled hydrogels did not significantly reduce elastase activity. Although this lack of significance with scrambled gels could be due to the smaller number of independent experiments conducted, it indicates that modulation of elastase was higher with the responsive hydrogels than scrambled ones at longer time points. This indicates that the partial improvement in cell migration with scrambled gels (Figure 7.10) could have been due to a higher passive release of inhibitor within the first 24 h, or that during this initial time period some gel degradation took place.

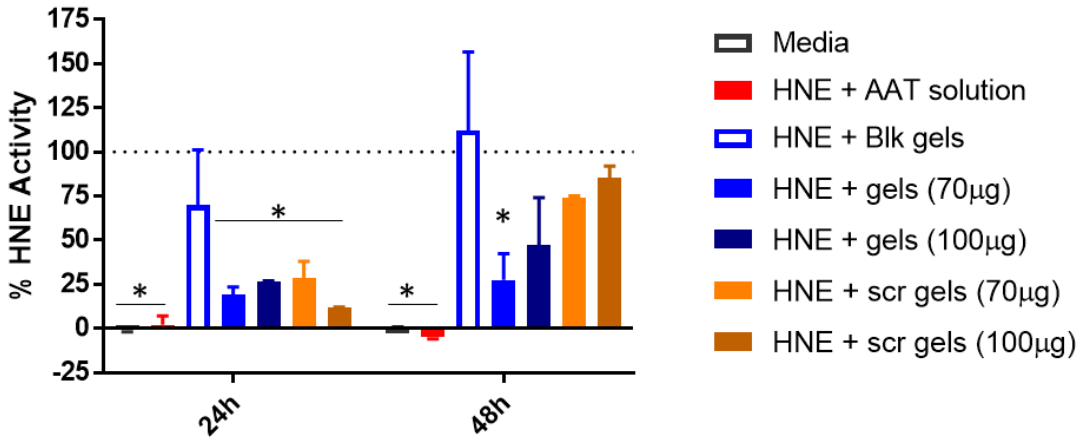

Figure 7.11. Effect of AAT-loaded hydrogels on HNE activity in cell supernatants of HNE-treated epithelial cells. *represents statistical significance by 2-way-ANOVA test with Tukey post-comparisons, for clarity only samples different from the HNE-incubated cell controls are noted, all statistical differences can be found in Table E3 of the Appendix. Individual experimental points can be found in the appendix on Figure E.8. Represented are mean ± error of the mean (N =3 of triplicates for samples not containing hydrogels, N=4 of duplicates for responsive hydrogels (70 µg), and N=2 of duplicates for responsive hydrogels (100 µg) and scrambled hydrogels (70 and 100 µg)).

7.4 Conclusions

4-PEGNB hydrogels and elastase inhibitor alpha-1-antitrypsin did not affect cell viability of epithelial cells, indicating their cytocompatibility.

In order to develop a model of elastase-induced epithelial damage the effects of elastase on epithelial cell viability and epithelial cell repair capabilities were established. Externally supplementing cells with elastase in the nanomolar range resulted in significantly reduced cell viability, in agreement with the majority of publications where elastase has been incubated with epithelial cells[227,244–246]. Elastase toxicity was time and concentration-dependant, and it could be attenuated by co-delivering the elastase inhibitor alpha-1antitrypsin at a high excess of respect to elastase. Similarly, the ability of epithelial cells to repair mechanically produced wounds in presence of elastase was decreased in presence of low concentrations of elastase. The co-administration of HNE with alpha-1antitrypsin led to an improvement in the repair abilities of

epithelial cells. Full epithelial repair comparable to untreated controls was only observed when cells were treated with a high excess of inhibitor of 10:1 respect to elastase concentration.

Hydrogels were then tested using this elastase-induced epithelial damage model to test their efficacy to reduce HNE activity in a biological context. Only hydrogels containing AAT improved the wound repair abilities of epithelial cells, confirming the amelioration is caused by release of the inhibitor. Although the epithelial repair observed with elastase-responsive hydrogels was better than in HNE-incubated cells, it did not lead to full epithelial repair as in untreated cell controls. Others have observed that even a 20:1 excess of inhibitor does not lead to full epithelial repair if the inhibitor is delivered once the cells have already started to suffer toxic effects from elastase incubation[195]. In this case, the observed partial improvement in repair may be due to the cells being exposed to HNE before the inhibitor is released. This delay in AAT release may be caused by the mechanism of inhibitor delivery, which depends on HNE-degradation HNE-inhibition cycles to degrade the hydrogel and release AAT. This was confirmed by the observation that the HNE activity was not fully reduced in the cells' supernatant. A partial reduction in HNE activity may explain why the improvement in wound repair was not as complete as when the inhibitor was administered in solution.

Then, the effect of passive released AAT on epithelial repair was assessed using scrambled hydrogels controls, since they were not expected to undergo significant degradation. Scrambled hydrogels promoted a similar level of repair compared to responsive hydrogels. This was attributed to a mixture of passive release and degradation mechanisms instead of the expected mechanism based purely on passive release, leading to an increase in AAT release. The mechanism of degradation has not been clarified, and it could be due to a small level of cleavage of the gels by other proteases, such as MMPs[163]. Additionally, hydrolysis of the esters on the 4-PEGNB polymer may be taking place to a small extent, which may be, for instance, due to changes in the pH of the medium common in cancer cells[255,256]. The scrambled hydrogels also significantly inhibited the HNE activity in the cell supernatant at 24 h, explaining the improvement in epithelial

cell repair at this time. Although, in contrast to responsive hydrogels, scrambled gels did not show significant inhibition of elastase at 48h, indicating that modulation of elastase activity was better with the responsive hydrogels at longer time points.

In summary, the reduction in elastase activity obtained with the elastase-responsive hydrogels, confirms the improvement in epithelial repair observed with these gels is caused by a partial inhibition of elastase. Although it could not be demonstrated that this release is exclusively caused by an elastase-controlled mechanism leading to self-inhibition of the enzyme activity, the use of elastase-responsive hydrogels to modulate elastase activity and improve epithelial repair has been demonstrated. The partial improvement in migration with scrambled gels suggests that elastase inhibition may also be achieved by non-elastase-controlled release of the inhibitor, therefore opening the possibility to other forms of hydrogel release taking place within the first 24 h.

Chapter 8.

Conclusions and outlook

The aim of this thesis was to develop an enzyme-responsive delivery system able to modulate protease activity in a self-regulated feedback manner, in response to the levels of protease activity. Elastase was selected as a clinically relevant target enzyme, since increased levels of activity of this serine protease are often associated with chronic inflammatory pathologies. This was achieved by designing hydrogels that were crosslinked with an elastase-responsive peptide incorporating an elastase inhibitor (alpha-1antitrypsin). In our studies multi-arm-PEG polymers with end-functionalities reactive towards thiols (norbornene and maleimide) that have been previously used in responsive drug delivery[39,43,160], were used as the building blocks for hydrogel structures. In order to increase the understanding of the hydrogel formation, the delivery system properties and the interactions of the materials with cells, the work was divided in several sections to address these objectives in detail: i) the characterisation of physical properties, gelation conditions and ability to physically entrap macromolecules (Chapter 3), ii) synthesis of the elastase-sensitive and incorporation into hydrogels (Chapter 4), iii) selectivity of release in response to elastase (Chapter 5), iii) ability to encapsulate the elastase inhibitor alpha-1-antitrypsin and inhibition profiles of elastase (Chapter 6), and iv) modulation of elastase activity in an *in vitro* model of epithelial repair (Chapter 7).

i) Hydrogels were initially prepared by crosslinking multiarm PEG-maleimide with a model short dithiol, in order to establish conditions that allowed uniform hydrogel formation, small mesh size and lower passive release. Reduction of the molecular weight of the polymer and high crosslinking densities together with using a low pH for gelation, led to uniform hydrogels with the lowest passive release of a model dextran.

ii) An elastase- responsive peptide with adequate solubility and elastase-responsive properties was synthesised and purified. The work conducted with the short dithiol was translated into forming peptide-crosslinked hydrogels, the optimal conditions of gelation and encapsulation established with the short crosslinker were utilised with the elastase-sensitive peptide to generate responsive hydrogels. Although peptide-crosslinked hydrogels prepared by Michael addition showed an elastase-controlled mechanism of release, they did not retain macromolecules very efficiently and were characterised by a high passive release. Therefore a multiarm PEG-norbornene, an alternative thiol-reactive polymer, was employed to produce peptide-crosslinked hydrogels.

iii) Hydrogels prepared with PEG-norbornene were able to reduce passive release of a model dextran and undergo a suitable elastase-controlled degradation, leading to almost 100 % release of a fluorescent dextran upon incubation with elastase. The specificity of the hydrogels to undergo elastase-controlled degradation and triggered release was confirmed by using a scrambled peptide (non-responsive to elastase) as crosslinker. It was shown that these hydrogels were not degraded by elastase, confirming the peptide elastase-responsive sequence determines the elastase-controlled release. Finally, elastase-responsive hydrogels were incubated with MMP-2 at concentrations that have shown to degrade MMP-responsive hydrogels. MMP-2 did not lead to an increase in degradation of elastase-responsive hydrogels or increased release of a model dextran. Therefore it confirms the selectivity of the hydrogels to be degraded by elastase, with no interference of other protease on the release mechanism.

iv) After confirming the stability of alpha-1-antitrypsin (AAT) under hydrogel preparation and release conditions, the inhibitor was encapsulated into hydrogels. The ability of AAT-loaded hydrogels to inhibit elastase was dependent on the amount of inhibitor encapsulated, with only hydrogels with 50µg AAT able to modulate elastase activity after 72h. Scrambled hydrogels were used as a control of the passively released AAT effects on elastase inhibition. A higher passive

release of the TRD70 with respect to responsive gels led to inhibition of elastase at short times. Thus elastase-responsive hydrogels showed an overall improved performance on elastase inhibition with respect to scrambled gels, suggesting that the elastase-controlled release of the inhibitor, is more efficient than only non-specific release mechanisms.

v) Before studying modulation of elastase activity *in vitro*, it was determined whether the hydrogels and AAT had a toxic effect on epithelial cells using A549 as a model cell line. It was observed that neither hydrogels nor AAT affected the viability of cells, as determined via a resazurin based cell metabolic activity assay. Then, the detrimental effects of elastase to epithelial cell viability and repair of A549 cells were established in order to develop a model for elastase-induced epithelial cell damage. HNE caused a time and concentration-dependent toxic effect on cells, and reduced the ability of cells to repair induced wounds on cell monolayers. Both detrimental effects of elastase on cells were ameliorated by the administration of AAT in solution, confirming that the *in vitro* model represented elastase-induced epithelial damage. Consequently, hydrogels were tested for their abilities to inhibit elastase activity and improve elastase-hindered epithelial repair with this model. Although AAT incorporating elastase-responsive hydrogels improved elastase-induced epithelial repair, it did not lead to full wound closure as observed in untreated cell controls. This partial improvement in wound repair was attributed to cell exposure to the medium-supplemented elastase before the inhibitor starts to get released from the hydrogels, and a partial rather than full inhibition of elastase in the medium. Scrambled hydrogels promoted a similar level of epithelial repair to that of responsive gels. It was observed that gels were partially degrading, indicating some non-specific mechanism of degradation had taken place. Although the degree of repair achieved with both types of hydrogels was similar, scrambled gels showed a reduced ability to inhibit elastase activity at longer times. In summary, the inhibitory abilities on elastase activity in the presence of cells with elastase-responsive gels was greater than the scrambled ones, although differences in epithelial repair were not observed. Although this demonstrates a greater inhibition effect due to elastase-controlled release, it cannot be confirmed

that elastase inhibition leading to improved cell repair is only caused by elastase-controlled release of AAT, but other non-specific mechanisms may be involved.

Overall, this work aimed to increase the knowledge on enzyme-responsive hydrogels for applications in drug delivery, addressing in particular the development of hydrogels capable of inhibiting enzymes in response to the activity of the target enzyme. In depth analysis of the release kinetics and enzyme-responsiveness were conducted by using scrambled hydrogels and studying release in enzyme-free medium, medium containing the target enzyme, and medium containing MMP-2 as an example of a non-targeted enzyme. Although high variability on the modulated levels of enzyme was observed, elastase-responsive hydrogels showed superior elastase inhibition with respect to non-responsive ones at longer times. Furthermore, the same effects were confirmed in a relevant biological model *in vitro*. Hydrogels achieved a partial inhibition of elastase activity that led to a partial improvement in elastase-hindered epithelial repair. Overall, this works signifies the first step in the development of a selective delivery system towards autonomous regulation of elastase activity, whereby the release of an elastase inhibitor is fully triggered by the level of enzyme in its environment.

8.1 Future work

Further investigations are required in order to gain a better understanding into the system and identify the source of variability, the degradation observed in scrambled gels and further insights into the system as well as potential clinical applications.

The ability of the hydrogels to release a loaded cargo in response to the target enzyme elastase has been proven, however some variability in the system has been observed. The passive release of a model fluorophore from hydrogels, and the results on elastase activity modulation, show some variability between hydrogel batches. It would be interesting to clarify whether this variability is linked to reproducibility on hydrogel preparation (e.g. crosslinking degree) or to variability during the release studies (E.g. enzyme-gel interactions). We have tried to minimise

these two possibilities by quantifying the free thiols of the peptides before gelation and measuring the activity of elastase batches. For instance, more regular tests of enzyme activity and quantification of free thiols could be useful with this regard. Additionally, fluorescently labelling of a small fraction of polymer or peptide followed by confocal analysis of the hydrogels could help identifying variability on gel uniformity and between different batches[173]. This could benefit in directing optimisations on reproducibility of the materials.

The ability of the hydrogels to achieve inhibitor release controlled by the target protease, and therefore on-demand enzyme activity modulation based on the levels of enzyme was of great importance in this work. For this reason, more investigations on the observed partial degradation of the scrambled controls would be important. If an unspecific release is taking place, then it could be the same case for the responsive hydrogels as well, meaning that the release of encapsulated inhibitor will not only be triggered by enzyme activity. For instance, it has been recently shown that ester linked 4-PEGNB (4-PEGNB) based gels, such as the ones used in this work, have lower stability than amide 4-PEGNB (4-PEGaNB) gels[239]. Hunckler *et al.*, have demonstrated that 4-PEGNB and 4-PEGaNB gels were equally stable in release buffer and had similar mechanical properties. While 4-PEGaNB gels were stable in cell culture conditions (37℃, 5 % CO_2 pH 7.4, cell medium with and without FBS), 4-PEGNB underwent slow degradation under cell culture conditions after two weeks and they were fully degraded *in vivo* 24 h after subcutaneous injection[239]. During the present work, the release studies of model fluorophores or the inhibitor in presence of elastase have been conducted under cell culture conditions (Chapter 5 and 6). It is possible that some of the slow degradation of the 4-PEGNB observed by Hunckler *et al.*, had started to take place over the length of our release studies and cell studies. It will therefore be of interest to either contemplate the possibility to move to a more stable polymer (4-PEGeNB), or conduct the proof of concept release experiments in release buffer instead of cell culture conditions in order to avoid unspecific instability mechanisms.

While this work focused on designing materials for selective delivery in response to elastase, it could be more widely applicable to target other proteases. For instance, there is precedence of MMP-responsive hydrogels where a MMP inhibitor (TIMP-3) has been encapsulated and released on-demand[115]. The key of responsive protease inhibition targeting relies on the selectivity of the peptide sequence and the inhibitor encapsulated towards the target enzyme. A careful selection of the peptide-inhibitor pair using the same delivery system could be used to address another protease. The combination of different materials, each able to individually and selectively modulate the activity of one protease, could provide simultaneous modulation of different enzyme activities. This would be of special interest in diseases where several enzymes are overexpressed and present variable activity levels over time such as chronic wounds[60]. The selectivity of release form the elastase-responsive materials in Chapter 5 demonstrated that MMP-2, an enzyme sometimes overexpressed in diseases with high elastase did not affect into drug release from the designed hydrogels. This data is promising as an initial assessment towards developing multiple enzyme-responsive delivery systems.

Finally, protease inhibitors can present inhibitory effects on proteases other than the target one. For instance, alpha-1-antitrypsin has inhibitory effects on other serine proteases such as proteinase-3 or trypsin[257]. Gene therapy based on siRNA (small interfering RiboNucleic Acid) could be a promising therapeutic modality for modulating protease activity by regulating the protease expression at a genetic level. Some recent studies have shown that enzyme-responsive siRNA achieved efficient inhibition of MMP-2 and tumour growth[127] and improved chronic wound healing[126] *in vivo.*

The final chapter of this work addressed the development of an *in vitro* model for elastase modulation in presence of cells and improvement in epithelial tissue repair, and subsequent testing of materials in the *in vitro* model. The testing of the efficacy of the materials in more complex models would be of great interest, in order to further understand the behaviour of the delivery system and their efficacy *in vivo. In vivo* models of high elastase activity associated with

inflammation and epithelial damage could be useful for this purpose. For instance wound models using Secretory Leukocyte Proteinase Inhibitor (SLPI) deficient mice[87], edema inflammation models of subcutaneous elastase injections[242,243], or intratracheal instillation of elastase causing pulmonary emphysema[88,89] are currently being used as preclinical models which give an insight on the damaging effects of elastase on chronic diseases.

Appendices

Appendix A: Supplementary data from Chapter 3

Table A.1. Effect of pH, crosslinker, Mw and percentage of polymer on 4-PEGMal gelation kinetics and storage modulus.

Mw PEG	Crosslinker	pH	%w/v	Gel point*	G' final
5 kDa	DTT	pH 3	5	30.9 ± 4.5	$3.4 \times 10^2 \pm 6.7 \times 10^1$
			10	9.6 ± 1.8	$1.2 \times 10^3 \pm 1.0 \times 10^3$
			20	1.8 ± 0.9	$9.2 \times 10^3 \pm 1.6 \times 10^2$
			30	1.4 ± 0.5	$1.1 \times 10^4 \pm 5.1 \times 10^3$
		pH 4	5	5.9 ± 5.0	$7.2 \times 10^2 \pm 4.2 \times 10^2$
			10	1.4 ± 0.7	$5.2 \times 10^3 \pm 2.7 \times 10^3$
			20	0.7 ± 0.1	$8.5 \times 10^3 \pm 9.6 \times 10^2$
			30	0.7 ± 0.1	$1.1 \times 10^4 \pm 4.3 \times 10^3$
	Peptide	pH 3	10	3.3 ± 0.7	$3.8\ 10^3 \pm 4.5 \times 10^2$
10 kDa	DTT	pH 3	10	27.2 ± 2.4	$2.2 \times 10^3 \pm 1.5 \times 10^3$
			20	7.4 ± 0.6	$14.7 \times 10^3 \pm 9.2 \times 10+$
		pH 4	5	12.5 ± 1.3	$8.9 \times 10^2 \pm 9.2 \times 10^1$
			10	3.8 ± 0.8	$1.9 \times 10^3 \pm 5.1 \times 10^2$
			20	1.3 ± 0.6	$6.3 \times 10^3 \pm 1.5 \times 10^2$
		pH 5	5	2.5 ± 0.5	$5.9 \times 10^2 \pm 2.9 \times 10^2$
			10	0.7 ± 0.1	$3.2 \times 10^3 \pm 7.0 \times 10^2$
		pH 6	5	0.3 ± 0.1	$7.9 \times 10^2 \pm 3.2 \times 10^2$
			10	0.4 ± 0.1	$8.9 \times 10^3 \pm 1.5 \times 10^3$
	Peptide	pH 4	10	2.63 ± 0.2	$7.9 \times 10^2 \pm 2.4 \times 10^2$

* Calculated with oscillatory rheology as the crossover point of G'>G''. Mean ± standard deviation, n=3 for DTT samples and n=2 for peptide samples.

Table A.2 : Influence of Mw and percentage of polymer on hydrogels swelling ratio (Qm), Mesh size, and 70 kDa dextran encapsulation efficiency (%) and maximum dextran released (D_{max})

Mw PEG	% w/v	Qm	Mesh size (nm)	Encapsulation Efficiency (%)	D_{max} (%)[a]
5 kDa	5	46.0 ± 5.6	11.0 ± 0.2	-	-
	10	17.2 ± 1.5	8.2 ± 0.3	96.5 ± 0.3	86.1 ± 10.5
	20	13.3 ± 1.0	7.4 ± 0.3	96.5 ± 0.6	56.4 ± 6.1
	30	10.2 ± 2.5	6.6 ± 0.9	-	-
10 kDa	5	29.5 ± 5.8	11.1 ± 0.2	-	-
	10	16.6 ± 1.1	11.0 ± 0.4	88.0 ± 6.4	69.2 ± 6.0
	20	12.8 ± 1.3	9.75 ± 0.6	81.4 ± 11.1	68.1 ± 10.5

[a] **D_{max}: % 70 kDa dextran released at endpoint (day 15). All samples were prepared at a 1:1 SH:C=C ratio, n=4, mean ± standard deviation.**

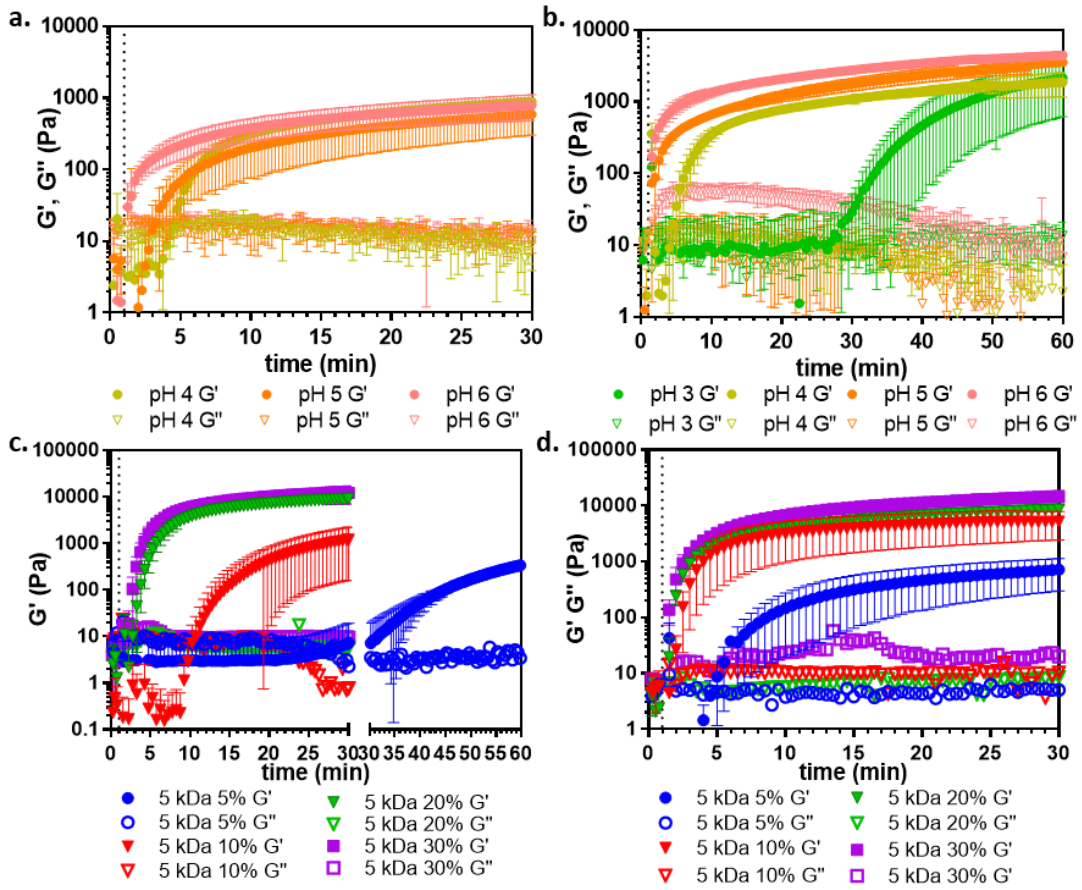

Figure A.1. Effect of pH, Mw and polymer percentage in gelation kinetics of 4-PEGMal gels. G' and G'' of **a.**) 5 % 10 kDa PEG at pH 4 - 6, **b**.) 10 % 10 kDa PEG at pH 3-6, **c**.) 5 kDa PEG at pH 3 from 5 to 30 % w/v, **d**.) 5 kDa PEG at pH 4 from 5 to 30 % w/v. All graphs include loss (G'') modulus in addition to storage (G') modulus already included in Figure 3.3 and Figure 3.4 (n=3, mean ± standard deviation).

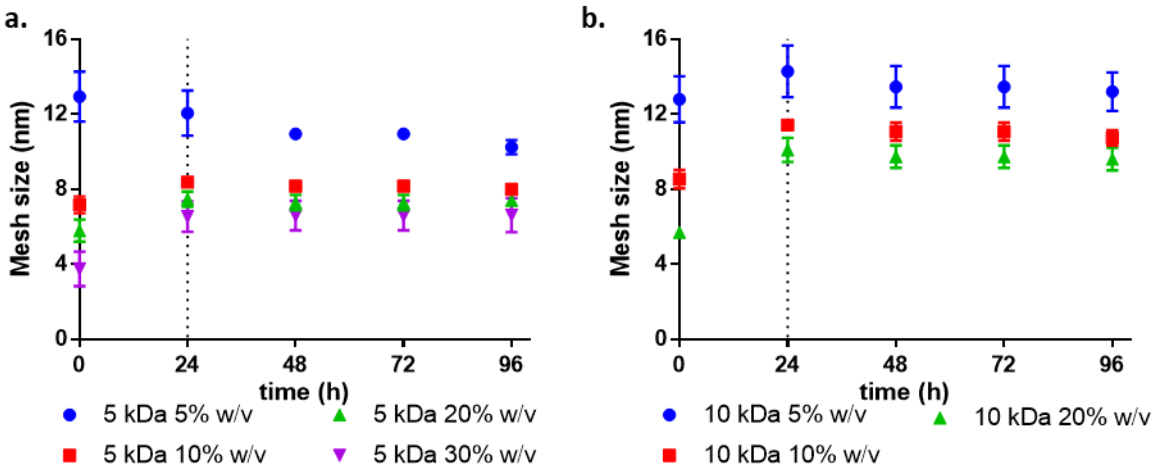

Figure A.2. Time- changes on mesh size of **a.**) 10 kDa and **b.**) 5 kDa 4-PEGMal hydrogels. Dashed lines show mesh size at 24 h, showing an increase on the mesh size from time cero to 24 h, when it reaches the equilibrium mesh size except for 5 kDa 5 % 4-PEGMal hydrogels.

Appendix B: Supplementary data from Chapter 4

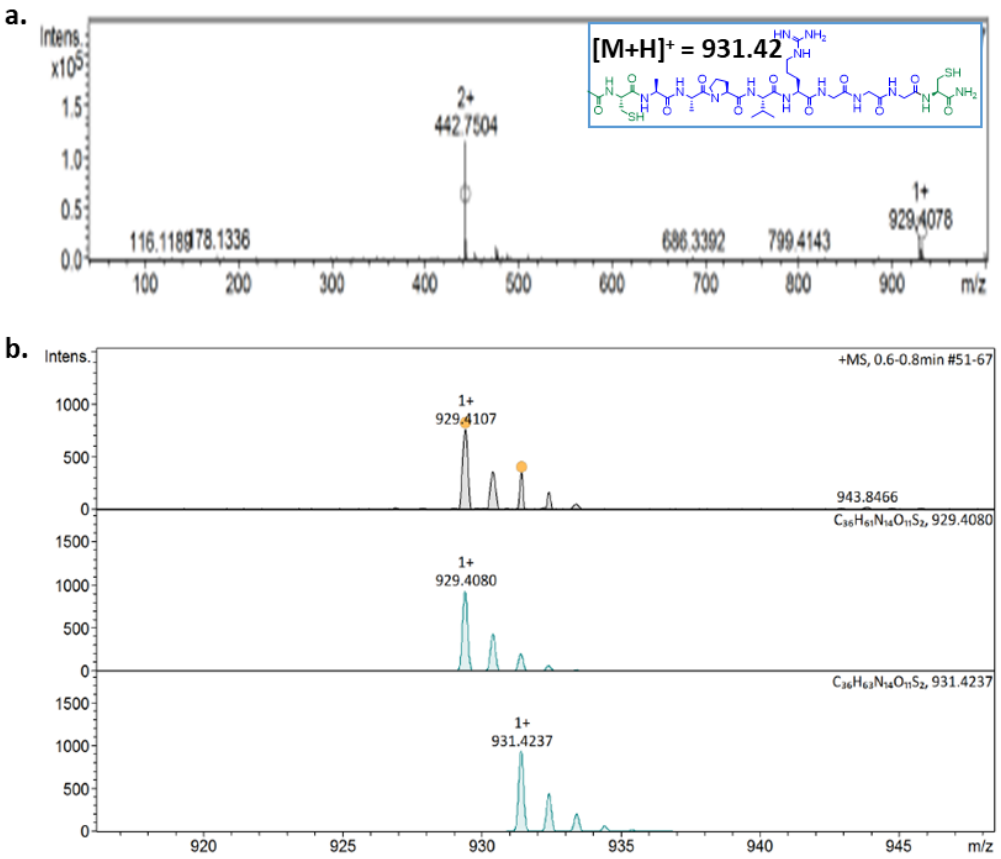

Figure B.1. ESI-MS of crude peptide Ac-CAAPVRGGGC-NH_2 (1). **a.**) Full spectra. **b**.) Detail of peptide m/z and isotope patterns between 920 and 950 Da, showing equilibrium between oxidised peptide ($[M+H]^+$ = 929.411) and reduced $[M+H]^+$ = 931.424).

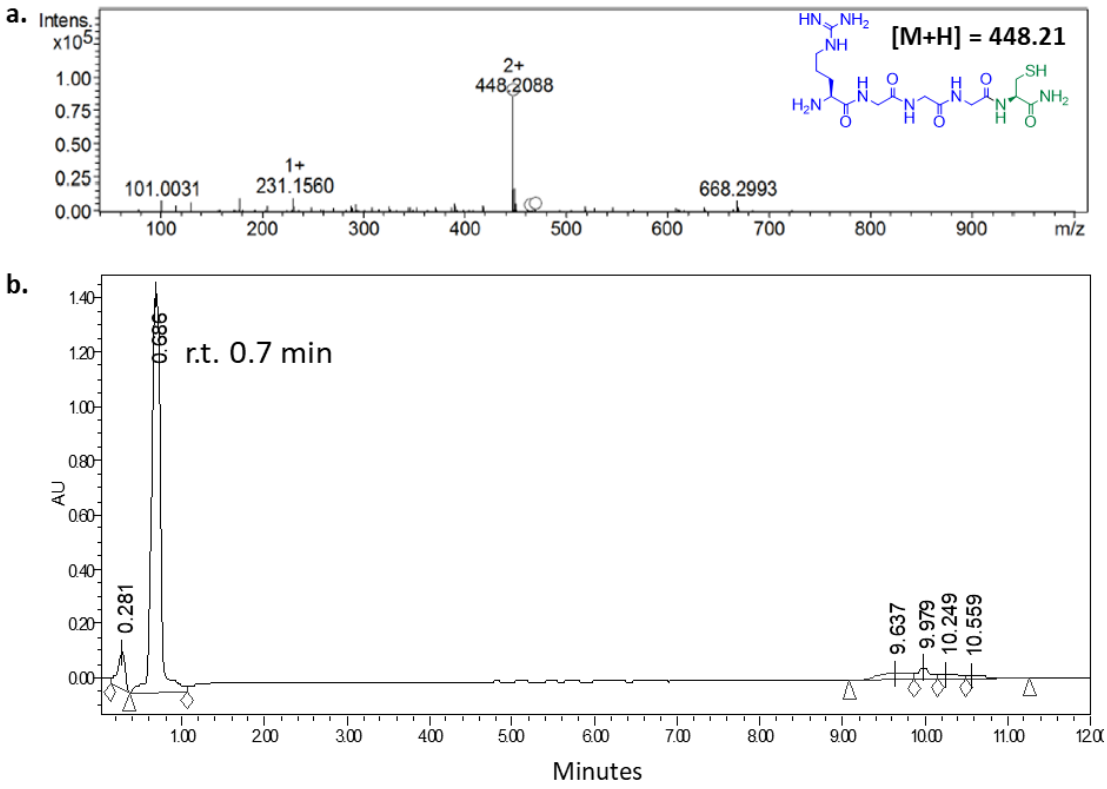

Figure B.2. Characterisation of purified peptide H-RGGGC-NH_2 (2). **a.**) ESI-MS spectra: $[M+H]^+$ predicted 448.2, observed 448.21. **b.**) RP-HPLC chromatogram (r.t. 0.7 min).

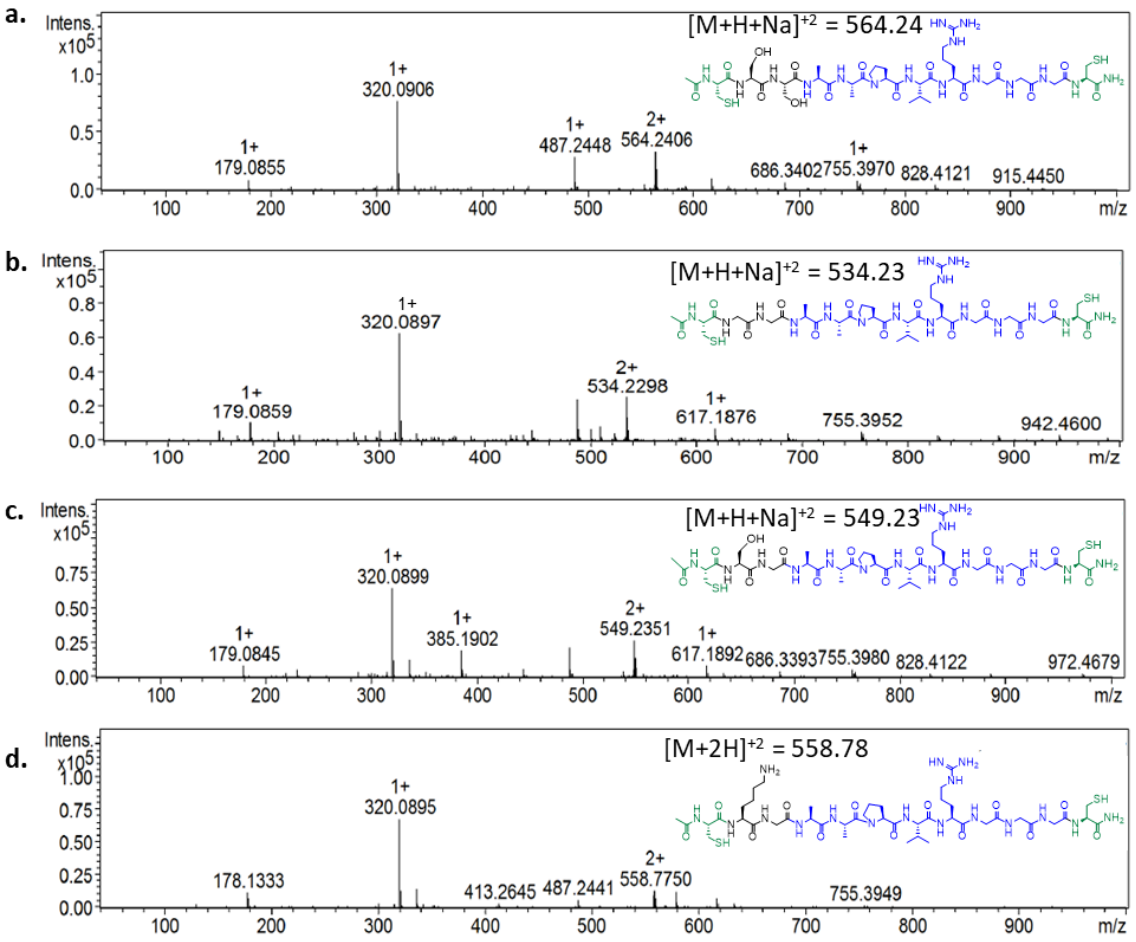

Figure B.3. ESI-MS spectra of elastase-responsive peptides 3 - 6. **a**.) Peptide 3 $[M+H+Na]^{+2}$ predicted 564.24, obtained 564.24. **b.**) Peptide 4: $[M+H+Na]^{2+}$ predicted 534.23, obtained 534.23. **c.**) peptide 5: $[M+H+Na]^{2+}$ predicted 549.23, obtained 549.23. **d.**) Peptide 6:$[M-2H]^{2+}$ predicted 558.78, obtained 558.78. Main peaks 320.09 and 617.18 belong to an internal Fmoc-Glycine standard added to all samples ($[M+Na]^{+}$ 320.09 and $[2M+Na]^{+}$ 617.19).

Table B.1 : Mesh size of 10 – 30 % w/v hydrogels fabricated with DTT as crosslinker and either 4-PEGMal or 4-PEGNB.

Mw PEG	% w/v	4-PEGMal Mesh size (nm)	4-PEGNB Mesh size (nm)
5 kDa	10	8.2 ± 0.3	7.1 ± 0.7
	20	7.4 ± 0.3	5.1 ± 0.2
	30	6.6 ± 0.9	4.4 ± 0.5

All samples were prepared at a 1:1 SH:C=C ratio, n=4, mean ± standard deviation .DTT + dithiothreitol, 4-PEGMal = 4-arm-PEG-maleimide, 4-PEGNB = 4-arm-PEG-norbornene

Appendix C: Supplementary data from Chapter 5

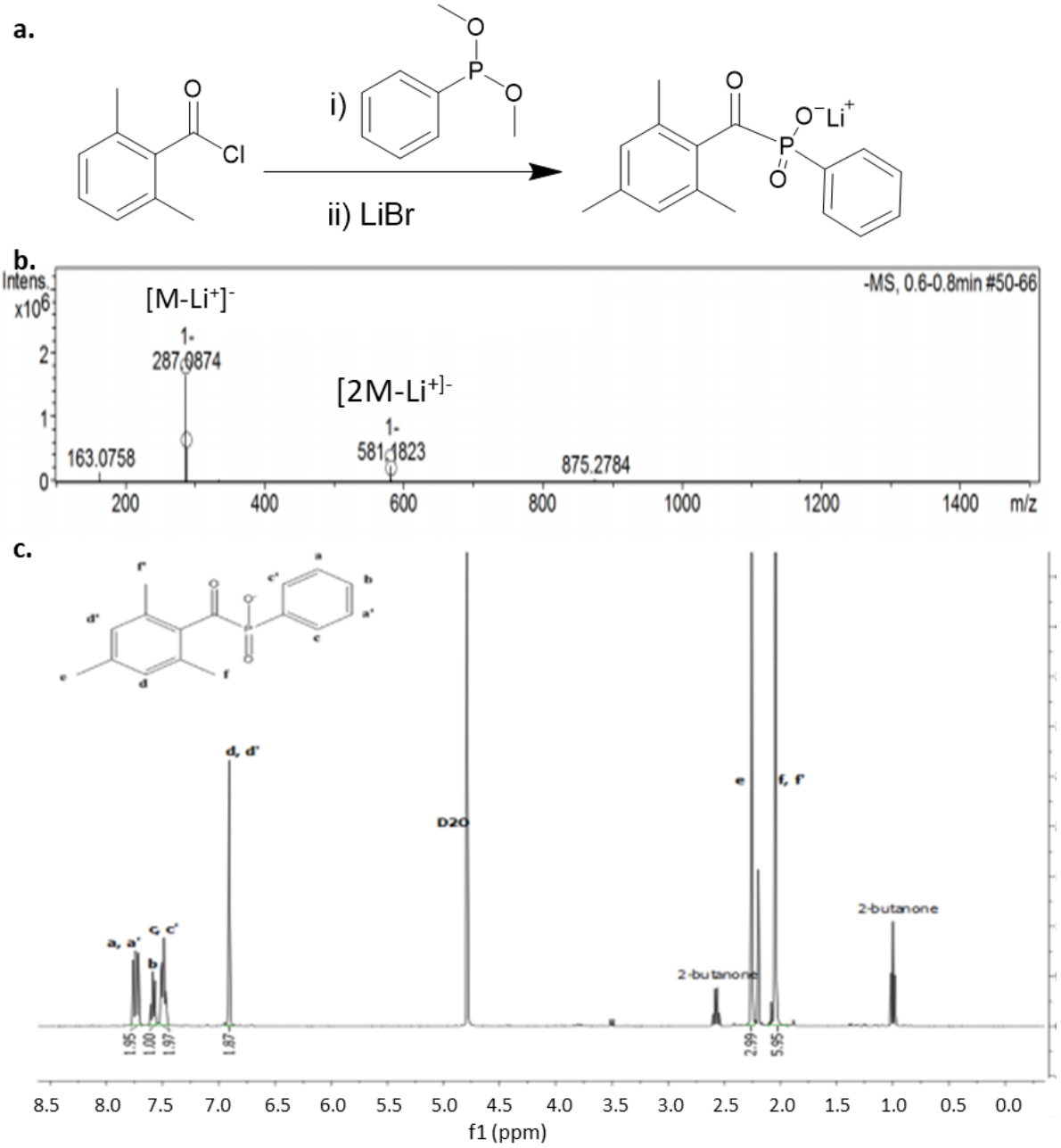

Figure C.1. Synthesis and characterisation of lithium phenyl-2,4,6-trimethylbenzoylphosphinate (LAP) photoinitiator. **A**.) Schematic of LAP synthesis as described by Fairbanks *et al.*[171]. **b**.)ESI-MS: $[M\text{-}Li^+]^-$ predicted 287.08, observed 287.09, $[2M\text{-}Li^+]^-$ predicted 581.18, observed 581.18. **c.**) ^1H NMR spectra (400 MHz, D_2O, δ, ppm): δ 7.77 – 7.70 (m, 2H), 7.61 – 7.55 (m, 1H), 7.52 – 7.45 (m, 2H), 6.91 (s, 2H), 2.26 (s, 3H), 2.04 (s, 6H).

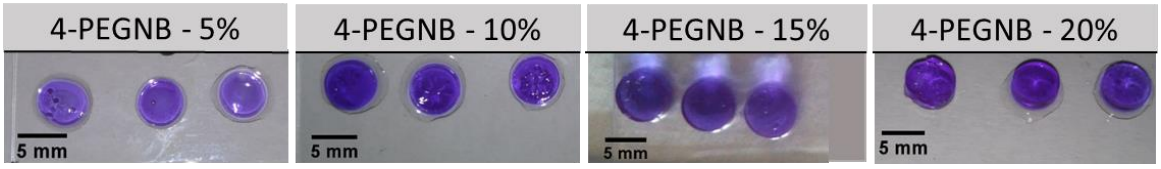

Figure C.2. Visual appearance of 4-PEGNB hydrogels (5, 10, 15 and 20 % w/v) at the end of passive release assay (day 6).

Table C.1 Statistically significant differences from post-hoc test from the comparison of the percent dextran released from 5, 10, 15 and 20 % w/v 4-PEGNB gels.

Time (h)	Tukey multiple comparisons test	P Value	Significant
1 h	5 % vs. 10 %, 5 % vs. 15 %,5 % vs. 20 %	<0.001	Yes (***)
2 h	5 % vs. 10 %, 5 % vs. 15 %,5 % vs. 20 %	<0.001	Yes (***)
4 h	5 % vs. 10 %, 5 % vs. 15 %,5 % vs. 20 %, 10 % vs. 20 %	<0.001 0.0432	Yes (***) Yes(*)
6 h	5 % vs. 10 %, 5 % vs. 15 %,5 % vs. 20 % 10 % vs. 20 %	<0.001 0.0365	Yes (***) Yes(*)
24 h	5 % vs. 10 %, 5 % vs. 15 %,5 % vs. 20 % 10 % vs. 20 %	<0.001 0.0066	Yes (***) Yes(**)
48 h	5 % vs. 10 %, 5 % vs. 15 %,5 % vs. 20 % 10 % vs. 20 %	<0.001 0.020	Yes (***) Yes(*)
96 h	5 % vs. 10 %, 5 % vs. 15 %,5 % vs. 20 % 10 % vs. 20 %	<0.001 0.0103	Yes (***) Yes(*)
144 h	5 % vs. 10 %, 5 % vs. 15 %,5 % vs. 20 % 10 % vs. 20 %	<0.001 0.0139	Yes (***) Yes(*)

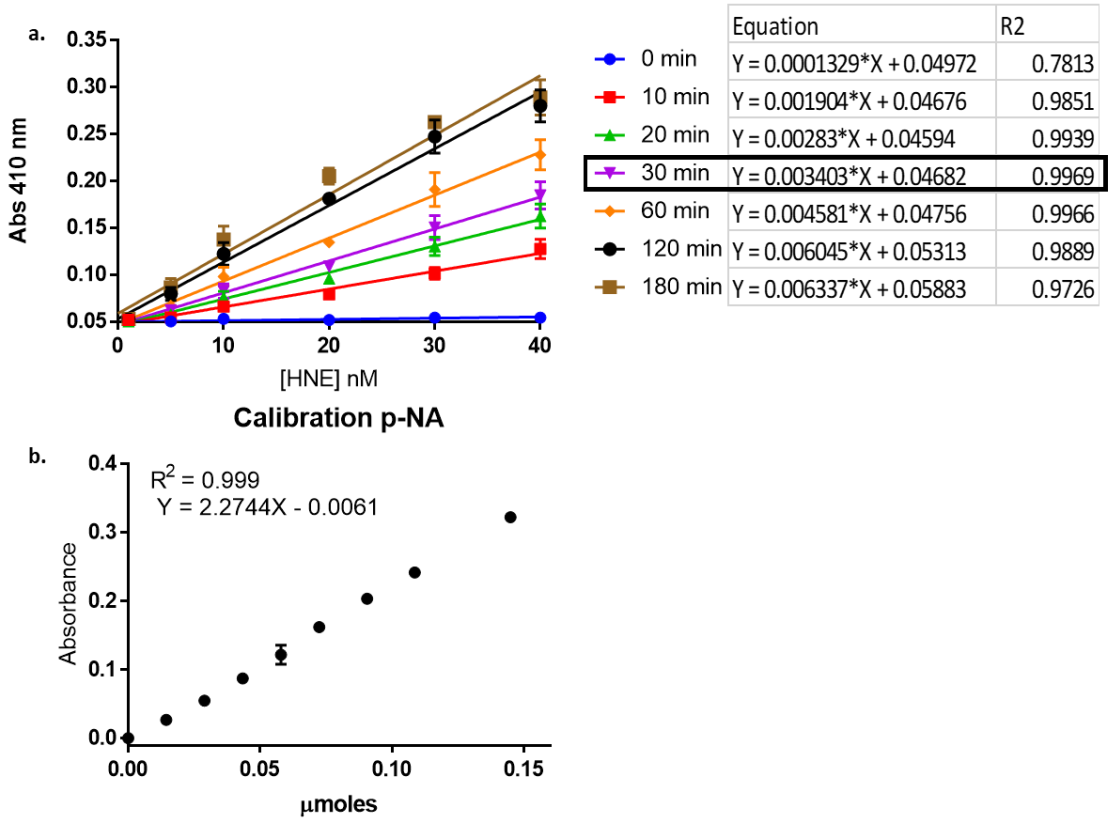

Figure C.3. Human Neutrophil Elastase activity assay. **a**.) Linearity of the quantified absorbance respect to HNE concentration under different incubation times. **b.**) Calibration curve of p-nitroanilide (p-NA) to convert absorbance of cleaved p-NA to micromoles and Units of human neutrophil elastase activity (HNE, 1U = 1umol p-NA).

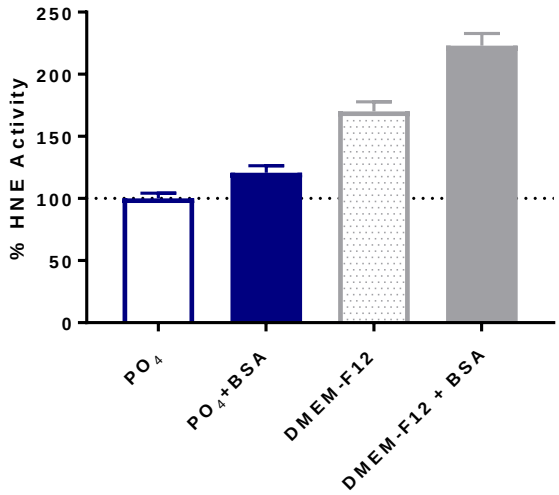

Figure C.4. Relative activity of Human Neutrophil Elastase in different release media: phosphate buffer pH 8 non-supplemented (PO_4), supplemented with 0.1 % BSA (PO_4 + BSA), cell culture medium (DMEM-F12) and 0.1 % supplemented cell culture medium (DMEM-F12 + BSA). Activity is represented as relative to phosphate buffer (n=3 ± mean standard deviation).

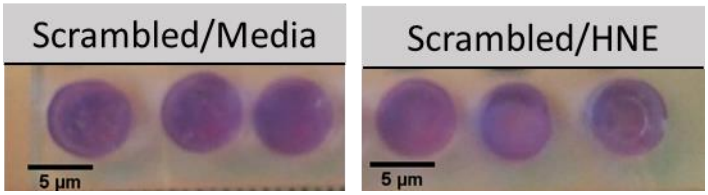

Figure C.5. Visual appearance of 4-PEGNB hydrogels prepared with elastase scrambled peptide incubated in medium (left) or with HNE (right) at the end of release assay (72 h).

Table C.2. Summary of all statistically significant differences in dextran release from MMP-responsive hydrogels in presence of HNE, MMP-2 and in buffer.

Tukey multiple comparison test	P Value	Significant
48 h +Buffer vs 48 h +MMP-2	0.0001	Yes (**)
48 h +HNE vs 48 h +MMP-2	0.0102	Yes (*)
72 h +Buffer vs 72 h +MMP-2	<0.001	Yes (****)
72 h +HNE vs 72 h +MMP-2	0.0115	Yes (*)

Appendix D: Supplementary data from Chapter 6

Table D.1 Statistically significant differences from post-hoc test from the comparison of the % activity with different amounts of AAT 10nM HNE. Multiple comparison between responsive gels containing 0, 5, 10, 20 and 50 µg of AAT at each time point. Multiple comparison between scrambled gels containing 0, 20 and 50 µg AAT at each time point.

Time	Tukey multiple comparisons test	P Value	Significant
24 h	Blank + HNE (n=3) vs. Blank + medium	0.0018	Yes(**)
	Blank + HNE (n=3) vs. 10µg AAT + HNE	0.0059	Yes(**)
	Blank + HNE (n=3) vs. 20µg AAT +HNE	0.0041	Yes(**)
	Scr blank+ HNE vs. Scr 20µg AAT +HNE	0.0045	Yes(**)
	Scr blank+ HNE vs. Scr 50µg AAT +HNE	0.0028	Yes(**)
48 h	Blank + HNE (n=3) vs. Blank + medium	0.0020	Yes(**)
	Blank + HNE (n=3) vs. 20mg AAT +HNE	0.0052	Yes(**)
	Blank + HNE (n=3) vs. 50mg AAT +HNE	0.0026	Yes(**)
	Scr blank+ HNE vs. Scr 20mg AAT +HNE	0.0495	Yes(*)
	Scr blank+ HNE vs. Scr 50mg AAT +HNE	0.0052	Yes(**)
72 h	Blank + HNE (n=3) vs. Blank + medium	0.0017	Yes(**)
	Blank + HNE (n=3) vs. 50mg AAT +HNE	0.0084	Yes(**)
	Blank + medium vs. 5mg AAT + HNE	0.0045	Yes(**)

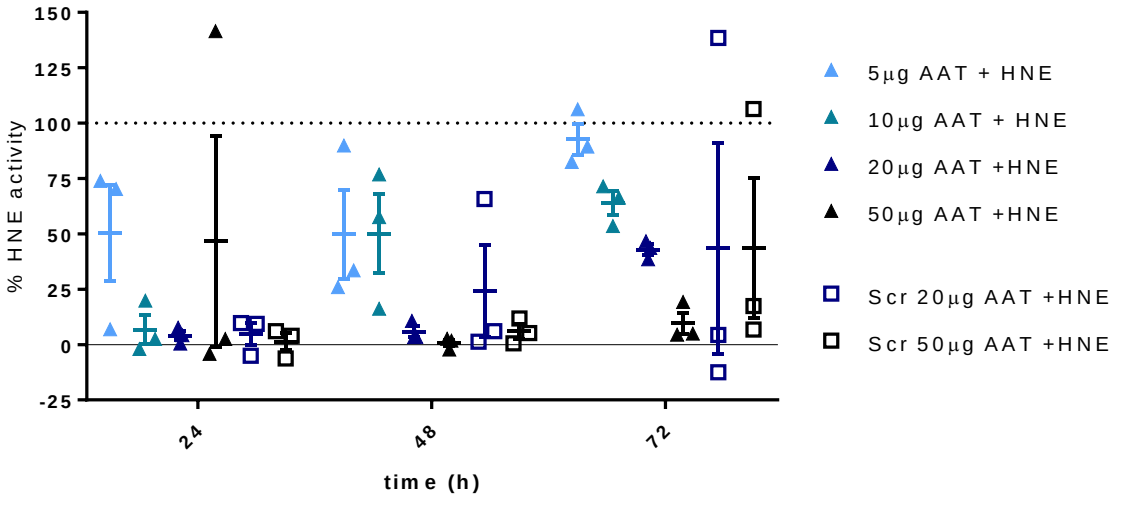

Figure D.1. Modulation of HNE activity using hydrogels with responsive and scrambled peptide crosslinkers encapsulating different amounts of AAT. Individual plot of HNE activity measured on the release medium with colorimetric activity assay with all hydrogels.

Figure D.2 Images of non-responsive hydrogels (scrambled peptide) at the endpoint of the release experiment showing hydrogels weak appearance and lost in dextran content

Table D.2 Statistically significant differences from post-hoc test from the comparison of the % TRD70 released of 50ug AAT hydrogels incubated with 10nM, 30nM and 50 nM HNE. Every sample is compared with every other sample at the same time point.

Time	Tukey multiple comparisons test	P Value	Significant
24 h	Medium vs. Blank gels + 10nM HNE	0.0019	Yes (**)
	Medium vs. Blank gels + 30nM HNE	0.0075	Yes (**)
	Medium vs. Blank gels + 50nM HNE	0.0023	Yes (**)
	AAT gels+ 10nM HNE vs. Blank gels + 10nM HNE	0.0047	Yes (**)
	AAT gels + 30nM HNE vs. Blank gels + 30nM HNE	0.0097	Yes (**)
48 h	Medium vs. AAT gels+ 50nM HNE	0.0009	Yes (***)
	Medium vs. Blank gels + 10nM HNE	0.0004	Yes (***)
	Medium vs. Blank gels + 30nM HNE	<0.0001	Yes (****)
	Medium vs. Blank gels + 50nM HNE	<0.0001	Yes (****)
	AAT gels+ 10nM HNE vs. Blank gels + 10nM HNE	0.0038	Yes (**)
	AAT gels + 30nM HNE vs. Blank gels + 30nM HNE	0.0004	Yes (***)
72 h	Medium vs. AAT gels+ 50nM HNE	0.0018	Yes (**)
	Medium vs. Blank gels + 10nM HNE	0.0133	Yes (*)
	Medium vs. Blank gels + 30nM HNE	0.0012	Yes (**)
	Medium vs. Blank gels + 50nM HNE	0.0012	Yes (**)

Appendix E: Supplementary data from Chapter 7

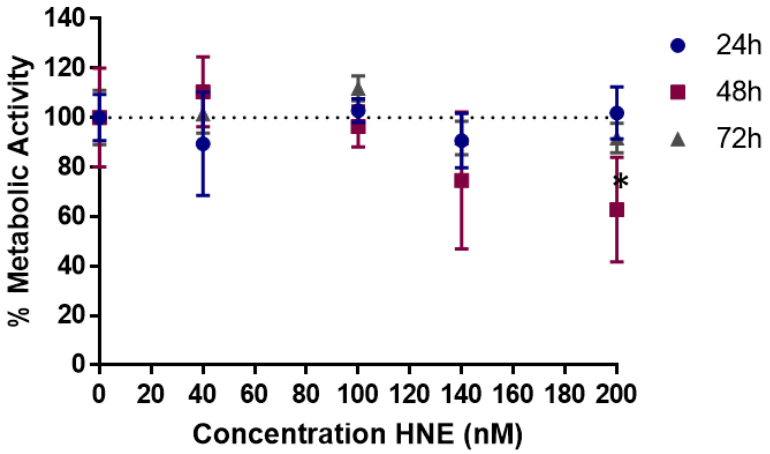

Figure E.1 Time and concentration-dependent effect of externally supplemented Human Neutrophil Elastase on the viability of epithelial cells in 10% v/v FBS supplemented DMEM-F12 (n=3, mean ± standard deviation). * represents statistical significance by 2-way-ANOVA test with Dunnets post analysis between each concentration respect the control with no HNE at the same time point (p Value ** < 0.05). Only 300nM HNE at 48h showed a significant reduction of cell viability, but not at 72h. All other concentration and time points did not show any effect on cell viability.

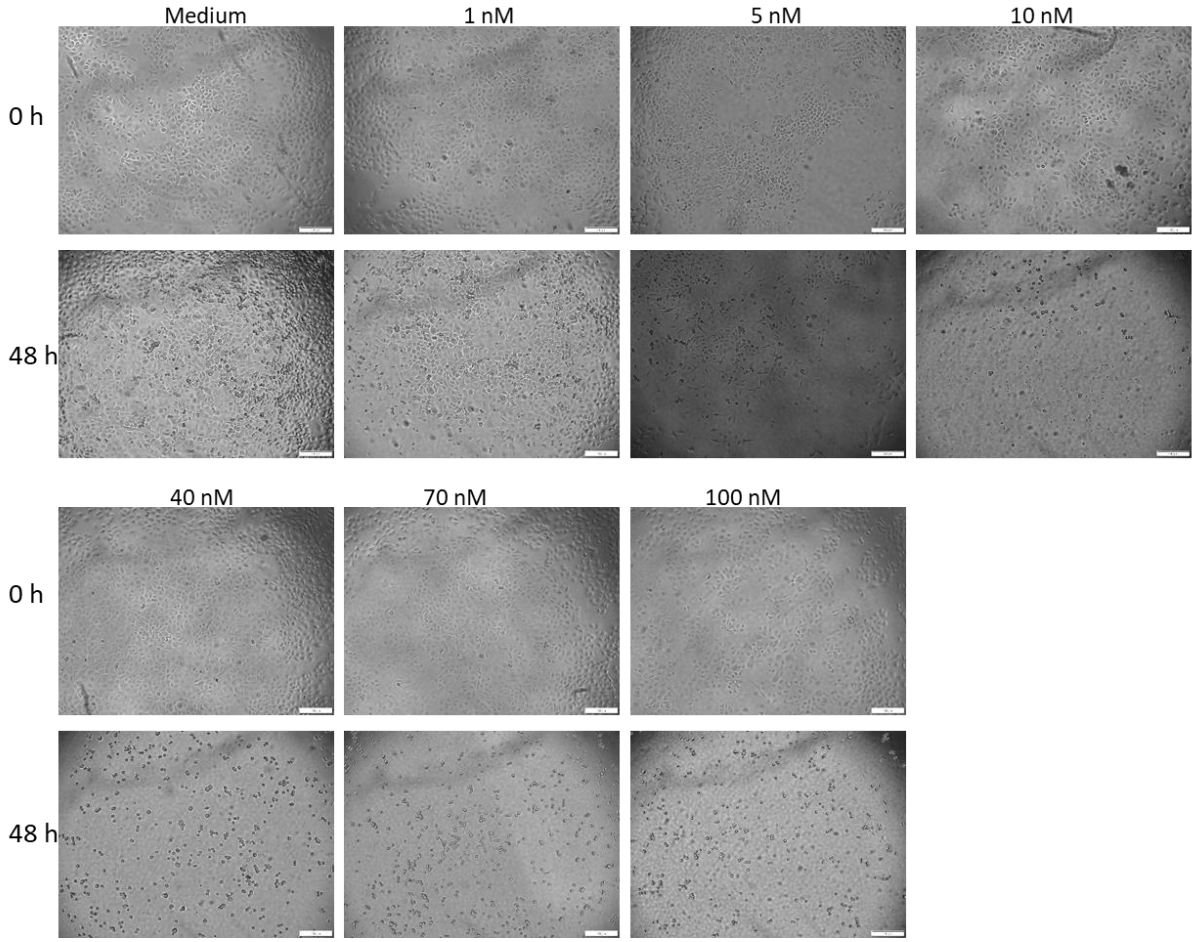

Figure E.2 Cell morphology of epithelial cells cultured on well plates after exposure to human neutrophil elastase for 48h. Scale bar is 200 µm.

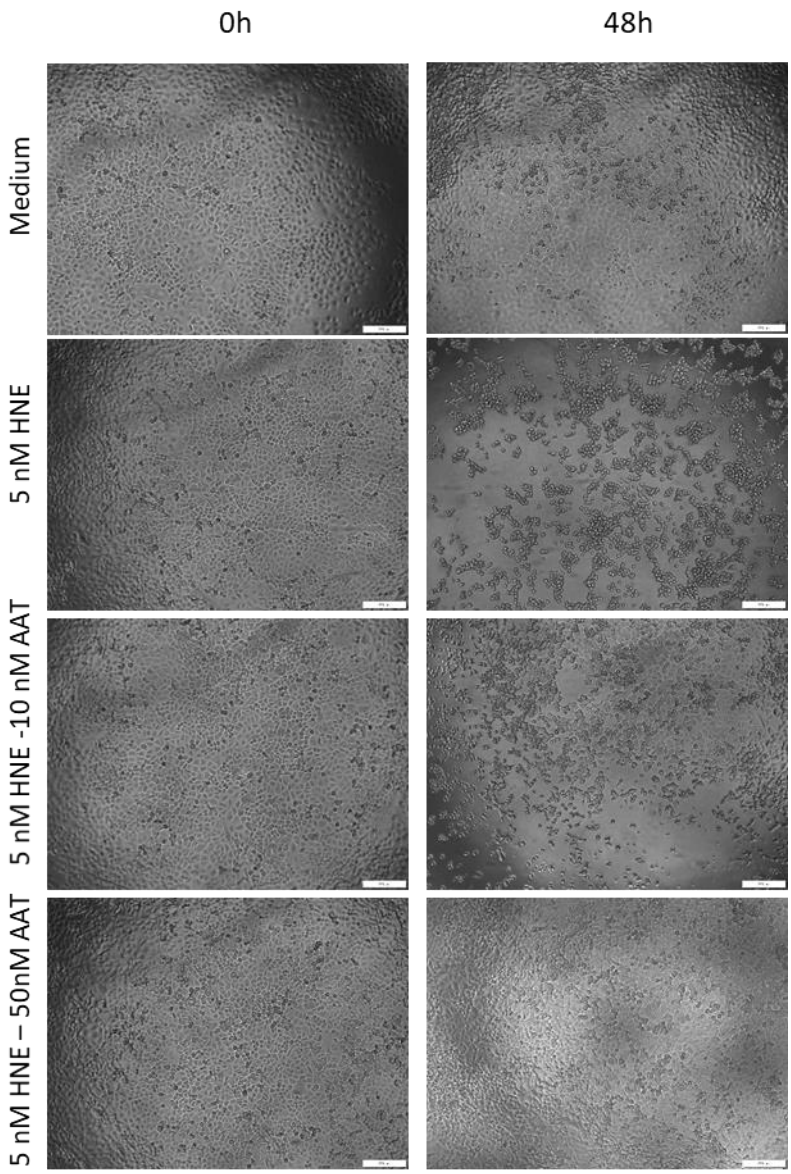

Figure E.3 Cell morphology of epithelial cells after exposure to different combinations of human neutrophil elastase and alpha-1antitrypsin for 48h. Scale bar is 200 µm.

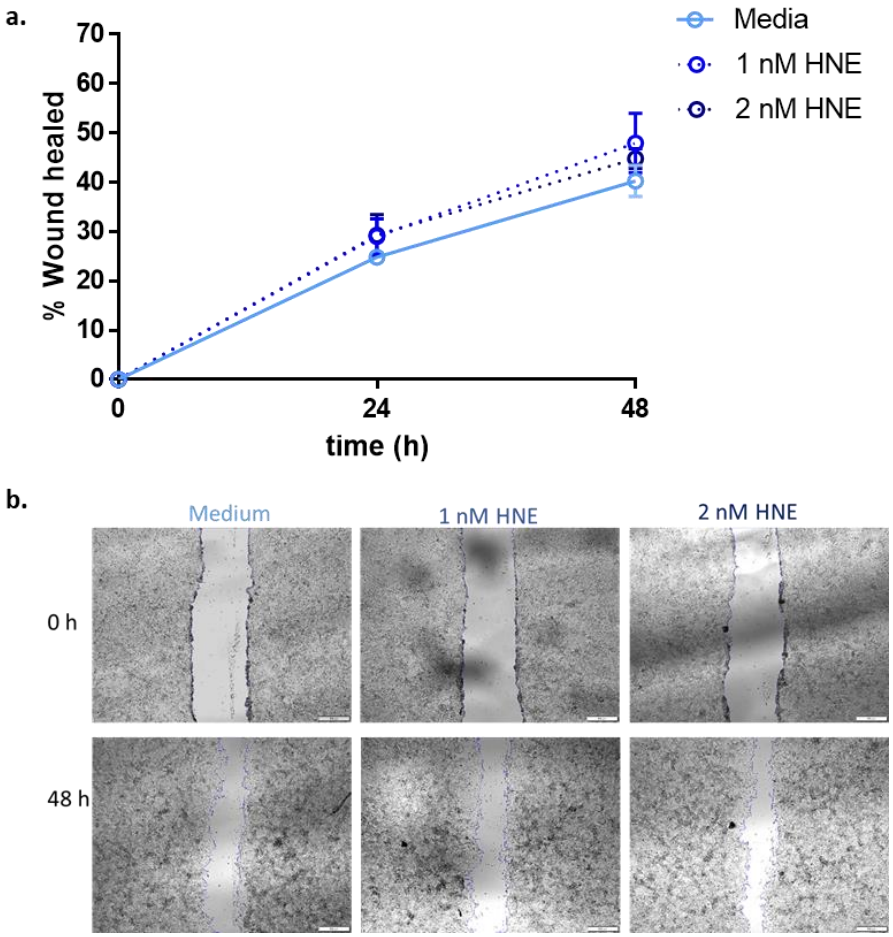

Figure E.4. Epithelial cell repair in presence of 1nM and 2nM Human Neutrophil Elastase, as determined by scratch assays of epithelial cells. **a.**) Percentage of wound healed at each time point and **b.**) optical microscope images of the wounded cell monolayer: top (immediately after scratching cells) and bottom (after 48 h). Scale bar is 500 µm.

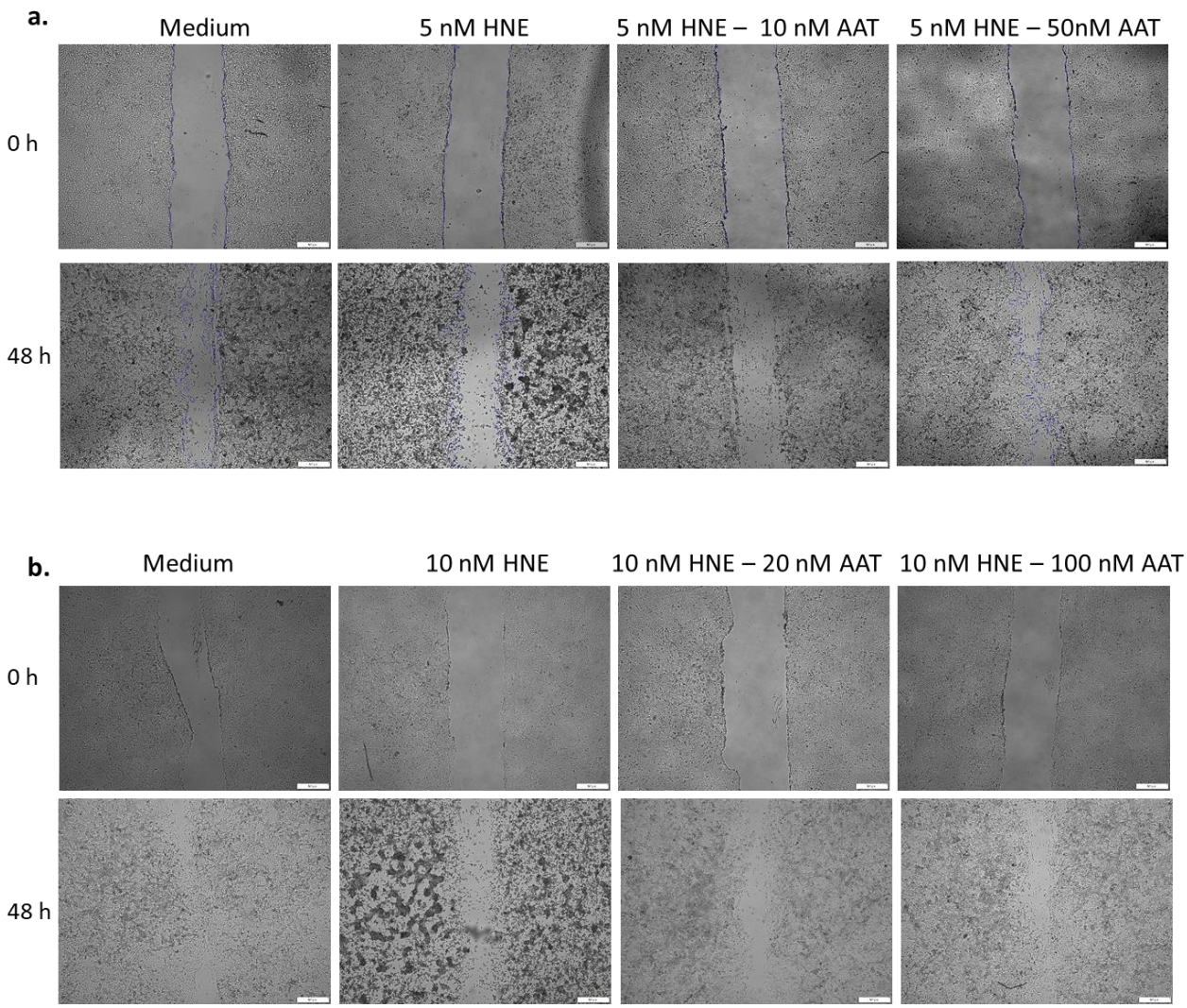

Figure E.5. Optical microscope images of wounded epithelial cell monolayers incubated with different combinations of human neutrophil elastase and alpha-1antitrypsin for 48h. Epithelial repair in presence of **a.**) 5 nM HNE and 5nM HNE and either 10nM or 50 nM AAT, **b.**) 10 nM HNE and 10 nM HNE and either 20 nM or 100 nM AAT. Scale bar is 500 µm.

Table E.1 Statistically significant differences from post-hoc test from the comparison of the % cell migration in presence of 5nM HNE and different AAT combinations.

Tukey multiple comparisons test	P Value	Significant
24 h 5nM HNE *vs* 24 h medium	0.0003	Yes (***)
24 h 5nM HNE *vs* 24 h 5nM HNE + 10nM AAT	0.0020	Yes (**)
24 h 5nM HNE *vs* 24 h 5nM HNE + 50nM AAT	<0.0001	Yes (****)
48 h 5nM HNE *vs* 48 h medium	<0.0001	Yes (****)
48 h 5nM HNE *vs* 48 h 5nM HNE + 10nM AAT	<0.0001	Yes (****)
48 h 5nM HNE *vs* 48 h 5nM HNE + 50nM AAT	<0.0001	Yes (****)
48 h 5nM HNE + 10nM AAT *vs* 48 h 5nM HNE + 50nM AAT	0.0342	Yes (*)

Table E.2 Statistically significant differences from post-hoc test from the comparison of the percentage of cell migration in presence of 10nM HNE and different AAT combinations

Tukey multiple comparisons test	P Value	Significant
24 h 10nM HNE *vs* 24 h medium	0.0003	Yes (***)
24 h 10nM HNE *vs* 24 h 10nM HNE + 20nM AAT	0.0020	Yes (**)
24 h 10nM HNE *vs* 24 h 10nM HNE + 100nM AAT	<0.0001	Yes (****)
48 h 10nM HNE *vs* 48 h medium	<0.0001	Yes (****)
48 h 10nM HNE *vs* 48 h 10nM HNE + 20nM AAT	<0.0001	Yes (****)
48 h 10nM HNE *vs* 48 h 10nM HNE + 100nM AAT	<0.0001	Yes (****)
48 h medium *vs* 48 h 10nM HNE + 20nM AAT	0.0342	Yes (*)

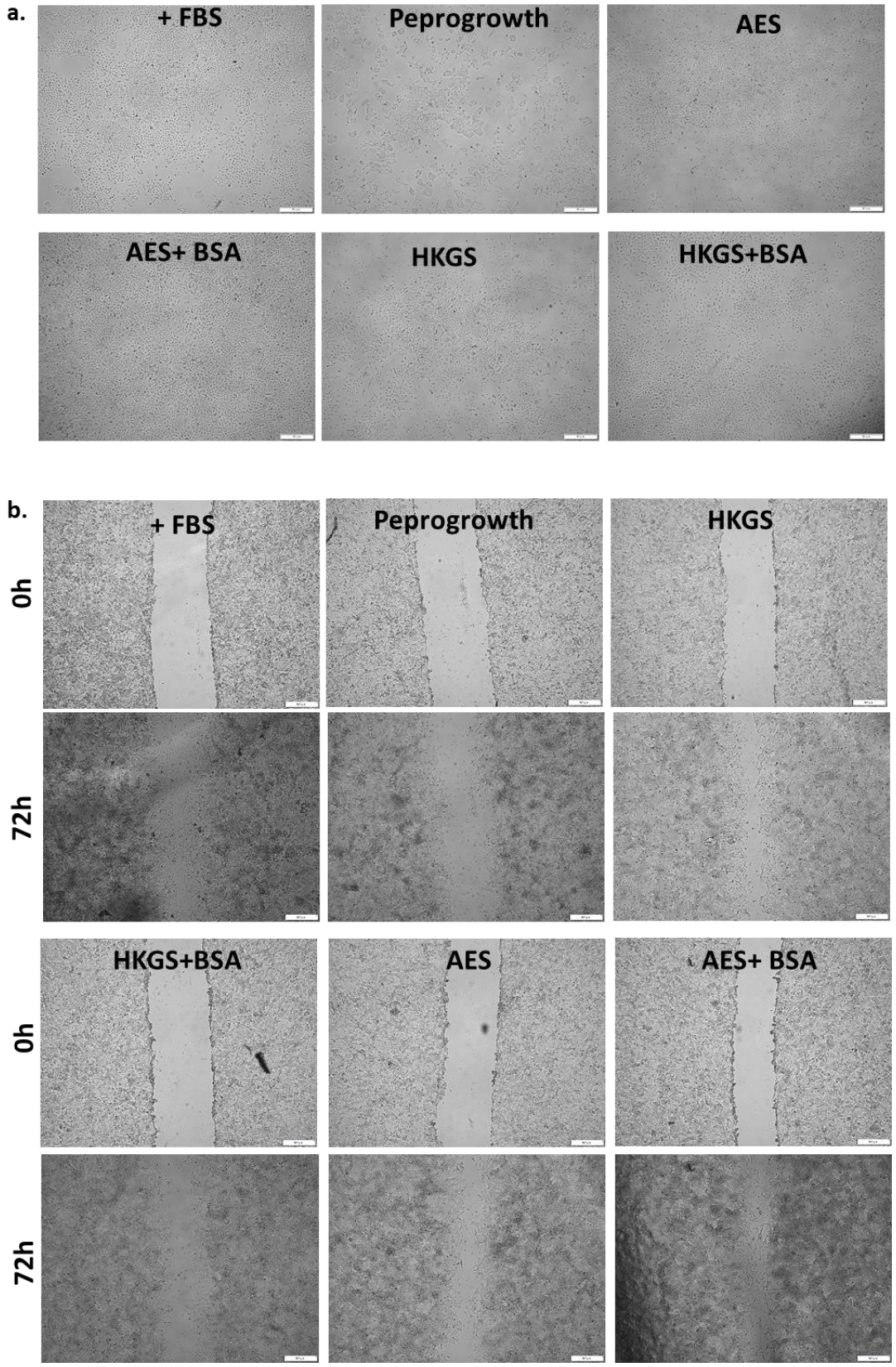

Figure E.6 Optical microscope images of wounded epithelial cell monolayers incubated with different DMEM-F12 supplemented medium**. a**.) Cell morphology after 24 h adaption in 1:1 10% FBS medium:Assay medium and 24 h in the indicated assay medium on each image (scale bar 50 µm). **b**.) Epithelial repair after 72h incubation in each medium, showing morphology and wound closure at each condition. Scale bar is 500 µm

Table E.3 Statistically significant differences from post-hoc test from the comparison of the percentage cell migration in presence of 10 nM HNE and different hydrogel types.

Tukey multiple comparisons test	**P Value**	**Significant**
24 h 10nM HNE *vs* 24 h medium	<0.0001	Yes (****)
24 h 10nM HNE *vs* 24 h AAT gels (70 µg)	0.0015	Yes (**)
24 h 10nM HNE *vs* 24 h AAT gels (100 µg)	0.0331	Yes (*)
24 h 10nM HNE *vs* 24 h AAT gels (70 µg)	0.0254	Yes (*)
24 h 10nM HNE *vs* 24 h AAT gels (100 µg)	0.0017	Yes (**)
24 h HNE + blank gels *vs* 24 h medium	<0.0001	Yes (****)
24 h HNE + blank gels *vs* 24 h AAT gels (70 µg)	0.0015	Yes (**)
24 h HNE + blank gels *vs* 24 h AAT gels (100 µg)	0.0331	Yes (*)
24 h HNE + blank gels *vs* 24 h AAT scrambled gels (70 µg)	0.0254	Yes (*)
24 h HNE + blank gels *vs* 24 h AAT scrambled gels (100 µg)	0.0017	Yes (**)
48 h medium *vs* 48 h 10nM HNE	<0.0001	Yes (****)
48 h Medium *vs* 48 h HNE + blank gels	<0.0001	Yes (****)
48 h Medium *vs* 48 h AAT gels (70 µg)	0.0007	Yes (***)
48 h Medium *vs* 48 h AAT gels (100 µg)	0.0289	Yes (*)
48 h Medium *vs* AAT scrambled gels (70 µg)	0.0035	Yes (**)
48 h Medium *vs* 48 h AAT scrambled gels (100 µg)	0.0222	Yes (*)
48 h 10nM HNE *vs* 48 h AAT gels (70 µg)	0.0019	Yes (**)
48 h 10nM HNE *vs* 48 h AAT gels (100 µg)	0.0026	Yes (**)
48 h 10nM HNE *vs* 48 h AAT scrambled gels (70 µg)	0.0222	Yes (*)
48 h 10nM HNE *vs* 48 h AAT scrambled gels (100 µg)	0.0035	Yes (**)
48 h HNE + blank gels *vs* 48 h AAT gels (70 µg)	0.0019	Yes (**)
48 h HNE + blank gels *vs* 48 h AAT gels (100 µg)	0.0026	Yes (**)
48 h HNE + blank gels *vs* 48 h AAT scrambled gels (70 µg)	0.0222	Yes (*)
48 h HNE + blank gels *vs* 48 h AAT scrambled gels (100 µg)	0.0035	Yes (**)

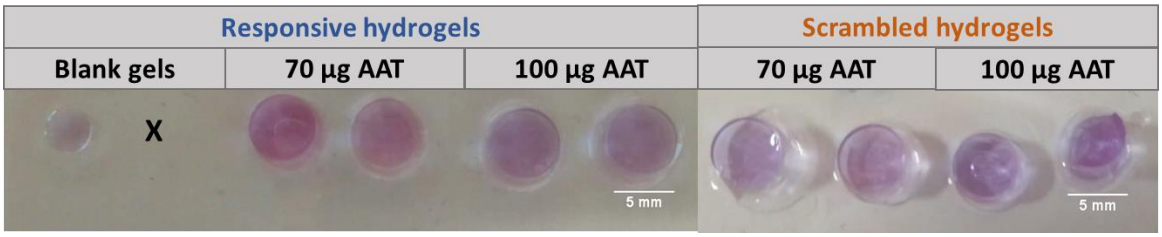

Figure E.7 Images of hydrogels at the endpoint of the scratch experiment. Scale bars are 5 mm, black cross indicates the hydrogel has been fully degraded.

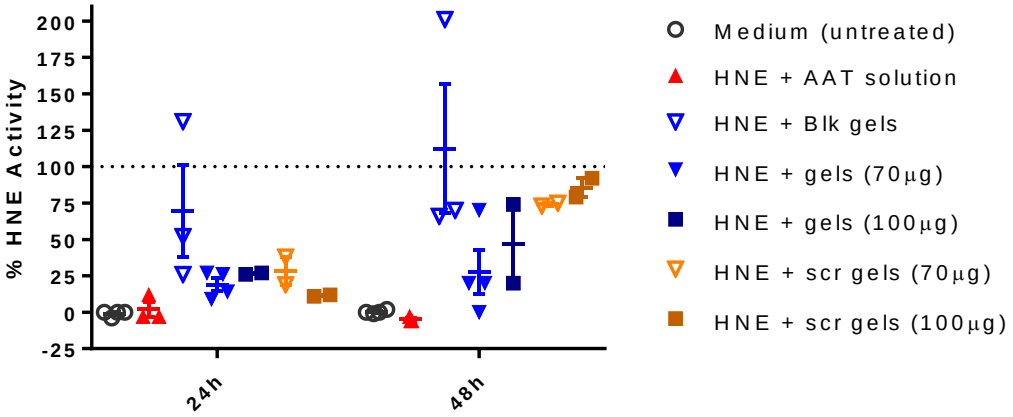

Figure E.8. Effect of AAT-loaded hydrogels on HNE activity in cell supernatants of HNE-treated epithelial cells corresponding to Figure 7.11. Individual experimental points are represented (N =3 and n=3 for samples not containing hydrogels, N=4 and n=2 for responsive hydrogels (70µg), and N=2 and n=2 for responsive hydrogels (100µg) and scrambled hydrogels (70 and 100µg)).

References

1. Li, J. & Mooney, D. J. Designing hydrogels for controlled drug delivery. *Nat. Rev. Mater.* **1**, 16071 (2016).

2. Weiss, R. G. Preface to the molecular and polymer gels; materials with self-assembled fibrillar networks special issue. *Langmuir* **25**, 8369 (2009).

3. Flory, P. Introductory lecture. *Faraday Discuss. Chem. Soc.* **57**, 7–18 (1974).

4. Hoare, T. R. & Kohane, D. S. Hydrogels in drug delivery : Progress and challenges *. *Polym. with aligned carbon Nanotub. Act. Compos. Mater.* **49**, 1993–2007 (2008).

5. Peppas, N. A., Hilt, J. Z., Khademhosseini, A. & Langer, R. Hydrogels in biology and medicine: From molecular principles to bionanotechnology. *Adv. Mater.* **18**, 1345–1360 (2006).

6. Eskandari, S., Guerin, T., Toth, I. & Stephenson, R. J. Recent advances in self-assembled peptides: Implications for targeted drug delivery and vaccine engineering. *Adv. Drug Deliv. Rev.* **110**–**111**, 169–187 (2016).

7. Chandrawati, R. Enzyme-responsive polymer hydrogels for therapeutic delivery. *Exp. Biol. Med.* **241**, 972–979 (2016).

8. Du, X., Zhou, J., Shi, J. & Xu, B. Supramolecular Hydrogelators and Hydrogels: From Soft Matter to Molecular Biomaterials. *Chem. Rev.* **115**, 13165–13307 (2015).

9. Angelerou, M. G. F. *et al.* Supramolecular Nucleoside-Based Gel: Molecular Dynamics Simulation and Characterization of Its Nanoarchitecture and Self-Assembly Mechanism. *Langmuir* **34**, 6912–6921 (2018).

10. Limón, D. *et al.* Microscale coiling in bis-imidazolium supramolecular hydrogel fibres induced by the release of a cationic serine protease inhibitor. *Chem. Commun.* **53**, 4509–4512 (2017).

11. Li, X. *et al.* pH-sensitive peptide hydrogel for glucose-responsive insulin delivery. *Acta Biomater.* **51**, 294–303 (2017).

12. Štaka, I. *et al.* A novel low molecular weight nanocomposite hydrogel formulation for intra-tumoural delivery of anti-cancer drugs. *Int. J. Pharm.* **565**, 151–161 (2019).

13. Wu, J., Su, Z. G. & Ma, G. H. A thermo- and pH-sensitive hydrogel composed of quaternized chitosan/glycerophosphate. *Int. J. Pharm.* **315**, 1–11 (2006).

14. Van De Wetering, P., Metters, A. T., Schoenmakers, R. G. & Hubbell, J. A. Poly(ethylene glycol) hydrogels formed by conjugate addition with controllable swelling, degradation, and release of pharmaceutically active proteins. *J. Control. Release* **102**, 619–627 (2005).

15. Yoon, S. D. *et al.* Cell recruiting chemokine-loaded sprayable gelatin hydrogel dressings for diabetic wound healing. *Acta Biomater.* **38**, 59–68 (2016).

16. Zhang, Y., Tao, L. & Wei, Y. Synthesis of Multiresponsive and Dynamic Chitosan-Based Hydrogels for Controlled Release of Bioactive Molecules. 2894–2901 (2011).

17. Li, Y., Rodrigues, J. & Tomas, H. Injectable and biodegradable hydrogels: gelation, biodegradation and biomedical applications. *Chem. Soc. Rev.* **41**, 2193–2221 (2012).

18. Liu, Z. Q. *et al.* Dextran-based hydrogel formed by thiol-Michael addition reaction for 3D cell encapsulation. *Colloids Surfaces B Biointerfaces* **128**, 140–148 (2015).

19. Luo, Y., Kirker, K. R. & Prestwich, G. D. Cross-linked hyaluronic acid hydrogel films: new biomaterials for drug delivery. *J. Control. Release* **69**, 169–184 (2000).

20. Anjum, F. *et al.* Enzyme responsive GAG-based natural-synthetic hybrid hydrogel for tunable growth factor delivery and stem cell differentiation. *Biomaterials* **87**, 104–117 (2016).

21. Song, A., Rane, A. A. & Christman, K. L. Antibacterial and cell-adhesive polypeptide and poly(ethylene glycol) hydrogel as a potential scaffold for wound healing. *Acta Biomater.* **8**,

41–50 (2012).

22. Rehmann, M. S. *et al.* Tuning and Predicting Mesh Size and Protein Release from Step Growth Hydrogels. *Biomacromolecules* **18**, 3131–3142 (2017).

23. Schweller, R. M. & West, J. L. Encoding Hydrogel Mechanics via Network Cross-Linking Structure. *ACS Biomater. Sci. Eng.* **1**, 335–344 (2015).

24. Karpushkin, E., Du, M., Slouf, M. & Du, K. Rheology and porosity control of poly (2-hydroxyethyl methacrylate) hydrogels. *Polymer (Guildf).* **54**, 661–672 (2013).

25. Turecek, P. L., Bossard, M. J., Schoetens, F. & Ivens, I. A. PEGylation of Biopharmaceuticals : A Review of Chemistry and Nonclinical Safety Information of Approved Drugs. *J. Pharm. Sci.* **105**, 460–475 (2016).

26. Grim, J. C., Marozas, I. A. & Anseth, K. S. Thiol-ene and photo-cleavage chemistry for controlled presentation of biomolecules in hydrogels. *J. Control. Release* **219**, 95–106 (2015).

27. Nehls, E. M., Rosales, A. M. & Anseth, K. S. Enhanced user-control of small molecule drug release from a poly(ethylene glycol) hydrogel via azobenzene/cyclodextrin complex tethers. *J. Mater. Chem. B* **4**, 1035–1039 (2016).

28. Merrill, E. W. *et al.* Platelet-compatible hydrophilic segmented polyurethanes from polyethyelene glycols and cyclohexane diisocianate. *Tansactions - Am. Soc. Artif. Intern. Organs* **28**, 482–487 (1982).

29. Bakaic, E., Smeets, N. M. B. & Hoare, T. Injectable hydrogels based on polye(ethylene glycol) and derivatives as functional biomaterials. *RSC Adv.* **5**, 35469–35486 (2015).

30. Fraser, A. K., Ki, C. S. & Lin, C. PEG-Based Microgels Formed by Visible-Light- Mediated Thiol-Ene Photo-Click Reactions. 507–515

31. Anumolu, S. N. S. *et al.* Doxycycline loaded poly(ethylene glycol) hydrogels for healing

vesicant-induced ocular wounds. *Biomaterials* **31**, 964–974 (2010).

32. Donahoe, C. D. *et al.* Ultralow protein adsorbing coatings from clickable PEG nanogel solutions: Benefits of attachment under salt-induced phase separation conditions and comparison with PEG/albumin nanogel coatings. *Langmuir* **29**, 4128–4139 (2013).

33. Pritchard, C. D. *et al.* An injectable thiol-acrylate poly (ethylene glycol) hydrogel for sustained release of methylprednisolone sodium succinate. *Biomaterials* **32**, 587–597 (2011).

34. Canal, T. & Peppas, N. A. Correlation between mesh size and equilibrium degree of swelling of polymeric networks. *J. Biomed. Mater. Res.* **23**, 1183–1193 (1989).

35. Lee, S., Tong, X. & Yang, F. Effects of the poly(ethylene glycol) hydrogel crosslinking mechanism on protein release. *Biomater. Sci.* **4**, 405–411 (2016).

36. Zustiak, S. P. & Leach, J. B. Characterization of protein release from hydrolytically degradable poly(ethylene glycol) hydrogels. *Biotechnol. Bioeng.* **108**, 197–206 (2011).

37. Thornton, P. D. & Ulijn, R. V. Enzyme responsive polymer hydrogel beads. *Chem. Commun.* **47**, 5913–5915 (2005).

38. Zustiak, S. P. & Leach, J. B. Hydrolytically degradable poly(ethylene glycol) hydrogel scaffolds with tunable degradation and mechanical properties. *Biomacromolecules* **11**, 1348–1357 (2010).

39. Aimetti, A. A., Machen, A. J. & Anseth, K. S. Poly(ethylene glycol) hydrogels formed by thiol-ene photopolymerization for enzyme-responsive protein delivery. *Biomaterials* **30**, 6048–6054 (2009).

40. Thornton, B. P. D., Mart, R. J. & Ulijn, R. V. Enzyme-Responsive Polymer Hydrogel Particles for Controlled Release. *Adv. Mater.* **19**, 1252–1256 (2007).

41. Foster, G. A. *et al.* Protease-degradable microgels for protein delivery for vascularization.

Biomaterials **113**, 170–175 (2017).

42. Mann, B. K., Schmedlen, R. H. & West, J. L. Tethered-TGF-β increases extracellular matrix production of vascular smooth muscle cells. *Biomaterials* **22**, 439–444 (2001).

43. Maitz, M. F. *et al.* Bio-responsive polymer hydrogels homeostatically regulate blood coagulation. *Nat. Commun.* **4**, 1–10 (2013).

44. Quinn, J. F., Whittaker, M. R. & Davis, T. P. Glutathione responsive polymers and their application in drug delivery systems. *Polym. Chem.* **8**, 97–126 (2017).

45. Yang, C., Mariner, P. D., Nahreini, J. N. & Anseth, K. S. Cell-mediated delivery of glucocorticoids from thiol-ene hydrogels. *J. Control. Release* **162**, 612–618 (2012).

46. Silva, E. A. & Mooney, D. J. Effects of VEGF temporal and spatial presentation on angiogenesis. *Biomaterials* **31**, 1235–1241 (2010).

47. Kim, M. & Cha, C. Modulation of functional pendant chains within poly(ethylene glycol) hydrogels for refined control of protein release. *Sci. Rep.* **8**, 1–12 (2018).

48. Stevens, D. M. *et al.* Semibranched polyglycidols as 'fillers' in polycarbonate hydrogels to tune hydrophobic drug release. *Polym. Chem.* **6**, 1096–1102 (2015).

49. auf dem Keller, U. & Sabino, F. Matrix metalloproteinases in impaired wound healing. *Met. Med.* **2**, 1–8 (2015).

50. Gill, S. E. & Parks, W. C. Metalloproteinases and their inhibitors: Regulators of wound healing. *Int. J. Biochem. Cell Biol.* **40**, 1334–1347 (2008).

51. Mohan, R. *et al.* Matrix metalloproteinase gelatinase B (MMP-9) coordinates and effects epithelial regeneration. *J. Biol. Chem.* **277**, 2065–2072 (2002).

52. International Consensus. The role of proteases in wound diagnostics. An expert working group review. *London: Wounds International* (2011).

53. Pandiella, A., Bosenberg, M. W., Huang, E. J., Besmer, P. & Massague, J. Cleavage of membrane-anchored growth factors involves distinct protease activities regulated through common mechanisms. *J. Biol. Chem.* **267**, 24028–24033 (1992).

54. McCarty, S. M. & Percival, S. L. Proteases and Delayed Wound Healing. *Adv. Wound Care* **2**, 438–447 (2013).

55. Troeberg, L. & Nagase, H. Proteases involved in cartilage matrix degradation in osteoarthritis. *Biochim. Biophys. Acta - Proteins Proteomics* **1824**, 133–145 (2012).

56. Roy, R., Yang, J. & Moses, M. A. Matrix Metalloproteinases As Novel Biomarkers and Potential Therapeutic Targets in Human Cancer. *J Clin Oncol* **27**, 5287–5297 (2009).

57. Hua, Y. & Nair, S. Proteases in cardiometabolic diseases: Pathophysiology, molecular mechanisms and clinical applications. *Biochim. Biophys. Acta - Mol. Basis Dis.* **1852**, 195–208 (2015).

58. Demidova-Rice, T. N., Hamblin, M. R. & Herman, I. M. Acute and Impaired Wound Healing: Pathophysiology and current methods for drug delivery, Part 1: Normal and chronic wounds: Biology, causes, and approaches to care. *Ski. Wound Care* **25**, 304–314 (2013).

59. Lazarus, G. S. *et al.* Definitions and guidelines for assessment of wounds and evaluation of healing. *Arch. Dermatol.* **130**, 489–493 (1994).

60. McCarty, S. M., Cochrane, C. A., Clegg, P. D. & Percival, S. L. The role of endogenous and exogenous enzymes in chronic wounds: A focus on the implications of aberrant levels of both host and bacterial proteases in wound healing. *Wound Repair Regen.* **20**, 125–136 (2012).

61. Guo, S. & DiPietrio, L. Factors Affecting Wound Healing. *J. Dent. Res.* **89**, 219–229 (2010).

62. Diegelmann, B. & Evans, M. Wound Healing: an Overview of Acute, Fibrotic and Delayed Healing. 1–8 (2004).

63. Wiegand, C. & Hipler, U. C. A superabsorbent polymer-containing wound dressing efficiently sequesters MMPs and inhibits collagenase activity in vitro. *J. Mater. Sci. Mater. Med.* **24**, 2473–2478 (2013).

64. Loots, M. A. M. *et al.* Differences in cellular infiltrate and extracellular matrix of chronic diabetic and venous ulcers versus acute wounds. *J. Invest. Dermatol.* **111**, 850–857 (1998).

65. Posnett, J. & Franks, P. J. The burden of chronic wounds in the UK. *Nurs. Times* **104**, 44–45 (2010).

66. Gottrup, F., Apelqvist, J., Price, P. & European Wound Management Association Patient Outcome Group. Outcomes in controlled and comparative studies on non-healing wounds: recommendations to improve the quality of evidence in wound management. *J. Wound Care* **19**, 237–68 (2010).

67. Guest, J. F. *et al.* Health economic burden that wounds impose on the National Health Service in the UK. *BMJ Open* **5**, e009283 (2015).

68. Eming, S. A. *et al.* Differential proteomic analysis distinguishes tissue repair biomarker signatures in wound exudates obtained from normal healing and chronic wounds. *J. Proteome Res.* **9**, 4758–4766 (2010).

69. Kurahashi, T. & Fujii, J. Roles of Antioxidative Enzymes in Wound Healing. *J. Dev. Biol.* **3**, 57–70 (2015).

70. Vaalamo, M. *et al.* Distinct populations of stromal cells express collagenase-3 (MMP-13) and collagenase-1 (MMP-1) in chronic ulcers but not in normally healing wounds. *J. Invest. Dermatol.* **109**, 96–101 (1997).

71. Wysocki, A. B., Staiano-Coico, L. & Grinnell, F. Wound Fluid from Chronic Leg Ulcers Contains Elevated Levels of Metalloproteinases MMP-2 and MMP-9. *J. Invest. Dermatol.* **101**, 64–68 (1993).

72. Trengove, N. J. *et al.* Analysis of the acute and chronic wound environments: The role of proteases and their inhibitors. *Wound Repair Regen.* **7**, 442–452 (1999).

73. Justet, C., Evans, F., Torriglia, A. & Chifflet, S. Increase in the expression of leukocyte elastase inhibitor during wound healing in corneal endothelial cells. *Cell Tissue Res.* **362**, 557–568 (2015).

74. Arpino, V., Brock, M. & Gill, S. E. The role of TIMPs in regulation of extracellular matrix proteolysis. *Matrix Biol.* **44–46**, 247–54 (2015).

75. Cullen, B., Smith, R., Mcculloch, E., Silcock, D. & Morrison, L. Mechanism of action of PROMOGRAN, a protease modulating matrix, for the treatment of diabetic foot ulcers. *Wound Repair Regen.* **10**, 16–25 (2002).

76. Yager, D. R. *et al.* Ability of chronic wound fluids to degrade peptide growth factors is associated with increased levels of elastase activity and diminished levels of proteinase inhibitors. *Wound Repair and Regen* **5**, 23–32 (1997).

77. Grinnell, F. & Zhu, M. Fibronectin Degradation in Chronic Wounds Depends on the Relative Levels of Elastase, α1-Proteinase Inhibitor, and α2-Macroglobulin. *J. Invest. Dermatol.* **106**, 335–341 (1996).

78. Ladwig, G. P. *et al.* Ratios of activated matrix metalloproteinase-9 to tissue inhibitor of matrix metalloproteinase-1 in wound fluids are inversely correlated with healing of pressure ulcers. *Wound Repair Regen.* **10**, 26–37 (2002).

79. Serena, T. E. *et al.* Defining a new diagnostic assessment parameter for wound care: Elevated protease activity, an indicator of nonhealing, for targeted protease-modulating treatment. *Wound Repair Regen.* **24**, 589–595 (2016).

80. Lee, W. L. & Downey, G. P. Leukocyte Elastase: Physiological Functions and Role in Acute Lung Injury. *Am. J. Respir. Crit. Care Med.* **164**, 896–904 (2001).

81. Jeske, L., Placzek, S., Schomburg, I., Chang, A. & Schomburg, D. BRENDA in 2019: A European ELIXIR core data resource. *Nucleic Acids Res.* **47**, D542–D549 (2019).

82. Korkmaz, B., Moreau, T. & Gauthier, F. Neutrophil elastase , proteinase 3 and cathepsin G : Physicochemical properties , activity and physiopathological functions. *Biochimie* **90**, 227–242 (2008).

83. Sand, J. M. B. *et al.* Accelerated extracellular matrix turnover during exacerbations of COPD. *Respir. Res.* **16**, 1–8 (2015).

84. Demkow, U. & van Oververld, F. J. Role of Elastases in the pathogenensis of Chronic Obstructive Pulmonary Disease: implications for Treatment. *Eur J Med Res* **15**, 27–35 (2010).

85. Groutas, W., D, D. & KR, A. Neutrophil elastase inhibitors. *Expert Opin Ther Pat* **21**, 339–354 (2011).

86. Sandhaus, R. A. a1-Antitrypsin deficiency 6: New and emerging treatments for a1-antitrypsin deficiency. *Thorax* **59**, 904–909 (2004).

87. Ashcroft, G. S. *et al.* Secretory leukocyte protease inhibitor mediates non-redundant functions necessary for normal wound healing. *Nat. Med.* **6**, 1147–1153 (2000).

88. Moreno, J. A. *et al.* High-density lipoproteins potentiate α1-antitrypsin therapy in elastase-induced pulmonary emphysema. *Am. J. Respir. Cell Mol. Biol.* **51**, 536–549 (2014).

89. Plantier, L. *et al.* Keratinocyte growth factor protects against elastase-induced pulmonary emphysema in mice. *Am. J. Physiol. - Lung Cell. Mol. Physiol.* **293**, 1230–1239 (2007).

90. Pu, S. *et al.* Effect of sivelestat sodium in patients with acute lung injury or acute respiratory distress syndrome: a meta-analysis of randomized controlled trials. *BMC Pulm. Med.* **17**, 1–9 (2017).

91. Nakayama, Y. *et al.* Clarification of Mechanism of Human Sputum Elastase Inhibition by a

New Inhibitor , ONO-5046 , Using Electrospray Ionization Mass Spectrometry. **12**, 2349–2353 (2002).

92. Von Nussbaum, F. & Li, V. M. J. Neutrophil elastase inhibitors for the treatment of (cardio)pulmonary diseases: Into clinical testing with pre-adaptive pharmacophores. *Bioorganic Med. Chem. Lett.* **25**, 4370–4381 (2015).

93. Eming, S. A. *et al.* A Novel Property of Povidon-Iodine: Inhibition of Excessive Protease Levels in Chronic Non-Healing Wounds. *J. Invest. Dermatol.* **126**, 2731–2733 (2006).

94. Barros, S. C., Martins, J. A., Marcos, J. C. & Cavaco-Paulo, A. Influence of secretory leukocyte protease inhibitor-based peptides on elastase activity and their incorporation in hyaluronic acid hydrogels for chronic wound therapy. *Biopolymers* **98**, 576–90 (2012).

95. Edwards, J. V. *et al.* Inhibition of elastase by a synthetic cotton-bound serine protease inhibitor: In vitro kinetics and inhibitor release. *Wound Repair Regen.* **7**, 106–118 (1999).

96. Schmutz, J. L. *et al.* Evaluation of the nano-oligosaccharide factor lipido-colloid matrix in the local management of venous leg ulcers: Results of a randomised, controlled trial. *Int. Wound J.* **5**, 172–182 (2008).

97. Francesko, A., Soares Da Costa, D., Reis, R. L., Pashkuleva, I. & Tzanov, T. Functional biopolymer-based matrices for modulation of chronic wound enzyme activities. *Acta Biomater.* **9**, 5216–5225 (2013).

98. Francesko, A. *et al.* GAGs-thiolated chitosan assemblies for chronic wounds treatment: control of enzyme activity and cell attachment. *J. Mater. Chem.* **22**, 19438–19446 (2012).

99. Nisi, G., Brandi, C., Grimaldi, L., Calabrò, M. & D'Aniello, C. Use of a protease-modulating matrix in the treatment of pressure sores. *Chir. Ital.* **57**, 465–468 (2005).

100. Vincent Edwards, J. *et al.* Modified cotton gauze dressings that selectively absorb neutrophil elastase activity in solution. *Wound Repair Regen.* **9**, 50–58 (2001).

101. Eming, S. *et al.* The inhibition of matrix metalloproteinase activity in chronic wounds by a polyacrylate superabsorber. *Biomaterials* **29**, 2932–2940 (2008).

102. Vasconcelos, A. *et al.* Tailoring elastase inhibition with synthetic peptides. *Eur. J. Pharmacol.* **666**, 53–60 (2011).

103. Cullen, B. M., Silcock, D. W. & Warrick, J. Controlled release therapeutic wound dressings. (2010).

104. Ashley, G. W., Henise, J., Reid, R. & Santi, D. V. Hydrogel drug delivery system with predictable and tunable drug release and degradation rates. *Proc. Natl. Acad. Sci. U. S. A.* **110**, 2318–2323 (2013).

105. Lu, Y., Aimetti, A. A., Langer, R. & Gu, Z. Bioresponsive materials. *Nat. Rev. Mater.* **2**, 16075 (2016).

106. Koehler, K. C., Anseth, K. S. & Bowman, C. N. Diels-alder mediated controlled release from a poly(ethylene glycol) based hydrogel. *Biomacromolecules* **14**, 538–547 (2013).

107. Huebsch, N. *et al.* Ultrasound-triggered disruption and self-healing of reversibly cross-linked hydrogels for drug delivery and enhanced chemotherapy. *Proc. Natl. Acad. Sci. U. S. A.* **111**, 9762–9767 (2014).

108. Khaled, S. Z. *et al.* One-pot synthesis of pH-responsive hybrid nanogel particles for the intracellular delivery of small interfering RNA. *Biomaterials* **87**, 57–68 (2016).

109. Koetting, M. C., Frank, J., Gupta, M., Zhang, A. & Peppas, N. A. pH-responsive and enzymatically-responsive hydrogel microparticles for the oral delivery of therapeutic proteins : Effects of protein size , crosslinking density , and hydrogel degradation on protein delivery. *J. Control. Release* **221**, 18–25 (2016).

110. Matsumoto, A. *et al.* Synthetic ‘smart gel’ provides glucose-responsive insulin delivery in diabetic mice. *Sci. Adv.* **3**, 1–13 (2017).

111. Chen, J. *et al.* Poly(N-isopropylacrylamide) derived nanogels demonstrated thermosensitive self-assembly and GSH-triggered drug release for efficient tumor Therapy. *Polym. Chem.* **10**, 4031–4041 (2019).

112. Pandey, K. C., De, S. & Mishra, P. K. Role of proteases in chronic obstructive pulmonary disease. *Front. Pharmacol.* **8**, 1–9 (2017).

113. Hu, Q., Katti, P. S. & Gu, Z. Enzyme-responsive nanomaterials for controlled drug delivery. *Nanoscale* **6**, 12273–12286 (2014).

114. Griffin, D. R., Weaver, W. M., Scumpia, P. O., Di Carlo, D. & Segura, T. Accelerated wound healing by injectable microporous gel scaffolds assembled from annealed building blocks. *Nat. Mater.* **14**, 737–744 (2015).

115. Purcell, B. P. *et al.* Injectable and bioresponsive hydrogels for on-demand matrix metalloproteinase inhibition. *Nat. Mater.* **13**, 653–61 (2014).

116. Itoh, Y., Matsusaki, M., Kida, T. & Akashi, M. Enzyme-responsive release of encapsulated proteins from biodegradable hollow capsules. *Biomacromolecules* **7**, 2715–2718 (2006).

117. Schulenburg, C., Faccio, G., Jankowska, D., Maniura-Weber, K. & Richter, M. A FRET-based biosensor for the detection of neutrophil elastase. *Analyst* **141**, 1645–1648 (2016).

118. Shin, D. S. *et al.* Synthesis of Microgel Sensors for Spatial and Temporal Monitoring of Protease Activity. *ACS Biomater. Sci. Eng.* **4**, 378–387 (2018).

119. Ulijn, R. V. Enzyme-responsive materials: a new class of smart biomaterials. *J. Mater. Chem.* **16**, 2217 (2006).

120. Zelzer, M. & Ulijn, R. V. Enzyme-responsive polymers: properties, synthesis and applications. in *Smart Polymers and their Applications* 166–203 (Woodhead Publishing Limited, 2014).

121. Zelzer, M., Todd, S. J., Hirst, A. R., McDonald, T. O. & Ulijn, R. V. Enzyme responsive

materials: design strategies and future developments. *Biomater. Sci.* **1**, 11–39 (2013).

122. Hu, J., Zhang, G. & Liu, S. Enzyme-responsive polymeric assemblies, nanoparticles and hydrogels. *Chem. Soc. Rev.* **41**, 5933 (2012).

123. Wade, R. J., Bassin, E. J., Rodell, C. B. & Burdick, J. a. Protease-degradable electrospun fibrous hydrogels. *Nat. Commun.* **6**, 6639 (2015).

124. Wanakule, P., Liu, G. W., Fleury, A. T. & Roy, K. Nano-inside-micro: Disease-responsive microgels with encapsulated nanoparticles for intracellular drug delivery to the deep lung. *J. Control. Release* **162**, 429–437 (2012).

125. Secret, E., Crannell, K. E., Kelly, S. J., Villancio-Wolter, M. & Andrew, J. S. Matrix metalloproteinase-sensitive hydrogel microparticles for pulmonary drug delivery of small molecule drugs or proteins. *J. Mater. Chem. B* **3**, 5629–5634 (2015).

126. Kim, H. S., Son, Y. J. & Yoo, H. S. Clustering siRNA conjugates for MMP-responsive therapeutics in chronic wounds of diabetic animals. *Nanoscale* **8**, 13236–13244 (2016).

127. Wang, H. *et al.* Matrix metalloproteinase 2-responsive micelle for siRNA delivery. *Biomaterials* **35**, 7622–7634 (2014).

128. Hou, W. *et al.* MMP2-Targeting and Redox-Responsive PEGylated Chlorin e6 Nanoparticles for Cancer Near-Infrared Imaging and Photodynamic Therapy. *ACS Appl. Mater. Interfaces* **8**, 1447–1457 (2016).

129. Veiman, K. *et al.* PEG shielded MMP sensitive CPPs for efficient and tumor specific gene delivery in vivo. *J. Control. Release* **209**, 238–247 (2015).

130. Linderoth, L., Peters, G. H., Madsen, R. & Andresen, T. L. Drug delivery by an enzyme-mediated cyclization of a lipid prodrug with unique bilayer-formation properties. *Angew. Chemie - Int. Ed.* **48**, 1823–1826 (2009).

131. Gu, Z. *et al.* Injectable Nano-Network for Glucose-Mediated Insulin Delivery. *ACS Nano* **7**,

4194–4201 (2013).

132. Aimetti, A. A., Tibbitt, M. W. & Anseth, K. S. Human Neutrophil Elastase Responsive Delivery from Poly(ethylene glycol) Hydrogels. *Biomacromolecules* **10**, 1484–1489 (2009).

133. Knipe, J. M., Chen, F. & Peppas, N. A. Enzymatic Biodegradation of Hydrogels for Protein Delivery Targeted to the Small Intestine. *Biomacromolecules* **16**, 962–972 (2015).

134. Lin, C. C., Raza, A. & Shih, H. PEG hydrogels formed by thiol-ene photo-click chemistry and their effect on the formation and recovery of insulin-secreting cell spheroids. *Biomaterials* **32**, 9685–9695 (2011).

135. Li, C. *et al.* Thrombosis-Responsive Thrombolytic Coating Based on Thrombin-Degradable Tissue Plasminogen Activator (t-PA) Nanocapsules. *Adv. Funct. Mater.* **27**, 1–11 (2017).

136. Zhu, S., Nih, L., Carmichael, S. T., Lu, Y. & Segura, T. Enzyme-Responsive Delivery of Multiple Proteins with Spatiotemporal Control. *Adv. Mater.* **27**, 3620–3625 (2015).

137. Kern, H. B. *et al.* Enzyme-Cleavable Polymeric Micelles for the Intracellular Delivery of Proapoptotic Peptides. *Mol. Pharm.* **14**, 1450–1459 (2017).

138. Holloway, J. L., Ma, H., Rai, R. & Burdick, J. A. Modulating hydrogel crosslink density and degradation to control bone morphogenetic protein delivery and in vivo bone formation. *J. Control. Release* **191**, 63–70 (2014).

139. Phelps, E. A., Templeman, K. L., Thule, P. M. & Garcia, A. J. Engineered VEGF-releasing PEG-MAL hydrogel for pancreatic islet vascularization. *Drug Deliv. Transl. Res.* **5**, 125–136 (2015).

140. Maitz, M. F. *et al.* Adaptive release of heparin from anticoagulant hydrogels triggered by different blood coagulation factors. *Biomaterials* **135**, 53–61 (2017).

141. Sabino, F. *et al.* In vivo assessment of protease dynamics in cutaneous wound healing by degradomics analysis of porcine wound exudates. *Mol. Cell. Proteomics* **14**, 354–370

(2015).

142. Cane, J. L. *et al.* Matrix metalloproteinases -8 and -9 in the Airways, Blood and Urine During Exacerbations of COPD. *COPD J. Chronic Obstr. Pulm. Dis.* **13**, 26–34 (2016).

143. Elbert, D. L., Pratt, A. B., Lutolf, M. P., Halstenberg, S. & Hubbell, J. A. Protein delivery from materials formed by self-selective conjugate addition reactions. *J. Control. Release* **76**, 11–25 (2001).

144. Insua, I., Zizmare, L., Peacock, A. F. A., Krachler, A. M. & Fernandez-Trillo, F. Polymyxin B containing polyion complex (PIC) nanoparticles: Improving the antimicrobial activity by tailoring the degree of polymerisation of the inert component. *Sci. Rep.* **7**, 1–10 (2017).

145. Zhao, Q. *et al.* Polysaccharide-based biomaterials with on-demand nitric oxide releasing property regulated by enzyme catalysis. *Biomaterials* **34**, 8450–8458 (2013).

146. Akama, S., Maki, T. & Yamanaka, M. Enzymatic hydrolysis-induced degradation of a lactose-coupled supramolecular hydrogel. *Chem. Commun.* **54**, 8814–8817 (2018).

147. Li, D., An, X. & Mu, Y. A liposomal hydrogel with enzyme triggered release for infected wound. *Chem. Phys. Lipids* **223**, 104783 (2019).

148. Lin, Y. A., Ou, Y. C., Cheetham, A. G. & Cui, H. Rational design of MMP degradable peptide-based supramolecular filaments. *Biomacromolecules* **15**, 1419–1427 (2014).

149. Chen, C. *et al.* Rational Design of Short Peptide-Based Hydrogels with MMP-2 Responsiveness for Controlled Anticancer Peptide Delivery. *Biomacromolecules* **18**, 3563–3571 (2017).

150. Kumada, Y., Hammond, N. a. & Zhang, S. Functionalized scaffolds of shorter self-assembling peptides containing MMP-2 cleavable motif promote fibroblast proliferation and significantly accelerate 3-D cell migration independent of scaffold stiffness. *Soft Matter* **6**, 5073 (2010).

151. Bremer, C., Tung, C. H. & Weissleder, R. In vivo molecular target assessment of matrix metalloproteinase inhibition. *Nat. Med.* **7**, 743–748 (2001).

152. Van Hove, A. H., Antonienko, E., Burke, K., Brown, E. & Benoit, D. S. W. Temporally Tunable, Enzymatically Responsive Delivery of Proangiogenic Peptides from Poly(ethylene glycol) Hydrogels. *Adv. Healthc. Mater.* **4**, 2002–2011 (2015).

153. Edwards, J., Caston-Pierre, S., Bopp, A. F. & Goynes, W. Detection of human neutrophil elastase with ethoxylate acrylate resin analogs. *J. Pept. Res.* **66**, 160–168 (2005).

154. Liu, S. Q., Rachel Ee, P. L., Ke, C. Y., Hedrick, J. L. & Yang, Y. Y. Biodegradable poly(ethylene glycol)-peptide hydrogels with well-defined structure and properties for cell delivery. *Biomaterials* **30**, 1453–1461 (2009).

155. Van Dijk, M., Van Nostrum, C. F., Hennink, W. E., Rijkers, D. T. S. & Liskamp, R. M. J. Synthesis and characterization of enzymatically biodegradable peg and peptide-based hydrogels prepared by click chemistry. *Biomacromolecules* **11**, 1608–1614 (2010).

156. Yang, J., Jacobsen, M. T., Pan, H. & Kopeček, J. Synthesis and characterization of enzymatically degradable PEG-based peptide-containing hydrogels. *Macromol. Biosci.* **10**, 445–454 (2010).

157. Deforest, C. A., Polizzotti, B. D. & Anseth, K. S. Sequential click reactions for synthesizing and patterning three-dimensional cell microenvironments. *Nat. Mater.* **8**, 659–664 (2009).

158. Purcell, B. P. *et al.* Delivery of a matrix metalloproteinase-responsive hydrogel releasing TIMP-3 after myocardial infarction: Effects on left ventricular remodeling. *Am. J. Physiol. - Hear. Circ. Physiol.* **315**, H814–H825 (2018).

159. Glangchai, L. C., Cristal, L., Caldorera-moore, M., Shi, L. & Roy, K. Nanoimprint lithography based fabrication of shape-specific , enzymatically-triggered smart nanoparticles. *J. Control. Release* **125**, 263–272 (2008).

160. Sawicki, L. A. & Kloxin, A. M. Design of thiol–ene photoclick hydrogels using facile techniques for cell culture applications. *Biomater. Sci.* **2**, 1612–1626 (2014).

161. Fairbanks, B. D. *et al.* A versatile synthetic extracellular matrix mimic via thiol-norbornene photopolymerization. *Adv. Mater.* **21**, 5005–5010 (2009).

162. Kyburz, K. A. & Anseth, K. S. Three-dimensional hMSC motility within peptide-functionalized PEG-based hydrogels of varying adhesivity and crosslinking density. *Acta Biomater.* **9**, 6381–6392 (2013).

163. Schultz, K. M., Kyburz, K. A. & Anseth, K. S. Measuring dynamic cell-material interactions and remodeling during 3D human mesenchymal stem cell migration in hydrogels. *Proc. Natl. Acad. Sci.* **112**, E3757-3764 (2015).

164. Phelps, E. A. *et al.* Maleimide cross-linked bioactive PEG hydrogel exhibits improved reaction kinetics and cross-linking for cell encapsulation and in situ delivery. *Adv. Mater.* **24**, 64–70 (2012).

165. Patterson, J. & Hubbell, J. A. Enhanced proteolytic degradation of molecularly engineered PEG hydrogels in response to MMP-1 and MMP-2. *Biomaterials* **31**, 7836–7845 (2010).

166. Lutolf, M. P. *et al.* Synthetic matrix metalloproteinase-sensitive hydrogels for the conduction of tissue regeneration: engineering cell-invasion characteristics. *Proc. Natl. Acad. Sci. U. S. A.* **100**, 5413–8 (2003).

167. Shih, H. & Lin, C. C. Cross-linking and degradation of step-growth hydrogels formed by thiol-ene photoclick chemistry. *Biomacromolecules* **13**, 2003–2012 (2012).

168. Mccall, J. D. & Anseth, K. S. Thiol − Ene Photopolymerizations Provide a Facile Method To Encapsulate Proteins and Maintain Their Bioactivity. *Biomacromolecules* **13**, 2410–2417 (2012).

169. Kharkar, P. M., Rehmann, M. S., Skeens, K. M., Maverakis, E. & Kloxin, A. M. Thiol-ene Click

Hydrogels for Therapeutic Delivery. *ACS Biomater. Sci. Eng.* **2**, 165–179 (2016).

170. Hoyle, C. E. & Bowman, C. N. Thiol-ene click chemistry. *Angew. Chemie - Int. Ed.* **49**, 1540–1573 (2010).

171. Fairbanks, B. D., Schwartz, M. P., Bowman, C. N. & Anseth, K. S. Photoinitiated polymerization of PEG-diacrylate with lithium phenyl-2,4,6-trimethylbenzoylphosphinate: polymerization rate and cytocompatibility. *Biomaterials* **30**, 6702–6707 (2009).

172. Kharkar, P. M., Kiick, K. L. & Kloxin, A. M. Designing degradable hydrogels for orthogonal control of cell microenvironments. *Chem. Soc. Rev.* **42**, 7335–7372 (2013).

173. Darling, N. J., Hung, Y. S., Sharma, S. & Segura, T. Controlling the kinetics of thiol-maleimide Michael-type addition gelation kinetics for the generation of homogenous poly(ethylene glycol) hydrogels. *Biomaterials* **101**, 199–206 (2016).

174. Nair, D. P. *et al.* The Thiol-Michael Addition Click Reaction: A Powerful and Widely Used Tool in Materials Chemistry. *Chem. Mater.* **26**, 724–744 (2013).

175. Li, G. *et al.* Investigation into thiol- (meth)acrylate Michael addition reactions using amine and phosphine catalysts. *Polym. Chem.* **1**, 1196–1204 (2010).

176. Chatani, S., Nair, D. P. & Bowman, C. N. Relative reactivity and selectivity of vinyl sulfones and acrylates towards the thiol–Michael addition reaction and polymerization. *Polym. Chem.* **4**, 1048–1055 (2013).

177. Lutolf, M. P., Tirelli, N., Cerritelli, S., Cavalli, L. & Hubbell, J. A. Systematic modulation of Michael-type reactivity of thiols through the use of charged amino acids. *Bioconjug. Chem.* **12**, 1051–1056 (2001).

178. Kim, J. *et al.* Characterization of the crosslinking kinetics of multi-arm poly(ethylene glycol) hydrogels formed via Michael-type addition. *Soft Matter* **12**, 2076–2085 (2016).

179. Jansen, L. E., Negrón-piñeiro, L. J., Galarza, S. & Peyton, S. R. Control of thiol-maleimide

reaction kinetics in PEG hydrogel networks. *Acta Biomater.* **70**, 120–128 (2018).

180. Lin, C., Sawicki, S. M. & Metters, A. T. Free-Radical-Mediated Protein Inactivation and Recovery during Protein Photoencapsulation. *Biomacromolecules* **9**, 75–83 (2008).

181. Williams, C. G., Malik, A. N., Kyun, T., Manson, P. N. & Elisseeff, J. H. Variable cytocompatibility of six cell lines with photoinitiators used for polymerizing hydrogels and cell encapsulation. *Biomaterials* **26**, 1211–1218 (2005).

182. Fleischmann, R. *et al.* Efficacy and safety of certolizumab pegol monotherapy every 4 weeks in patients with rheumatoid arthritis failing previous disease- modifying antirheumatic therapy : the FAST4WARD study. *Ann Rhem Dis* **68**, 805–811 (2009).

183. Chapman, A. P. *et al.* Therapeutic antibody fragments with prolonged in vivo half-lives. *Nat. Biotechnol.* **17**, 780–783 (1999).

184. Rybinski, B., Franco-Barraza, J. & Cukierman, E. The wound healing, chronic fibrosis, and cancer progression triad. *Physiol. Genomics* **46**, 223–244 (2014).

185. West, J. & Hubbell, J. Polymeric biomaterials with degradation sites for protease involved in cell migration. *Macromolecules* **32**, 241–244 (1999).

186. Jo, Y. S. *et al.* Biomimetic PEG hydrogels crosslinked with minimal plasmin-sensitive tri-amino acid peptides. *J. Biomed. Mater. Res. - Part A* **93**, 870–877 (2010).

187. Watarai, A. *et al.* TGFb functionalized starPEG-heparin hydrogels modulate human dermal fibroblast growth and differentiation. *Acta Biomater.* **25**, 65–75 (2015).

188. Salimath, A. S. *et al.* Dual Delivery of Hepatocyte and Vascular Endothelial Growth Factors via a Protease-Degradable Hydrogel Improves Cardiac Function in Rats. *PLoS One* **7**, 1–12 (2012).

189. Zhang, Y. *et al.* Thrombin-Responsive Transcutaneous Patch for Auto-Anticoagulant Regulation. *Adv. Mater.* **29**, 1–7 (2017).

190. Riener, C. K., Kada, G. & Gruber, H. J. Quick measurement of protein sulfhydryls with Ellman's reagent and with 4,4'-dithiodipyridine. *Anal. Bioanal. Chem.* **373**, 266–276 (2002).

191. Lu, S. & Anseth, K. S. Release behavior of high molecular weight solutes from poly(ethylene glycol)-based degradable networks. *Macromolecules* **33**, 2509–2515 (2000).

192. Merrill, E. W., Dennison, K. A. & Sung, C. Partitioning and diffusion of solutes in hydrogels of poly(ethylene oxide). *Biomaterials* **14**, 1117–1126 (1993).

193. Garesse, R., Castell, J. V, Vallejo, C. G. & MArco, R. A Fluorescamine-Based Sensitive Method for the Assay of Proteinases, Capable of Detecting the Initial Cleavage Steps of a Protein. *Eur J Biochem* **99**, 253–259 (1979).

194. Insua, I. *et al.* Enzyme-responsive polyion complex (PIC) nanoparticles for the targeted delivery of antimicrobial polymers. *Polym. Chem.* **7**, 2684–2690 (2016).

195. Garratt, L. W. *et al.* Alpha-1 antitrypsin mitigates the inhibition of airway epithelial cell repair by neutrophil elastase. *Am. J. Respir. Cell Mol. Biol.* **54**, 341–349 (2016).

196. Liang, C., Park, A. Y. & Guan, J. In vitro scratch assay: a convenient and inexpensive method for analysis of cell migration in vitro. *Nat. Protoc.* **2**, 329–333 (2007).

197. Schneider, C. A., Rasband, W. S. & Eliceiri, K. W. NIH Image to ImageJ: 25 years of image analysis. *Nat. Methods* **9**, 671–675 (2012).

198. Secret, E., Crannell, K. E., Kelly, S. J., Villancio-Wolter, M. & Andrew, J. S. SI_Matrix metalloproteinase-sensitive hydrogel microparticles for pulmonary drug delivery of small molecule drugs or proteins. *J. Mater. Chem. B* **3**, 5629–5634 (2015).

199. Bae, K. H. & Kurisawa, M. Emerging hydrogel designs for controlled protein delivery. *Biomater. Sci.* **4**, 1184–1192 (2016).

200. El-Sherbiny, I. M. & Smyth, H. D. C. Biodegradable nano-micro carrier systems for sustained pulmonary drug delivery: (I) Self-assembled nanoparticles encapsulated in

respirable/swellable semi-IPN microspheres. *Int. J. Pharm.* **395**, 132–141 (2010).

201. Baldwin, A. D. & Kiick, K. L. Reversible maleimide-thiol adducts yield glutathione-sensitive poly(ethylene glycol)-heparin hydrogels. *Polym. Chem.* **4**, 133–143 (2013).

202. Tung, C. M. & Dynes, P. J. Relationship between viscoelastic properties and gelation in thermosetting systems. *J. Appl. Polym. Sci.* **27**, 569–574 (1982).

203. Patrick, A. G. & Ulijn, R. V. Hydrogels for the Detection and Management of Protease Levels. *Macromol. Biosci.* **10**, 1184–1193 (2010).

204. Korkmaz, B. *et al.* Design and use of highly specific substrates of neutrophil elastase and proteinase 3. *Am. J. Respir. Cell Mol. Biol.* **30**, 801–807 (2004).

205. Edwards, J. V., Prevost, N. T., French, A. D., Concha, M. & Condon, B. D. Kinetic and structural analysis of fluorescent peptides on cotton cellulose nanocrystals as elastase sensors. *Carbohydr. Polym.* **116**, 278–285 (2015).

206. Edwards, J. V., Caston-Pierre, S., Howley, P., Condon, B. & Arnold, J. A Bio-Sensor for Human Neutrophil Elastase Employs Peptide-p-Nitroanilide Cellulose Conjugates. *Sens. Lett.* **6**, 517–523 (2008).

207. Guan, J. & Wagner, W. R. Synthesis, characterization and cytocompatibility of polyurethaneurea elastomers with designed elastase sensitivity. *Biomacromolecules* **6**, 2833–2842 (2005).

208. Mann, B. K., Gobin, A. S., Tsai, A. T., Schmedlen, R. H. & West, J. L. Smooth muscle cell growth in photopolymerized hydrogels with cell adhesive and proteolytically degradable domains: Synthetic ECM analogs for tissue engineering. *Biomaterials* **22**, 3045–3051 (2001).

209. Habraken, G. J. M., Peeters, M., Thornton, P. D., Koning, C. E. & Heise, A. Selective Enzymatic Degradation of Self-Assembled Particles from Amphiphilic Block Copolymers

Obtained by the Combination of N -Carboxyanhydride and Nitroxide-Mediated Polymerization. *Bioma* 1371–1379 (2011).

210. Roberts, J. N. *et al.* Dynamic Surfaces for the Study of Mesenchymal Stem Cell Growth through Adhesion Regulation. *ACS Nano* **10**, 6667–6679 (2016).

211. Masood, A. *et al.* Neutrophil elastase-induced elastin degradation mediates macrophage influx and lung injury in 60% O2-exposed neonatal rats. *Am. J. Physiol. Lung Cell. Mol. Physiol.* **309**, L53-62 (2015).

212. Lutolf, M. P. *et al.* Repair of bone defects using synthetic mimetics of collagenous extracellular matrices. *Nat Biotechnol* **21**, 513–518 (2003).

213. Zustiak, S. P. & Leach, J. B. Characterization of Protein Release From Hydrolytically Degradable Poly (Ethylene Glycol) Hydrogels. **108**, 197–206 (2011).

214. Lutolf, M. P. & Hubbell, J. a. Synthesis and Physicochemical Characterization of End-Linked Poly (ethylene glycol) -co-peptide Hydrogels Formed by Michael-Type Addition. *Biomacromolecules* **4**, 713–722 (2003).

215. Majima, T. & Schnabel, W. Phenyl-2,4,6-trimethylbenzoylphosphinates as water-soluble photoinitiators. Generation and reactivity of O=b(C6Hs)(O-) radical anions. *Makromol Chem* **192**, 2307–2315 (1991).

216. McKinnon, D. D., Kloxin, A. M. & Anseth, K. S. Synthetic hydrogel platform for three-dimensional culture of embryonic stem cell-derived motor neurons. *Biomater. Sci.* **1**, 460–469 (2013).

217. Law, B., Weissleder, R. & Tung, C. H. Peptide-based biomaterials for protease-enhanced drug delivery. *Biomacromolecules* **7**, 1261–1265 (2006).

218. Leight, J. L., Alge, D. L., Maier, A. J. & Anseth, K. S. Direct masurement of matrix metalloproteinase activity in 3D cellular microenvironments using a fluorogenic peptide

substrate. *Biomaterials* **34**, 7344–7352 (2013).

219. Bremer, C., Tung, C.-H. & Weissleder, R. In vivo molecular target assessment of matrix metalloproteinase inhibition. *Nat. Med.* **7**, (2001).

220. Harris, T. J., Von Maltzahn, G., Derfus, A. M., Ruoslahti, E. & Bhatia, S. N. Proteolytic Actuation of Nanoparticle Self-Assembly. *Angew. Chemie - Int. Ed.* **45**, 3161–3165 (2006).

221. Song, J. *et al.* PROSPER: An Integrated Feature-Based Tool for Predicting Protease Substrate Cleavage Sites. *PLoS One* **7**, 1–23 (2012).

222. Cutting, K. F. Wound exudate: composition and functions. *Br. J. Community Nurs.* **8**, S4–S9 (2003).

223. Secret, E., Kelly, S. J., Crannell, K. E. & Andrew, J. S. SI_Enzyme-responsive hydrogel microparticles for pulmonary drug delivery. *ACS Appl. Mater. Interfaces* **6**, 10313–10321 (2014).

224. Nagase, H. Substrate specificity of MMPs. in *Matrix Metalloproteinase Inhibitors in Cancer Therapy* 39–66 (Humana Press, 2001).

225. Polverino, E., Rosales-mayor, E., Dale, G. E. & Dembowsky, K. The Role of Neutrophil Elastase Inhibitors in Lung Diseases. *Chest* **152**, 249–262 (2017).

226. Navia, M. A. *et al.* Structure of human neutrophil elastase in complex with a peptide chloromethyl ketone inhibitor at 1.84-Å resolution. *Proc. Natl. Acad. Sci. U. S. A.* **86**, 7–11 (1989).

227. Oltmanns, U., Sukkar, M. B., Xie, S., John, M. & Chung, K. F. Induction of human airway smooth muscle apoptosis by neutrophils and neutrophil elastase. *Am. J. Respir. Cell Mol. Biol.* **32**, 334–341 (2005).

228. Stockley, R. *et al.* Phase II study of a neutrophil elastase inhibitor (AZD9668) in patients with bronchiectasis. *Respir. Med.* **107**, 524–533 (2013).

229. Stevens, T. *et al.* AZD9668 : Pharmacological Characterization of a Novel Oral Inhibitor of Neutrophil Elastase. **339**, 313–320 (2011).

230. Stevens, T. *et al.* AZD9668 : Pharmacological Characterization of a Novel Oral Inhibitor of Neutrophil Elastase. *J. Pharmacol. Exp. herapeutics* **339**, 313–320 (2011).

231. U.S. National Library of Medicine. Subcutaneous Elafin in Healthy Subjects. Identifier NCT03522935.

232. Baker, A. H., Edwards, D. R. & Murphy, G. Metalloproteinase inhibitors: Biological actions and therapeutic opportunities. *J. Cell Sci.* **115**, 3719–3727 (2002).

233. Sandhaus, R. A. *et al.* The Diagnosis and Management of Alpha-1 Antitrypsin Deficiency in the Adult. *Chronic Obstr. Pulm. Dis. J. COPD Found.* **3**, 668–682 (2016).

234. Gettins, P. G. W. Serpin structure, mechanism, and function. *Chem. Rev.* **102**, 4751–4803 (2002).

235. Silverman, G. A. *et al.* The serpins are an expanding superfamily of structurally similar but functionally diverse proteins. Evolution, mechanism of inhibition, novel functions, and a revised nomenclature. *J. Biol. Chem.* **276**, 33293–33296 (2001).

236. Dobó, J. & Gettins, P. G. W. α1-Proteinase Inhibitor Forms Initial Non-covalent and Final Covalent Complexes with Elastase Analogously to Other Serpin-Proteinase Pairs, Suggesting a Common Mechanism of Inhibition. *J. Biol. Chem.* **279**, 9264–9269 (2004).

237. Rose, A. S. *et al.* NGL viewer: Web-based molecular graphics for large complexes. *Bioinformatics* **34**, 3755–3758 (2018).

238. Fisher, J. F. & Mobashery, S. Recent advances in MMP inhibitor design. *Cancer Metastasis Rev.* **25**, 115–136 (2006).

239. Hunckler, M. D. *et al.* Linkage Groups within Thiol–Ene Photoclickable PEG Hydrogels Control In Vivo Stability. *Adv. Healthc. Mater.* **1900371**, 1–7 (2019).

240. Wiegand, C. *et al.* Protease and pro-inflammatory cytokine concentrations are elevated in chronic compared to acute wounds and can be modulated by collagen type I in vitro. *Arch Dermatol Res* **302**, 419–428 (2010).

241. Zeng, Y. *et al.* PEGylated Cationic Vectors Containing a Protease-Sensitive Peptide as a miRNA Delivery System for Treating Breast Cancer. *Mol. Pharm.* **14**, 81–92 (2017).

242. Tsai, Y. F. *et al.* Sirtinol Inhibits Neutrophil Elastase Activity and Attenuates Lipopolysaccharide-Mediated Acute Lung Injury in Mice. *Sci. Rep.* **5**, 1–10 (2015).

243. Fujie, K. *et al.* Inhibition of elastase-induced acute inflammation and pulmonary emphysema in hamsters by a novel neutrophil elastase inhibitor FR901277. *Inflamm. Res.* **48**, 160–167 (1999).

244. Suzuki, T. *et al.* Proteinase-activated receptor-1 mediates elastase-induced apoptosis of human lung epithelial cells. *Am. J. Respir. Cell Mol. Biol.* **33**, 231–247 (2005).

245. Suzuki, T. *et al.* Leukocyte elastase induces lung epithelial apoptosis via a PAR-1-, NF-κB-, and p53-dependent pathway. *Am. J. Respir. Cell Mol. Biol.* **41**, 742–755 (2009).

246. Fischer, B. M., Zheng, S., Fan, R., Voynow, J. A. & Carolina, N. Neutrophil elastase inhibition of cell cycle progression in airway epithelial cells in vitro is mediated by p27 kip1. *Am. J. Physiol. - Cell Mol. Physiol.* **293**, 762–768 (2007).

247. Song, J. S. *et al.* EFFECTS OF ELASTASE INHIBITOR ON THE EPITHELIAL CELL APOPTOSIS IN BLEOMYCIN- INDUCED PULMONARY FIBROSIS. *Exp. Lung Res.* **2148**, (2009).

248. Ginzberg, H. H. *et al.* Neutrophil-mediated epithelial injury during transmigration: role of elastase. *Am. J. Physiol. Gastrointest. Liver Physiol.* **281**, 705–717 (2001).

249. Kuwahara, I. Neutrophil elastase induces IL-8 gene transcription and protein release through p38/NF- B activation via EGFR transactivation in a lung epithelial cell line. *AJP Lung Cell. Mol. Physiol.* **291**, L407–L416 (2006).

250. Akram, K. M., Lomas, N. J., Spiteri, M. A. & Forsyth, N. R. Club cells inhibit alveolar epithelial wound repair via TRAIL-dependent apoptosis. *Eur. Respir. J.* **41**, 683–694 (2013).

251. Sonnaert, M., Papantoniou, I., Luyten, F. P. & Schrooten, J. Quantitative Validation of the Presto Blue™ Metabolic Assay for Online Monitoring of Cell Proliferation in a 3D Perfusion Bioreactor System. *Tissue Eng. - Part C Methods* **21**, 519–529 (2015).

252. Stamm, A., Reimers, K., Strauß, S., Vogt, P. & Scheper, T. In vitro wound healing assays – state of the art. *BioNanoMat* **17**, 79–87 (2016).

253. Xiaokaiti, Y. *et al.* EGCG reverses human neutrophil elastase-induced migration in A549 cells by directly binding to HNE and by regulating α1-AT. *Sci. Rep.* **5**, 1–14 (2015).

254. Chin, A. C. *et al.* Neutrophil-mediated Activation of Epithelial Protease-Activated Receptors-1 and -2 Regulates Barrier Function and Transepithelial Migration. *J. Immunol.* **181**, 5702–5710 (2008).

255. Pugin, J. *et al.* Cyclic stretch of human lung cells induces an acidification and promotes bacterial growth. *Am. J. Respir. Cell Mol. Biol.* **38**, 362–370 (2008).

256. Kato, Y. *et al.* Acidic extracellular microenvironment and cancer. *Cancer Cell Int.* **13**, 1 (2013).

257. Korkmaz, B., Horwitz, M., Jenne, D. & Gauthier, F. Neutrophil elastase, proteinase 3, and cathepsin G as therapeutic targets in human diseases. *Pharmacol. Rev.* **62**, 726–759 (2010).